UNIVERSITY OF LIVERPOOL

Role of microRNAs and effects of substrate, age and stretch in experimental models for IPF.

Thesis submitted in accordance with the requirements of the University of Liverpool for degree of Doctor in Philosophy

By
Michele Scotto di Mase

February 2020

Abstract

Pulmonary fibrosis (IPF) is a debilitating progressive disease mostly affecting the elderly, and due to dysregulated wound healing repair. It is characterised by increased matrix production and altered ECM composition, leading to increased tissue rigidity, and eventually, death.

In mammalian lungs, mechanical stretch is generated by the diaphragm and chest muscles and transferred first to lung septa and then at cellular level. In lung fibrosis the increase in ECM causes mechanical stretch impairment due to the increase in tissue stiffness, which is thought to be mostly dependant on increased fibrillar collagen.

Using an ad hoc in vitro system, the effects of collagen as culture substrate, age and mechanical stretch on several ECM genes were investigated in both primary and immortalised lung cells. My results indicated profibrotic roles for collagen as a substrate and age, while mechanical stretch appeared to have a protective role against fibrosis.

Pharmacological use of microRNAs to fine tune mRNA expression is a novel field of research. MicroRNA based therapies either aim to increase expression of a microRNA to repress a target mRNA (mirmimics), or decrease microRNA expression to upregulate a target mRNA (antagomir). Analysis of microRNA expression in the Bleomycin mouse model of lung fibrosis identified more than 20 microRNAs that were significantly modified in their expression during fibrosis induction and progression.

Using the Bleomycin model, I identified 4 microRNAs (miR-21a-5p, miR-34a- 5p, miR-29a-3p and miR-378-5p) as potential pro-fibrotic microRNAs due to progressively increased expression correlated with progression of fibrotic features.

Results from primary mouse fibroblast cultures showed that overexpression of miR-29a-3p results in a reduction of Col1a1 expression, suggesting an antifibrotic role for this microRNA. miR-21a-5p expression decreased Smad7 expression in both primary mouse lung fibroblasts and in the Bleomycin model of lung fibrosis. Treatment with a miR-21a mirmimic resulted in increased lung fibrosis in the Bleomycin mouse model, while treatment with a miR-21a antagomir resulted in reduced lung fibrosis. My results identify miR-21a repression as a potential novel strategy to treat IPF.

List of presentations

Oral Communications

Scotto di Mase M, Whysall K, Bou-Gharios G, van't Hof RJ. Mechanical stretch, age and substrates affect expression of ECM gene and microRNAs in lung fibroblasts. IACD Musculoskeletal Biology Science day 2017. **Oral presentation.**

Scotto di Mase M, Whysall K, Bou-Gharios G, van't Hof RJ. Mechanical stretch and age affect fibrosis-related gene expression in lung fibroblast. British Society of Extracellular Matrix (BSMB) annual meeting, 2017, London, UK. **Oral presentation.**

Poster Communications

Scotto di Mase M, Whysall K, Bou-Gharios G, van't Hof RJ. A miR-21a antagomir decreases lung fibrosis in the mouse model of Bleomycin induced fibrosis. British Society of Extracellular Matrix (BSMB) spring meeting, 2019. **Poster presentation.**

Scotto di Mase M, Whysall K, Bou-Gharios G, van't Hof RJ. Matrix composition affects fibrosis-related gene expression in response to TGF-ß and mechanical stretch in A549 epithelial cell line. British Society of Extracellular Matrix (BSMB) spring meeting, 2018. **Poster presentation.**

Scotto di Mase M, Whysall K, Bou-Gharios G, van't Hof RJ. Role of miR-34a- 3p in IPF. IACD Musculoskeletal Biology Science day 2016. **Poster presentation.**

Scotto di Mase M, Whysall K, Bou-Gharios G, van't Hof RJ. Role of miR-34a- 3p in IPF. IACD Musculoskeletal Biology Science day 2015. **Poster presentation.**

A Pasquale,

Per sempre nella mia vita quotidiana

Acknowledgment

This part of my thesis is dedicated to the people that filled my life with love in the past 4 years in Liverpool.

First of all, I have to thank the University of Liverpool and the Crossley Barnes fund that funded my project.

Second, I would like to thank Sue Jones for her fundamental support when I had to pause my PhD. I would like also to thank Simon Tew and Aphrodite Vasilaki for the support to all the IACD PhD student "community".

I want to express my gratitude to Sheila Ryan, Brenda Smith, Sharon Power, Joni Roachdown, Joe Tancock, Andy Houghton and the other members of IACD staff, for their help in this project.

This project would not have been possible without the members of my group, who helped me when I was pulled down for problems bigger than me. To my desk mate, Francesca Manuela de Sousa Brito, who always pushed me through difficulties telling me that everything will be all right (she still does). Friends like her remain forever. To Cat, Mandy and Gemma thanks for the cake and tea, thanks to you I learned something great about the British Culture. To Mandy Prior and her life stories, maybe the only person who can make me silent. To Gemma Charlesworth thanks for your kindness, patience and happiness, you can fill a room with good vibes! To Cat Sperinck the person with the best music taste in all IACD, thanks for all the laugh together. To Jacqueline Siew Yeen Lin the hardest worker that I ever seen in my life. You will remain an amazing example for me for your strength and kindness. To Anna Daroszewska, thanks for all the interest expressed in my research, you helped me in becoming a better researcher. To Andy Butcher, a surprising party animal!

My sincere thanks go also to Kasia Whysall, who helped me in establishing my Science at IACD. To Jack Sharkey who showed me the difficulties of *iv* injection and to Harrish Poptani for the support and the possibility to use the Quantum GX-2 at the CPI unit. To Rees Sweeney, Sarah Roper and Ké Liu for all the help in all *in vivo* procedures I learned. To Kazu Yamamoto who helped me in the last period of my PhD with stimulating queries. To Kevin Hamill and his effort to make the lab a happier and more professional working place.

To George Bou-Gharios, who taught me the power of scientific doubt. I also want to

thank George for his door always being open and to the mental support he gave me. Without you I do not think I could have finished this PhD.

The life of a researcher is not an easy journey, similar to the one in the *Inferno of Divine Comedy*, where *Dante Alighieri* is able to reach the Paradise thanks to *Virgilio.* For that, I want to thank to my first supervisor Rob van 't Hof, my *Virgilio,* who guided me in this path with intellectual honesty and passion. I will miss to knock on your door and spend hours talking about Science, cheese and wine, without any Academic borders.

Living IACD meant a lot for me, because I become a better researcher and a better person. Therefore, thanks to Alessandro Riccio, Brandan Norman and Mohd Azuradi (Eddy), for the time together in and out the lab. To Lorenzo Ramos who gave me a roof when I did not have one. To Conor Sugden for the *Bella Ciao*. To Lee Throughton, Umar Sharif, Aibek Smagul, Wazu Supharattanasitthi, Panos Balaskas, Lina Zaripova, Martina Meschis, Caroline Staunton, Rachel Lawless, Craig Keenan, Abdullah Y Mandourah and Ayed Al-Qahtani for the trivial and not conversations. To my pal Steph Frost for the pints after work. To my great friend Sahem Alkharabsheh and all the cigarette of the weekend outside of the lab. To Thiago Ramos, one of the greatest brain that I found in this path. To my little Ify Giakoumaki a great friend who took care of me in the past 4 years. To Valentina Barrera my big sister, always there when I had the problem, and a source of inspiration for the person she is.

In Liverpool, I had the chance to meet amazing people outside the lab. People that filled my days of bad experiments, who listened all complains trying to understand what I really do in a lab, who I hope will never leave my life. To Adrien, Marc, Andrea, Tea and Lesley, Dani, Alberto, Montalbano, Ryan and Alhalanna, Bianca and Maria, Corrado, Chris, Lesley, John and Yasmine thanks for all the laugh and cry, for all the time together that truly filled my time in Liverpool. To Joana the first person I met in Liverpool, who introduce me to the best Pub in town.

To my family that always supported me in some of the darkest years of our story. To my father who pushed me in achieving what I really want, to my mother who will never lose their faith in me and to my sister who was always there when something was wrong. To my friends from Italy Skiattarella, Lucci, Elio, Rosario, Perna, Nico and Renald who with a simple Skype calling gave me their support.

At last but not least to my Giulia, who demonstrated me that distances are not an issue when there is love. Thanks for making me clear that in this life we are not alone as soon as we are together.

Author's Declaration

I declare that the work in this dissertation was carried out in accordance with the regulations of the University of Liverpool. The work is original except where indicated by references in the text.

Any views expressed in this thesis are those of the author and in no way represent those of the University of Liverpool.

This thesis has not been presented to any other university for examination in the United Kingdom or overseas.

Index of figures

Index of Tables

Table of contents

1. Introduction

1.1. Tissue Fibrosis overview

Tissue fibrosis is a multifactorial disease characterized by an excessive production and deposition of extracellular matrix (ECM). The accumulation of ECM disrupts tissue architecture and eventually leads to organ failure. Tissue fibrosis accounts for more than 45% of all cases of death in developed countries (Jun & Lau, 2018). The excessive production of ECM underlays dysregulation in the wound healing repair system, a feature common to all fibrotic disease. Tissue fibrosis can affect virtually every tissue and can rise from a broad range of pathological conditions such as heart failure, Scleroderma, cancer or without a certain aetiology (as for Idiopathic Pulmonary Fibrosis or IPF). Interestingly, liver fibrosis can originate also from Hepatitis B and C (HVB HVC) virus, leading eventually to cirrhosis, while kidney fibrosis can develop as a consequence of metabolic dysregulation such as in diabetes or hypertension (Jun & Lau, 2018).

Wound healing is a finely regulated mechanism which, when impaired leads to development of fibrosis. Tissue repair consists of three distinct and overlapping mechanisms: immune recruitment after damage, activation of immune cells and myofibroblasts, and myofibroblast renewal of ECM (Jun & Lau, 2018). The wound healing repair system allows to repopulate a damaged tissue and it is a key mechanism for individual survival.

After damage, platelets form a fibrin clot to protect tissue parenchyma and they release chemokines and cytokines to recruitment immune cells. Tissue injury is also sensed through damage-associated-molecular-patterns (DAMPs) by innate immune granulocytes. DAMP-activity is not confined to native immunity cells, as DAMPs are constantly released during all phases of wound healing repair and also activate non-immune cells (mesenchymal, epithelial, and endothelial cells). Once activated, innate immunity cells protect a damaged tissue from any possible infections and remove cells debris. Innate immune cells produce and release of cytokines and chemokines to mount a specific immune response, known as adaptive immunity (Jun & Lau, 2018). Therefore, innate immune response is unspecific and rapid.

Innate immunity response starts with neutrophils, which are the first cells to be

recruited as the most abundant granulocyte population in the bloodstream. Subsequently, macrophages arrive on the site of damage to produce a more robust inflammatory response. Innate immunity through cytokines and chemokines then recruits cells from adaptive immunity, which mount a more specific immune response. However, the release of cytokines has a plethora of cellular effectors that can either boost or repress inflammatory response. In this context, macrophages have a key role in the development of inflammation, which dramatically impacts fibrotic development. This is because during wound healing repair, macrophages can change their cytokine expression profile, which affects mesenchymal ECM turnover.

Macrophages are leucocyte cells deriving from either the mother yolk sac or the bone marrow. The first type forms the organ resident macrophage (alveolar macrophages, Kupffer cells as example) and the second the monocyte population in the circulation (fig. 1.1) (Distler et al., 2019).

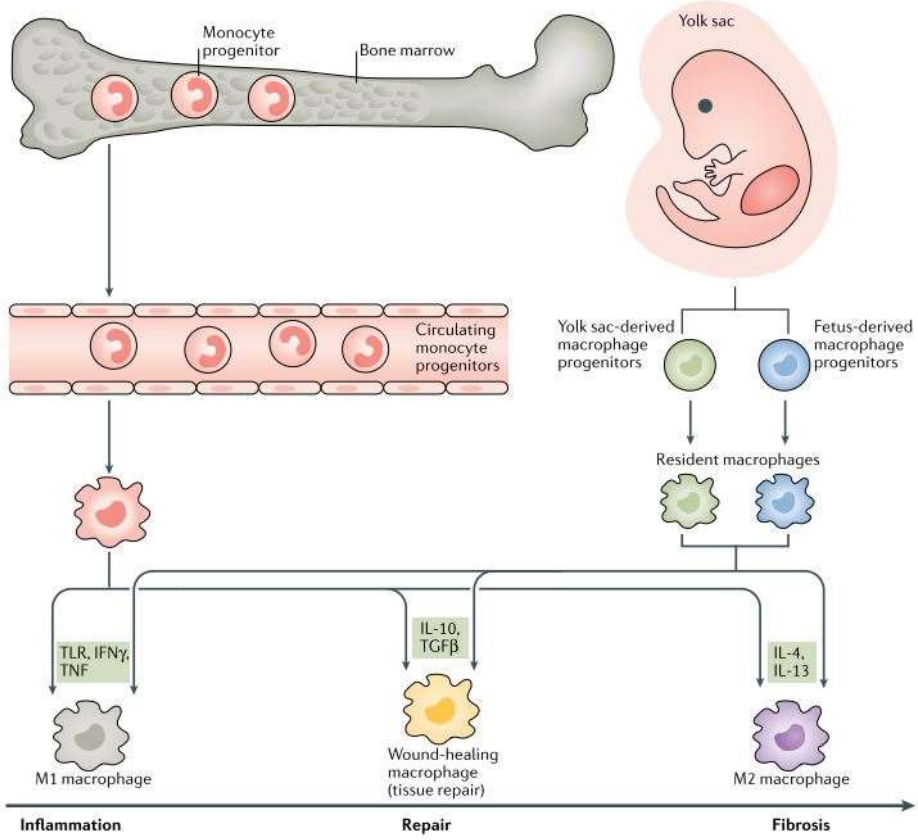

Figure 1.1 Macrophage activation and differentiation in tissue repair and fibrosis. Tissue resident macrophages and circulating bone marrow derived macrophage progenitors can differentiate into M1 and M2 with specific cytokine production profile. (from Distler et al, 2019).

For long macrophages have been distinct in two types, based on the difference in cytokine expression (known as M1 and M2 polarization), which triggers a diverse adaptive immune response.

M1 polarization sees the expression of IFN-Ɣ, LPS, TNF-α, while IL-4, IL-13, IL-1, IL-12 and TGF-ß are expressed during the M2 polarization. Evidence from studies on fibrosis demonstrated that macrophages can change the polarization state in response to tissue environment (Mack, 2018). Macrophages switch from M1 to M2 to calm the inflammation and to stimulate ECM production through TGF-ß (see below). However, when the M2 response is persistent, it stimulates an excessive production of ECM, which can evolve into a fibrotic phenotype. ECM turnover is strongly influenced by a family of enzymes known as Metalloproteinases (MMPs), which if dysregulated, may induce a fibrotic development. Macrophages control and regulate MMP expression and activation, and they also regulate their inhibitors (TIMPs) expression and their activity (Mack, 2018). Therefore, macrophages switch from M1 and M2 and *vice versa* based on the cytokine environment, influencing the type of immune response and ECM turnover, both mechanisms crucial in tissue fibrosis. Collectively, a large number of publications show that monocytes/macrophages play important but multifaceted roles in regulation of inflammation, regeneration, and fibrosis, depending on their polarization within tissues and the type and stage of diseases (Mack, 2018). Possibly fine tuning the macrophage polarization state can be a future pharmacological strategy for cellular therapies against tissue fibrosis. (Jun & Lau, 2018).

As mentioned, macrophages (and other antigen presenting cells) activate adaptive immunity through MHC complex interaction with T-cells receptor (TCR). This allows the correct mounting of the specific immune response to damage. Releasing specific subsets of cytokines and chemokines, T-cells produce inflammation to eradicate the source of damage (infective, tissue damage neoplastic, etc.), which subsequently activates mesenchymal cells involved in the tissue repair. Mesenchymal cells produce and release both ECM and enzymes able to metabolise ECM (MMPs). Mesenchymal cells are usually in a quiescent state, but after activation through cytokines (TGF-ß) first expand and then start producing large amounts of ECM. Dysregulation in this crosstalk between immune and mesenchymal cells can boost a series of signals that increase ECM production and leads to development of fibrosis.

In healthy wound healing, inflammation should stop once the cause of damage is eradicated, while mesenchymal cells remodel the ECM and repair the damage. By contrast, in tissue fibrosis the inflammatory response is persistent, and the repair machinery is constantly activated. The persistent inflammation and mesenchymal activation are chronic hallmarks of tissue fibrosis (Wynn, 2004). White and Mantovani in a short review defined inflammation in fibrosis as “too much of a good thing”, highlighting inflammation duality (White & Mantovani, 2014). However, results from several fibrotic experimental models do not correlate the severity of inflammation with the amount of fibrosis, indicating that fibrogenesis and inflammation hold diverse roles in fibrosis outcome (Wynn, 2004).

Cytokines can activate signalling pathway networks with dramatic changes on the surrounding environment. This is because cytokines possess autocrine and paracrine tropism on all cells present in a parenchyma. Therefore, in case of damage, cytokine release can rapidly change tissue structure through the recruitment and activation of specialised cells. The subsets of cytokines generally associated with a fibrotic response are the ones produced by Th2 cells, although TNF-α and IL-1ß are also produced by Th1 cells have been found in patients affected by IPF and SSc (Distler et al., 2019). In addition, Th-17 cells may regulate TNF-α and IL-1ß release by Th1 cells, and stimulate ECM production in fibrosis (Mack, 2018). It is probable that the Th1 and Th-17 cells control the first acute adaptive response to tissue damage, while Th2 cells control the progression into inflammation and tissue remodelling. This possibility is supported by evidence identifying a more important role of Th2 response in fibrosis progression, rather than initiation (Wynn, 2004).

Typical cytokines released by Th2 cells are IL-4, IL-5, IL-10, IL-11, IL-13, and TGF-ß which activate the mesenchymal tissue remodelling. IL-4 can dampen the inflammation and increase ECM release; while IL-13 although profibrotic can attenuate fibrosis through IL-13 receptor decay (Mack, 2018). Interestingly, IL-4 expressing macrophages have been identified as a class of fibrosis related macrophages, while inhibition of IL-11 reduced fibrosis in the Bleomycin mouse model of lung fibrosis. IL-4 and IL-13 have pleiotropic effects and similar targets, which result in both anti-inflammatory and profibrotic responses.

TGF-ß is the most important cytokine in the context of tissue fibrosis. This pleotropic cytokine is upregulated in all forms of tissue fibrosis and several studies have associated TGF-ß activation with the molecular and cellular dysregulation underlying fibrotic disease. For this reason, treatment with TGF-ß or analogues are well-establish methods used in experimental biology to reproduce fibrotic phenotypes. TGF-ß can activate fibroblasts and other mesenchymal and non-mesenchymal cells to become pro-fibrotic myofibroblasts (Wynn, 2011). However, TGF-ß is also involved in other cellular processes such as metastasis and angiogenesis. Myofibroblasts are mesenchymal cells fundamental in wound healing repair. This cell population originates from different progenitors such as fibroblasts, pericytes, fibrocytes, and epithelial and endothelial cells. Dysregulation of normal myofibroblast activity triggers fibrotic “un-healing” which culminates in the excess in ECM. In tissue fibrosis, myofibroblasts accumulate, crosslink, and overproduce collagen fibres and other ECM components. The excessive increase in ECM augments tissue stiffness, impairing the diffusion of nutrients and oxygen, which further propagate the dysregulated wound healing repair (D. J. Tschumperlin et al., 2018). In vitro studies investigating the actions of TGF-ß indicate that even at a concentration of 0.5 ng/mL, TGF-ß can rapidly stimulate collagen synthesis (Fragiadaki et al., 2011). In connective tissues, TGF-ß is present as either a free homodimer or attached to fibrillin through latent TGF-ß binding protein (LTBP) (Theocharis et al., 2019). This allows fast release of the cytokine to induce tissue restoration in case of damage.

The TGF-ß superfamily includes TGF-ß1-ß3, activins, Bone morphogenic proteins (BMPs) and myostatin, which, after binding to their receptors, all transduce their intracellular signal through a phosphorylation cascade. TGF-ß receptors are heterodimers consisting of a serine/threonine kinase type I, also known as ALK 1-7, and a structural subunit (Hartmann & Yang, 2020). Free TGF-ß activates receptor dimerization, allowing autophosphorylation of the serine/threonine residues in the ALK domains (Chaudhury & Howe, 2009). The then leads to kinase activity resulting in the phosphorylation of activatory SMADs (SMAD1, SMAD2, SMAD3, SMAD5 and SMAD9). Generally, SMAD1 and 5 are also activated by BMP7, while SMAD2 and 3 are only activated by TGF-ß. SMAD2 and 3 are activated through a mechanism involving an anchor protein, known as SARA (Smad Anchor for Receptor Activation). Binding to phospho-SMAD 2 and 3, SARA brings this complex in close proximity to the TGF-ß receptor, increasing the affinity to SMAD4. SMAD4 is a regulatory member of the SMAD family and it is necessary for nuclear translocation and DNA binding, which enhances ECM gene transcription (fig 1.2)

(X. Yan, Liu, & Chen, 2009). The SMAD2/3/4 complex acts as transcription factor binding to SBE (Smad binding elements) stimulating transcription of a variety of genes (Col1a1, Col1a3, CCN2, Snail, Slug, Fibulin-1, PDGRFRα, TGF-ß1 receptor, IL-1ß etc.). This pathway also triggers a positive feedback loop on TGF-ß1 receptor expression, which further increase the expression of key genes involved in organ fibrosis. This mechanism rapidly augments ECM production by mesenchymal cells (Troncone et al., 2018). However, to limit the power of this pathway, inhibitory Smads (SMAD6 and -7) are upregulated by TGF-ß as well. SMAD6 and -7 serve as a negative feedback loop to limit the activity of the TGF-ß signalling cascade (Troncone et al., 2018).

Through this canonical pathway, fibrillar collagens, CCCN2/CTGF, laminins, fibronectins and other structural protein are upregulated in their expression (Wynn, 2011). This activation results in increased ECM synthesis and secretion by fibroblasts and partially by epithelial cells (Chaudhury & Howe, 2009). In healthy repair conditions, ECM production creates a barrier to pathogens and helps to sustain the epithelial regeneration. In contrast, in fibrosis, this activation, for reasons that are as yet unknown, triggers an excessive production of ECM and tissue disruption (X. Yan et al., 2009).

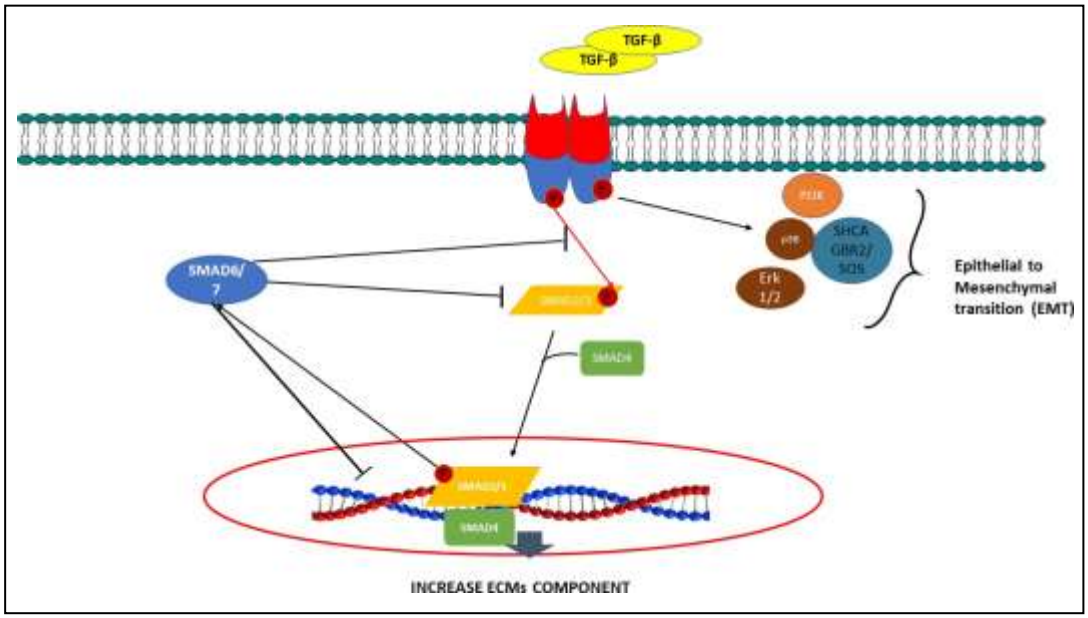

Figure 1.2 Schematic cartoon of TGF-ß canonical pathway (see SMAD pathway). On the right side of the cartoon pathways at the basis of EMT activation from TGF-ß (see text).

Non-canonical TGF-ß pathways, although starting from the same TGF-ß receptor, differ from the canonical pathway in the downstream effectors (PI3K/Akt, Rho, Rock, and Grb2). The

activation of this signalling pathway results in epithelial to mesenchymal transition (EMT), a fibrosis-related mechanism.

EMT is a biological mechanism that is the opposite of mesenchymal to epithelial transition (MET, which is rarer). EMT was first discovered in gastrulation and neural crest formation, processes controlled by SNAIL, a DNA repressor protein family (Kalluri & Weinberg, 2009). An EMT-dependent increase in mesenchymal cells appears to participate in tissue fibrosis, as it increases the mesenchymal cell pool in a damaged tissue. Evidence from *in vitro* studies identified TGF-ß as master regulator of EMT (Chaudhury & Howe, 2009). In epithelia associated with a fibrotic cytokine environment, TGF-ß triggers Snail and Slug activation through a SMAD dependent mechanism (Thiery et al., 2009), leading to an increase in myofibroblasts.. This mechanism can trigger a fibrotic development. However the importance of EMT has only been conclusively shown in kidney fibrosis *in vivo*, while there is still a lack of information regarding the role of EMT in liver and lung fibrosis (Kalluri & Weinberg, 2009).

The 2007 EMT meeting has decided to classify EMT in three categories related to: embryogenesis (type 1), wound healing/tissue regeneration and fibrosis (type 2) and cancer/metastasis (type 3) (Kalluri & Weinberg, 2009). However, this classification was made to distinguish between the same molecular mechanisms in three different biological processes that differ dramatically.

At the cellular level EMT is governed by a finely tuned transcriptional regulation, which determines cytoskeletal remodelling and dramatic changes in the expression of cell adhesion molecules and surface markers. The resulting cells present mesenchymal markers and respond to mesenchymal stimuli. The type 2 EMT (fibrotic) is the process that allows an epithelial cell to become a mesenchymal cell after an inflammatory stimulation or in response to TGF-ß. However, once the damage has been repaired, the mesenchymal cells should undergo apoptosis or MET to revert to normal tissue homeostasis. In fibrosis, however, the constant level of inflammation potentiates EMT, giving rise to abnormal mesenchymal cell numbers (Kalluri & Weinberg, 2009). EMT is not an instant mechanism, but a progressive series of changes associated with phenotypical alteration in terms of adhesion, cytoskeleton, and protein secretion. Non-canonical TGF-ß activation promotes epithelial polarization through Smurf (Smad associated E3-ubiquitin ligase)-dependent Rho GTPase degradation, which triggers tight junction disruption (Massagué, 2012). Gradually the epithelial cells gain mesenchymal markers such as N-cadherin, instead of E-cadherin (Thiery et al., 2009). Next,

surface integrins gradually change, switching from E- to N-cadherin. For example, integrin the expression of β4 is decreases, leading to decreased contacts with basal membrane. Then, in later stages of this process, cells will start to increase expression of α-smooth actin and fibrillar collagens The non-canonical TGF-ß pathway also contributes to this transformation through Phoshoinositol-3 kinase (PI3K) and p38 (MAP kinase) activation (Massagué, 2012). However, it is not clear if cytoskeletal modification results from the non-canonical pathway activation or as a secondary effect of TGF-ß canonical activation. Moreover, PI3K and p38 signalling pathways also occur in type 3 EMT (metastatic EMT) and SMAD signalling is over-expressed in tumour initiating cell stemness and is considered pro-metastatic (Massagué, 2008). However, in metastasis ECM remodelling leads to cancer stem cell escape, while in tissue fibrosis ECM remodelling triggers parenchymal disruption, two phenotypical distinct processes.

The contribution of EMT to fibrosis can be quite dramatic, it has been estimated that EMT accounts for the 30% of the mesenchymal cell population in kidney fibrosis. Increasing evidence currently also demonstrates the role of endothelial to mesenchymal transition (EndoMT) in tissue fibrosis (Hashimoto et al., 2010) (Kalluri & Neilson, 2003).

Mesenchymal fibroblasts are considered to be the most important cell type in tissue fibrosis. Fibroblasts are slow contractile cells, with unique proliferative capabilities (Abercrombie, 1979). As mentioned, fibroblasts are mesenchymal cells, distributed sparsely in the connective tissue, where they create (in development) and model (in adult life) ECM. In adult life fibroblasts remodel ECM by increasing fibre cross-linking, which makes fibres resist digestion by degrading enzymes. Fibroblasts regulate enzymatic crosslinking via lysyl-oxidase (LOX) and tissue transglutaminase (TG2), which crosslink diverse collagen fibres and can also cross-link collagens to fibronectin (see paragraph on fibrillogenesis). This mechanism dramatically increases in pathological condition and with ageing (Theocharis et al., 2019). Fibroblasts maintain ECM stability moving across connective tissue and organ interstitium through chemotaxis (Kendall & Feghali-Bostwick, 2014). Without environmental stimulation, adult fibroblasts do not produce large quantities of ECM (Laurent, 1986). In contrast, after tissue damage fibroblasts activate into myofibroblasts, which rapidly respond to damage, remodelling ECM. As described above, myofibroblasts can originate from mesenchymal cell lineage such as fibroblasts, fibrocyte, smooth muscle cells, and from epithelial and endothelial cells through EMT and Endo-MT respectively (Kendall & Feghali-Bostwick, 2014). Although

myofibroblasts have a key role in wound healing repair, excess myofibroblast activity underpins all known forms of tissue fibrosis. Exacerbation and persistent TGF-ß signalling activation can lead to fibrotic development. TGF-ß expression can rapidly increase through a positive feedback mechanism. Although SMAD6 and SMAD7 suppress the canonical TGF-ß pathway, this inhibition does not seem to be able to prevent development of fibrosis (X. Yan et al., 2009). The positive feedback loop in the TGF-ß signalling potentiates ECM release by myofibroblasts, leading to fibrosis (Kendall & Feghali-Bostwick, 2014). The effects induced by TGF-ß in this cell population are not limited to ECM expression. Interestingly, TGF-ß rapidly increases CTGF/CCN2 and IL-6 expression, two proteins that boost collagen expression in myofibroblasts (Kendall & Feghali-Bostwick, 2014). As mentioned above, TGF-ß is often bound to a protein complex that reduces cytokine availability and to fibrillin (Theocharis et al., 2019). Matrix remodelling through activation of MMPs, mostly derived from macrophages, can degrade fibrillin fibres, leading to release of the TGF-ß, and increased pro-fibrotic signalling.

Understanding the role of TGF-ß in fibrotic fibroblasts or myofibroblasts, is a challenge, as myofibroblasts can originate from different sources (as mentioned above). Excluding EMT, myofibroblasts involved in fibrosis originate from different mesenchymal sources, however, understanding the single sub-type contribution is challenging. Moreover, there is not a univocal cluster of cell markers that clearly identify myofibroblasts. Myofibroblast activation changes cell morphology due to cytoskeletal rearrangement, highlighted by α-smooth actin expression (Rybinski et al., 2014). This mechanism allows myofibroblasts to move across the septa and the damaged epithelium to repair the damage. The repair dysregulation taking place in fibrosis is thought to be due to a prolonged activation in response to chronic damage, which exacerbates myofibroblasts activation (Rybinski et al., 2014).

Studies from animal models have shown that fibrosis might be reversible in early stages and once the aetiology is eliminated. However this is not the case for idiopathic lung fibrosis (Jun & Lau, 2018). Although organ fibrosis presents a similar mechanism of action, it has distinct phenotypes in each organ, reflecting differences in tissue structure and organization as well as ECM composition. For this reason liver and kidney fibrosis appear more treatable than heart and lung fibrosis (Jun & Lau, 2018).

Liver contains highly specialized cells involved in metabolisms and hepatocytes have

considerable regenerative capability. Cellular therapies using macrophages have demonstrated the possibility to decrease collagen deposition in animal models of liver fibrosis (Mack, 2018). Therapies for kidney fibrosis are demonstrating the possibility to recapitulate disease phenotype as well. Tim Johnson developed a selective inhibitor of transglutaminase 2 TG2, which appears to revert disease hallmarks. This TG2 inhibitor has now passed pre-clinical trial, as it was extensively demonstrated the possibility to revert increase in collagen deposition in a model of chronic kidney fibrosis in rabbits (Atkinson, Pullen, Da Silva-Lodge, Williams, & Johnson, 2015). By contrast, cardiac fibrosis can be irreversible in some severe conditions. In cardiac fibrosis, hypertension and cardiac infraction can dramatically change disease outcome, despite cardiomyocytes have little regenerative capability and therefore they cannot deposit enormous quantity of collagen (Jun & Lau, 2018). On the other hand, pericyte and smooth muscle cells becoming myofibroblasts can dramatically increase fibrotic formation. At the state of art there are no effective therapies to revers cardiac fibrosis.

In summary, after tissue damage, megakaryocytes release chemokines and cytokines. Cytokines activate cells of the innate immune system and alveolar epithelial type-II cells, which release inflammatory mediators for host-protection, while chemokines recruit immune cells. Neutrophils and macrophages are usually the first cells that mediate innate immunity. Neutrophils possess a high secretory activity of lytic enzymes and inflammatory mediators, which recruit lymphocytes and activate macrophages to switch from M1 to M2. This mechanism starts a more robust inflammatory response, activating leucocytes Th2-response with secretion of IL-1ß, TNF-α, IL-4, IL-11, IL-13 and TGF-ß. Those cytokines activate myofibroblasts, which remodel ECM to repair the damaged tissue. Then, if wound healing repair apparatus is altered, this results in a persistent response to damage which gradually leads to fibrosis, as shown in figure 1.3.

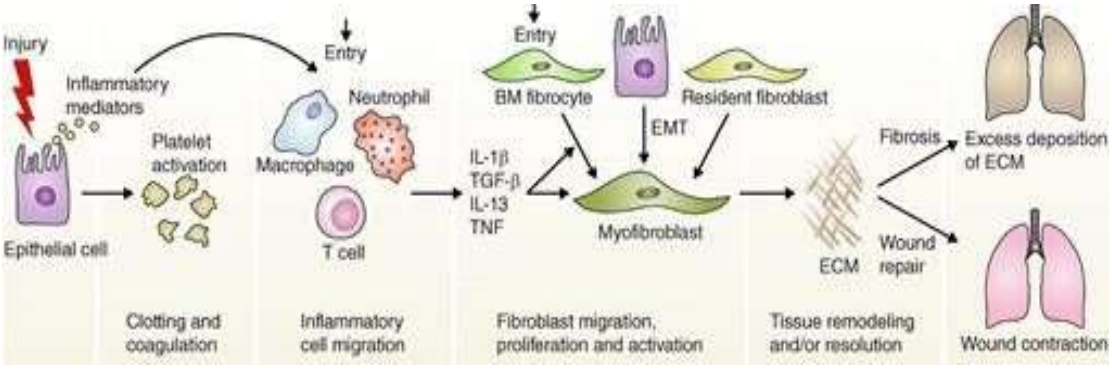

Figure 1.3 Schematic mechanism of fibrosis. After an epithelial injury, inflammatory mediators recruit innate immune cells and T cells mount an inflammatory response. T-cells secrete proinflammatory cytokines and TGF-ß. Cytokine environment activates fibrocyte, resident fibroblast, epithelia cells (through EMT) to remodel ECM. In healthy condition ECM is produced to trigger epithelia regeneration, once this result is achieved ECM is degraded, myofibroblasts undergoes apoptosis and tissue integrity is restored. In IPF (as well in other fibrotic development) myofibroblasts persistence increase ECM content leading to fibrotic development (From Wynn, 2011).

1.2. Interstitial lung disease, IPF and Bleomycin usage as model for lung fibrosis

Interstitial lung disease (ILD) and pulmonary fibrosis comprise a wide range of lung diseases (Kalchiem-Dekel, Galvin, Burke, Atamas, & Todd, 2018). Figure 1.4 shows a schematic clinical classification of ILD, including six type of ILD included in Kalchiem-Dekel review.

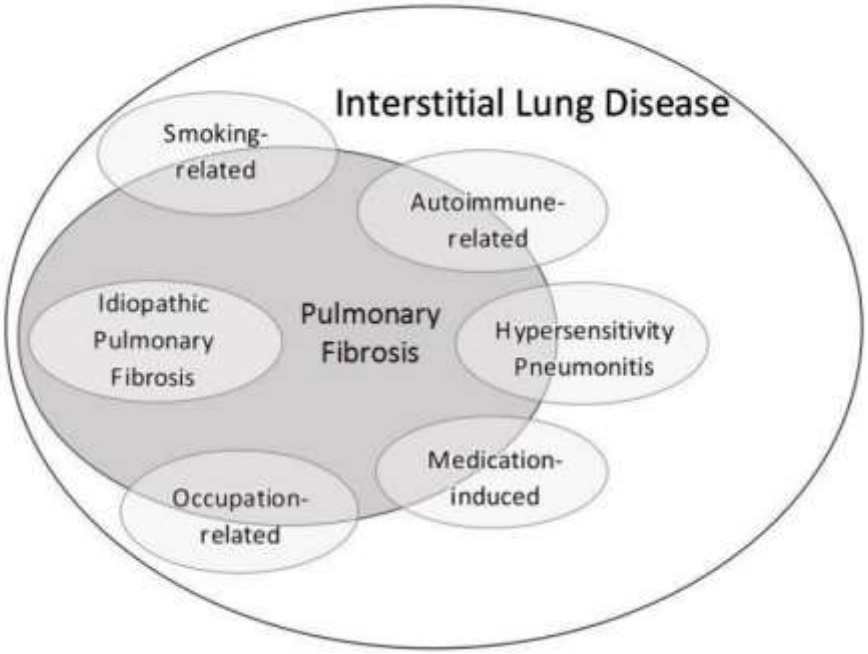

Figure 1.4 Set-theoretic classification of ILD phenotypes. Pulmonary fibrotic outcome is one of most likely pathological progression of ILD, IPF holding the worst prognosis (from Kalchiem-Dekel et al., 2018)

ILDs start with acute inflammation and little fibrotic development, therefore treatment with anti-inflammatory drugs are quite effective in early stages of disease (Kalchiem-Dekel et al., 2018). By contrast, in IPF or severe forms of pulmonary fibrosis, pulmonologists advice against the use of immunosuppressive and anti-inflammatory treatments (Fujimoto, Kobayashi, & Azuma, 2015).

ILDs are usually classified in interstitial pneumonia (UIP), organizing pneumonia (OP) and non-specific interstitial pneumonia (NSIP). UIP and NSIP show sparse dense fibrotic areas with necrotic fibroblasts immerse in ECM (fibroblasts foci), whereas OP shows spindle-shaped fibroblasts and oval-shape ECM (Kalchiem-Dekel et al., 2018). Without considering diseases

aetiology, in most of cases, ILDs show progressive evolution into fibrosis from an inflammatory state. However, IPF and PF phenotypes are associated more with UIP than NSIP (Murray et al., 2012). Both diseases present differences in aetiology, histopathological pattern, and in biomarker associated with the disease. However, lack of a precise histopathological classification of clinically recognized pulmonary fibrosis resulting from conflicting reports has been for long a problem in diagnosis (Kalchiem-Dekel et al., 2018). ILD induced by systemic sclerosis (SSc-ILD) can be confused with IPF and vice versa, as both present fibrotic development, similar biomarkers (IL-13, IL-1R, CCN2/CTGF as example),and similar histopathological and CT scan patterns (Lagares et al., 2017). This limitation in diagnosis has critical consequences in disease treatment, as an anti-inflammatory treatment can worsen IPF. (Murray et al., 2012). Although SSc-ILD (autoimmune ILD in fig. 1.4) appears phenotypically very similar to IPF, in the last decade high resolution tomography has evolved to discern between the two phenotypes (Lagares et al., 2017). Tomography scans from both SSc-ILD and IPF consist in sparse attenuation of X-ray (also called GGO, ground-glass opacities) across lung subpleural cross-sections. However, GGO has a different appearance in SSc-ILD versus IPF, and honeycombing is a feature (in some cases) present only IPF patients (fig. 1.5) (Kalchiem-Dekel et al., 2018).

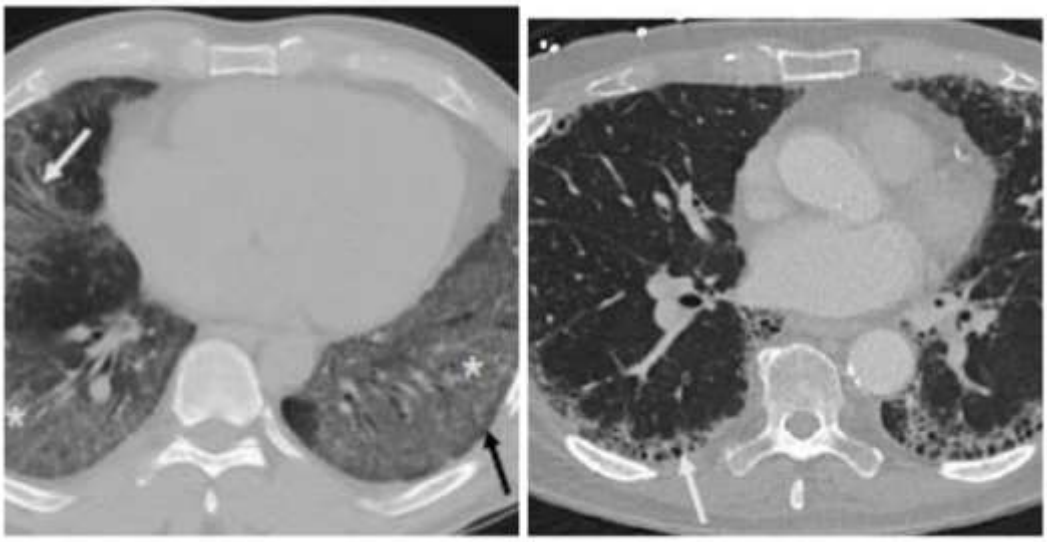

Figure 1.5 HRCT scan from patients affected by ILD. ILDs presents a high level of overlapping. SSc-ILD (left) and IPF (right) similarities become limitation in clinical practise (see text). The figure shows differences in ground-glass opacity and similarities in subpleural fibrotic development, highlighted with white arrow (SSc-ILD left) and black arrow (IPF right)

There is substantial variation in the appearance of fibrosis between individual patients. For example, fibroblast foci or honeycomb formations are correlated with more severe fibrosis, however they are only present in a minority of IPF patients (Kalchiem-Dekel et al., 2018).

ILD biodiversity represents a limit also in experimental biology. Reproducing the wide spectrum of fibrotic features of human lung fibrosis within a single animal model is currently not possible Therefore, different animal models of lung fibrosis have been developed using exposure to toxic molecules, irradiation and gene overexpression (Degryse & Lawson, 2011). The single exposure to a profibrotic concentration of Bleomycin remains the most used model and perhaps the most established as well. A single intratracheal or oropharyngeal administration of Bleomycin leads to an initial immune phase, followed by fibrosis (Wynn, 2011).

Bleomycin is drug used for treatment of patients with lung cancer, however, the drug is used in experimental biology as it induces fibrosis very similar to human lung fibrosis. Bleomycin induces both single and double strand DNA breaks (ssDNA or dsDNA) which lead to fibrosis. Subcutaneous administration of Bleomycin initiates a SSc-ILD like disease (Murray et al., 2012). The intratracheal/oropharyngeal route is the gold standard method to induce

lung fibrosis in rodents. Interestingly, Lakatos and collaborator compared intratracheal and oropharyngeal silica administration in the mouse, demonstrating that both administration routes were equivalent for drug delivery. Oropharyngeal localized in the distal parenchyma, while intratracheal more close to the hilum (see 2.2) (Lakatos et al., 2006). Although the Bleomycin model of lung fibrosis is fast and quite reproduceable, it has technical limitations due to the lack in hyperplastic alveolar type II cells, usually induced by chronic damage. Moreover, in rodents, Bleomycin-induced-fibrosis resolves after 21 days from the first injection (Mouratis & Aidinis, 2011).

Another disadvantage is that the Bleomycin model reproduces fibrotic features also common to SSc-ILD. This limitation is important in drug development, as drugs for both SSc-ILD and IPF are tested with a very similar animal model, despite the differences in disease aetiology. As mentioned, anti-inflammatory drugs are not recommended in patients with lung fibrosis. As a result of limitations in the Bleomycin model, drugs that appeared successful in initial animal studies failed in the further studies. Examples of this are INF-ϒ, Pirfenidone, Etanercept (TNF mAb) and bosentan (Murray et al., 2012).

Nevertheless, the Bleomycin model of lung fibrosis remains a fundamental tool in this field of research. However, disease variability, with overlap across IPF, PF and SSc-ILD represents major limitation of this system. In recent years organoids have become a novel model for the study of complex disease, such as lung fibrosis. However, the structural and cellular complexity of the lung has so far prevented the development of a suitable organoid model system for lung fibrosis.

1.2.1. Diagnosis of Pulmonary fibrosis

In lung pathophysiology, diagnostic uncertainty has been a historical limitation due to overlap in disease phenotypes. IPF and PF main distinction is in their aetiology, which is unknown for IPF. However, due to conflicting histological reports there is no clear disease classification. The high variability among lung fibrotic features, is a big limitation and has to be taken in account in both experimental and clinical practice (Kalchiem-Dekel et al., 2018).

Formulating a straightforward and accurate diagnosis for IPF for clinicians has been a challenge. The most common symptoms are considered to be “dry cough”, as well as weight loss, fever, and arthralgia (Meltzer & Noble, 2008). IPF symptoms are common to many other

lung diseases, such as chronic obstructive pulmonary disease (COPD) and lung cancers. This unspecific symptomatology is driven by the magnitude of response to damage, which is typical during early stages of the disease. Clearer signs of fibrosis are detectable during the late stages of the disease, where treatments cannot revert the fibrotic phenotype. Moreover, there are no specific and sensitive routine laboratory test that can univocally diagnose IPF in a patient. However, physiologic changes in spirometry parameters, such as lung capacity or lung volume are historically well- established methods to detect IPF (Wynn, 2011). Spirometry changes are due to changes in lung architecture due to a in decrease in ECM turnover. However, routine laboratory tests (blood test) and spirometry evaluations cannot be considered as gold standard due to technical limitations. On the other hand, imaging techniques such as high-resolution computerized tomography (HRCT) have become crucial in IPF diagnosis and is considered the gold standard for IPF diagnosis (Martinez et al., 2017). The presence of honeycombing is considered a clear hallmark of disease physiology. Honeycomb is a multiple unshaped thin fibrotic-like wall cysts which modifies the acinar lung architecture. The result of honeycomb formations is an enlargement of both lung bronchiole and epithelial. Honeycombs are composed mostly of ECM and they appear translucent at HRCT. Although honeycombing shares similarities with emphysema, honeycombing is considered as a clear manifestation of fibrosis in later stages of IPF (Arakawa et al., 2011). Nevertheless, only 30% of IPF patients present honeycombing in HRCT scans. More invasive tests, such as surgical lung biopsies, are generally used to overcome an uncertain diagnosis. Histological stains permit identification of clear fibrotic features, such as parenchymal disruption, fibroblast foci, tissue scaring and immune infiltration. Limitation to this is the possibility to produce false negative results due to the presence of fibrotic lesion only in a localised area. Therefore, as a single step diagnosis might fail in the identification of fibrosis, there is an increasing interest to develop a multidisciplinary approach. Although the increase in the number of tests also raises the possibility of systematic error, a multidisciplinary approach seems to improve the accuracy in the diagnostic process. Of note is the discovery of a number of serum markers such as specific microRNAs (X. Yang et al., 2015), metalloproteinases (MMP-1 and MMP-7) (Rosas et al., 2008) or proteins (endotelin- 1 and surfactant protein), which might lay the foundation for a better diagnosis in lung fibrosis. The clinical challenge is then to set standardized guidelines applicable to large scale populations for diagnosis. However, HRCT together with surgical lung biopsy remain the clinical gold standard for diagnosis (Martinez et al., 2017). Interestingly,

Burgstaller and collaborators identified possible molecular signature in lung diseases analysing ECM through a proteomic approach, which might be a new strategy for a fast and clear diagnosis for ILDs (Burgstaller et al., 2017).

1.3. Lung Structure and Physiology

The lung is an evolutionary unique organ, a vertebrate adaptation to air for oxidative metabolism. The lung provides oxygen to tissues and the release of carbon dioxide during each breathing cycle. In alveolar sacs and in transitional bronchioles oxygen is exchanged with carbon dioxide and *vice versa* in a diffusion process (Hsia et al., 2016). Tissues need oxygen to complete aerobic respiration, which is fundamental to produce ATP in mitochondria. Carbon dioxide is the final product of aerobic metabolism, and it can be considered as "waste". Vertebrates constantly breathe through a controlled mechanism involving involuntary innervation. This gas exchange necessary to live, is brought in from the trachea to the bronchiole through convention, while gases diffuse through the alveolar and transitional bronchiole. This latter is the actual location for gas exchange through circulation and provides oxygen and releases carbon dioxide (Hsia et al., 2016). Lung is characterised by an inhomogeneous stratified epithelia, composed of a wide range of different cell types, which reflects functional differences between proximal and distal regions (fig. 1.6).

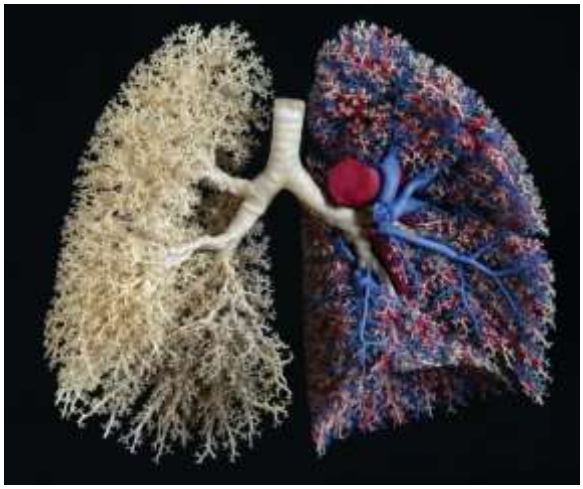

Figure 1.6 Cast of human bronchial tree with airways (yellow), pulmonary arteries (red), and pulmonary veins (blue) (From Hsia et al., 2016).

Proximal and distal lung can be then divided in two different compartments based on their function and cell population. Regarding cell heterogeneity, Whitsett and his collaborators produced in November 2018 a fundamental publication for lung biologist (Whitsett et al., 2018). Through single cell RNA analysis and bioinformatic tools they clustered each cellular lineage identifying 1) Epithelial cell (Ciliated, Club, alveolar epithelial type I and type II) 2) Immune cells (T and B lymphocytes, basophils and macrophages) 3) Mesenchymal (smooth muscle cells, pericyte, matrix and lipo-fibroblast and myofibroblast) and Endothelial

(lymphatic and vascular endothelial) (fig. 1.7).

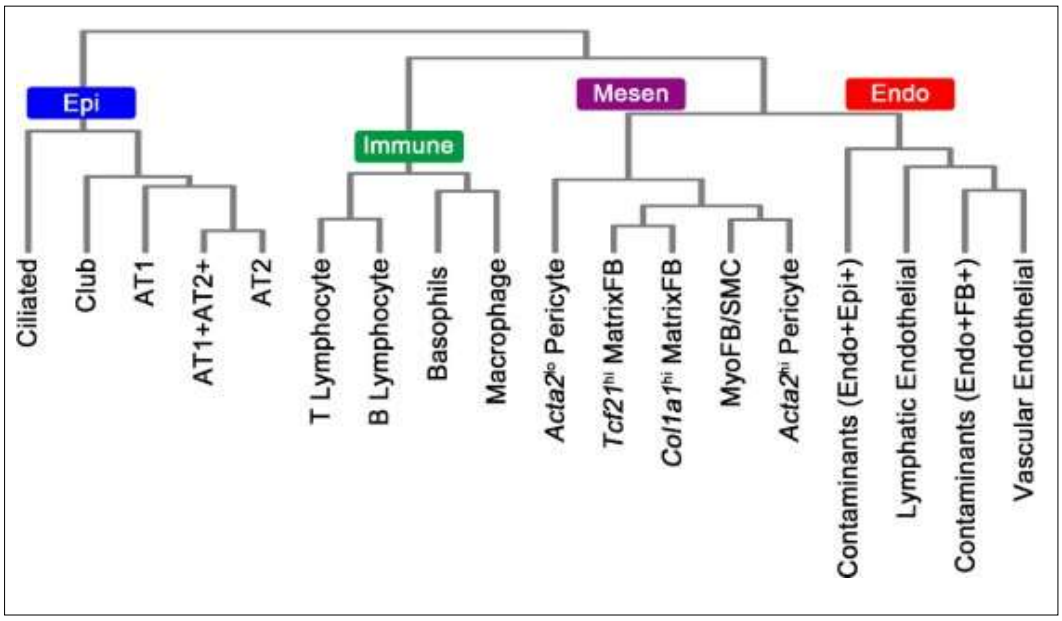

Figure 1.7 Hierarchical clustering for major lung cell types predicted from the RNA-sequencing data, from Whitsett and collaborator analysis from whole mouse lung. Endo, endothelial cells; Mesen, mesenchymal cells; Epi, epithelial cells; Immune, immune cells; FB, fibroblast cells; AT1, alveolar type 1 cells; AT2, alveolar type 2 cells; MyoFB, myofibroblast cells; SMC, smooth muscle cells; MatrixFB, matrix fibroblast cells. (From Whitsett, Kalin, Xu, & Kalinichenko, 2018).

Proximal airways are generally referred as conducting airways. Their main role is to conduct air in the direction of transition bronchioles and alveoli, generating O_2 and CO_2 gradients (Hsia et al., 2016). Conducting airways are composed of cartilaginous cells (trachea and bronchi) and a mixture of basal epithelia cells, comprising ciliated, goblet, club, and immune cells. In adults, basal cells serve as a pool for epithelial cells, however in distal airways basal cells differs from proximal ones in morphology, molecular signature, and molecular function (Whitsett et al., 2018). Lung basal cells possess secretory activity fundamental for host protection and for production of surfactant molecules involved in gas exchange. The basal cell proliferation state depends on interaction with mesenchymal cells through production of growth factors (TGF-ß and IL-1). Ciliated, club and goblet cells possess a high secretory activity and participate in innate immunity (Schittny, 2017). Brush cells compose a first barrier in lung apex. Club, goblet, and brush cells are activated in response to intoxicant, and represent the first host defence against pathogens, whereas ciliated cells remove the debris. Club and brush cells produce lactoferrin and defensin, while goblet cells mucins MUC5A and MUC5B. Club cells produce surfactant protein A and B, but not C, involved in the surface tension that allows gas exchange (fig. 1.8). Other cells composing this track are

neuroendocrine cells, which are as “gas sensors” (Whitsett et al., 2018).

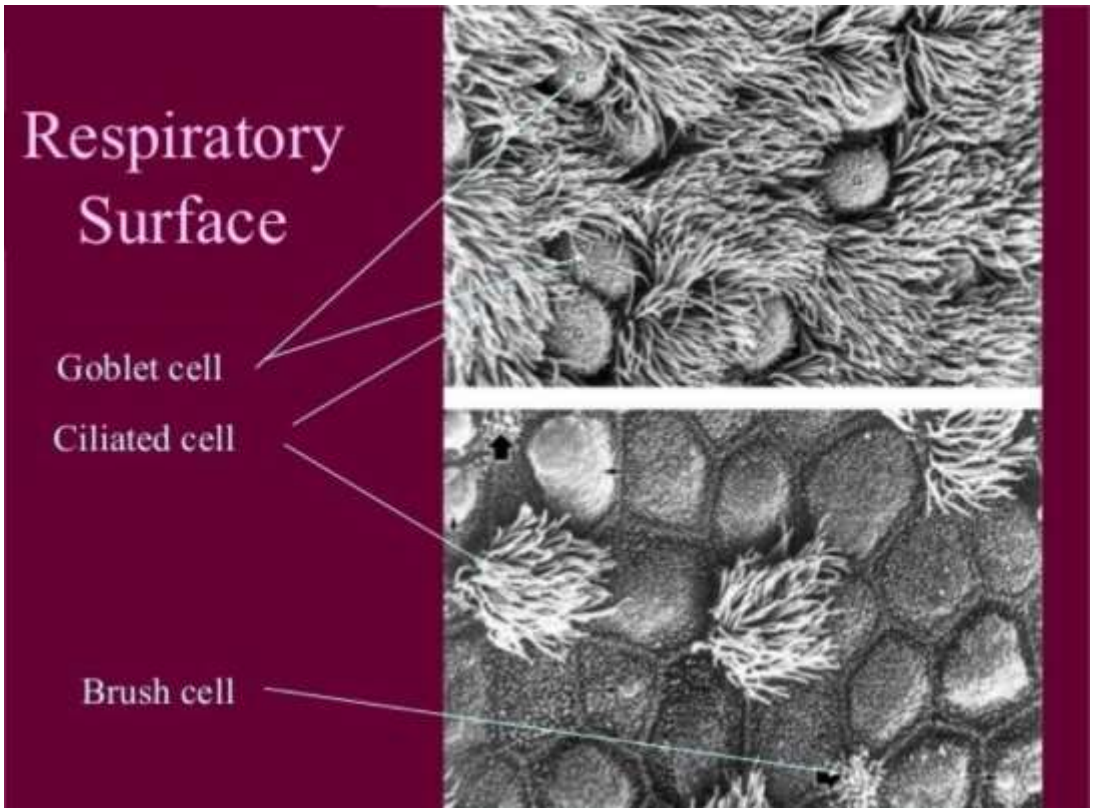

Figure 1.8 Electron microscopy image of proximal conductive airways. Image are identified as Goblet cells indicated by G; Ciliated cells can be identified by flagellum structures. Brush cells are identified by black arrows in the lower image. [Image from google image).

The distal airway, as mentioned above, composes the gas exchange unit and relative branches. Gas exchange is achieved through the diffusion of O_2 and CO_2 between the alveolar wall and lung microcirculation. A dense capillary network connected to terminal branches is the prolongation of pulmonary arteries and veins. This brings arterial walls and capillaries, separated by septa, in proximity favouring gas exchange. To optimize gas exchanges between epithelia, the contact surface is spread out over the surface. Capillaries and alveolar walls are in close contact, to maximize the volume of air, by contrast conductive airways minimize dead space and flow resistance, allowing air flow into the alveoli (fig.1.9).

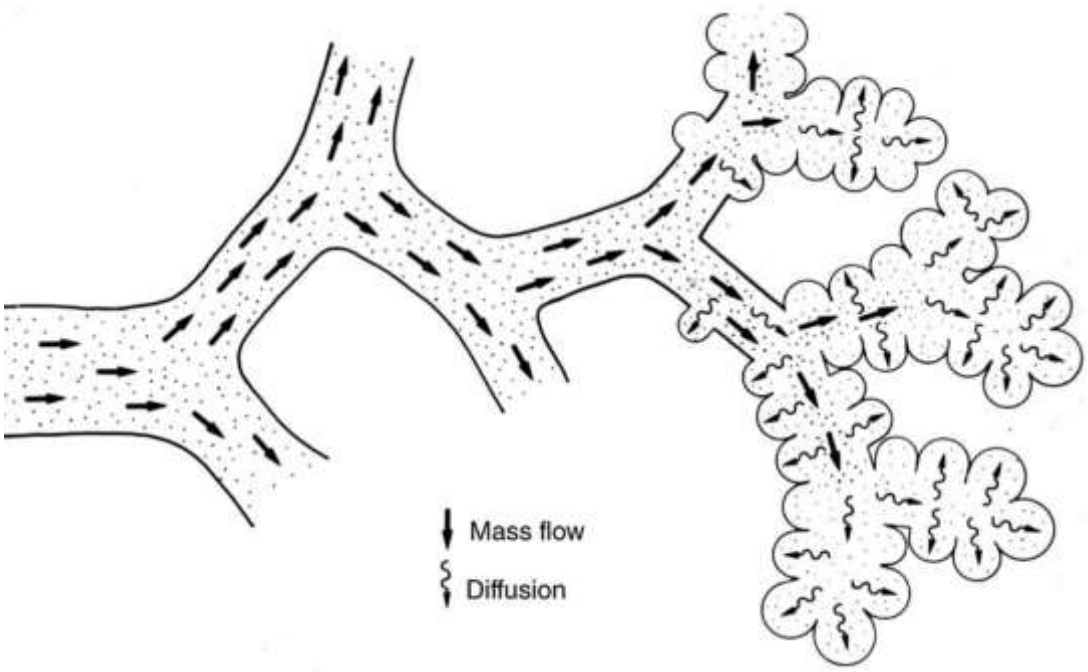

Figure 1.9 Proximal airway allows the mass flow of air in the conductive airways, while alveolar structures allow the gas exchange through a diffusion mechanism. Therefore, conductive airway generates a flow, which allows diffusion of gasses due to irregular structure of distal airways (from transitional bronchiole to alveoli)(from Hsia et al., 2016).

Moreover, capillaries are smaller and denser than alveoli, which are also not homogenous between them (Hsia et al., 2016). Alveolar epithelium is a mosaic of alveolar type-I and II epithelial cells and originate from the same squamous alveolar epithelial precursor cell. Those cells originated once the structure of bronchoalveolar duct is formed, through myofibroblast ECM deposition. Interestingly, the alveolar epithelia progenitor originates from the foregut (endoderm) and are already present during conductive airway budding. However, only in the canalicular and saccular phase do they start to differentiate into mature alveolar epithelia (Whitsett et al., 2018). After branching morphogenesis, these cells accelerate their proliferation, colonizing the scaffold built by myofibroblasts. In the adult lung, alveolar epithelial type-II cells originate during cannulation are able to differentiate into alveolar type-I cells (Schittny, 2017). Alveolar epithelia type-II cells are in a lower abundance and cover less than the 5% of the entire alveolar parenchyma, where they produce and recycle lipids to obtain surfactant proteins (Hsia et al., 2016). Surfactant proteins are produced in the canicular phase and released in the airways in order to promote increase in gas tension and promote gas exchange (Whitsett et al., 2018). Alveolar epithelia type-I cells cover more than

95% of the total alveolar parenchyma and appear as an unaligned leaflet, which extends over capillaries surface, where they promote O_2 diffusion. Alveolar epithelial cells are separated by a thin interstitium from endothelial cells, where the gas exchange takes place (fig. 1.10) (Hsia et al., 2016). Lung mesenchymal cells generate the alveolar scaffold in the saccular- alveolar phase, while they are involved in wound healing repair in adult life. Mesenchymal cells are associated with both the alveolar epithelium and endothelium of the capillaries (fig. 1.10) (Whitsett et al., 2018). Lung fibroblasts include lipofibroblasts, myofibroblasts and matrix fibroblasts. Lipofibroblasts participate in lung fibre organization and contribute to surfactant protein synthesis (McGowan & Torday, 1997). Myofibroblasts are associated with the alveolar interstitium, where they are orientated in the direction in which the alveolar walls contract, and they express α-smooth actin although they are different from smooth muscle cells. Matrix-fibroblasts produce ECM during alveorization and in wound healing repair (Whitsett et al., 2018).

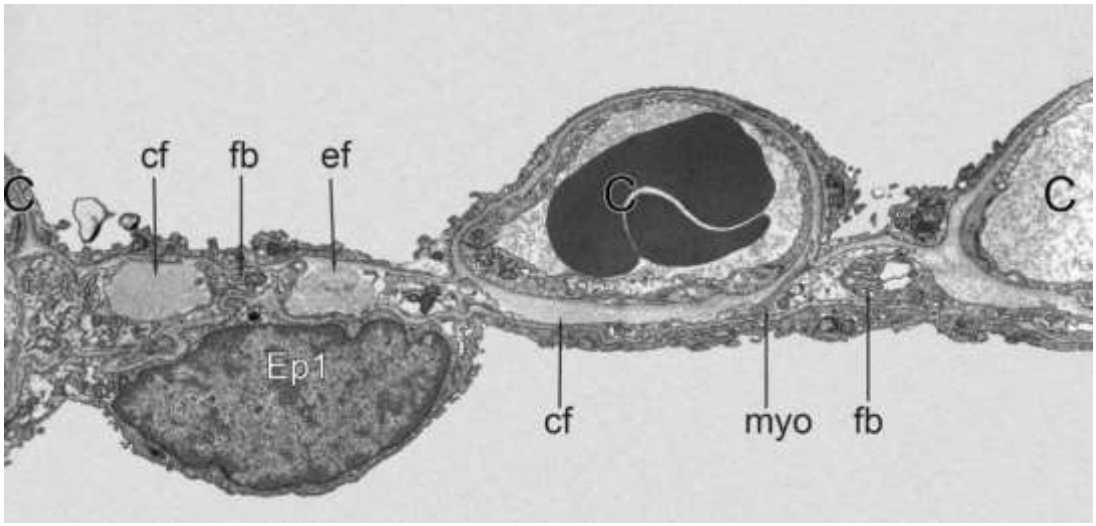

Figure 1.10 Electron micrographs of alveolar human lung showing capillaries (C), type-1 alveolar epithelium (Ep1) and elements of the interstitium such as collagen (cf) and elastic (ef) fibres and fibroblast (fb) that focally can form myofibrils (myo) and serve as myofibroblasts bracing the interstitial space. (From Hsia et al., 2016).

Lung function is maintained during each air cycle thanks to a tree-like structure composed of a network of fibres and filament. This structure allows influx and efflux of air and to overcome mechanical stretch induced by ventilation, where ventilation is the movement of fresh bloom of air (Béla Suki et al., 2011). Conductive airways increase air flow velocity as the cross-section area decreases following proximal direction. Once airflow reaches alveoli the uneven alveolar geometry induces an increase in cross-section area and a decrease in flow velocity (fig. 1.9) (Hsia et al., 2016). Therefore, the new air will diffuse only after energy dissipation. For these reasons, lung architecture is defined as a tensegrity structure, where stiffer fibres (in conductive airway) support and propagate the mechanical stretch without structural collapse (Béla Suki et al., 2011). Tensegrity is a building principle where structures that stabilize the shape of a system are in continuous tension or “tensional integrity” rather than constant compression (fig.1.11) (Ingber, 2003).

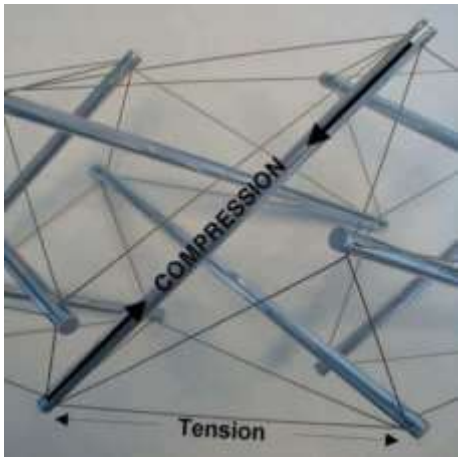

Figure 1.11 Example of Tensegrity represented by Snelson sculpture, where the tensegrity force balance is based on local compression and continuous tension (From Ingber, 2003).

This system can resemble the lung connective component, although a certain amount of compression is exerted by respiratory muscles on the pleura (Hsia et al., 2016; Béla Suki et al., 2011). The architectural structure of mammalian lungs undergoes a number of volume pressure modifications induced by respiratory cycles. Connective tissue elastic properties guarantee volumetric variation in lung expansion and recoil. Lung architecture is composed of an integral connective tissue continuum that expand from conductive airways into alveolar, which spans the entire lung until the pleura (Hsia et al., 2016). Moreover, this scaffold connects and separates (as septa) airway epithelium from vascular endothelium. This flexible connective tissue presents a hierarchical composition formed by 1) axial fibres that connect bronchi and bronchioles continues into the alveolar ducts 2) peripheral fibres from the pleura to lung parenchyma 3) septa fibres from the intra-alveolar space to capillaries, this latter point of connection with axial and peripherical fibres (fig. 1.12) (Hsia et al., 2016).

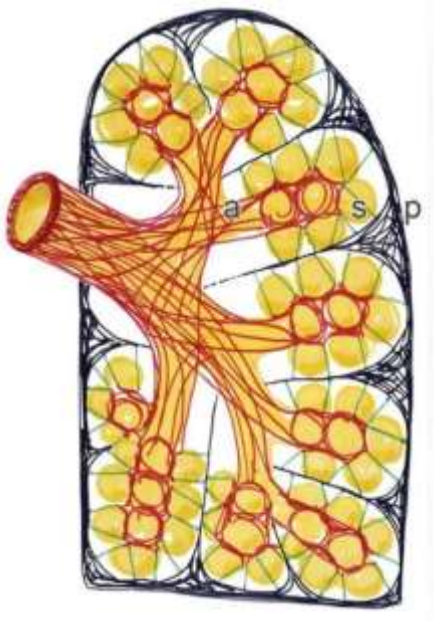

Figure 1.12 Schematic cartoon representation of lung fibres architecture. Axial fibres are coloured in red and indicated by a. Axial fibres represent ECM that goes from bronchi to alveoli. Peripheral fibres are coloured in black and indicated by p. They connect lung edge to the pleura and are also attached to fibres that compose alveolar-capillary interface, which is represented by septa fibres coloured in green and indicated by letter s (From Hsia et al., 2016).

This structure allows chest and diaphragm movement to be propagated through fibres onto cells composing the alveolar and capillaries tissue. This transmission of stretch pulls fibres extending the contact surface between alveoli and capillaries also determining gas diffusion. The connective tissue associated with lung is composed by cells and ECM including water and biological macromolecules. Pulmonary ECM is organized into two main structural types; basement membranes (covers basal side of epithelial and endothelial cells) and interstitial matrix. Basal membrane and interstitial matrix together form tissue-specific niches, fundamental sources of stem cells (Burgstaller et al., 2017). Interstitial matrix forms lung scaffolding fibres, which compose the connective tissue mentioned above. The major ECM components that make up lung structure are collagen, elastin, and proteoglycans. Each ECM component has a different structural role in response to lung deformation, resulting in differences in mechanobiological properties. In addition, ECM contains secreted proteins, such as growth factors, ECM-modifying enzymes and other ECM-associated proteins which do not contribute to the structure of ECM, but affect its function (Burgstaller et al., 2017).

Collagen is the most abundant and rigid protein present in the lung, and it is considered a determinant factor in lung mechanobiology. Collagen type-I, III and IV constitute around the 15% of total lung dry weight and are the major protein group (Laurent, 1986). Type-I and III

form fibres that support the entire lung parenchyma, where collagen fibres are the most abundant component (fig. 1.7). They extend from a central axial fibre network down to peripherical alveoli, passing through bronchoalveolar ducts, which also extend from the visceral pleura and a parenchymal interstitium that connects the two (Hsia et al., 2016). From a biomechanics point of view, collagen fibres are structural filaments that influence the non-linear elastic behaviour of the lung, expressed as lung hysteresis in cyclic breathing. More detailed information on collagen fibres and the role of collagen type-I and III in lung fibrosis are discussed in 1.3.1. Collagen type IV is less abundant and forms a sheet layer as part of the epithelial basement membrane (Béla Suki et al., 2011). Collagen type-IV forms a network in which four molecules are assembled forming tetramers, however its role in conferring stability to lung deformation is poorly studied (Ricard-Blum, 2011).

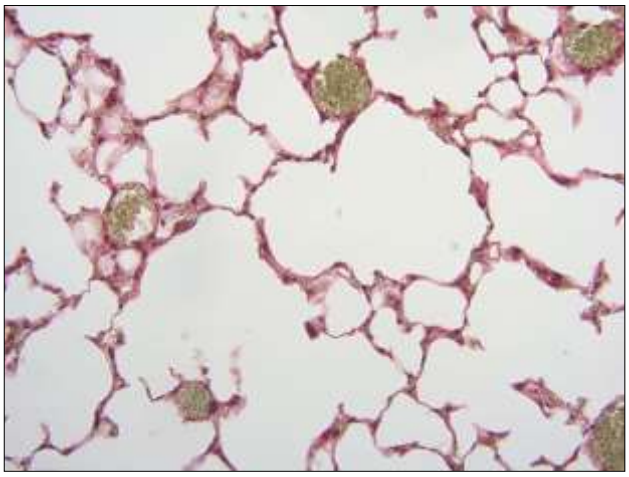

Figure 1.13 mouse lung stained for collagen fibres indicated by the red colour due to the staining with Sirius Red, which stains collagen fibres. From the picture it is possible to appreciate hexagonal like structure representing alveoli. A major blood vessel can be discriminated by an increased stain for Sirius Red and by the presence of red blood cells, in which appear as green-yellow in this stain.

Elastin provides elasticity to the lung scaffold and is synthetized as tropo- elastin by mesenchymal and endothelial cells. Elastin molecules in combination with other ECM proteins (fibulins fibrillin and glycoproteins) form microfibrils in a self- assembling mechanism. In addition, separated elastin molecules cross-link through hydrophobic bonds forming fibres of elastin (Béla Suki et al., 2011). In alveolar walls, those fibres overlap and bind collagen fibres via RGD-motifs (Burgstaller et al., 2017). This matrix composition allows a proper hysterical deformation of lung parenchyma, allowing the serial alveolar opening during gas exchange.

However, elastic fibres are less important than collagen fibres in properly maintaining lung structure.

Proteoglycans (PGs) or Glycosaminoglycans (GAGs) are the second most abundant ECM component in the lung. PGs and GAGs possess a protein core connected to long chains of repeated disaccharide units soluble in water and therefore charged. PGs and GAGs dissolved in water become the ground substance, which embedded the connective tissue (Béla Suki et al., 2011). The main role of PGs and GAGs is to sequester water that might change secondary and tertiary collagen structure. In the expiratory phase surfactant molecules together with PGs and GAGs avoids the alveolar collapsing through trapping a residual volume of air in the lung (Béla Suki et al., 2011).

1.4. Genes

The following subparagraphs provide detailed information regarding genes studied in this experimental thesis on microRNAs and lung fibrosis. In the experimental sections fibrillar collagens, CCN2/CTGF, Snail family associated with EMT, and inhibitory Smad; have been studied as they represent key markers for fibrosis and EMT.

1.4.1. Collagens

Collagens are the most abundant proteins in mammals, and they comprise 28 isotypes (Tab. 1.1), numbered with Roman numerals numbers in vertebrates. Each collagen has a different role and abundance in each body compartment. They are formed by triple α-chain helix structure folded in a rope-like shape.

Table 1.1 Collagens type (From Ricard-Blum, 2011).

Collagen type	α Chains	Molecular species
Collagen I	α1(I), α2(I)	$[\alpha1(I)]_2$, α2(I) $[\alpha1(I)]_3$
Collagen II	α1(II)	$[\alpha1(II)]_3$
Collagen III	α1(III)	$[\alpha1(III)]_3$
Collagen IV	α1(IV), α2(IV), α3(IV), α4(IV), α5(IV), α6(IV)	$[\alpha1(IV)]_2$, α2(IV) α3(IV), α4(IV), α5(IV) $[\alpha5(IV)]_2$, α6(IV)
Collagen V	α1(V), α2(V), α3(V), α4(V)[a]	$[\alpha1(V)]_2$, α2(V) $[\alpha1(V)]_3$ $[\alpha1(V)]_2\alpha4(V)$ α1(XI)α1(V)α3(XI)
Collagen VI	α1(VI), α2(VI), α3(VI), α4(VI)[b], α5(VI)[c], α6(V)	
Collagen VII	α1(VII)	$[\alpha1(VII)]_3$
Collagen VIII	α1(VIII)	$[\alpha1(VIII)]_2$, α2(VIII) α1(VIII), $[\alpha2(VIII)]_2$ $[\alpha1(VIII)]_3$ $[\alpha2(VIII)]_3$
Collagen IX[e]	α1(IX), α2(IX), α3(IX)	[α1(IX), α2(IX), α3(IX)]
Collagen X	α1(X)	$[\alpha1(X)]_3$
Collagen XI	α1(XI), α2(XI), α3(XI)[d]	α1(XI)α2(XI)α3(XI)
Collagen XII[e]	α1(XII)	$[\alpha1(XII)]_3$
Collagen XIII	α1(XIII)	$[\alpha1(XIII)]_3$
Collagen XIV[e]	α1(XIV)	$[\alpha1(XIV)]_3$
Collagen XV	α1(XV)	$[\alpha1(XV)]_3$
Collagen XVI[e]	α1(XVI)	$[\alpha1(XVI)]_3$
Collagen XVII	α1(XVII)	$[\alpha1(XVII)]_3$
Collagen XVIII	α1(XVIII)	$[\alpha1(XVIII)]_3$
Collagen XIX[e]	α1(XIX)	$[\alpha1(XIX)]_3$
Collagen XX[e]	α1(XX)	$[\alpha1(XX)]_3$
Collagen XXI[e]	α1(XXI)	$[\alpha1(XXI)]_3$
Collagen XXII[e]	α1(XXII)	$[\alpha1(XXII)]_3$
Collagen XXIII	α1(XXIII)	$[\alpha1(XXIII)]_3$
Collagen XXIV	α1(XXIV)	$[\alpha1(XXIV)]_3$
Collagen XXV	α1(XXV)	$[\alpha1(XXV)]_3$
Collagen XXVI	α1(XXVI)	$[\alpha1(XXVI)]_3$
Collagen XXVII	α1(XXVII)	$[\alpha1(XXVII)]_3$
Collagen XXVIII	α1(XXVIII)	$[\alpha1(XXVIII)]_3$

Individual α chains, molecular species, and supramolecular assemblies of collagen types.
[a]The α4(V) chain is solely synthesized by Schwann cells.
[b]The α4(VI) chain does not exist in humans.
[c]The α5(VI) has been designated as α1(XXIX).
[d]The α3(XI) chain has the same sequence as the α1(II) chain but differs in its posttranslational processing and cross-linking.
[e]FACIT, Fibril-Associated Collagens with Interrupted Triple helices.

The length of the Amino acid chains varies in number from 622 to 3152 amino acids acid per α-chain between the different collagens. Although each collagen has a unique α-chain amino acid sequence, there are similarities in the amino-acid sequence with characteristic Gly-X-Y repeats, where X and Y are either proline, alanine or hydroxyproline. Collagens can be subdivided in into subfamilies based on their super-molecular assemblies: fibrils, beaded filaments, anchoring fibrils, and networks (Ricard-Blum, 2011). Fibrillar collagen have a dedicated paragraph in this thesis, because of their importance in fibrosis (see below). Fibrillar associated collagens do not form fibres, but they are covalently bound to the fibres. Beaded filaments, between different epithelial layers composed mostly of collagen type VI, it is thought that they can interact with basal membranes and as well to fibrillar collagens. Network collagens possess a peculiar structure due to the lack in glycine, as composed by collagen type IV, which accounts for different mechanical properties. They form network structure through N-C terminal binding.

1.4.1.1. Fibrillar Collagens

Fibrillar collagens account for the structural environment and hold a key role in lung mechanics and fibrosis. They are formed by one major triple-helix structure folded in a zipper-like fashion. The presence of hydroxyproline in the α- chain of both collagen type-I and type-III is fundamental for the formation of the fibrils. At the super molecular level, rigidity is achieved as in the procollagen molecule (the pro-peptide) the hydroxyproline-lysine of single α-chains forms a so called “rope-shape” structure able to resist to mechanical force, thus assembling fibres. The lack of hydroxyproline, in both inter and intra molecules binding, accounts for the elastic capability, that allow the stretch of the fibres without the disruption of the rod-like super molecular structure (Béla Suki et al., 2011). As example, collagen type I is longer and more united in the structure than collagen IV, that contains fewer hydroxyproline binding sites. Therefore, Collagen type-I can assemble more rigid fibres through triple α-chain helix link together by covalent bounds, which would need then a higher amount of energy to be broken compared to Collagen type-IV (Shoulders & Raines, 2009).

Fibrils are assembled as a quasi-hexagonal rod-like structure. This structure is at the basis of the mechanical properties of this subfamily. Of particular interest is the lysine-hydroxyproline-lysin bonds between different triple helix that maintains collagen structure

integrity (Orgel, Irving, Miller, & Wess, 2006). Collagen type I and III provide the structural component of many body compartments, including bone and muscle, providing physical support against mechanical forces.

The organisation and tensile properties of the collagen fibres in the lung allows mechanical forces to propagate from the diaphragm and chest muscles through the major airways, and into the alveoli, without triggering a collapse of the organ.

Lung deformation or mechanical stretch strongly influence fibrillar collagen and it has been proposed that lung elastic properties are the result of a balance between collagen strength and elasticity.

Collagen molecules are crosslinked through the Milliard reaction, where a sugar group interacts with an amine giving rise to a covalent bond. This cross linking prevents degradation of collagen type I by metalloproteinases and it is at the basis of increased collagen during ageing, although lung epithelial cells seem to downregulate Col1a1 gene expression during ageing. Other fundamental crosslink reactions are disulphide bonds and glycation reduction of crosslinks and N-ε (γ-glutamyl) lysine iso-peptide, this latter catalysed by transglutaminase-2. Inhibitors of transglutaminase-2 are currently in currently in phase II clinical trials in kidney fibrosis, and if effective could also be used in pulmonary fibrosis (Johnson et al., 2007). The level of collagen crosslinking is tissue-specific, with the musculoskeletal system showing higher rates of crosslinking in comparison with the respiratory or cardiovascular systems (Ricard-Blum, 2011).

Each collagen α-chain is composed of a N- terminal, a repeated helix and C- terminal domains. The N-terminal contains a signal sequence and a globular sequence present as well in the C-terminal, rich in Cys, which allow collagens to form Cys-Cys disulphide bridge. The level of N-terminal divergence is in the number of exons present in this domain; it is thought to be at the basis of collagens diameter size. Cleaved N-terminal is also considered to hold a paracrine effect on collagens expression level. C-terminal also contains a globular site fundamental for intra and inter-binding interaction between different α-chain of procollagen. Both the N- and C- terminal domains are removed from the procollagen peptide, once secreted into the extracellular space. This allows multiple molecules of procollagen to bind together forming a fibre.

The α-chain of fibrillar collagens is synthesized as precursor pro α-chain, after posttranslational modifications, three pro α-chain molecules form a procollagen structure. Procollagen is synthetized in ER as pro-peptide. α-chain peptides are bound together through lysin-hydroxyproline, disulphide bridges. N- and C- terminal proteolytic cleavage through metalloproteinases (MMPs) allows the binding of pro-collagen molecules. The majority of post-translational modifications in procollagen take place in the Golgi. Hydroxylation, disulphide bridge creation and glycosylation are fundamental steps for procollagen correct folding that take place in both ER and Golgi. Of note is the pH sensitive transportation from ER to Golgi, which involves the heat shock protein 47 (HSP47). This chaperone is able to guide only correctly folded α-chains. Depletion of HSP47 in knock out mice lead to retarded body development (fig. 1.14) (Ishida & Nagata, 2011).

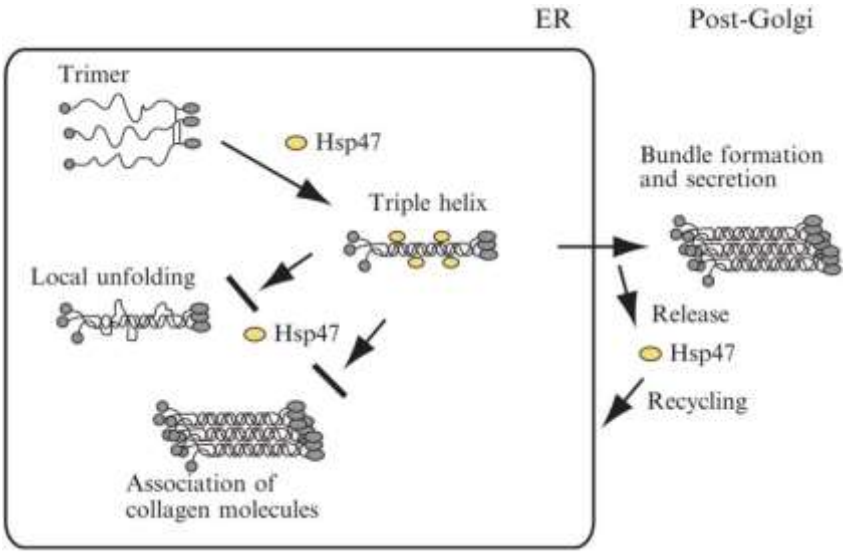

Figure 1.14 Collagen undergoes a number of post-transcriptional modification. HSP47 actively participates in the transportation of collagen molecules assembled correctly (From Ishida & Nagata, 2011).

Collagens are highly conserved between species, even in non-vertebrate organisms such as sea urchins (Niederreither et al., 1995). Loss of function of collagen type I or III leads to severe disorders such as Osteogenesis Imperfecta (IO) and the Ehler-Danlos syndrome (EDS). Interestingly, in EDS the low amount of collagen can lead to pneumothorax (collapse of a lung). Mutations in Collagen type-I have been referred to as “procollagen suicide”, as the lack in fibrillogenesis is associated with a body weakness (in particular in bones) not compatible with a long survival. Col1a1 transgenic models generated by exon depletion in one allele only

lead to bone weakness, body shortening and a high rate of premature death (Pereira, Khillan, Helminen, Hume, & Prockop, 1993).

Collagen can be seen as structured scaffold that maintains tissues integrity; however, collagens have roles beyond structural support as well. Collagens in the ECM play important roles in both ECM-ECM and cell-ECM cross-talk. In 1966 Hauschka and Königsberg demonstrated that a collagen substrate induces chicken embryo fibroblasts to differentiate into myofibroblasts. Fibrillar collagen interacts also with other components of ECM such as fibronectin (Hauschka & Konigsberg, 1966). Interestingly, fibronectin can bind different collagens overlapping and competing with metallo-proteinase-2 for the same binding site rendering the collagens resistant to several proteases (Steffensen, Xu, Martin, & Zardeneta, 2002). This latter fact may be crucial in early stages of fibrosis when expression of fibronectin is increased. Collagens contain RGD motifs which allow interaction with cells *via* binding to integrins (Burgstaller et al., 2017).

More than 15% of lung wet weight is composed of collagen fibres, mostly collagen type-I and III. In lungs, collagen fibres are arranged to form single fibres around alveoli and/or as networks of the single fibres (Béla Suki et al., 2011). The lung is one of the most perfused organs, as it is the centre of the gas exchange and oxygen delivery. The blood vessels are formed by different layers composed mostly of collagen I and III, that give the strength and elasticity fundamental for blood to flow. Differences in collagen content reflects lung physiology, where alveoli contain more collagen type-III than bronchioles, leading to reduced rigidity.

1.4.1.1.1. Collagen Type I

Collagen type-I is the most abundant collagen type, expressed in almost all connective tissues and it is the major component in bone, skin, tendon and blood vessels. Type-I collagen accounts around ~80% of the total protein present in bone and it is the most abundant protein in vertebrates (Henriksen & Karsdal, 2016). Collagen type-I can be found as homo or hetero-trimer composed of either two α1 and one α2 chains (2:1), or as homotrimer of three α1 chains. The α1 chain is encoded by COL1A1 and α2 chain by COL1A2 in human, and in mice by Col1a1 and Col1a2. Although there is no clear correlation between homotrimer formation and pathological phenotypes, the presence of COL1A1 homodimers has been associated with tumours and fibrotic lesions (Makareeva & Leikin, 2014).

The COL1A1 gene is located on the long arm of chromosome 17 in humans, and on the long arm of chromosome 11 in mice. This gene consists of 51 exons and it has 13 isoforms in humans and 4 in mice, all due to alternative splicing. The length of the Col1A1 gene is ~18kbp in both humans and mice (ENSG00000108821).

COL1A2 encoding for the type-I collagen α2 chain is located on the long arm of chromosome 7 in humans, and on the long arm of chromosome 6 in mice. The Col1a2 gene has a length of ~36 kbps and is organised in 52 exons. It has 13 isoforms in humans and 8 in mice (ENSG00000164692).

Like for collagen type-III, both α chains of Collagen type-I are highly conserved between species and contains repeated sequences as LINE-1 Alu in its genomic sequence. During maturation, the collagen type-I protein undergoes several post-translational modification, such as hydroxylation of Proline and Lysin residues that allow the correct folding of the pro-peptide. Glycosylation and other post- translational modifications proceed simultaneously with the synthesis in the ER (Engel & Bächinger, 2005). Folding of the collagen type-I triple helix is guided by chaperones prevent formation of an unfolded structure. Any unfolded triple helixes are degraded in lysosomes through a chaperone-dependent mechanism. For collagen type-I the most important chaperone is HSP47, which delivers the unfolded α chains into autophago-lysosomes (Makareeva & Leikin, 2014).

Collagen type-I is secreted a as pro-peptide, followed by proteolytic cleavage to remove the N- and C- terminal domains from the pro-peptide, necessary for a correct fibrillogenesis. Alteration in Collagen type-I secretion can be also a result of polymorphism in promoter

sequences, that have been observed in osteoporosis.

During foetal development Col1a1 and Col1a2 are highly expressed in the lung. Up-regulation in COL1A1 and COL1A2 synthesis during the post-foetal period allows correct development of the lung. Tissue damage as well as pathological conditions like fibrosis led to a collagen type-I upregulation. In those pathological conditions ECM reorganization triggers increase in organ stiffness. Physiologically, collagen type-I, as mentioned above, is expressed in lung in response to damages, as it is a key protein for wound healing repair. Dysregulation in wound healing repair due to repeated damage are able to trigger fibrotic lesion.

Type-I collagen, in particular the α1 chain, is involved in a number of pathway related to cascade coagulation, mitogenesis, inflammation and cell differentiation. *In vitro* studies have demonstrated that TGF-ß modulates type-I collagen expression in a dose dependent manner. Concentrations higher than 10 ng/mL trigger a downregulation in Col1a1 expression, in a mechanism involving CUX-1, a DNA binding protein (Fragiadaki et al., 2011). Collage type-I activates a number of intracellular signalling pathways through cell surface receptors such as integrins and tyrosine kinase receptors.

Ageing is a natural mechanism that impacts type-I collagen metabolism, and ageing has been correlated with increased collagen abundance (Kühn, 1987). However, studies on Col1a1/Col1a2 demonstrated instead a reduction in collagen synthesis in aged samples (Guilbert et al., 2016). This apparent increase in collagen fibre content is due to increased fibre crosslinking during ageing. Collagen crosslinks make fibres impervious to degradation by MMPs, leading to an increase in collagen protein content (Miller, 2010). Increased collagen crosslinking is also thought to be at the basis of the higher incidence of pulmonary fibrosis in the elderly population (Burgstaller et al., 2017).

Interestingly, collagen type-I crosslinking is a result not only of hydroxylation but also of Glycosylation, which is thought to contribute even more to collagen insolubility. Glycation end products (AGEs) are considered at the basis of fibrotic lesion development and ageing (Henriksen & Karsdal, 2016). AGEs can activate the Smad3 pathway, even without TGF-ß receptor activation, through a p38 activation (Lan, 2008).

Collagen type-I makes up more than 10-15% of the entire lung structure and it can be found in all pulmonary substructures (from the bronchioles to the alveoli). Assembled in fibres together with collagen type-III it provides ECM rigidity to the lung. Moreover, type-I collagen is considered as monomers or brick that constitutes collagen fibres, as it is highly represented.

Interestingly, Collagen type-I as monomer holds different mechanical properties than collagen type-I in fibres, underlaying physiological differences in the supra-molecular structure. Recent advances in Atom Force Microscopy (AFM) have highlighted that type-I collagen as single molecules possess a higher resistance to tensile stretch compared to a fibrillar collagen. The reason lay in the non-covalent bounds on the fibrillar collagen (0.5 GPa of force to be broken), whereas a single molecule of type-I collagen to be broken need a higher force to "unwrap" a secondary structure as it contains more covalent bounds (11 GPa) (Shoulders & Raines, 2009). This molecular organization is at the basis of energy dissipation during breathing. Moreover, it is thought that they can control contractile movement or organ and also cells *via* binding specific receptors as dimeric discoidin receptors DDR1 and DDR2, which possess an active tyrosine kinase activity (Ricard-Blum, 2011).

1.4.1.1.2. Collagen Type III

Collagen type-III was first identified by Miller et al in 1971 and it constitutes between 5-20% of all collagen in mammals.

Collagen type-III is a homotrimer formed of three collagen type-III α-chains encoded by the COL3A1 gene, in humans located on the long arm of the chromosome 2. Collagen type-III is highly conserved among species, in particular in mouse and dog. The 38kbp gene in both human and mice contains 51 exons, with an amino acid sequence composed of Gly-X-Y repeats similar to all other fibrillar collagens and fundamental for super molecular structure and crosslink formation (see above). Alternative splicing mechanisms or use of alternative promoters, leads to 6 transcript variants in human and 7 in the mouse (ENSG00000168542).

Collagen type-III is synthetized as pre-peptides, which undergo post- translational modification, between ER and *cis*-Golgi. Triple helix formation is obtained through disulphide and hydroxyproline-lysine bonds of three identical α- chains. The pro-peptide is secreted as tropocollagen, containing a globular N- and C- terminal, which are further cleaved, allowing the formation of fibrillar structures (see above).

Collagen type-III is highly expressed in hollow organs and in developmental organs as placenta and endometrium and it is one of the most important components of blood vessels. We found high levels of Col3a1 expression in lung fibroblasts isolated from C57BL/J mice.

Collagen type-III, as mentioned above, plays a key role in tensile stress and it is the

second major component of collagen fibres. Fibrillar collagen, as mentioned above, possess the ability to form covalent bond that crosslinking together different collagens, giving rise to fibres. A collagen fibre is composed mostly of collagen type-I (around 85%) which is considered as the “brick-module” of fibres, whereas collagen type-III accounts for 10-15%. Collagen type-III is localised in the peripheral part of the fibres suggesting a more regulative role. Thus, collagen type-III presence confers a variability to the supra-molecular structure, regulating fibril diameter and also interactions between fibrils and other ECM components. The peripherical localization is considered to influence fibre formation during the wrapping of the fibre (Fleischmajer, Douglas MacDonald, Perlish, Burgeson, & Fisher, 1990).

Collagen type-III displays a high overlapping with collagen type-I expression, although the molecular mechanism underlying this is not clear (Niederreither et al., 1995).

TGF-ß, Wnt/ß-catenin, p38 mitogen-activated protein kinase (MAPK) and hypoxia-inducible factor 1a (HIF-1a) generally activate collagen type-III expression. However, Col3a1 expression can be influenced by ageing, cell origin, and concentration of Col3a1-inducing cytokines, resulting in differential and complex regulation. As example, HIF-1a leads to Col3a1 expression decrease in chondrocytes, whereas it increases Col3a1 expression in primary endothelial rat fibroblasts (Kuivaniemi & Tromp, 2019). The only clear mechanism able to induce Col3a1 expression is through the neural precursor cell expressed (NEDD9), which has been demonstrated to regulate vascular remodelling and pulmonary hypertension (Haley et al., 2018).

Accumulation of collagen type-III is strongly involved in several fibrosis mechanisms, but also accounts to systemic sclerosis and liver cirrhosis. The role of Col3a1 in pulmonary fibrosis is not entirely clear, as in lungs, type-III collagen accounts for the elasticity of the fibres. Moreover, Col3a1 reduces stiffness, and biopsies from patients affected by IPF showed a reduction in production of type-III collagen (Seyer, Hutcheson, & Kang, 1976; D. Tschumperlin, Boudreault, & Liu, 2011). In 1997 Liu and collaborators, discovered that Col3a1 knock out mice showed a dysregulated fibrillogenesis, where the triple helix of collagen type-III was replaced by collagen type-I, resulting in an increase in rigidity of collagen fibres, lacking in Col3a1. This latter highlights the possibility of an anti-stiffness, and therefore anti-fibrotic role of Col3a1. Therefore, the balance between collagen type-I and type-III may be very important in the severity of the effects of the pulmonary fibrosis.

1.4.2. Connective Tissue growth factor (CCN2/CTGF)

Connective Tissue growth factor or CCN2 (CTGF was changed to CCN2 in 2015 by the HUGO Gene Nomenclature Committee HGNC) is a protein discovered in 1991 and originally named “fibroblast-inducible secreted protein-12”. CCN2 is a member of the CCN family of proteins, that comprises six subgroups with similar structural and mitogenic characteristics. Historically, CCN2 was discovered as a matricellular protein associated with organ fibrosis and angiogenesis. (Gonzalez & Brandan, 2019). The CCN2 gene is located on the long arm of chromosome 6 in humans, and on the long harm of chromosome 10 in mice. The human encodes a single 349 amino acid protein. Mouse *Ccn2* expresses three mRNA splice variants; two of 23 kbps and one of 34 bps, which encode for a 348, 293 and 80 amino acid proteins respectively (ENST00000367976).

CCN2 is composed of an insulin-like growth factor -binding domain (IGF-BP), a von Willebrand domain (VWC), a thrombospodin-1 domain (TSP) (similar to non- fibrillar collagens) and cysteine knot domain. The IGF-BP domain possesses only structural similarity as it has very low affinity for insulin. The VWC domain is fundamental for interaction with αvß3/ß5 integrins (present on mesenchymal cells) and with growth factors such as TGF-ß and bone morphogenic proteins (BMPs). The TSP domain is fundamental for interaction with ECM, MMPs, VEGF and LRP1. The C- terminal contains the Cys knot domain, homologous to a number of growth factors, which mediates interaction with elastic ECM components (Takigawa, 2018).

To address the role of CCN2 *in vivo* different transgenic mice have been developed, either with overexpression or deletion of CCN2. A transgenic mouse model, where the CCN2 gene was under control of Col1a2 promoter, leading to fibroblast- specific overexpression of CCN2, showed several fibrotic features in skin, lung, kidney and vasculature (Sonnylal et al., 2010). On the other hand, systemic CCN2 knock out prevents mice from Bleomycin induced skin fibrosis (S. Liu et al., 2011). Taken together these two studies demonstrate a key role of CCN2 in fibroblast-mediated tissue fibrosis.

CCN2 is expressed during development in the thin wall surrounding bronchioles and alveoli. CCN2 knock out litters were very small in number; the high incidence of mortality was thought to be due to lung problems. The surviving mice showed poor susceptibility to bleomycin induced fibrosis, whereas CCN2 over- expression leads to thickening in alveolar

space between alveoli due to cell proliferation and secretion. Interestingly, foetal regulation of CCN2 expression is controlled differentially by different genetic enhancers, which show time and tissue specific regulation (Frost et al., 2018). CCN2 has both a regulatory and structural roles in lung. CCN2 is one of the earliest transcripts induced by TGF-ß r and it has autocrine and paracrine effects on the expression of major ECM genes (Col1a1, fibulin-1, PDGFR) (Kendall & Feghali-Bostwick, 2014).

1.4.3. Snai1 (SnaiL) and Snai2 (Slug)

Snail family proteins are zinc-finger DNA binding proteins involved in several mechanisms during foetal development and in epithelial to mesenchymal transition (EMT). They are composed of a highly conserved C-terminal region, which contains from four to six zinc-finger region and a N-terminal with differences between species. Snail proteins are expressed in the nuclei where they function as sequence specific transcription factors, where they o repress target genes. They were discovered first in *Drosophila melanogaster* mesoderm and subsequently discovered in different vertebrate and non-vertebrate organisms, including mouse and human (Nieto, 2002).

The human and mouse genomes encode two snail proteins: Snail (or Snai1) and Slug (or Snai2). Snail is a 17 kbp gene in both human and mouse, located on the long harm of chromosome 20 long in human and on the long harm of chromosome 2 in mouse. Both genes encode a protein of 264 amino acid which is the only protein translated (ENSG00000124216).

The Slug gene consists of 24 kbp and is located on the long harm of chromosome 8 in human and on the long harm of chromosome 16 in mouse. The human gene encodes 4 translated variants from alternative splicing events, whereas mouse Slug encodes only for the full-length protein of 268 amino acids (ENSG00000019549).

Snail family proteins bind to DNA in a sequence specific manner (consensus sequence: CAGGTG) through a basic helix-loop-helix motif, similar to the E-box common to a variety of transcriptional factors. Snail superfamily in vertebrate consists of Snail and Slug subgroups, with different roles in embryonic development (mesodermal for Snail and neural crest for Slug) (Thiery et al., 2009).

Snail and Slug compete for the same binding sites in the DNA. This competition leads to a preferential expression of a single family member in a positive feedback manner (Y. Chen &

Gridley, 2013).

Epithelial to mesenchymal transition (EMT) is a mechanism historically associated with development, where characteristic transition in surface proteins from E-cadherin to N-cadherin is a sign of change in cell polarity. This mechanism is fundamental during embryogenesis for the creation of the germinal layers, during gastrulation. The genetic regulation in development identified the different roles of Snail and Slug in mesoderm and neural crest location (Kalluri & Weinberg, 2009). However, EMT is not confined only in germ layer development, but also in angiogenesis and wound healing, and pathological events such as organ fibrosis and metastasis in cancer.

Snail and Slug are induced by TGF-ß in epithelial cells where this activation mediate the inhibition of caveolin and sequestration of TGF-ß receptor 1 recycle. Both mechanisms are connected with EMT and are thought to participate to lung fibrosis, resulting in EMT for ATII (Hwangbo et al., 2016). In conclusion, Snail and Slug are thought to play an important role in the development of IPF by increasing the size of the fibroblast pool through induction of EMT. In addition, Slug and Snail may trigger increased mobility in mesenchymal cells, as has been observed in cancer cells. Mobility is a key characteristic of myofibroblasts in fibrosis.

1.4.4. Mothers against decapentaplegic homolog 6 and 7

Inhibitory Smad proteins constitute the inhibitory feedback loop in the Smad activatory pathway. Inhibitory Smads present similarity in structure with activatory Smad, (https://www.omim.org/entry/600993). Differences in the protein structure from other activatory Smads are located in the N-terminal domain, where inhibitory Smads lack a TGF-ß phosphorylation site (X. Yan et al., 2009). All Smad proteins are composed of two main domains (MH1 and MH2) that compete in the DNA binding activity, where Smad proteins compete to give rise to expression of distinct sets of mRNA (X. Yan et al., 2009).

SMAD6 is a 38 kbps gene located on the long harm of chromosome 15 in human and of 30 kbps located on the long arm of chromosome 9 in mouse. The human gene encodes a 496 amino acid long protein in its full-length translation and 5 other splice variants, whereas mouse presents 3 splice variants (ENSG00000137834)

Smad7 is a ~44 kbps gene located on the long harm chromosome 18 encoding for a 426 amino acid full-length protein in both human and mouse, with 8 splice variants in human and

5 in mouse (ENSG00000101665).

As mentioned above, both inhibitory Smads mediate activatory Smad inhibition through three major mechanisms, which reflects similarity in the supramolecular structure: 1) competition in phosphorylation cascade to activatory Smads after TGF-ß receptor 1 dimerization. 2) Phosphate removal through a phosphatase activity. 3) E3-ubiquitin-dependent lysosomal degradation of TGF-ß1 receptors achieved through Smad-Specific E3-ubiquitin ligase 1 and 2 (Smurf1 and 2) (X. Yan et al., 2009). Another possible mechanism of inhibition of TGF-ß signalling pathway demonstrated *in vitro* for Smad7 highlighted a transcriptional factor activity for this protein. Atomic Force Microscopy (AFM) experiments aiming at investigating interactions between SBE and PAI-1 oligonucleotide consensus sequences with Smad7 showed a similar force of binding compared to activatory Smad. Interestingly, Smad7 was able to bind SBE in a 17 nucleotide sequence different from Smad4 (Shi et al., 2008). Although it is not clear if there is an exclusive relationship in this binding, it results in a decrease in effector gene expression (Zhang et al., 2007). Another possible mechanism still not well understood is the indirect inhibition of TGF-ß and BMP pathways, through inhibitory SMADs combination with histone deacetylases (Bai, Shi, Yang, & Xu, 2000). The mechanism proposed referred that Smad6 regulates ECM gene transcription in combination with Hoxc-8, mediating an inhibition on Smad1 DNA binding activity.

Smad-dependent signalling affects fibrosis through the regulation of myofibroblast activation, synthesis and secretion of matrix proteins, T cell cytokine upregulation, and mesenchymal differentiation. Therefore, as Smad6 Smad7 limit TGF-ß-induced Smad signalling, they may play an important role in fibrosis.

Excess synthesis and secretion of collagen is a major feature of lung fibrosis, and TGF-ß strongly increases Collagen expression. Therefore, TGF-ß has been a major target for the development of anti-fibrotic therapies (Chaudhary, Schnapp, & Park, 2006). However, none of strategies so far have succeeded in reverting lung fibrosis. Increasing inhibition of Smad signalling by increasing Smad7 has shown to ameliorate the Bleomycin model of fibrosis, indicating that Smad7 is a promising candidate for targeting fibrosis (Bonniaud et al., 2014).

1.4.5. Platelet derived grow factor receptor α (PDGFRα)

Platelet-derived growth factor receptor alpha (PDGFRα) belongs to the platelet-derived

growth factor receptor family. PDGFRα signalling plays an important role in wound healing repair.

PDGFRα encodes a 6kbp gene located on the long arm of chromosome 5 in humans and the long arm of chromosome 4 in mice. The PDGFRα protein serves as a tyrosine kinase receptor for PDGF. PDGFRα encodes 10 splice variants in humans and 2 isoforms and 9 splice variants in mice (ENSG00000134853).

The PDGFRα protein consists of a c extramembrane domain for ligand binding, a transmembrane domain and an intra-cellular tyrosine kinase domain that undergoes transphosphorylation inducing the subsequent intracellular signalling cascade. PDGFRα activation can lead to uncontrolled cellular proliferation and increased matrix production (Mori et al., 1993). Two phosphorylation sites are located in the insert-region between the actual kinase subdomains. Those sites are rich in Ser and Thr, which upon ubiquitination mark the protein for proteasomal degradation (P. H. Chen, Chen, & He, 2013).

PDGFRα selective knock-out experiments shows that PDGFRß can compensate the lack of PDGFRα, forming homodimers able to activate the same signalling cascades (P. H. Chen et al., 2013).

Binding of the PDGF ligands induces tyrosine autophosphorylation of PDGFRα , leading to activation of a number of SH-adaptor transducers such as Sos, Grb, which can then transduce to downstream kinase/phosphatases such as PI3k and PLCγ (Tallquist & Kazlauskas, 2004).

PDGFRα is a common marker for mesenchymal cells and variation to its activation or expression level is strongly associated with a variety of pathological states including fibrosis. Anomalies in activatory pathways can be cell-specific and can also induce changes in cell polarity as in EMT.

1.4.6. Granzyme ß (GRMß)

Granzyme ß (GzmB) is a serine protease enzyme mostly known for its pro- apoptotic role in epithelial and in cytotoxic T and natural killer lymphocytes. It mediates the cell-mediated killing in combination with perforin, which forms a transient pore in cell membranes allowing targeting of Grmß. Granzyme ß has been associated with a number of immunological

mechanisms and it is at the basis of acute phases lung injury (Russo et al., 2018).

Granzyme ß is encoded by GZMB gene, located on the long arm of chromosome 14 in both humans and mice. GZMB is a 10 and 14 kbp gene, respectively in humans and mice. The protein is 247 amino acid long and it presents 8 additional non-coding splice variants only in human (ENSG00000100453).

Although GzmB plays a fundamental role in apoptosis, this enzyme when is not targeted through perforin can mediate cellular receptor cleavage and ECM degradation. The serine protease activity is at the basis of GzmB role in apoptosis, as it cleaves a variety apoptotic target proteinssuch as caspase 3 leading to programmed cell death. (Heibein et al., 2000). Organ fibrosis is characterised by insufficient apoptosis of mesenchymal cells, and excessive apoptosis in the lymphocyte population (Wynn, 2011). Excessive lymphocyte cell death leads to an increase of inflammatory mediators. Among all those molecules, perforin and GzmB are thought to play an important role in acute lung injury (Miyazaki et al., 2004). Excessive and prolonged lung injury is a common mechanism in lung fibrosis. In this context apoptosis is a key mechanism for mesenchymal removal after the replacement of the scar tissue, whereas an excessive immune cells apoptosis increases the level of perforin/GzmB. As demonstrated by perforin knock out mouse, GzmB and perforin might be involved not only in the acute inflammatory phase in fibrosis, but also in its progression (Miyazaki et al., 2004).

1.5. Lung biogenesis

Lung development is a complex mechanism that reflects the high level of cellular heterogeneity mentioned above. Lung is derived from both endoderm and mesoderm through a mechanism involving sequential signalling interactions between epithelia and mesenchyme, composed of four phases; embryonic, pseudoglandular, canalicular and saccular-alveolar (Whitsett et al., 2018).

In the embryonic phase, the foregut divides into oesophagus and trachea, forming the future inner lung parenchyma as two buds. Mesodermal cells interact with endodermal foregut cells (fig.1.15), leading to laryngotracheal track and pleura formation (Schittny, 2017). In more detail, mesenchyme in embryogenesis creates the lung pleura and the cartilaginous ring surrounding the trachea and bronchi. During lung embryogenesis, vascular and neuroectoderm tissues associated to lung develop at the same time (Schittny, 2017). Thus, in embryogenesis, there is the formation of the trachea, main stem, lobar and segmental bronchi, and hilum, through a process generally referred to as branching morphogenesis (Schittny, 2017). Epithelial-Mesenchymal interactions are finely controlled during the embryonic developmental process, fundamental for progression in the further phase of lung development.

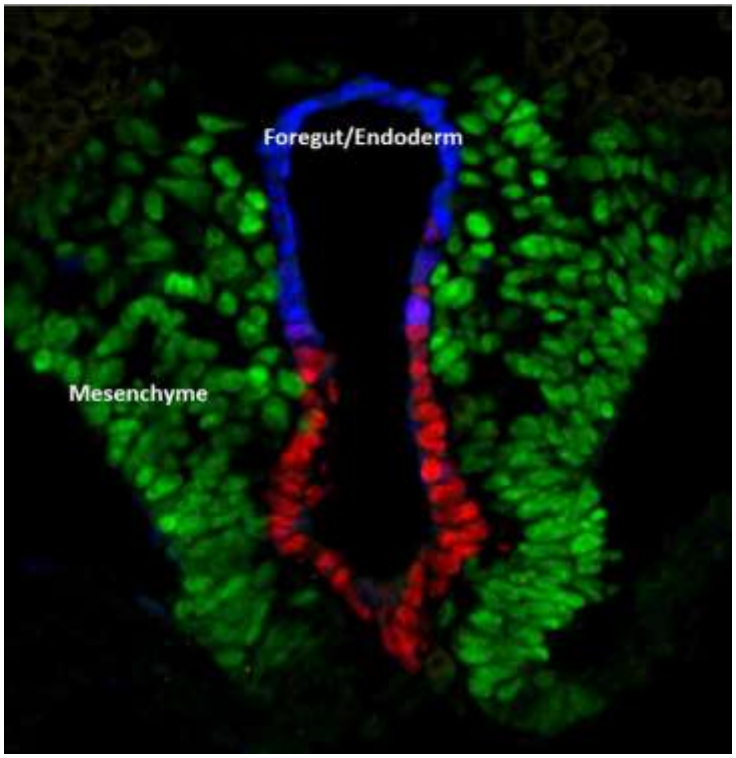

Figure 1.15 Differentiation of the embryonic foregut endoderm. Dorsal ventral axis is represented in blue (SOX2) and lung in red tubules (NKX2). While the mesenchyme is represented in green (FOXF1)(From Whitsett et al., 2018).

The pseudoglandular phase is characterised by branch formation from lung buds, which resemble a classical lung tree-like structure. From each "father" segment two "daughter" segments will form in a process dominated by inhomogeneous dichotomy. Inhomogeneous dichotomy is characteristic of lung biogenesis only for bipedal apes, where branches grow as separated units, each newly formed branch is defined as a "generation" (fig.1.9) (Hsia et al., 2016; Whitsett et al., 2018).

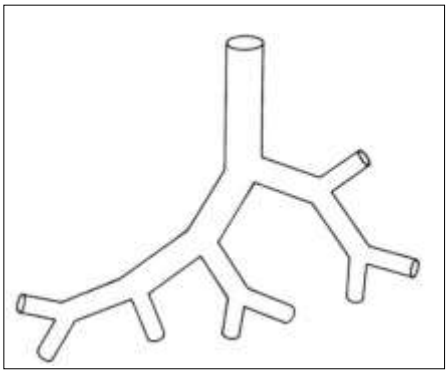

Figure 1.16 Example of inhomogeneous dichotomy.

From a father branch two structural different daughter branches will be formed, resulting in the inhomogeneous structure. By contrast, rodents show a monopodial inhomogeneous branching formation, where one daughter branch is formed from a father main branch (Schittny, 2017). The diverse branching development between bipedal apes and rodents represents one of the main structural difference between these two species.

Transition from the embryogenic to the pseudoglandular stage is governed by Sox2 and Sox9 expression, where Sox2 activates epithelial cells for the branching, while Sox9 is active during budding and in later stages of saccular acinar formation (see below). Other key genes in this process are Transcriptional terminator factor, which control the embryogenic phase and FGF10 which serves as signal from mesenchyme to epithelia promoting branching morphogenesis (Whitsett et al., 2018).

Following branching, the canalicular phase starts with formation of the first respiratory unit (Schittny, 2017). From this phase on, developmental mechanisms vary between mammalian species, and the following description applies only to humans. The canalicular phase is characterised by epithelial differentiation in the proximal airways, while respiratory epithelia start to form the terminal buds, with formation of the early respiratory units. A respiratory unit is composed by airway epithelia and capillaries, which permit gas exchange. Airway epithelia are still generated through a branching morphogenesis with inhomogeneous characteristics, while capillaries form trough angiogenesis. Interestingly, in branch morphogenesis before the canalicular phase, each generation shows a progressive 50% reduction in the diameter for conducting airways, while in respiratory units this relationship is lost. Newly formed respiratory bronchioles show a decrease in diameter length through generation resulting in a reduction in lung capacity, which will allow O_2 diffusion through bronchioles walls (Hsia et al., 2016). Pre-respiratory units generated in the canalicular phase originate from small buds, which differentiate giving rise to alveolar epithelial cells type-I and II (Whitsett et al., 2018). Alveolar epithelia type differentiation marks a discontinuity in epithelia layer, resulting in an evident morphological change from conducting airways to respiratory unit. The respiratory unit starts from the bronchioalveolar duct junction, which

represent a connection point of conductive airway with respiratory airway (fig. 1.17) (Winkelmann & Noack, 2010).

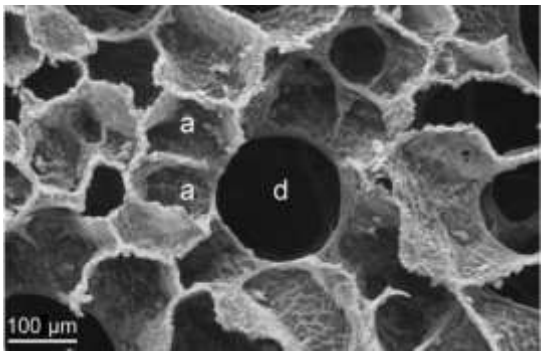

Figure 1.17 Scanning electron micrograph of human lung parenchyma. Alveolar ducts (d) are surrounded by alveoli (a). Alveoli represent lung section with the highest diffusion capability due to the reduce structure. In the figure it is possible to appreciate the differences in size and structure between alveolar ducts and alveoli. Bronchioalveolar duct development provide the structural basis for alveolar development in canalicular-alveolar phase (From Hsia et al., 2016).

Bronchioalveolar duct formation lays the basis for saccular-alveolar development from transitional bronchiole units. As mentioned, angiogenesis forms capillaries from primitive blood vessels. Pericyte and smooth muscle are recruited on vessels edge to extend their networks, ending in capillary formation at the end of respiratory units. Endothelial cells migrate internally newformed vessel, to remodel basal lamina producing a proper vascular lamina, in a process regulated by VEGF-A (Schittny, 2017; Whitsett et al., 2018).

In humans, branching morphogenesis ends at the start of the saccular stage when alveorization begins. In human, rat and mouse, the saccular stage starts shortly before birth and leads to the formation of the first alveoli. From bronchoalveolar ducts, squamous epithelial cells, precursors of alveolar epithelia type-I and II, determines an epithelia growth in length and width, forming a pre- alveolus. Both type-I and II cells are derived from the same undifferentiated cuboidal squamous progenitor, which serves as a stem niche (Schittny, 2017).

As mentioned above, microvasculature follows airway progression, depositing connective tissue, which separate endoderm and mesoderm. At the saccular stage smooth muscle cells produce a thick, immature septum that covers type-I and type-II epithelia cells around double layer capillaries. Maturation of capillary layers and alveolar septa is thought to take place in parallel, at the start of alveorization (Schittny, 2017). Lipofibroblasts and myofibroblasts build alveolarsepta (see below) and boost alveolar epithelial expansion

through FGF10 release in alveorization (Whitsett et al., 2018). Alveorization is a developmental mechanism starting after birth and continuing as long as lung is growing, consisting in alveolar formation (Schittny, 2017). Microvasculature developing in here is driven by VEGF and TGF-ß and by hypoxia, which can retard or accelerate lung development (Whitsett et al., 2018). This phase in lung biogenesis is characterized by the gas exchange unit ultimate generation. New septa generated by mesenchyme, lift up the primary septa deposited during canalicular phase, separating capillary from pre-alveolar space. Then, smooth muscle cells release ECM components forming the fibrillar alveolar structure. Then the septum rises up to its full length and a proper alveolus is formed. In this process, septa thinning and the two capillaries fuse to form a single layer capillary network in the septum (Schittny, 2017). This allows formation of a respiratory unit, which continues in human until around 2 years post birth, or in response to a pneumonectomy (Hsia et al., 2016).

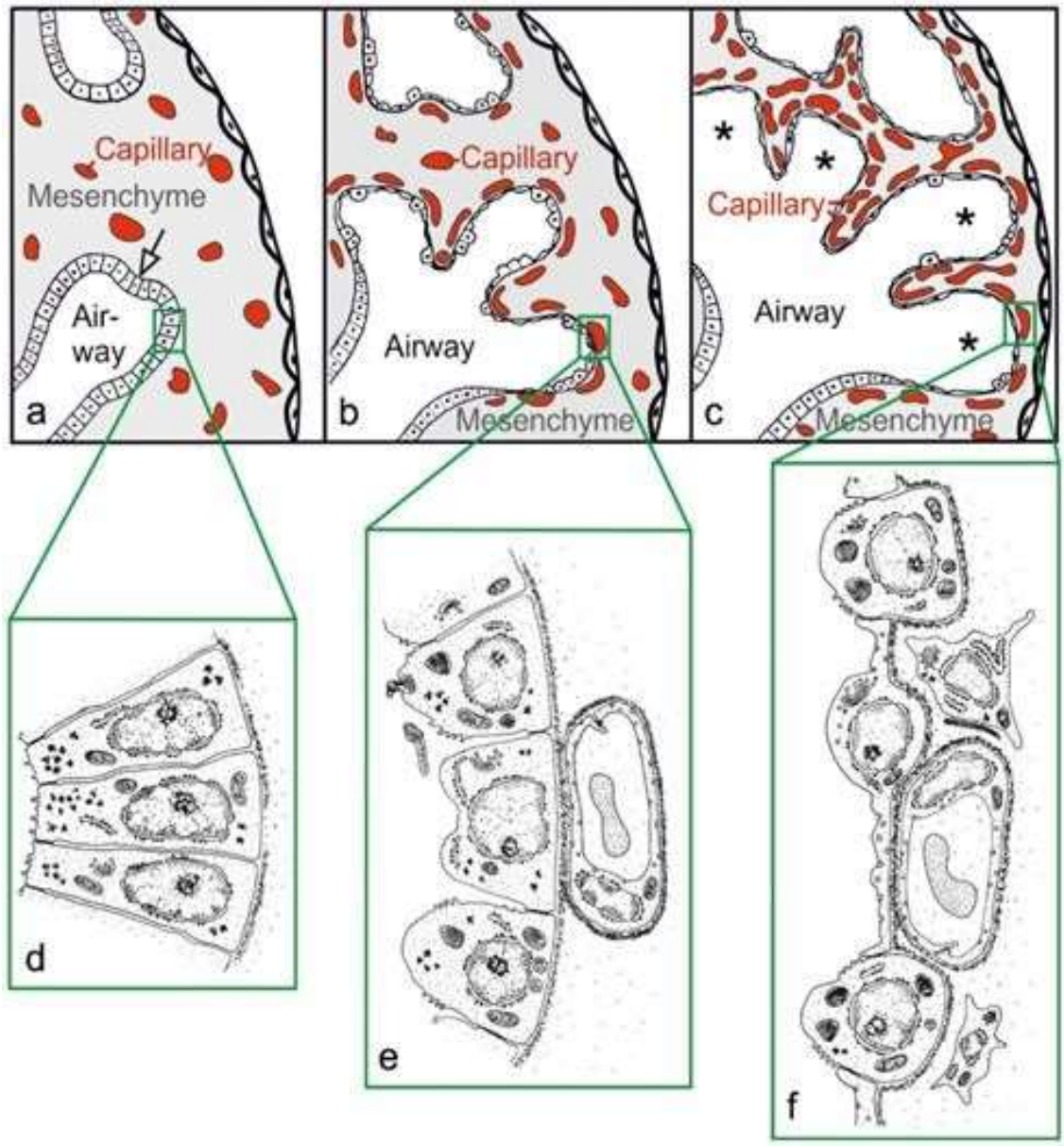

Figure 1.18 Morphological development of the lung parenchyma during the pseudoglandular, canalicular and saccular stage. In the pseudoglandular stage, epithelial tubules branches penetrate into the surrounding mesenchyme (a). The canalicular stage (b) is characterized by a differentiation of the epithelial cells into type I and type II epithelial cells (e, f), forming the future airways. Capillaries maturation starts once the mesenchyme is close contacts to the epithelium (b, e) and by the formation of first future air−blood barriers (e, f). Thick immature inter-airspace septa is formed by mesenchyme ECM expression, which in the terminal ends of the bronchial tree represent air-blood phase (Schittny, 2017).

1.6. Lung Biomechanics

Pulmonary fibrosis repair impairment alters organ function, resulting in variation to the Volume/Pressure ratio. Fibrosis is characterised by volume decrease and pressure increase in terms of air during each breathing cycle, resulting from the increase in ECM (Bela Suki, Stamenovic, & Hubmayr, 2011). This fact inevitably alters lung mechanical properties.

Lung movement is controlled by chest muscles and diaphragm, which control lung expiration and inspiration through involuntary innervation. This creates a tension which is then further propagated to ECM and finally this force is transferred from ECM to cells cytoskeleton. Inflammatory signals and cytokines key in fibrosis, such as TGF-ß and TNF-α, prompt cytoskeletal remodelling that alters cell-generated forces and cellular mechanical properties (D. J. Tschumperlin et al., 2018). Tissue damage alters normal tissue "mechanical" homeostasis, with collagen deposition by myofibroblasts that increases tissue stiffness. Transition from a lower to a higher level of stiffness seems to propagate collagen deposition and crosslink. Stiffness, or rigidity, of a material is based on how well a material resists to a force applied on it. This resistance depends on ECM composition, which varies between body compartments, and is altered in a wide range of pathological conditions (Handorf et al., 2015).

Interestingly, stiffening seems to amplify mesenchymal activation. Normal tissue repair decreases stresses in the wound bed, through signals that bring myofibroblasts to either a quiescent state or induce myofibroblast apoptosis. By contrast, stiffer ECM, generated by impairment in wound healing repair, increases collagen deposition and myofibroblasts activation (D. J. Tschumperlin et al., 2018). One possible explanation to this mechanism is that stiffer materials increase activation of Focal Adhesion Kinases (FAKs). FAKs are activated by integrins and growth factor receptors, which can respond to changes in the extracellular space. Those change possibly can be transduced to FAK, which might activate Rho/Rock signalling pathways, triggering cell polarity activation and results in myofibroblasts persisting in their activation state (Handorf et al., 2015). Moreover, acquisition of cell polarity seems to trigger myofibroblast migration towards stiffer matrix. Marinkovic and collaborators demonstrated that lung fibroblasts from IPF patients were more responsive when cultured on rigid Col1a1 based matrix, whereas soft matrix inhibits fibrotic phenotype, in terms of cells contractility (Marinković, Liu, & Tschumperlin, 2013). Therefore, tissue biomechanics influences fibrosis outcome. Although most of the evidence regarding these behaviours rely

on *in vitro* studies, the interest in this field has largely increased.

Stiffness is not the only variable used in biomechanics; mechanical stress (force per unit area) is a key parameter to take in account to understand fibrotic response over time. Mechanical stress (or stretch) changes biomaterials size and shape, when a force is applied onto an elastic material (Béla Suki et al., 2011). When a force has a direction, stretch is equal to the product of material length increase $\varepsilon = (l-l_0)/l_0$ with Young's modulus of elasticity, *Y*. Where l_0 refers to material starting length and *l* to the length after a force is applied. Young's modulus refers to material elastic properties (Béla Suki et al., 2011). In addition, Young's modulus is indirectly proportional with tissue flexibility. Soft tissue possesses a lower Young's modulus compared to rigid materials. Increase in tissue stiffness, as in fibrosis, augments parenchyma rigidity, resulting lung volume pression changes ratio. Therefore, fibrotic ECM possess a higher Young's modulus compared to healthy ECM. Therefore, the tension or force required (considered as mechanical work during time) to stretch highly crosslinked ECM fibres is higher.

This increase in tissue stiffness seems to generate a positive feedback on collagen deposition and crosslinking. Biomechanics have extensively proved that all tissues respond to mechanical changes, through sensors of biomechanical alterations. Cell to cell and cell to ECM interactions represent a fine-tune system that controls tissue biomechanics and senses alterations. The understanding of molecular mechanisms beyond bio-mechanic can lead to new pharmacological strategy aiming at as example inhibition of mesenchymal movement towards stiff ECM (which increase ECM production, see above).

Adhesion molecules play a key role in cell-cell communication. FAKs and cadherins prompt cytoskeletal changes due to mechanical stimulation. Cadherins are adhesion membrane proteins that connects adjacent cells. Those adhesion molecules allow cells to sense and transfer information regarding alteration in shear force and stretch, resulting in cytoskeleton remodelling. Mechanical stimulation increases actomyosin tension, inducing acquisition in cell polarity and collective migration (D. J. Tschumperlin et al., 2018). Modification to cytoskeletal tension is thought to participate activate mechanism as EMT in response to damage. VE-cadherin in the vasculature represents a well-studied example of mechano-transduction. On cell surface a complex formed by VE-cadherin, PECAM-1, and VEGF receptor type II and III form a well-studied mechanosensitive system. Mechanical forces and fluid flows trigger PECAM-1 interaction with vimentin, which activating Src kinase family,

regulating vasculature tone. In addition, this mechanism leads to increase in VEGF receptor activation; inhibitors for this vascular tyrosine kinase receptor appear promising novel pharmacological strategy against fibrosis as they promote myofibroblast “deactivation”. Another intracellular sensor for mechanical forces is represented by the Notch and Rho/Rock signalling pathways, whose seem to prompt vimentin and α-smooth actin expression in response to mechanical stimulation, mechanisms occurring also EMT (D. J. Tschumperlin et al., 2018). Interestingly, this relationship might underlie a synergistic mechanism on EMT, where the acquisition of cell polarity, perhaps, depends on mechanical stimulation.

Cell-matrix forces are sensed mostly though integrins, αß heterodimer transmembrane cells surface receptors (D. J. Tschumperlin et al., 2018). Integrins are important in biomechanics as they bind specific ECM domains, activating signal transduction in response to mechanical stimulations. RGD motif represents a high conserved aminoacidic triplet presents in fibronectin, vitronectin, osteopontin, fibrinogen and von Willebrand factor, which possess affinity for a wide range of integrins (Burgstaller et al., 2017). Integrin-RGD interaction allow mesenchymal cells population to move across connective tissue and epithelium. Activated integrins are bound to actomyosin system through dynamic association with integrin- or F-actin binding protein. This association transfers information regarding matrix stiffness from fibronectin to cytoskeleton. Another cell-matrix force sensor recently identified, is Thy-1, a GPI-anchored glycoprotein, which seems to amplify or attenuating stiffness sensing to cell-matrix adhesions. Proteomic analysis have identified more than 500 individual protein in the “adhesome” (adhesion proteins omic) influenced by changes in mechanical environment, which might contain future target against fibrosis (D. J. Tschumperlin et al., 2018).

At the intracellular level, the transcriptional factors YAP and TAZ were identified as mechano-sensors in endothelial and mesenchymal cells. YAP and TAZ might regulate gene expression in response to mechanical stress through indirect association with other transcriptional factors implicated in fibrosis, such as SMAD and Notch/ß-catenin (D. J. Tschumperlin et al., 2018). Another important mechano-sensor intracellular transcription factor family associated with fibrosis is MRTF, which after activation induced by TGF-ß, moves to the nucleus where it activates SNAIL2. Through this mechanism MRTFs induce cytoskeletal remodelling occurring in EMT (Thiery et al., 2009).

Biomechanics present technical limitation as most of those studies have been

conducted *in vitro* through tension force microscopy or similar techniques. There is the necessity to corroborate this evidence in experimental animal models. Multidisciplinary approaches might in the future highlight mechanisms not totally clear nowadays.

1.6. Genetic factors influencing pulmonary fibrosis

Understanding the genetic and epigenetic factors involved in IPF is a powerful tool for both diagnostic and therapeutic advances. IPF is a multifactorial disease where genetic predisposition and environmental cause the IPF phenotype. Therefore, pulmonary fibrosis does not act as a classical Mendelian disease "one gene : one phenotype".

Despite the fact that there is not a single predominant mutation associated with the disease, inheritability of IPF, known as familial IPF, has been documented. Familial IPF is characterised by higher incidence in the younger population, without a significant environmental cause triggering IPF. Where classic IPF predominantly affects the elderly, familial IPF predominantly affects people in the 18-25 year old age bracket (King et al., 2000). Familial IPF is transferred in an autosomal dominant fashion with high penetrance.

Only a few mutations have been associated with an early age IPF and with a worsening of the fibrotic phenotype (Leslie et al., 2012). Familial IPF seems to follow the "double hit theory", where the inherited genetic factors lead to a higher susceptibility to environmental conditions. As example, in a study using a cohort of 111 families with familial IPF, only 8% of people were un-affected. However, those subjects showed subclinical manifestation of the disease (Steele et al., 2005). Therefore, they might be predisposed to develop IPF.

Studies into the genetic basis of fibrosis have revealed several genes associated with pulmonary fibrosis.

Polymorphisms are changes in the genome that occur in more than 1% of the population Genome wide studies have identified polymorphisms in the MUC5B gene, which encodes a lipoprotein fundamental for gas exchange, related to a poorer IPF prognosis in Hispanic and Caucasian cohorts (Borie et al., 2013). Moreover, this MUC5B variant was not associated with SSc-ILD but only with IPF. SNPs in interlukin-1 (IL-1) and in tumour necrosis factor α (TNFα) in Italian and British cohorts have been associated with higher susceptibility to IPF. However, those SNPs were found only in a small number of patients, and hence cannot be used for diagnostic purposes (Borie et al., 2013).

Gene mutations in telomerase as well as mutations leading to telomere shortening have been reported to be correlated to IPF (M. Armanios, 2012). Telomerases are polymerase enzymes with a reverse transcriptase activity specialised in chromosome end duplication. In mammals, telomerases are composed of two components: a catalytic unit named hTERT with

a reverse transcriptase activity and an RNA unit (hTR in humans) which contains the RNA template (TTAGGG)n for telomere repeat addition (Ramlee, Wang, Toh, & Li, 2016). Healthy somatic cells decrease in telomere length as a normal process during ageing. Deficiencies in the normal duplication of telomeres give rise to a series of diseases, known as telomeropathies. Telomeropathies have been extensively associated with pulmonary fibrosis. Primary telomeropathies are due to mutations in the genes related to telomere maintenance, such as mutations in DKC1 and hTERT. While secondary telomeropathies are due to dysregulation of the DNA repair system that leads to impairment in telomere length, as can occur in progeria and cancer. Mutations in either telomerase gene or in gene related to telomerase biogenesis gives rise to Dyskeratosis congenital (DC) (M. Y. Armanios et al., 2007). In DC, telomere shortening generates an early cell death or an early cell cycle arrest; pathological features of DC are bone marrow failure and pulmonary fibrosis. For DC patients, IPF is the second most common cause of death after bone marrow failure (M. Y. Armanios et al., 2007). One explanation why DC can lead to IPF lays in the high cell turnover of lung epithelial cells. A high cell turnover implies that lung cells at each replication will present mutation in telomeres, which will reduce the cell turnover. This might then increase susceptibility to damage, with a stronger dysregulation in wound healing repair system. In general DC patients present clinical features similar to familiar IPF, such as the high penetrance in young adults (M. Armanios, 2012).

Mutations in the DCK1 gene, a gene fundamental for correct telomerase biogenesis, lead to the most common form of DC with IPF. Patients with DCK1 mutations often develop IPF after bone marrow transplantation due to treatment with immunosuppressive that are toxic to the pulmonary system (M. Armanios, 2012). Unfortunately, bone marrow transplantation is the only available treatment in severe DC. Adjustment in anti-rejection therapies only slow IPF development, which is the main cause of death in these patients. IPF can also arise in DC patients without bone marrow failure. Mutations, in hTERT and hTR (telomerase genes) create a more severe type of DC with anticipated IPF (similar to familiar IPF). The transmission follows, as for familiar IPF, an autosomal dominant heritability. Usually mutations in hTERT and hTR lead to loss of function of telomerase, which triggers either IPF or bone marrow failure or a combination of the two (M. Y. Armanios et al., 2007). Loss of function mutations in those genes show a more severe phenotype, although mutations leading DC do not present a fully progeroid phenotype. Young patients show “symptoms of

ageing", such as, hair loss, liver cirrhosis, and osteoporosis. Ageing is a multifactorial mechanism in which both genetic and environmental events can deregulate its normal progression (Lidzbarsky et al., 2018). Telomere shortening is one of the most studied mechanisms related to ageing. Therefore, clarifying this overlap between DC and IPF might provide new insight into the role of ageing in IPF, and may explain why IPF is more common in the elderly.

One of the most interesting genetic insights into IPF comes from Nogee and collaborators, who in 2001 identified a series of point mutations in the surfactant protein C gene (SFTP-C) (Nogee et al., 2001). SFTP-C is a key protein for lung stability and for lung embryonic development. SFTP-C is expressed and secreted only by Alveolar epithelial cell type II (AECII) and it maintains lung integrity (Whitsett et al., 2018). When secreted, SFTP-C, together with mucins, shields alveolar parenchyma from irritants and pathogens. Moreover, SFTP-C is required for correct lung inflation and recoil, as through reducing lung surface tension, it prevents lung collapse. Unfolded mutant SFTP-C protein accumulates in the alveolar parenchyma where it induces epithelial injury. Those injuries in the parenchyma then lead to familial IPF (Van Moorsel et al., 2010).

1.7. Environmental factors influencing pulmonary fibrosis

Environmental factors can contribute to the development of IPF. Although there is not a univocal correlation between a single identified environmental factor and IPF, a number of risk factors have been described. Exposure to asbestos, smoke from cigarettes, and silicosis seem to accelerate IPF progression from a ILD phenotype, in particular for subjects constantly exposed to a toxic environment (Olson, Gifford, Inase, Fernández Pérez, & Suda, 2018). Other factors that increase the risk of IPF regards to workers exposed to metal, stone and wood dust, hair dressing and farming products. Microbial agents such as viral infection by EBV or cytomegalovirus have been identified in alveoli from patients with IPF and it was considered as a source of risk. However, current treatment for IPF uses drugs with immunosuppressive effect, which can influence the analysis (King et al., 2000).

UK is the country with the highest incidence of IPF per inhabitant in Europe. Gribbin and collaborators found a 100% increase in the number of cases from 1993 to 2003, with higher incidence in the male population (Gribbin et al., 2006). The male predominance may be caused by the fact that specific professions (such as miner), are historically associated with males, possess a higher risk to develop IPF. Moreover, the number of smokers is higher in males than females, according to "Facts on Gender and Tobacco" from the World Health Organization.

1.8.Ageing in pulmonary fibrosis

Ageing is a multifactorial biological process, in which genetic and environmental factors contribute to its progression. Genetic mechanisms driven by age progression are telomere shortening, decreased cell turnover and autophagy. Unhealthy life-styles, such as smoking, have shown to accelerate ageing and decrease life-span (Lidzbarsky et al., 2018). Age increases susceptibility to several diseases due to cellular senescence and organ structural deterioration, which influences fibrosis (Lidzbarsky et al., 2018). An example is represented by IPF, which mostly affects the elderly population with high significant increase after 75 years old compared to 40-60 aged (King et al., 2000). As mentioned in the paragraph *Genetic factor influencing IPF*, mutations in DKC1 and telomere shortening are genetic conditions that correlate age with pulmonary fibrosis (M. Armanios, 2012). Ageing leads to accumulation of

damages over time, and this can result in changes in matrix biosynthesis and modification of cell-ECM and ECM-ECM interactions (Kurtz & Oh, 2012). Furthermore, during ageing there is an increase in the alveolar space, which is not related to inflammation or alveolar wall destruction (Miller, 2010). This changes lung mechanics perhaps influences ECM composition and turnover in aged subjects. Collagen type-I and III are strongly influenced qualitatively and quantitatively by age, although it is debatable whether age quantitatively increases fibrillar collagens. Collagen fibre turnover decreases with age in particular for type-I collagen (Parola, 2016). One possible explanation for this could be that collagen crosslinking increases with age or that ageing increases advanced glycosylation end products (AGE) (Reiser, Hennessy, & Last, 1987). Therefore, ageing determines a more "favourable" environment for fibrosis, which might explain the lack of response to antifibrotic therapies in the elderly (Raghu et al., 2011). Understanding the impact of age alone and in combination with other fibrotic *stimuli* may clarify the role of ageing in pulmonary fibrosis.

Age-related disease phenotypes are difficult to reproduce due to the low efficacy in reproducing such phenotypes. There are a wide range of animal model that can be used for age-related research, rodents have been extensively used for this propose. However, understanding the genetic variability of mouse strains is important to generate a consistent model, because each strain possesses specific genetic characteristics, which can translate to variation to the desired model. The C57BL/6J mouse strain represents the genetically most well-characterised animal used in experimental biology. Models of progeria syndromes, models of accelerated or retarded ageing are well-established animal model, able to reproduce complex age-related features (Kõks et al., 2016).

Mouse and human organs age differently at different rates. For ageing studies, the age at which a mouse is considered "aged" for the organ or tissue under study is generally chosen by comparing the ageing-related features in the mouse by those in humans. This age can vary considerably between organs. For example, the age range used to study age-related osteoarthritis in mice is 15 to 17- months , while *in vivo* models for studying ageing lungs require mice older than 19 months (Kõks et al., 2016; Schulte et al., 2019, Mühlfeld, & Brandenberger, 2019).

Interestingly, Schulte and collaborators have pointed out the key role of age for the development of mice animal models of lung disease. They have reported a clear significant increase in inspiratory capacity, compliance, hysteresis, and lung volume, while tissue

resistance, tissue elastance and alveolar cellular volume showed significant decrease from in mice older than 18 months (Schulte et al., 2019).

1.9. microRNA

microRNAs are small non-coding nuclear RNAs with a length of 17-22 base pairs, involved in gene regulation (Cai et al., 2009). microRNAs play a key role in transcriptome regulation through a 3'-UTR binding repression mechanism on mature mRNA, which stops ribosome translation. Only the central part of a mature microRNA sequence is actually bound to its 3'-UTR binding site on the target mRNA. This part of the sequence is composed of 8-9 base pairs, whereas the rest of the sequence is key for ribozyme-like interaction with protein co-factors involved in the microRNA repression mechanism (see below). A single microRNA can modulate the expression of many genes. As well as of directly decreasing the expression of target mRNAs, microRNAs can also indirectly regulate gene expression by inhibiting the expression of transcription factor. The inhibition of a inhibitory transcription would in principle increase the expression of genes repressed by this transcription factor. The actions of microRNAs are based on sequence complementarity between the microRNA and its target mRNAs (see below).

microRNAs are named using a specific nomenclature, where the first three letters identify the species ("hsa" for human and "mmu" for mouse). microRNA coding sequences are located in both intronic and exonic regions, where polymerase II transcribe a pre-form of microRNAs from a single or polycistronic unit. microRNAs located in intronic regions are expressed from a single open reading frame (ORF), while the ones located in exons are co-expressed with the relative gene (Cai et al., 2009). The coordinated expression of microRNAs is strongly regulated at the epigenetic level. DNA methylation accounts for 10% of changes in the entire microRNA expression during some forms of cancer (Cai et al., 2009). DNA methylation represses gene transcription and therefore microRNA expression. microRNAs located near CpG island tend to be most affected by hypermethylation (Cai et al., 2009). For instance, miR-34b and miR-34c showed expression suppression related to hypermethylation of a nearby CpG island. This mechanism has been extensively studied as the miR-34 family targets p53 expression, a fundamental cell cycle *gate keeper*. Changes in p53 expression as a

result of miR-34a inhibition, have been shown to be linked with cancer cell proliferation. however, in the Bleomycin model of lung fibrosis miR-34a inhibition appears to reverse lung fibrosis (Disayabutr et al., 2016; Hermeking, 2010).

microRNAs were first detected in *C. elegans* in 1993 by Ambros and Ruvkun, who identified an inhibitory element involved in larval development in *lin-4*. It is now estimated that microRNAs compose around 1% of the mammalian genome (Bartel, 2009).

As mentioned, microRNAs are transcribed by polymerase II as either a cluster or as a single microRNA unit, produced as pri-miRNAs. miR biogenesis is classified as either canonical or non-canonical (O'Brien et al., 2018). In canonical biogenesis, after polymerase transcription, pri-miRNAs assume a secondary hairpin structure and undergo a first catalytic cleavage mediated by DGCR8 and Drosha. While DGCR8 recognises a N6-methyladenylated GGAC motif, Drosha operate the endonuclease cut forming a 2 nt 3' overhang, generating a pre-miRNA. Once the pre-miRNA is obtained, the exportin-5/RanGTP complex exports the miRNA to the cytoplasm, where further cleavage by the RNase III endonuclease activity of Dicer results in mature microRNA (O'Brien et al., 2018). This mature duplex sequence represents a mature ds microRNA, the direction of the two strand determines the name of the mature single strand microRNA. The 5p strand arise from the 5'-end of the pre-miRNA hairpin while the 3p strand originates from the 3'-end. Both strands can be loaded in a protein complex known as microRNA-induced silencing complex (miRISC), which is mainly composed of the Argonaute 2 protein (AGOII) (fig. 1.16) (O'Brien et al., 2018).

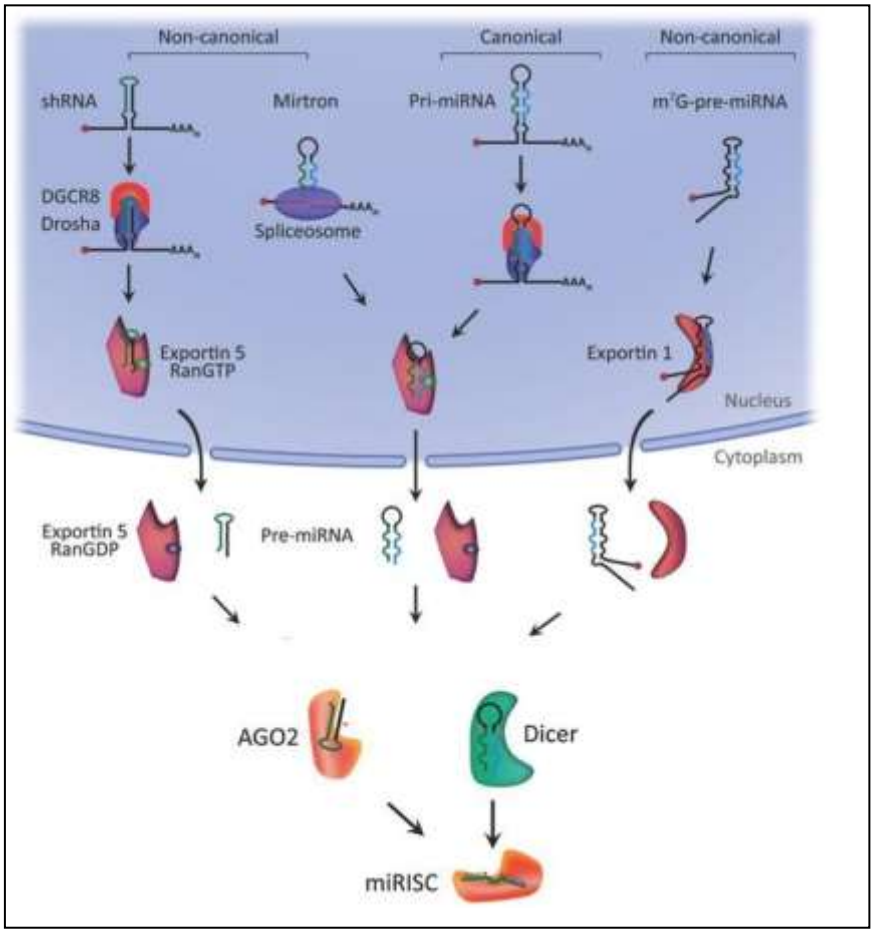

Figure 1.19 microRNA biogenesis. See text for details
See text for the details (From O'Brien et al., 2018).

However, only one strand is favoured in this preferential binding on the RISC. Therefore, only one strand can operate the inhibition of a target mRNA and the two strands have different targets, based on sequence complementarity. Interestingly, microRNAs compete not only for the RISC complex, but also for the binding at the target mRNA. The competition between the 5p and 3p depends on thermodynamic stability of the 5'-ends of the miRNA duplex or by the presence of a 5' Uracil at nucleotide position 1 of mature miRNA. Lower 5' stability or 5'-uracil are inducing events leading to a preferential microRNA strand loading (O'Brien et al., 2018). Therefore, miRNA binding to the inhibitory complex is influenced by the sequence. Interestingly, 5'-end low stability loading, permits AGOII conformational changes occurring in miRISC-dependent recognition and degradation (Bartel, 2009).

Non-canonical microRNA biogenesis results from different combinations of proteins involved in the canonical biogenesis. There are two distinct mechanisms grouped as

Drosha/DGCR8-indipendent and Dicer-independent biogenesis. First group resemble on Dicer substrates, which are directly exported to the cytoplasm without cleavage. Dicer-independent miRNAs are processed by Drosha from short hairpin RNAs (shRNA), which can be directly exported in the cytoplasm and loaded on AGOII (O'Brien et al., 2018).

Modification at the post-transcriptional level, such as RNA editing, or SNPs can influence microRNA target interaction. This because change in the sequence can change both binding to RISC complex and target mRNA binding (Bartel, 2009). Approximately 16% of human pri-miRNAs are subject to A-to-I editing, where an adenosine is transformed in an inosine (Cai et al., 2009). This modification alters normal microRNA:mRNA interaction, creating wobble base pairing, which is considered to trigger inosine-cytosine interaction. Single base pair polymorphism alters microRNAs sequence determining, as well as for the A-to-I editing, changes in recognition between microRNA-mRNA microRNA interferes with translation through a selective binding at complementary sequences in the 3'-UTR of a mature mRNA. Although microRNA-mRNA interaction is not the only mechanism affecting mRNA expression, it accounts for most of transcriptional repression (O'Brien et al., 2018). Other less frequent mechanisms are a 5'-UTR binding, which can even induce transcription through microRNA binding at a gene promoter (Rocha et al., 2007).

Nevertheless, transcription repression consists in a sequence specific mechanism, where AGOII recognizes an mRNA through microRNA-mediated binding, which acts as an RNA guide. AGOII or AGO2 is the endonuclease composing miRISC complex. In the microRNA repression, the core sequence, composed of 7-8 nucleotide represent the RNA guide that guides AGO2 to cleaves and degrades mature mRNA and stop translation. AGO2 is overexpressed in several pathological conditions, which sees increase in microRNA repression machinery, as in cancer. In those cases, AGO2 overexpression results in repression (or suppression) in the translation of a set of gene by miRISC complex. Diseases phenotypes induced by alteration to those mechanisms are still not clear, but they might in future exploited for molecular therapies. AGO2 augmented expression potentiates microRNAs or siRNAs repression rate, as it increases the number miRISC complexes activity in the cytoplasm (Ye, Jin, & Qian, 2015). When the microRNA guide binds mature mRNA, it destabilizes AGOII association with microRNA at the 3'-end, activating a conformational change that activates enzyme nuclease activity. Thus, miRISC-dependent degradation starts after GW182 recruitment, which act as mediator between AGO2 and PAN2-PAN3. This protein together

with CCR4-NOT complex mediates poly-A de-adenylation, which follow the 5'-mRNA de-capping by exonuclease DCP2, resulting in mRNA degradation (O'Brien et al., 2018).

The regulatory function of microRNAs depends on target identification, which is based on Watson and Crick rules. microRNAs from metazoans differ from those in plants in the repression mechanism, as the first one does not need a perfect match between sequences to repress a transcript. By contrast, in plants microRNAs translational inhibition can result only from perfect complementarity between sequences. Nevertheless, microRNA core and mRNA 3'-UTR interaction can repress translation only when the binding between nucleotides is energetically favourable. Therefore, interaction between mRNAs 3'-UTR and miRs core can be predicted from sequence complementarity. However, those predictions need experimental procedures, either measuring both microRNA and mRNA expression levels or immunoprecipitating mRNA:microRNA complex to prove such interaction. Through transcriptomic techniques a complex network of interactions was discovered, where each microRNA has multiple targets. This fact also means that family of protein with a similar 3'-UTR can virtually be inhibited by the same microRNA. An example of this is represented by miR-29a, which shows sequence complementarity for fibrillar collagens and for collagen IV, in the basal membrane (Montgomery et al., 2014). Moreover, these sequences (both mRNA and miR) show a remarkable evolutionary conservation between species in metazoans. Interesting, several studies in the last 10 years have proven that groups of microRNAs have pathway-related preferential expression correlated to biological mechanism, such as ageing, cancer, development, and fibrosis (Bartel, 2009). Therefore, in metazoans microRNAs regulate mRNAs translation through a partial sequence complementarity, which is additionally highly conserved between species. The 7-8 bp long core microRNA shows for many microRNA:mRNA interactions an homology in the interacting sequence, also conserved in most model organisms. Although microRNA expression is governed by epigenetics, increased microRNA levels result from *stimuli* of different origin. miR upregulation increases the probability of interaction with a set of target mRNAs, which can ultimately lead to pathology. microRNA networks influence cell cycle arrest, apoptosis, proliferation, ECM metabolism, development, and diseases. This means that microRNAs have the potential to be important for both diagnosis and treatment of diseases. In humans hsa-miR-19a and hsa-miR-34a were significantly increased in ageing and muscle wasting. miR-34a also showed an age dependent expression in muscle. The mechanism proposed is a repression of VEGF-A and decrease in

endothelial growth. In this clinical study, the miR-34a increase was correlated mostly to SIRT1 decrease, which might trigger mitochondrial degeneration in the aged cohort (Zheng et al., 2018). miR-34a is a perfect example of a microRNA with multiple targets and involvement in different biological mechanisms. Increased miR-34a expression in lung epithelial cells in response to TGF-ß is thought to be at the basis of EMT in fibrosis. TGF-ß, EMT and ageing are three mechanisms that at the molecular, cellular and organism level are connected with fibrosis, where miR-34 is thought to possess a key role (Cui et al., 2017; Takano et al., 2017). miR-21a comprises two isoforms known as miR-21a-3p (or miR-21-1) and miR-21a-5p (or miR-21-2); and represents another microRNA involved in multiple biological mechanisms. The gene is transcribed from the vacuole membrane protein-1 (VMP-1) ORF. Transfection with this ORF sequence has been used to induce miR-21a-5p expression in cancer cells (Ribas et al., 2012). miR-21a-5p levels were found increased in the bronco-alveolar lavage from patients with IPF together with miR-155 (Li et al., 2013). miR- 21a is highly conserved between species, and its expression is increased in the Bleomycin model of lung fibrosis (Xie et al., 2011). This miR appears to play a role in the regulation of EMT in alveolar epithelial cells, and in fibrinogenic activation in fibroblasts, two mechanism related to fibrosis (Yamada et al., 2013). Moreover, increased miR-21a expression has been documented in several forms of tissue fibrosis at both the inflammatory and tissue remodelling stages.

Through translational repression microRNAs can change the proteomic composition of cells, and through this can alter cellular and physiological functions. Bartel in 2009 has summarized microRNA repression activity on proteins as switch interaction, tuning interaction, and neutral interaction. In switch interaction, a microRNA is upregulated in response to augmented protein level, which, as example, can prevent a pathological outcome. Switch interaction in some cases can be accounted for a “failsafe” target where protein repression is important for survival (Bartel, 2009). An example is miR-9a expression during embryogenesis in *Drosophila melanogaster* epithelial cells, which prevents from extra-neural differentiation. Tuning interaction is similar to switch interaction, but in a more dynamic way, as based in microRNA sinusoidal expression to compensate a transient protein increase. The possibility to tuning microRNAs expression is also a good strategy in experimental microRNAs validation. Neutral interactions reduce protein expression for proteins that do not have functional role. microRNA protein repression is considered a two-step mechanism. First microRNA binds on the 3’-UTR accounting for a moderate 2-fold change decrease in mRNA

translation. From this moment on, protein synthesis by ribosome gradually reduces, reaching a final 10-fold repression (Bartel, 2009). This model takes in account AGOII conformational changes and the 3'-end pairing, which might explain why 6-mer bindings are also a possible alignment.

Major rules that govern miR-mRNA interactions are based on sequence homology and conservation between species. A number of different open source bioinformatic software systems have been developed to identify possible targets for specific miRs. Assumptions regarding binding probability are based on experimental evidence of microRNA-mRNA interactions (Agarwal, Bell, Nam, & Bartel, 2015). microRNAs showing a high level of conservation between species have been observed to be more likely to effectively repress mRNA translation. microRNA-target interactions are classified on the basis of the type of interaction between miR core sequence and mRNAs 3'-UTRs. microRNA-mRNA recognition results from a match between these two sequences, where the position 1 and the last match shows to be more important. Thus, binding nomenclature states 8mer and 7mer interactions accounting for matches in position 2-8; 7-mer A1 accounting for 2-8 match position followed (as match in the last nt) by an adenosine in the mRNA sequence and then 6-mer with 2-6 base pair complementarity (rarely taken in account) (Agarwal, Bell, Nam, & Bartel, 2015). Another important determinant which can influences positively microRNA action is the supplementary 3'-pairing. When a 7 or 8-mer interaction presents also a 3 base pairing, it has more probability to repress that target (Bartel, 2009). This latter mechanism results in more stable mRNA binding to the miRISC. During classical miR:MRE without mismatches, the binding in position 2-8 is strong enough to trigger mRNA degradation.

As mentioned above, microRNAs participate in a number of biological process, and it is now agreed that microRNA expression profiles are cell and organ specific. As a consequence, a microRNA could affect different targets depending on the tissue studied. Moreover, it appears that microRNAs possess paracrine and autocrine functions. Because of their small size, microRNAs are more resistant to endonucleases, and they can be found either complexed with exosomes or free in the tissue environment. Although it is not totally clear how this affects the tissue transcriptome, microRNAs complexed with exosomes appear to participate in cell communication (O'Brien et al., 2018). It has been postulated that through distribution through the circulation microRNAs can affect distant organs, however this mechanism might

be true only for body compartments in close proximity. In lungs, capillary-alveolar epithelial cross talk seems an interesting possibility that can be applied to microRNAs. The progress in this understanding is highlighting the possibility to use microRNA to diagnose diseases, based on microRNA expression variance. Tests based on microRNA profiling, from blood serum or bronco-alveolar lavage, have produced interesting results for microRNAs as diagnostic parameter in a wide range of diseases (G. Yang et al., 2015). As mentioned, miR-21a and miR-155 were found upregulated in broncho-alveolar lavage from patients affected by IPF, while miR-34a was found downregulated in patients affected by lung cancer. However, to develop diagnostic applications, miR profiling in large cohorts are necessary to establish the actual predictive capability of those tests. This diagnostic possibility becomes an interesting possibility to apply to lung fibrosis pathology, in particular for early stages of the disease, when the fibrosis is more reversible.

1.10. Antifibrotic Therapies

As mentioned in the first chapter of the whole spectrum of lung fibrosis, IPF appears the most resistant to treatment. IPF is resistant to all major antifibrotic treatments, and current drugs only reduce disease symptoms, and in some cases, slow disease progression(Fujimoto et al., 2015). There are currently no treatments that are able to revert disease outcome, although to some extend fibrosis appears to be reversible. However, depending on the stage of disease the response can vary dramatically. For more severe cases, the only successful therapy is lung transplantation (Fujimoto et al., 2015). However, lung transplantation is an invasive and risky procedure, which can result in transplant rejection. Therefore, it is a strategy to consider only for high risk cases.

One of the main reasons why antifibrotic therapies are not successful in IPF is because of its unknown underlying cause. The removal of causal factors resulted in disease amelioration in several similar lung fibrotic phenotype(Fujimoto et al., 2015). IPF has long been classified as an inflammatory-related disease, which explains why the first treatment for IPF was with corticosteroids and other immunosuppressives. One example is represented by the failure of a therapy using prednisone and azathioprine with or without NAC (N-acetylcysteine). Unfortunately, this therapy led to 23 cases of premature hospitalization and did not show any disease amelioration (King et al., 2000).

Pirfenidone and Nintedanib are at the moment approved for the treatment of IPF and other lung fibrotic diseases in the EU, Japan, and the USA. Pirfenidone is a low-molecular-weight compound that showed anti-inflammatory and antifibrotic effects, with inhibition of fibroblast proliferation, collagen biosynthesis and reduction in the positive TGF-ß feedback effect (Troncone et al., 2018). Nintedanib blocks the activity of VEGF and FGF, resulting in improved lung respiratory function. These two compounds have been also compared for their efficacy by the FDA, which reported that Nintedanib showed a stronger effect against acute symptoms, while Pirfenidone improved survival time (Fujimoto et al., 2015).

Interestingly, new leads using monoclonal antibodies (mAb) against profibrotic proteins might be more successful strategies, of note is a mAb targeting CCN2/CTGF which is in phase II clinical trials for IPF (FDA). It is still necessary to develop new effective therapies to improve the quality of life of patients affected by lung fibrosis. The strategies currently employed have benefitted from a better understanding of the molecular mechanisms involved in lung fibrosis. Examples of this are represented by monoclonal antibody and synthetic nucleotide therapies, including miRNA, siRNA, Crisper/Cas9, Tales; which might represent the future of pharmacology (Ramazani et al., 2018). However, most of those novel drugs have so far failed in clinical trials, due to differences between animal models and humans.

microRNAs represent a good strategy for diseases that that affect parts of an organ, such as fibrosis or cancer. In cancer an intra-tumoral injection of miRNA directly into the pathogenic site could enhance target specificity, efficacy and minimize side effects (Hanna et al., 2019). microRNAs have been shown to be differentially expressed during fibrosis progression and in many other pathologies such as cancer, diabetes, neuropathy. Moreover, drugs used in clinical practise against cancer, such as cisplatin or doxorubicin show a response in a set of microRNAs, which have been identified at the basis of drug resistance to those systemic drugs. Moreover, as many of those compounds are considerably toxic a resistance can worsen the clinical outcome. microRNA repression activity correlated to drug resistance have been explained by inhibition of ATP-binding cassette proteins (ABC). Drug resistance to cisplatin, widely used for non-small lung cancer adenocarcinoma, through miR-495 repression to ABCG2 protein, involved in drug trafficking. (Hanna et al., 2019). Although a promising possibility, none of the microRNAs at the moment have passed to phase III clinical trials, also for evaluation in the cost and profit in drug development, as for miR-21 (RG-012) used to cure

Alport syndrome, which is a fibrosis related kidney disease and suspended for apparently no scientific reasons (Ivan G. Gomez et al., 2015). However, there are promising results from mirmimic miR-34 for the treatment of liver and lung cancer, mirmimic miR-29 for scar tissue (and maybe fibrosis); and antagomir strategy using LNA-based miR-92 for a broad range of cancers. Of note microRNA therapy for mesothelioma represents a promising possibility to cure one of the most lethal diseases (Hanna et al., 2019). The main issues are possible off-target effects, possibility to inhibit RNA binding protein motifs, long-terms effects, effective absorption and distribution, and Toll-like receptor activation. However, because the lung is a highly vascularised tissue, miR Adsorption, Distribution, Metabolism and Excretion (ADME) is probably less of a problem in the lung than in many other tissues. Another option for effective drug delivery to the lung is the use of aerosols, which might be a future strategy for microRNA treatments. Interestingly, non- invasive inhalation of polyplexes formed by mRNA complexed with hyperbranched polyesters were adsorbed by lung epithelial cells and expressed in mouse lung lobes (Patel et al., 2019). Considering that microRNAs are at least 10 times smaller in nucleotide number compared to mRNAs, drug production might be even easier for miRs.

1.11. Aims

There is currently no treatment for IPF that can cure the disease or stop progression. It is therefore essential to identify novel targets for the development of new drugs. microRNAs might be a potential novel strategy to treat IPF and other types of fibrosis. Therefore, the overall aim of my thesis was to identify microRNAs that can be targeted to cure or stop progression of IPF. The achieve this, I addressed the following specific aims:

Aim 1: Analyse the expression patterns of microRNAs in the Bleomycin model of IPF.

Aim 2: Study the effects of the microRNAs identified in Aim 1 in *in vitro models* of fibrosis.

Aim3: Study the effects of extracellular matrix composition, mechanical forces and ageing on expression of the microRNAs identified and fibrosis-related-mRNAs in *in vitro models* of fibrosis.

Aim 4: Test miRmimics and antagoMirs for the most promising miRs identified in the first two aims as treatments for IPF using the Bleomycin model of lung fibrosis.

2 Materials and Methods

2.1 Reagents

Table 2.1. Reagents

Reagent	Catalogue number	Company
Alexa Fluor 488	A32723	Life technologies, USA
Alexa Fluor 555	A32727	Life technologies, USA
Alexa Fluor 594	A32740	
Blocking buffer	(TBS)927-50010	LICOR, UK
Chloroform	C2432	Sigma Aldrich, UK
Collagenase, type 1a	C9891	Sigma Aldrich, UK
Custom miRIDIAN Hairpin Inhibitor	MIMA000530	Dharmacon, GE, USA
Custom miRIDIAN MIMICS	MIMAT000530	Dharmacon, GE, USA
Cutom miRIDIAN Negative Control	IN-001005-01-50	Dharmacon, GE, USA
DMEM	21885025	Gibco, UK
DMEM F-12	D9785	Sigma Aldrich, UK
DMSO	0231	VWR, USA
Fetal Bovine Serum	S1810	Biowest, USA
EDTA	E6758	Sigma
Ethanol Absolute	E7023	Honeywell, USA
Ethanol (histology)		Fisher scientific
EvoScript Universal cDNA Master	07912455001	Roche, Switzerland
Glacial acetic acid	305238	Scientific Laboratory Supplies, UK
HBSS	14025	Life Technologies, USA
HEPES	H3874	Sigma Aldrich, UK
Isopropanol	278475	Sigma Aldrich, UK
Lightcycler 480 probes master	04887301001	Roche, Switzerland
Lipofectamine 2000	11668019	ThermoFisher, USA
miRScript II RT Kit	218161	Qiagen, UK
miScript miRNA Inhibitor (antagomir)	219300	Qiagen
miRScript Negative Control (scramble)	1027271	Qiagen, UK
miScript miRNA Mimic	219600	Qiagen, UK
miScript SYBR Green PCR Kit	218076	Qiagen, UK

Neutral buffer formalin	HT501128	Leica, UK
Non-immune goat serum	S-1012-50	Vector, USA
Paraformaldehyde	#P6148	Sigma Aldrich, UK
PBS	D8537	Sigma Aldrich, UK
Penicillin/Streptomycin	P4333	Sigma Aldrich, UK
Qiazol	79306	Qiagen, Germany
SDS	L4509	Sigma Aldrich, UK
Sodium hydrogen carbonate	S6014	Sigma Aldrich, UK
Sirius Red (Picric Acid)	STPSRPT	StatLab
Recombinant TGF-β1	100-21	Peprotech, USA
Tween 20	P7949	Sigma Aldrich, UK
Vectashield mounting medium with DAPI	H1200	Vector, USA
Xylene	X0250	Fisher scientific, USA

2.2 In vivo Procedure

2.2.1 Animal information and power calculations

C57BL/6J were purchased from JAX, male mice were used for all *in vivo* procedure, while female mice for all *in vitro* procedure. C57BL/6J employed for the Bleomycin model of lung fibrosis in chapter 3 were housed in a pathogen free facility; C57BL/6J used for miR-21a-5p inhibition in the Bleomycin model of lung fibrosis in chapter 6 were housed in the Centre for Preclinical Imageing (CPI) facility, both at the University of Liverpool. All procedures were in accordance with the Animals (Scientific Procedures) Act 1986 and the EU Directive 2010/63/EU and after the local ethical review and conducted under the PPL of Prof. Bou-Gharios after the approval of Liverpool University's Animal Welfare and Ethical Review Body (AWERB).

Sample size for both *in vivo* experiments were conducted in order to find the optimal number of animal to use, as requested by the 3R (replacement, reduction, and refinement). Power calculation for sample size were performed using OpenEpi an free on-line platform for calculation as advised in "How to calculate sample size in animal studies?", published by Journal of Pharmacology and Pharmacotherapeutics (Charan & Kantharia, 2013). Although in

this publication authors advise a sample size for each group equal or higher than 10, the level of confidence should be the most important value to take in consideration. However, this value for novel drug, as a treatment with microRNA, should be quite low, to prevent an unnecessary pain to an animal.

For Bleomycin experiment in chapter 3, I used a level of bilateral confidence of 90% as the method was efficient in reproducing the desired phenotype. As the experiment aim was to reproduce fibrosis in term of progressively increase of disease hallmarks, an expose to non-expose ratio equal to 0.25 was used. A percentage of outcome in the control group was set at 3% as no treatment was administered in control group, as PBS being a liquid might induce a parenchymal damage.

Table 2.1 Power calculation used for Bleomycin experiment

Bilateral confidence	90%
Power	80% (as adviced by OpenEpi)
Expose/ not Expose (ratio)	0.25
Not Exposed with outcome	3%

OpenEpi calculated a total number sample size of 19 mice divided in 15 for treated group (Bleomycin) and 4 for control group.

For miR-21a-5p mirmimic and antagomir treatments the confidence was set as 25%, as literature, *in silico, and in vitro* evidence suggested changes in the system due to the treatment. Not exposed versus expose ratio was set at 0.5 as it was necessary to evaluate miR-21a background effect. Therefore, the percentage adverse event in control group was set at 20% as treatment were non-toxic at 2 mg/mL (from Dharmacon customer service).

Table 2.2 Power calculation used for miR-21a experiment

Bilateral confidence	25%
Power	80% (as adviced by OpenEpi)
Expose/ not Expose (ratio)	0.33
Not Exposed with outcome	20%

OpenEpi calculated a total number sample size of 12 mice divided in 4 for treated group (Bleomycin) and 4 for control group

2.2.2 *Bleomycin model of lung fibrosis*

As mentioned in the previous chapter, Bleomycin is not the only method use to induce fibrosis in experimental models. Administration of silica or asbestos, irradiation of gamma rays, infections with adenovirus overexpressing TGF-ß, or other techniques are equally valuable methods able to reproduce a fibrotic phenotype. All of them present benefits and drawbacks, however as the model was already established by Dr Ke Liu, from Bthe ou-Gharios group, it has been easier to follow his method rather than optimise a new one.

Bleomycin is an antibiotic produced by *Streptomyces verticillus* and was discovered by the Japanise scientist Hamao Umezewa in 1969. Bleomycin induces cell death through single and double strand DNA breaks. Bleomycin activity is particularly high in lung due to a lack in the inactivating enzyme, Bleomycin hydrolases, which trigger an higher cell death in lung parenchyma (Mouratis & Aidinis, 2011). The main benefit in the use of Bleomycin is the low cost of the entire procedure, the reproducibility in a wide range of model organism (from mouse to primates). Bleomycin allows to reproduce a fibrotic phenotype in short therapeutic window, of 14-28 days, despite the induction of fibrosis is more acute than chronic, as in all ILDs with fibrotic characteristic. Moreover, Bleomycin has been extensively reported that in rodents the fibrotic Bleomycin-induced phenotype is rescued after 28 days, consisting in the major limitation of this technique (Mouratis & Aidinis, 2011).

The second thing that was important to consider was the route of administration, as in an interesting paper from 2006, H. Lakatos and collaborators compared the efficacy of

oropharyngeal and intratracheal administration routes to induce fibrosis (Jun & Lau, 2018). Although in this study researcher used silica instead of Bleomycin, this paper highlighted for oropharyngeal route a localization of damage in distal lung, while intratracheal administration was more effective in the proximal lung. (Lakatos et al., 2006). Intratracheal administration is also a more complex technique, as the catheter is surgery installed might trigger pathogen infections, which will alter the response to a drug, as example. Therefore, oropharyngeal administration was used to induce a lung fibrotic phenotype in experimental animal.

7 mg of Bleomycin was dissolved in sterile PBS to achieve a concentration of 1 mg/mL and stored at -20°C. Anesthetised mice were suspended by the cranial incisors on a thin rubber band, animal tongue was gently extracted in order to close through forceps and the Bleomycin was administered in the posterior pharynx at the base of the tongue (fig. 2.1). A single dose treatment of Bleomycin was used in all procedure, the volume of drug to administer was calculated based on weight in order to reach a concentration of 0.15 mg/mL for each experimental animal. As Bleomycin referred to a moderate procedure in ASPA for the level of pain induced in the experimental animal, I monitored at different intervals changes in body weight (see appendix 1) and any sign of distress.

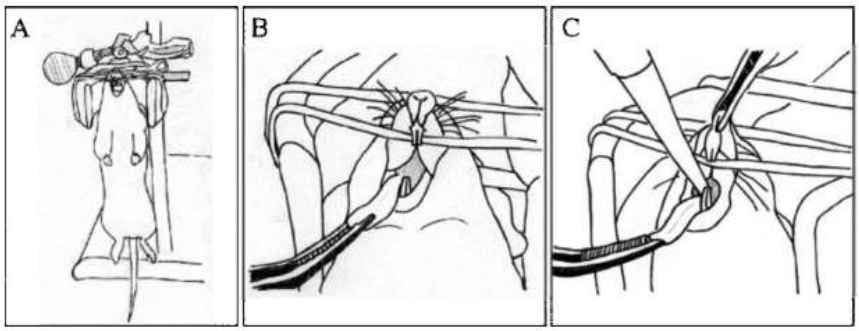

Figure 2.1 Methodology for oropharyngeal aspiration. Anesthetised mice were suspended by the cranial incisors on a thin rubber band, animal tongue was gently extracted in order to close through forceps and the Bleomycin was administered in the posterior pharynx at the base of the tongue.

2.2.3 microRNA treatment in mice

Customised sequences and hairpin inhibitor from the miRIDIAN product line (GE Dharmacon) were used for miR-21a gain and loss of function in the *in vivo* model of Bleomycin induced lung fibrosis. Customised sequences contained a phosphonothioate group (containing a sulphite group instead of a phosphoric group in nucleic acid backbone) in the terminal ends of the sequence, a cholesterol group at 3'-RNA (synthetic) and also a 2-OMe substitution. mirmic sequence referred to miR-21a-5p, while scramble sequence was random generated and as the sequence used did not match with any other miRNA. miRIDIAN hairpin inhibitor consisted of a double strand sequence able to inhibit miR-21a-5p expression, which present specific chemical changes that are covered by industrial secret.

ID	Sequence	modification	Isolation method
Scramble	5'-C*A*GUACUUUUGUGUAGUA*C*A*A-3'	* = P > S, 3'Chl , 2'OMe	HPLC/Desalt
mirmic	5'-U*A*GCUUAUCAGACUGAUG*U*U*G*A-3'	* = P > S, 3'Chl , 2'OMe	HPLC/Desalt

Mice received a 2 µg/mg dose of microRNAs every 7 days, according to treatment half-life. microRNAs were injected *via* tail vein by Dr. Sharkey from CPI unit from University of Liverpool facility.

Mice were preconditioned with miR-21a treatment at time starting of the experiment (day 0), and at day 8, while Bleomycin was administered at day 2 as described in 2.2.2. After 18 days from the starting of the procedure mice were sacrificed (fig. 2.2).

Figure 2.2 Treatment timeline. microRNAs treatment for miR-21 mirmimic, antagomir and scramble were performed before the administration of Bleomycin in order to reach a concentration in the animal bloodstream before the acute damage induce by Bleomycin. The day after (day 1) Bleomycin was administered as described in 2.2.2. To maintain an effective miR-21a concentration, another microRNA treatment was performed at day 8. Mice were culled after 18 days from the first treatment and 17 days after the treatment with Bleomycin, to avoid a rescue of phenotype (which is usually 21 days after the single dose of Bleomycin).

2.2.4 Dissection and inflation of lung

Mice were culled through intraperitoneal injection (IP) of 0.2 mL of Pentobarbital, then the abdominal cavity was opened using sterile scissors and forceps and skin was removed. Liver portal vein was cut, and diaphragm removed. Chest ribs were then opened without touching lung and heart through transversal cutting using blunt scissors. Neck muscles were removed leaving trachea opened. A sterile string was then passed underneath and then up tracheal space through the use of blunt forceps and wrapped around tracheal rings, leaving an opened knot. A blunt syringe filled with air was then placed in the tracheal space and the knot was closed around syringe blunt needle. Air was then pushed in the lung space for the procedure used in Chapter 3; O.C.T. at 30% v/v Sucrose/PBS was used instead for procedure in Chapter 6. Once the lung was inflated, syringe was gently removed, and the knot closed. Lung was dissected out from the dorsal cavity as inflated lung. Knotted lungs filled with air (Chapter 3) were placed in a 7 mL bijou containing 4°C PBS supplemented with 3% of Potassium Iodine and imaged by µCT *ex vivo.* Post-caval lobes were dissected out for histology while all other lobes were stored at -80°C for RNA extraction. Samples used for histology were placed in PBS supplemented with 4% of PFA and placed at 4°C. After less than 24 hours, PBS at 4% PFA was discarded in a dedicated bin under a fume hood and replaced with cold 70% Ethanol.

The left lobe was dissected out from lungs filled with O.C.T.at 30% v/v of Sucrose/PBS (Chapter 6) for RNA extraction while right and post-caval lobes were snap frozen with Iso-Pentane and stored in -80°C and used for Histology.

2.2.5 Ex vivo lung imageing with µCT scan

Lung filled with air and in PBS supplemented with 3% of Potassium Iodine and scanned by µCT using Skyscan1272 system (SKYSCAN, Belgium) with a resolution of 20 µm, using a 0.25 mm aluminium filter and 0.3° rotation step. Images were reconstructed using Skyscan "NRecon" software (SKYSCAN, Belgium), which allows scans reorientation and to define a volume of interest for the analysis. Using "CTAN" software (SKYSCAN, Belgium) the data set is then analysed with a macro measuring the lung volume. *Ex vivo* scans allows to produce tomographic images extremely precise, due to an accuracy of the order of micrometres. However, for lung application *ex vivo* CT has limitation due by a considerable intrasample variability as the amount of air in the explanted lung can dramatically vary during the dissection.

2.2.6 In vivo live imageing with µCT scan

Mice used for the experiment conducted in Chapter 6 were imaged by *in vivo* µCT using a Quantum GX-2 system (PerkinElmer, USA). *In vivo* µCT allow to produce images from a living organism, which are key in preclinical studies, as they provide evidence in real time on the effectiveness of a treatment. Mice were imaged at day 0, at day 8 to obtain information on the early stage of disease, and at 12 and 18 for the late stage of disease. The machine produces two image one; regarding to inspiration and expiration phase of each breathing cycle, producing a volumetric image, representing the lung in all three dimensions through synchronising of single images collected during inflation and expiration.

An X-ray filter of copper (Cu) 0.06mm and aluminium (Al) 0.5mm was used for lung scans. Live CT view allowed then to position the camera in the region of interest before the starting of the CT scanning. Lungs were scanned with a 50 µm voxel size and at high speed (4 minute). Post-scan sorting of respiratory phases was used to produce inhalation and exhalation images. Once the scan of a lung was finished, mice were acclimatised in a dedicated

box at 37°C for recovery.

2.3 Histology

2.3.1 Paraffin wax histology

Lungs fixed with PBS at 4% of PFA were after dehydrated using Et-OH at 70% and embedded using Leica EMTP6 tissue processor following the following protocol:

Table 2.4 Processing protocol using Leica EMTP6 tissue processor

Reagent	Processing time	Temperature	Drain time (seconds)
70% Et-OH	30 min	Ambient	80
90% Et-OH	30 min	Ambient	80
100% Et-OH	10 min	Ambient	80
100% Et-OH	10 min	Ambient	80
100% Et-OH	10 min	Ambient	80
100% Et-OH	15 min	Ambient	80
Xylene	10 min	Ambient	120
Xylene	20 min	Ambient	120
Xylene	30 min	40°C	120
Wax	4 h	60°C	140

Lungs were then embedded in wax using a Leica EG1150 Tissue Embedder with a caudal orientation. Sections of 5 µm thickness were obtained using a RM2265 Leica microtome.

2.3.2 Cryogenic histology

Lungs filled with O.C.T. at 30% v/v of Sucrose/PBS were place in -20°C 20 minutes before cryostat and then cut with a Leica CM1850 cryostat producing slides of 5-7 µm.

2.3.3 Picosirius red Staining

PFA fixed sections were dewaxed through Xylene for 5 minutes and hydrated through decreasing ethanol concentrations, while cryosections were incubated for 1 minute in PBS.

PFA sections were incubated with Weigert's haematoxylin for 8 minutes allowing nuclear staining. Slides were then washed in running tap water. This step was not used for Cryosections as the procedure destroyed tissue architecture. Slides were then incubated for 1 hour in Picrosirius red, which colours collagen fibres. Sections were washed through two dips in water with 1% of Acetic Acid. Slides were dehydrated in ethanol, cleared in xylene and mounted in a resinous medium with a coverslip. Slides were then incubated for 1 hour in a fume hood at room temperature to evaporate traces of xylene.

2.3.4 Histology imaging

Slides were imaged using an Olympus BX60 microscope with or without a polarized filter (Nikon) as Brightfield microscopy and polarized light microscopy. Slides were imaged at 4X, 10X and 20X magnification with or without polarised filter. Polarised light was obtained positioning the polarising filter at 90° orientation. This technique was used as it allows to image repeating structures with a refractive index, such as collagen fibres (Wolman & Kasten, 1986).

Quantitative measurement of the dichroism was calculated through ImageJ Fiji using a macro, which measured the area of colour developed by dichroisms (see appendix 2).

2.4 Cell culture

2.4.1 Immortalised cell lines

2.4.1.1 A549

A549 adenocarcinoma alveolar lung cells were purchased from the American Type Culture Collection (ATCC) cultivated with DMEM F-12 (Sigma-Aldrich) supplemented with 10% foetal bovine serum (FBS) (Gibco) and 1% Penicillin/Streptomycin (Sigma-Aldrich) in a humidified incubator at 37°C and 5% CO_2. Cells at passage lower than 20 were defrosted from liquid nitrogen tanks and first pre-cultured in a T75 flask for 3-4 days until confluency was reached. Then, cells were split in a 1:10 ratio.

Cells were washed with sterile Phosphate buffered saline (PBS) to remove any trace of conditioned media and incubated with 1.5 mL of TripLE express (Gibco) per T75 flask for cells detachment for 5 minutes. Subsequently, cells were visualised at phase contrast microscope (Nikon TiE) to confirm surface detachment. Cells were washed using 7-8 mL of complete DMEM F-12, used to neutralise TripLE express action, and resuspended and collected in a 15 mL tube (Falcon). Cells were spun down at 300 g for 5 minutes, allowing pellet formation. After supernatant removal, cells were resuspended in 10 mL of complete DMEM F- 12 and used for cell expansion or in experiments.

2.4.1.2 MRC5

MRC5 immortalised lung fibroblast cell lines at passage 5 were kindly donated by Dr Kazuhiro Yamamoto (Institute of Ageing and Chronic disease) and after amplification were stored in liquid nitrogen. MRC5 at passage lower than 10 were cultured with DMEM (Gibco) supplemented with 10% FBS and 1% Penicilin/Streptomycin in a humidified incubator at 37°C and 5% CO_2. Cells were cultured until confluency was reached and then washed with Phosphate buffered saline (PBS) to remove any trace of conditioned media and incubated with 1.5 mL of TripLE express (Gibco) per T75 flask for cells detachment for 5 minutes. Subsequently, cells were visualised at phase contrast microscope (Nikon TiE) to confirm surface detachment. Cells were washed using 7-8 mL of complete DMEM F-12, used to neutralise TripLE express action, and resuspended and collected in a 15 mL tube (Falcon). Cells

were spun down at 300 g for 5 minutes, allowing pellet formation. After supernatant removal, cells were resuspended in 10 mL of complete media and used for cell expansion or in experiments.

2.4.2 Primary cells

2.4.2.1 Primary mouse lung fibroblasts culture

Primary mouse lung fibroblasts were cultured in complete DMEM in a humidified incubator at 37°C and 5% CO_2. Lung fibroblasts after 5 days of culture were transferred to a T75 flask (see 2.4.3). After overnight incubation cells reached full confluency of the flask and were then used for further experiment. Cells were sub-cultured according to 2.4.1. Cells used for all *in vitro* procedure were then at a passage 2.

2.4.2.2 Primary mouse lung fibroblasts isolation

Three different methods were attempted to obtain the best fibroblasts cellular yield.

For the first method slices of around 1 mm^2 of lung tissue were cut. Slices were placed in a sterile incubator at 37°C and 5% CO_2 with 1-2 mL of complete DMEM for 30 minutes. Media volume was increased until reaching 7-8 mL and half replaced every 1-2 days after first incubation (fig 2.3), until fibroblasts had grown out of the tissue.

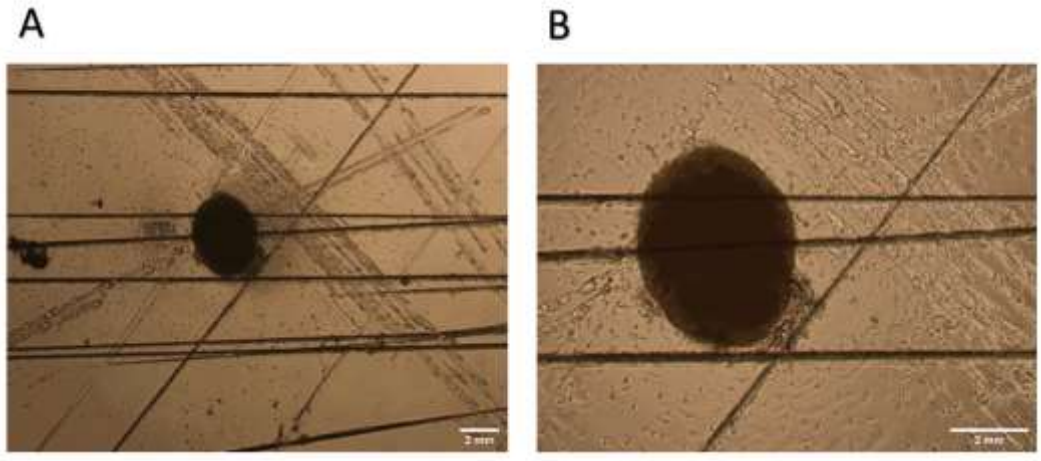

Figure 2.3 Possible primary fibroblasts culture obtained using the second method described (see text). Cells at 4X magnification (A) and at 10X magnification (B). Please note that we refer as "possible primary fibroblasts culture" as we did not test the efficiency of this isolation. Images were obtained using phase contrast microscopy. [scale bar 2 mm].

Next, I tried a method developed by Seluanov and collaborators, but using collagenase instead of Liberase (Seluanov, Vaidya, & Gorbunova, 2010). Liberase is a mixture of collagenase and other proteases which was developed to obtain a better cell release from ECM. However, as it was reported that there is no change in terms of cellular yield, using liberase or collagenase (Hyder, n.d.), we used collagenase. Moreover, I compared Seluanov method of isolation with another method provided by Dr Vanja Pekovic-Vaughan (IACD). The substantial difference between the two methods lay in the use of Hanks Buffer supplemented with at 0.47% of $NaHCO_3$, 1% of Hepes buffer and 1% of Penicillin/ Streptomycin and with 10% w/v of Collagenase, instead of using 10% w/v Collagenase in DMEM media. Testing the two methods in parallel showed that after 5 days of culture we consistently were able to obtain a much higher yield using modified Hanks buffer, leading to a fully confluent culture of primary cells (fig. 2.2).

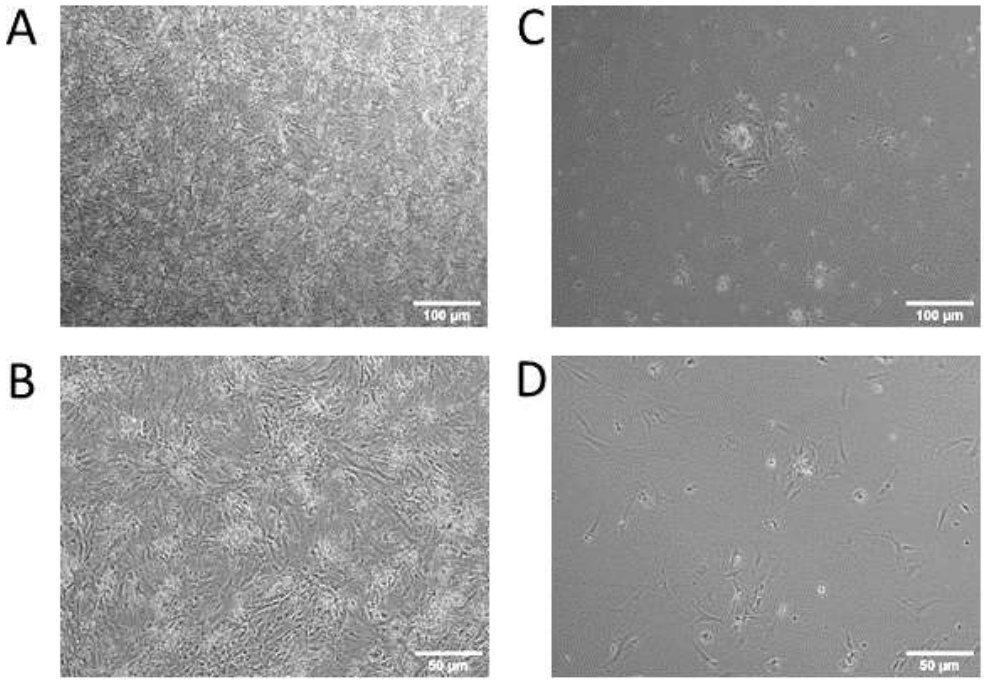

Figure 2.4 Primary fibroblasts isolation methods comparison. Figure shows images from primary mouse lung isolation protocols using the method provided by Dr V. Pekovic- Vaughan (A 4X magnification and B 10X magnification) and Seluanov method (C 4X magnification and 10X magnification). [scale bar 100 and 50 µm].

The method developed from Dr. Pekovic-Vaughan resulted in a better yield and therefore was used for all procedures (fig. 2.2). In detail: lungs were placed in a Petri dishes and dissected to remove hearts and trachea. Using a sterile scalpel, tissues were chopped

producing slices of ˜1 mm^2. The tissue fragments were then incubated for 1.5 h in a modified Hanks buffer supplemented with at 0.47% of $NaHCO_3$, 1% of Hepes buffer 1% of Penicillin/ Streptomycin and 10% w/v of crude collagenase Type 1 (Sigma-Aldric) from Clostridium histolyticum. The Petri dish was then washed with 1-2 mL of the enzyme to obtain the best yield. Cell suspensions after resuspension, were filtered through a 100 µm cell stretcher, to avoid larger pieces in the following isolation steps. Subsequently, the mixture was centrifuged at 300 g for 5 minutes, to obtain a cellular pellet. The cell pellet was resuspended in in complete Hanks buffer, and centrifuged gain at 300g. After centrifugation, the supernatant was discarded, and the pellet resuspended in complete DMEM. The cells were cultured in complete DMEM at 37°C and 5% CO_2 for five days, in order to obtain a fully confluent culture, as shown in figure 2.3. Next, cells were harvested using trypsin, as macrophages are resistant to trypsin digestion. The resulting cell suspension was then spun down at 300 g for 5 minutes and resuspend again in DMEM media at 10% FBS 1% Penicillin/Streptomycin. After 16h of further culture, cells were usually forming a fully confluent T75 culture ready for further applications.

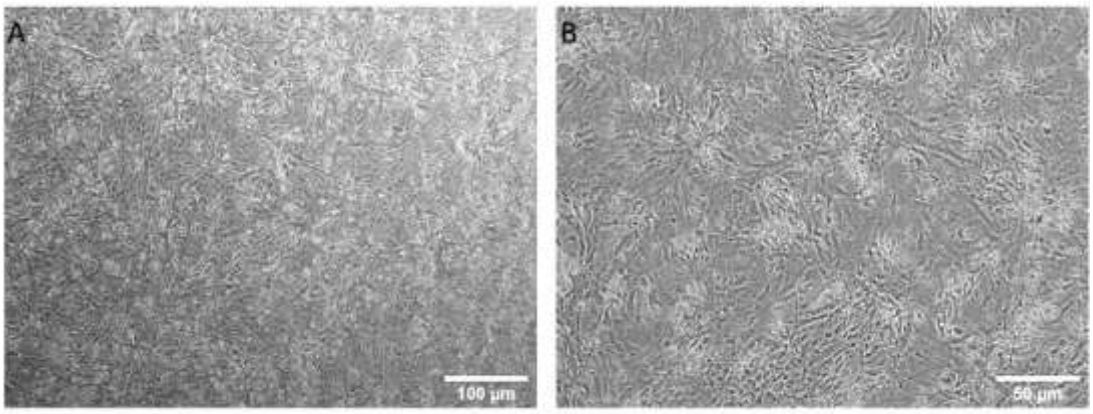

Figure 2.5 Cultured mouse fibroblast isolated from the lung five days after the isolation. Figure A shows the culture at 4X magnification while B is showing 10X magnification. Images were obtained using phase contrast microscopy. [scale bar 100 and 50 µm].

To characterise the cells isolated, $0.5X10^3$ lung fibroblasts were cultured on sterile 25mm circular coverslips in a 12 well plate for 1.5 days in complete DMEM at 37°C and 5% CO_2. Once cultures were reaching 50-60% confluency of the coverslip, medium was removed, cells washed with PBS, and the cells fixed for 10 minutes with cold 4% v/v of paraformaldehyde in PBS. Cells were subsequently washed 3 times for 10 minutes with sterile

PBS at 4°C. Fixed cells were then stored at 4°C to avoid protein degradation and used for immunocytochemistry.

As fibroblasts do not possess a unique marker that allows to distinguish this cell population, a panel of 3 positive and 1 negative marker were used (tab. 2.3). α- Smooth actin, vimentin and HSP/47 were used as positive markers as these are highly expressed in fibroblasts, while F4/80 was to verify macrophage/monocyte contamination.

Table 2.5 Table 2.4 Primary and secondary antibodies list used to validate primary fibroblasts isolation.

Ab Target	HOST	Concentration used	Second Ab
a-SMA	Mouse	10 μg/mL	AF594 Goat anti-mouse
Vimentin	Rat	10 μg/mL	AF555/AF594 Goat anti-rat
F4/80	Rat	10 μg/mL	555 Goat anti-rat
HSP47	Rabbit	10 μg/mL	488 Goat-anti-rabbit

Coverslips were removed from 12-well plates and placed on a parafilm layer and incubated with PBS at 4°C supplemented with 0.5% v/v Tween 20 for 20 minutes to permeabilise fixed cells. Coverslip were then washed with PBS at room temperature. Fixed cells were then incubated with goat blocking serum at room temperature (VECTOR) for 45 minutes. Subsequently, coverslips were incubated overnight (16 hours) at 2-8 °C with one of the primary antibodies shown in Table 1. Primary antibodies were diluted at 1 in 100 v/v in goat blocking serum. After the overnight incubation, coverslips were washed with PBS at 4°C, then incubated with the secondary antibody at 1 in 100 dilution in Goat Blocking serum for 1 hour at room temperature in the dark to prevent loss of fluorescence.

After the incubation with the secondary antibody, coverslips were washed in PBS at 4°C in the dark. After this step, except for mF4/80 immunostaining, a second primary antibody was incubated overnight again to produced double stained specimens. The combination of first and second antibody to evaluate fibroblast markers was based on fluorophore excitation spectrum and species compatibility. Negative control without employing antibodies was used

to measure background fluorescence for vimentin, α-smooth actin and HSP47. Images were produced using a LSM800 laser confocal microscope (Zeisss) at 10X and at 20X magnification. All images with the confocal microscopy were 512 x 512 pixels at 16 bit obtained through a bidirectional scanning of the coverslips.

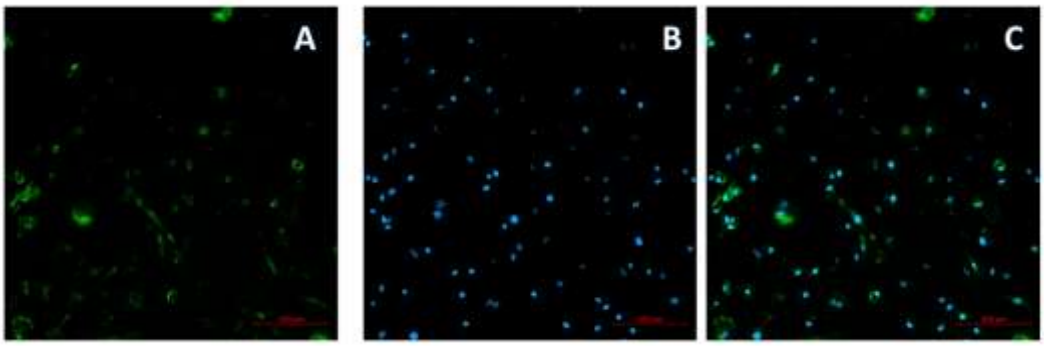

Figure 2.6 Lung fibroblasts isolation efficiency (1): Immunocytochemistry (ICC) from primary Macrophages positive control for F4/80. Macrophages were kindly provided by my colleague Jacqueline Lim, imaged using confocal microscopy with a 20X magnification lens from ZeissLSM800 for: (A) F4/80 conjugated with AF555 in green (A); (D) DAPI for nuclear stain and with DAPI (B); and a merge of the two antibodies used (C) [scale bar = 100 µm].

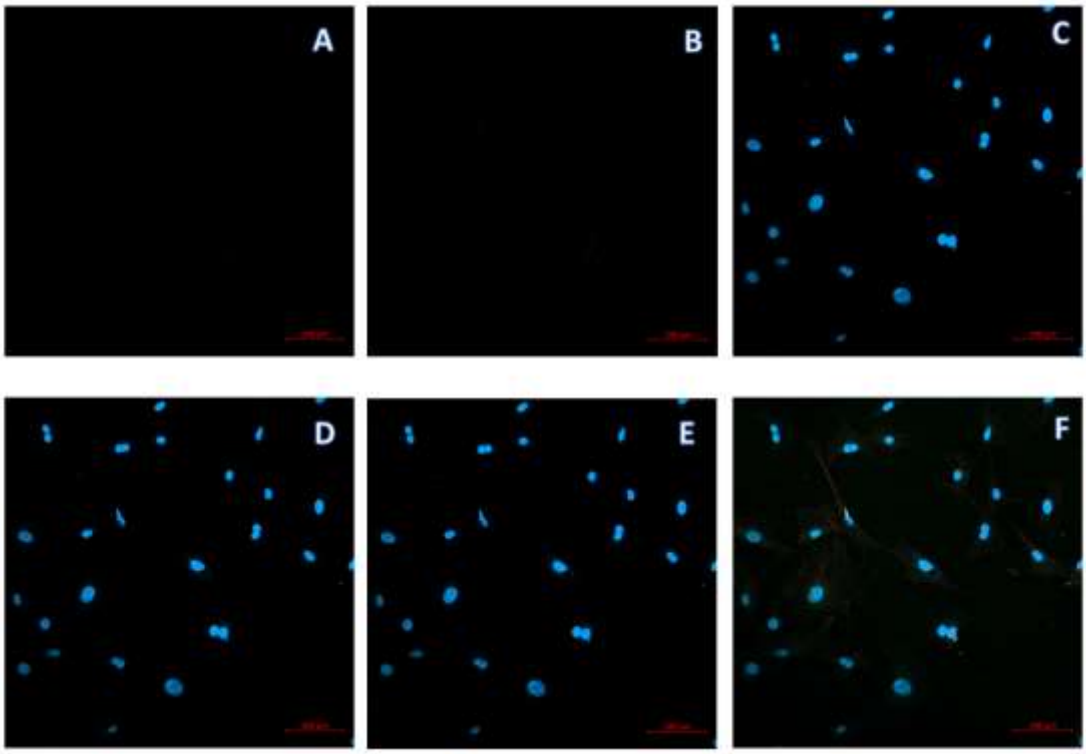

Figure 2.7 Lung fibroblasts isolation efficiency (2): Immunocytochemistry (ICC) from primary lung cells imaged negative control. Primary cells were imaged using confocal microscopy with a 20X magnification lens from ZeissLSM800 for: DAPI for nuclear stain (C); vimentin negative control conjugated with AF555 in green (A) and with DAPI (D); α-smooth actin negative control conjugated with AF594 in red (B) and with DAPI (E); and an overexposed merge of the three antibodies used (F) [scale bar = 100 µm].

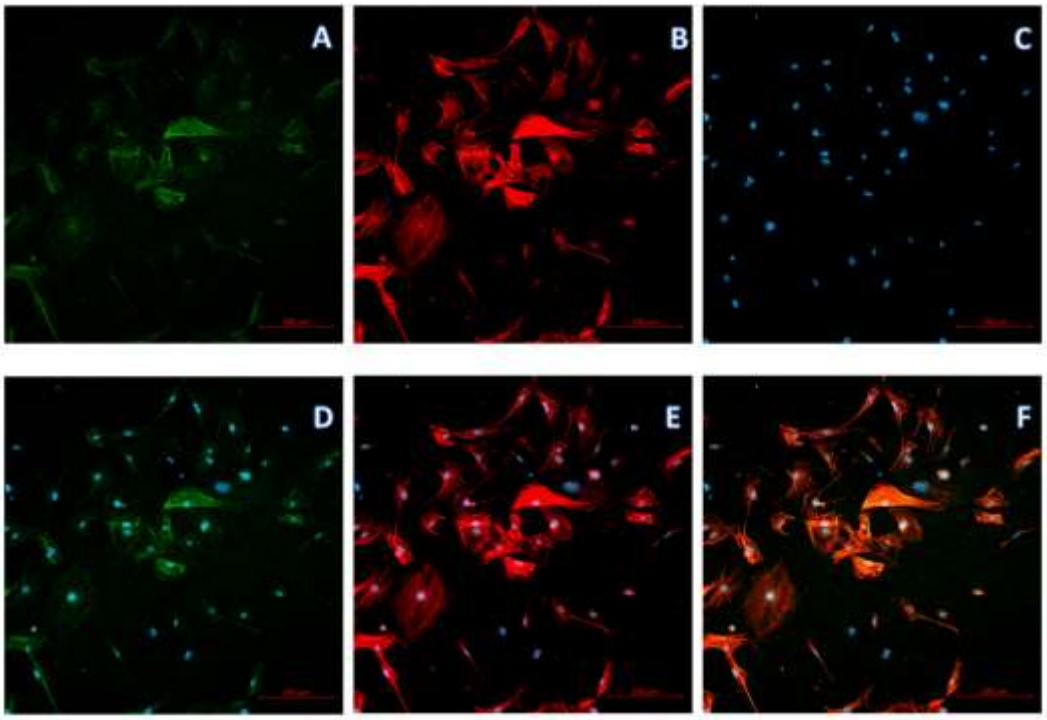

Figure 2.8 Lung fibroblasts isolation efficiency (4): Immunocytochemistry (ICC) from primary lung cells imaged using confocal microscopy with a 10X magnification lens from ZeissLSM800 for: DAPI for nuclear stain (C); Vimentin conjugated with AF555 in green (A) and with DAPI (D); α-smooth actin conjugated with AF594 in red (B) and with DAPI (E); and a merge of the three antibodies used (F) [scale bar = 200 µm].

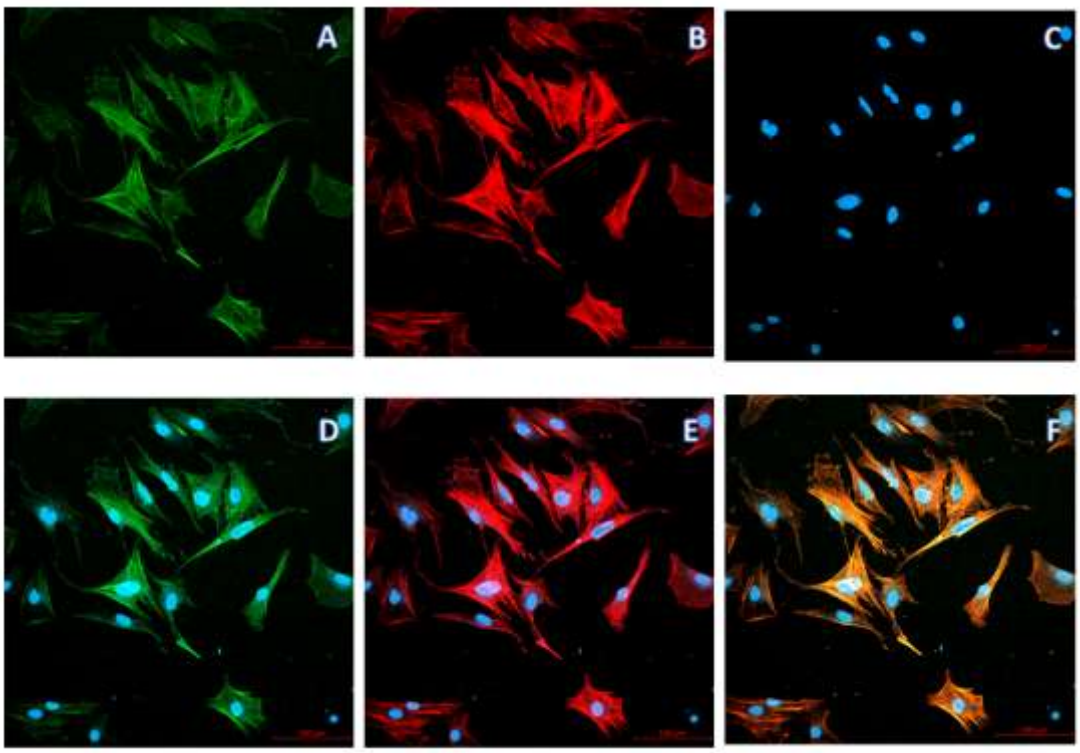

Figure 2.9 Lung fibroblasts isolation efficiency (5): Immunocytochemistry (ICC) from primary lung cells imaged using confocal microscopy with a 20X magnification lens from ZeissLSM800 for: DAPI for nuclear stain (C); Vimentin conjugated with AF555 in green (A) and with DAPI (D); α -smooth actin conjugated with AF594 in red (B) and with DAPI (E); and a merge of the three antibodies used (F) [scale bar = 100 µm].

Primary mouse lung fibroblasts were positively stained for vimentin and α- smooth actin. Both cytoskeleton proteins are considered markers for fibroblasts as expressed in mesenchymal cells. Vimentin is associated with microtubules and with tubulin, whereas α-smooth actin to actin filaments. Primary cells show an abundant cytoskeletal presence for both fibroblast markers, with merged images highlighting a cytoskeletal co-localization (orange colour in fig. 2.8 and 2.9).

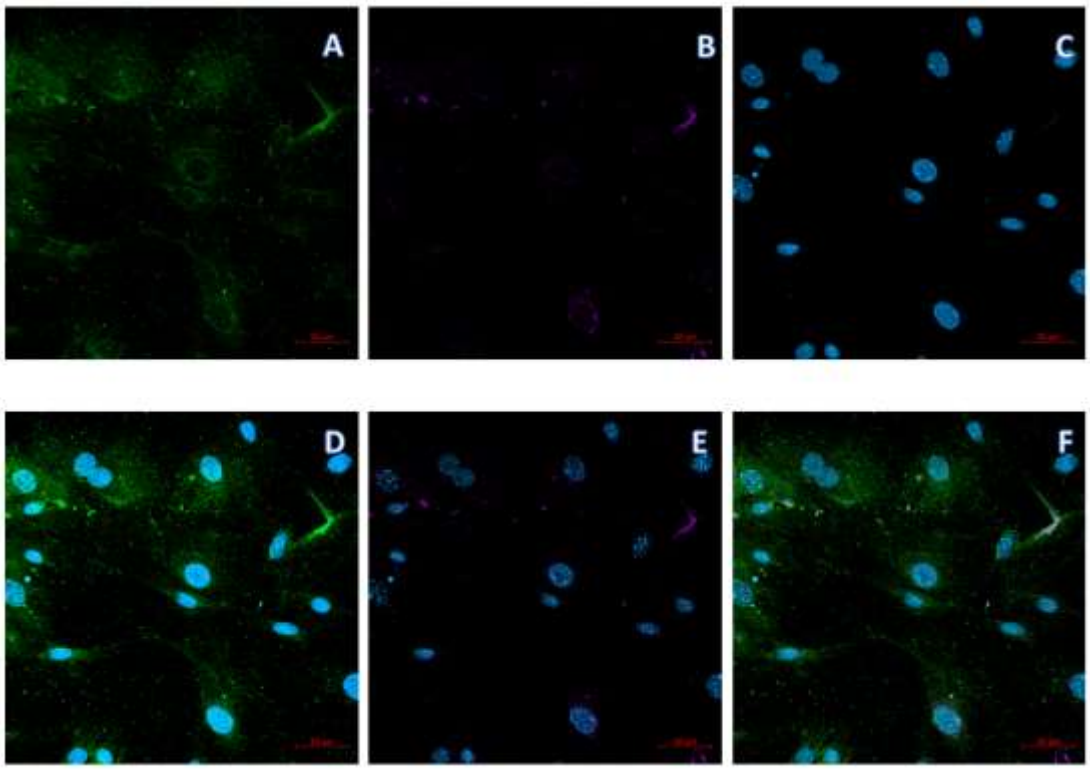

Figure 2.10 Lung fibroblasts isolation efficiency (6): Immunocytochemistry (ICC) from primary lung cells imaged using confocal microscopy with a 20X magnification lens from ZeissLSM800 for: DAPI for nuclear stain (C); Vimentin conjugated with AF594 in green (A) and with DAPI (D); HSP47 conjugated with AF594 in red (B) and with DAPI (E); and a merge of the three antibodies used (F) [scale bar = 50 µm].

HSP47 is a chaperone protein fundamental in collagen α-chain transportation from endoplasmic reticulum, therefore it can be used as marker for mesenchymal cells. Vimentin showed again a cytoskeletal localization, although less bright than in other samples, while HSP47 around nuclei, suggesting the identification of collagen producing primary cells (fig. 2.9).

2.4.3 TGF-ß treatment

TGF-ß is one of the most important cytokines to reproduce experimentally a fibrotic environment. TGF-ß alone is able to induce EMT in epithelial lung cells, and activate fibroblast activation in myofibroblasts. Human recombinant TGF-ß from Peprotech was used for all *in vitro* application as human and murine TGF-ß share more than 80% of sequence similarity in DNA and protein sequence homology (from Blast).

Therefore, the following methodology was used for TGF-ß treatments in A549, MRC5 and primary lung fibroblast. Cells were detached from a T75 fully confluent flask as described in section 2.4.1. $1x10^5$ cells per well were seeded on either RGD-motif or collagen I coated plate purchased from Flexcell. In each experiment, four 6-well plates, paired for each substrate condition, were used at the same time. After 48 hours cells were reaching 60-70% of confluence. Complete media (DMEM for fibroblasts and DMEM F-12 for A549 only) was replaced for 16-18 hours with DMEM or DMEM F-12 (A549) at 1% Penicillin/Streptomycin and 1% of defined serum replacement specific for human (TCH) or mouse (TCM) cells. Next, 3 wells per plate were treated with 2 ng/mL of recombinant TGF-ß and other 3 wells with BSA at 0.1% in PBS. The 2 ng/mL concentration was used as TGF-ß at concentration equal or higher than 10 ng/mL can suppress collagen expression via CUX-1 (Fragiadaki et al., 2011). Moreover, from a trial test I have conducted at the beginning of my PhD it appears that 2 ng/mL was the concentration with less variability in the system (however, data cannot be included in this thesis as this test was performed in 3T3/NIH, with different kit for mRNAs extraction, retro-transcription, and qPCR).

Two 6-well plates out of 4 were placed in a Tension system for cell stretch (Flexcell) in a dedicated sterile humidified incubator at 37°C and at 5% CO_2. Tension was then set at 6% of stretch and at 1 Hz of frequency using a continuous stretch for 6 hours. After completion, the plates were removed from the physical support, imaged using phase contrast microscopy (Nikon TiE), washed with sterile PBS for 2 times and lysed using Trizol, and the lysate collected in a sterile Eppendorf tube and stored at - 80 °C.

2.4.4 Flexcell tension system

The Flexcell Tension system allows coated plates to stretch. Stretch is the percentage of total surface elongation, and it is expressed as percentage of increase from starting state. The main purpose of this experimental procedure was to evaluate stretch contribution to gene expression in a system that include fibrotic stimulation in terms of cytokine and ECM. Flexcells plates surface can be functionalised with ECM components, such as RGD-motif, collagen I or IV, laminin and fibronectin. The experimental plan for this procedure was to evaluate difference in mRNAs due to different ECM coat. Therefore, the effect of collagen over RGD-motif were evaluated, assuming collagen type I coating fibrotic-like. As explained in 1.6, in fibrosis there is an increase in the organ stiffness, due to dysregulation in wound healing repair, which dramatically augments collagen content. Collagen is among protein in the mammalian with the highest Young's modulus (Young's modulus monomer is 7 GPa), therefore a quantitative increase in course of fibrosis might be act as stimulation on expression of gene and microRNA involved in fibrosis (Shoulders & Raines, 2009). The rational in the use of the Flexcell system was to produce interdependent data on the role of collagen and stretch. However, the system cannot provide information regarding tissue stiffness which appears (as mentioned in 1.6) more important than stretch in a context of lung fibrosis. This was a limitation due to the system used.

The Flexcell Tension System is composed by a loading coated post, plates are physically placed and a controlled vacuum pump. Pumps compressing air in the space between the loading post and the coated surface creates the vacuum, which allows to mechanical stretch the culture as indirect movement of the loading post (fig. 2.10). To avoid air leaking, which cause a weaker stretch (as vacuum cannot be created), Vaseline was spread around the physical support. The Flexcell Tension System was inserted in a dedicated humidified incubator, having tubes connected to the vacuum pump outside of the incubator.

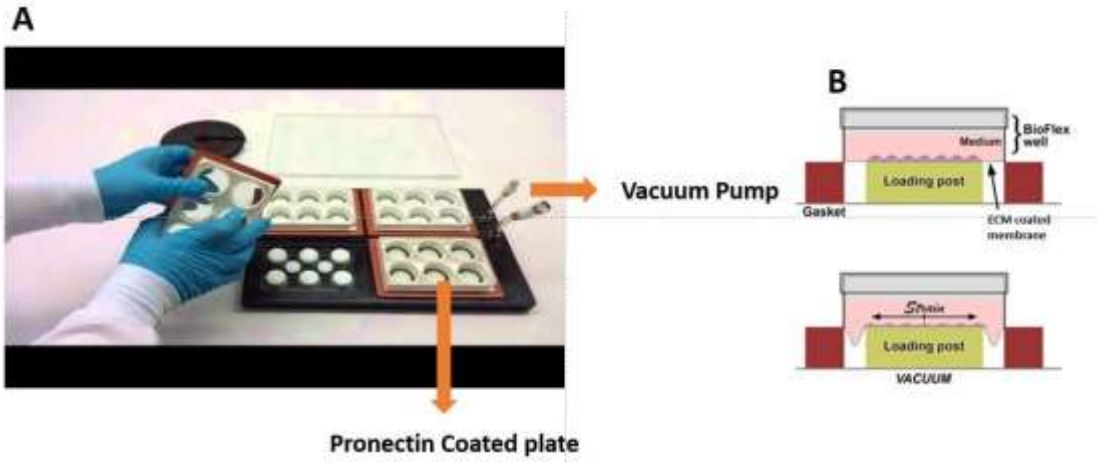

Figure 2.11 Schematic representation of Flexcell Tension System. The plate is placed with a brown rubber on top of a black support as shown in A. An air pump then creates vacuum, the air removal allows the plate surface to extend over the loading post, producing a stretch of surface as shown in B. (Please note that the figure in B contains the world strain although it should be stretch. The figure was not altered as taken from Flexcell website).

2.4.5 *In vitro microRNA treatments*

Primary mouse lung fibroblasts were growth in T-75 and detached as described in 2.4.1. $2X10^5$ cells per well were seeded in 6-well plates. Once cultures reached full confluency, the DMEM was removed, and fibroblasts incubated for 30 min in sterile PBS in a humidified incubator at 37°C and at 5% CO_2. For each mouse donor 3 different conditions were established. A scramble sequence for control, containing a random sequence not associated with any specific microRNAs; a mirmimic for the gain and a synthetic hairpin inhibitor for loss of function.

Primary mouse lung fibroblasts were treated with synthetic sequence for miR-29a at 0.05 µM. Treatments for miR-21a-5p used scramble at 0.1 µM, mirmimic at 0.05 µM and antagomir at 0.15 µM. Primary cell transfection was achieved using Lipofectamine 2000. After 48 hours of incubation in a humidified incubator at 37°C and at 5% CO_2 cells were washed with sterile PBS and lysed using Trizol and stored at -80°C.

2.5 Molecular Analysis

2.5.1 Lung Homogenization

Lungs were homogenised using liquid Nitrogen (N2) and a mortar, and the resulting tissue powder was lysed in 0.5 mL of Trizol and vortexed for 5 min at maximum speed.

2.5.2 Total RNA extraction

0.5 mL of Trizol (Thermofisher) was added to cells in 6-well plates for 5 minutes for each well and the lysate collected with the use of a sterile scraper and stored in Eppendorf tubes at -80°C. After defrosting, 0.12 mL of Chloroform was then added to each tube and the tubes centrifuged at 12,000 x g for 15 min at 4°C. Only the aqueous phase, containing the total RNA, was collected for further steps. Next, 0.2 mL of Isopropanol was added to each tube and mixed with the lysate and incubated for 30 minutes in -80° C. Tubes were centrifuged at 12,000 x g for 10 min at 4°C to precipitate the RNA. The liquid phase was then discarded, and the pellet washed with 0.5 mL of molecular grade 75% ethanol and centrifuged at 7.500 x g for 5 min at 4°C. The ethanol phase was discarded, and the pellet was air dried for 5 min at room temperature. RNase free water (volume depending on pellet size) was then added and the tubes incubated in a thermo-block at 55°C for 10-15 min. Total RNA concentration was then determined using a Nanodrop from Thermofisher. RNA with a 260/280 and a 260/230 ratio respectively higher than 1.65 and 1.4 were used in further applications.

2.5.3 Reverse transcription

Per sample, 1 µg of total RNA was used for all reverse transcriptase reactions. Evoscript from Roche LifeScience was used as it contains both random hexamers and oligo-dT as primers. Next, 4µl of 5x concentrated Reaction buffer and PCR grade water to a final volume of 18µl was added. Tubes were mixed well, centrifuged briefly and incubated for 5 minutes at room temperature. After incubation, 2µl of 10x concentrated Enzyme mix was added and mixed well. Tubes were then placed in a SimpliAmp Thermal Cycler (Thermo Fisher, USA) and incubated using the protocol in Table 2.5.

Per sample, 100 ng of total RNA was used for all miRNA reverse transcriptions. Reverse-

transcription was performed using miScript II Hispec technology. A mastermix composed of 2:1 of 5X miscript Buffer with 10X miscript Nucleic Mix was added to the RNA. After 5 minutes of incubation, 1 µL of miScript reverse transcriptase mix was added to the solution. Tubes were then placed in a SimpliAmp Thermal Cycler (Thermo Fisher, USA) and incubated using the protocol in Table 2.6.

Table 2.6 Reverse-transcription run program mRNAs.

Step	Temperature	Time
1st	42°C	15 min
2nd	85°C	5 min
3rd	65°C	15 min
4th	4°C	∞

Table 2.7 Reverse transcription run program microRNAs.

Step	Cycle	Temperature	Time
1st Incubation	1	37°C	60 min
2nd Incubation	1	95°C	5 min
Cooling	1	40°C	30 sec

2.5.4 *Quantitative Polymerase chain reaction*

Genes were analysed using primer-probe sets from either Real Time Ready Assay© or Universal probe library©, while microRNAswas analysed using validated primers from miRScript technology. First the number of reactions were calculated according to the following formula:

$$n^{\circ}\ of\ reaction = (n^{\circ}\ of\ samples + 1) \times 3 + 1$$

Formula 1: Calculation of number of reactions

The resulting number was multiplied for each reagent single volume according to the following tables:

Table 2.8 Master mix ingredients and volumes used for Universal probe library©

Reagent	Volume (µL)
MasterMix	5
Fw Primer	0.4
Rw Primer	0.4
Probe	0.2
Water	3

Table 2.9 Master mix ingredients and volumes used for Realtime Ready Assay©.

Reagent	Volume (µL)
Mix	5
miR Primer	0.5
Water	3.5

Table 2.10 Mastermix ingredients and volumes used for mirScript ©.

Reagent	Volume (µL)
Syber Green	5
miR Primer	0.7
Universal primer	1
Water	2.3

Each reagent was mixed together and 9 µL of the mix was loaded in each well in a 96 well plate. Then, 1 µL of cDNA per well was added in triplicate for each sample. For miR-qPCRs

I used a Roche LightCycler480 (Roche, Switzerland) with the following protocol:

Table 2.11 miR-qPCR protocol used for Roche LightCycler480.

Step	Cycle	Temperature	Time
Enzyme activation	1	95°C	15 min
Amplification	45	95°C	15 sec
		56°C	30 sec
		71°C	30 sec
Cooling	1	4°C	∞

while for qPCRs a LightCycler96 (Roche, Switzerland) with the following protocol:

Table 2.12 qPCR protocol used for Roche LightCycler96.

Step	Cycle	Temperature	Time
Pre-incubation	1	95°C	10 min
Amplification	45	95°C	10 sec
		60°C	30 sec
		72°C	1 sec
Cooling	1	4°C	∞

Results were analysed with two different dedicated software packages, depending on the machine used.

Relative miR expression was calculated using SNORD68 as housekeeping gene as suggested in the miRScript manual. Only miR-qPCRs results showing similar melting profile were used for further analysis as prove of technical specificity. Table

2.11 lists information regarding the validated primers used for all miR-qPCRs.

Table 2.13 microRNA primers list.

miScript Primer Assay	Cat. no.	Sequence
SNORD68_11	MS00033712	5'UGAGUUUCGAUGUGUACGCUUG AACUUAAUUUCUGAGUUUAC3'
miR-21_2	MS00011487	5'UAGCUUAUCAGACUGAUGUUGA3'
miR-34a_1	MS00001428	5'UGGCAGUGUCUUAGCUGGUUGU3'
miR-29a_1	MS00001372	5'UAGCACCAUCUGAAAUCGGUUA3'
miR-378_1	MS00032781	5'UAGCACCAUCUGAAAUCGGUUA

Relative mRNA expression was calculated using ß2-microglobulin for all *in vitro* experiments and HMBS for all the *in vivo* experiments. This is because HMBS showed a stable expression between samples, while ß2-microglobulin expression was stimulated by Bleomycin treatment. Mouse Col1a1 primers were the only using Universal probe library© technology (Tab. 2.12). Table 2.13 lists information regarding the validated Primer/Probe used for qPCRs.

All qPCRs calculation for microRNAs and genes of interest followed delta CT relative expression, this allowed to compare each experiment in a more absolute way than relative to the control. To accomplish that housekeeping gene should not vary more than two between all technical replicates. Relative expression is therefore equal to the quadratic difference of housekeeping gene and gene of interest, obtained from each sample average from three technical replicates.

The reason why I used two different qPCR machines for my experiments lay in the possibility to exploit peculiar characteristic of each qPCR machines. LightCycler 480 can be customed with temperature, time and in the trend of increase or decrease in the temperature. Therefore, it suited better with SYBR GREEN technology as the custom setting for melting temperature allowed to choose more accurate temperatures of annealing. 0.5 °C variation in temperature can results in not specific signals, as fluorescence depends by the number of probe molecule attached to DNA minor groove. By contrast, LightCycler 96 has a more rapid execution time, which fitted better with Taqman technology, more specific and sensible than SYBR GREEN.

Table 2.14 Universal probe library© mus musculus Col1a1 primer information.

GENE ID	FORWARD (5'-3)	REVERSE (5'-3')	PROBE SEQ	AMPLICON BP
Col1a1	CTCCTGGCAAGAATGGAGAT	AATCCACGACCCTGA	CCTCCTGG	91

Table 2.15 Real Time Ready Assay© primer/probe list.

ASSAY ID	GENE SYMBOL	ALIAS	DESCRIPTION
100861	COL1A1 *H. sapiens*	OI4	collagen, type I, alpha 1 [Source:HGNC Symbol;Acc:2197]
148603	CTGF *H. sapiens*	CCN2, HCS24, IGFBP8, MGC102839, NOV2	connective tissue growth factor [Source:HGNC Symbol;Acc:2500]
144082	SNAI1 *H. sapiens*	dJ710H13, SLUGH2, SNA, SNAH	snail homolog 1 (Drosophila) [Source:HGNC Symbol;Acc:11128]
105613	PDGFRA *H. sapiens*	CD140a, MGC74795, PDGFR2, RHEPDGFRA	platelet-derived growth factor receptor, alpha polypeptide [Source:HGNC Symbol;Acc:8803]
104699	SMAD7 *H. sapiens*	CRCS3, FLJ16482, MADH7, MADH8	SMAD family member 7 [Source:HGNC Symbol;Acc:6773]
143711	B2M*H. sapiens*	beta-2-microglobulin	beta-2-microglobulin [Source:HGNC Symbol;Acc:914]
317785	Col3a1 M. musculus	AW550625, Col3a-1, KIAA4231, mKIAA4231, MMS10-W, Ms10w	collagen, type III, alpha 1 Gene [Source:MGI (curated);Acc:MGI:88453]
311697	Snai2 M. musculus	Slug, Slugh, Snail2	snail homolog 2 (Drosophila) Gene [Source:MGI Symbol;Acc:MGI:1096393]
316448	Snai1 M. musculus	AI194338, Sna, Sna1, Snail, Snail1	snail homolog 1 (Drosophila) Gene [Source:MGI (curated);Acc:MGI:98330]
316877	Ctgf M. musculus	Ccn2, fisp-12, Fisp12, Hcs24,	connective tissue growth factor Gene [Source:MGI (curated);Acc:MGI:95537]
300938	Smad6 M. musculus	Madh6, Smad 6	MAD homolog 6 (Drosophila) Gene [Source:MGI (curated);Acc:MGI:1336883]
301088	Smad7 M. musculus	Madh7	MAD homolog 7 (Drosophila) Gene [Source:MGI (curated);Acc:MGI:1100518]
301208	B2m *M. musculus*	beta 2 microglobulin, beta2-m, beta2m, Ly-m11	beta-2 microglobulin Gene [Source:MGI (curated);Acc:MGI:88127]
307872	HmbsM. musculus	PBGD, porphobilinogen deaminase, T25658, Ups, Uros1	hydroxymethylbilane synthase Gene [Source:MGI Symbol;Acc:MGI:96112]

2.6 *Bioinformatics tools*

microRNA target discovery was performed with TargetScan 7.2 (http://www.targetscan.org/vert_71/), while general information about each microRNA used were obtained from miRBase database (http://www.mirbase.org/). This database provides specific information regarding microRNA nomenclature, hairpin structure, sequence peculiarity and a list of related publications. Moreover, it distinguishes the mature microRNA in seed sequence and passenger strand, which present an asterisk after the name. This is because pre-microRNAs are composed of a stem hairpin united dsRNA, where the two strands are separated by exonuclease cleavage, as only mature microRNA can be assembled in the RISC complex (Cai et al., 2009). Although both strands can operate a transcript inhibition, only the "seed strand" is usually considered for target analysis (O'Brien et al., 2018). In this study, only microRNAs conserved between human and mouse were taken in consideration.

TargetScan 7.2, as many other target discovery platform, allows target discovery in most studied model organisms trough either microRNA or gene ID or name, as shown in figure 2.14.

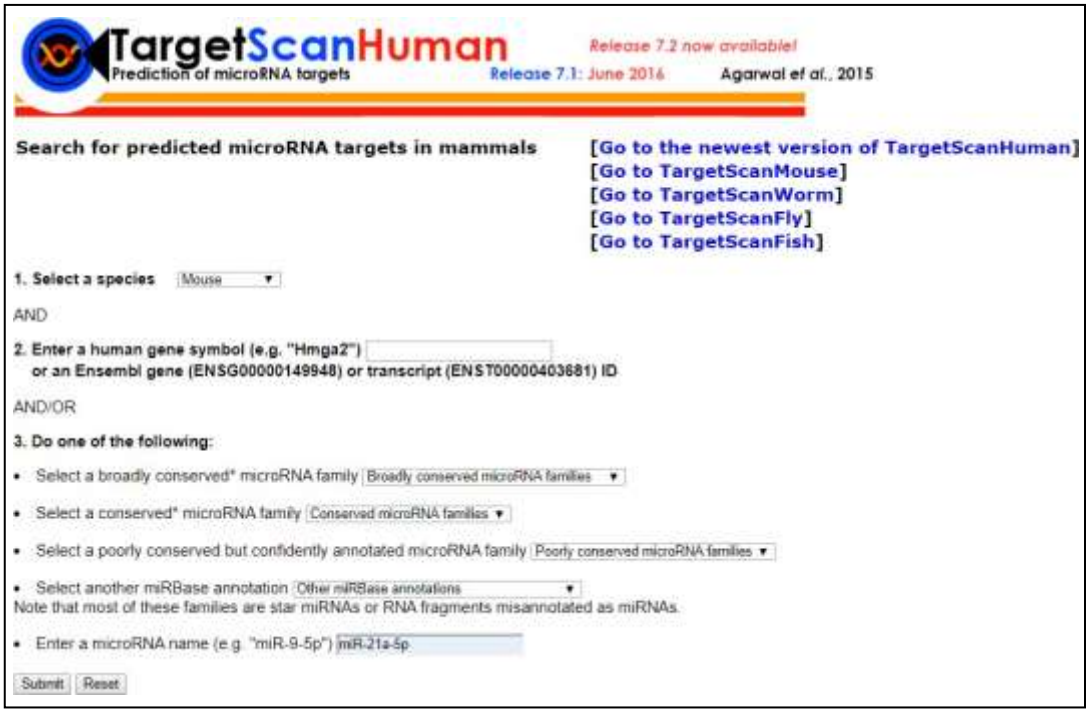

Figure 2.12 TargetScan 7.1 open page screen shot

Then, in case of mRNAs target discovery from a microRNA name, TargetScan generates a table representing a list of mRNAs that satisfy algorithm requirements (Tab. 1 in Chapter 6 and

Chapter 7). For search from a gene name or ID, the platform produces a diagram, illustrating the entire 3'-UTR (as 5'-3') with coloured boxes regarding the location and type of binding (fig. 2.15).

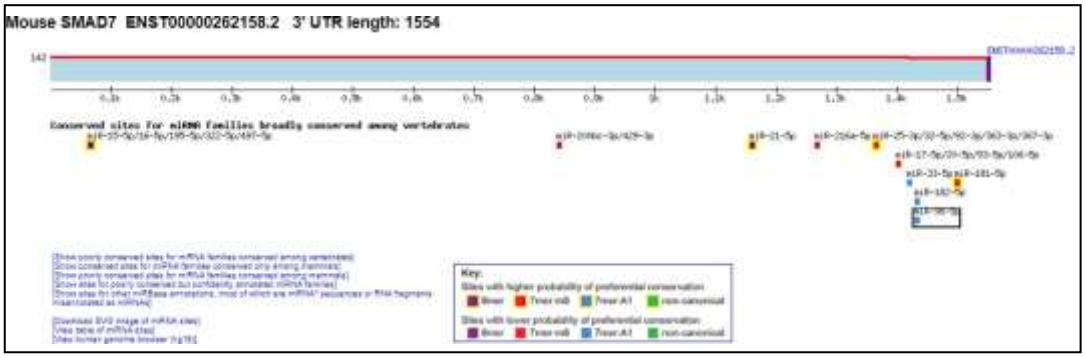

Figure 2.13 TargetScan output from mRNA name search. The output provides information regarding selected gene 3'-UTR gene (in this case Smad7 in mouse, on top) and location (below gene UTR) and type (see legend in the central box) of predicted binding site

This selection system is based on a number of assumptions that are quite often expanded, as new mechanisms or inhibition preference are discovered. TargetScan follows Watson and Crick pairs complementarity between microRNA seed sequence and corresponding 3'-UTR. The seed sequence represents the inhibitory core in the ribonucleic complex and therefore, represents the most important selection requirement. Selection requirements are based on the analysis of preferential conserved miRNA binding motif presents in the 3'-UTRs, which identify several classes of target sites. An 8-mer site is a match on miRNA of interest in position 2-8 with an adenosine on mRNA opposite to position 1, a 7-mer A1 site matching in position 2-7 with an adenosine on mRNA opposite to position 1, a 7- mer site matching in position 2-7 and a 6-mer site matching in position 2-7 with lower efficacy (Agarwal et al., 2015). Adenosine in microRNA sequence at position 1 regarded to increase in affinity in the binding, seen in mammalian species and therefore present only in algorithms for vertebrates (Bartel, 2009). Other parameter affecting microRNA binding included position 11-15 in the miR sequence, which promote binding when in contiguous complementarity to the mRNA sequence. Moreover, 3'-UTR accessibility is quite important parameter that can influence microRNA-mRNA interaction for steric reasons. miR-binding at the central of gene

3'-UTR occurs less as the silencing complex might be destabilised by ribosomal rRNA (Bartel, 2009). With that TargetScan7.2 provided reliable predictions for mRNA and microRNA target identification. However, Fromm and collaborators extensively explained that TargetScan prediction algorithm main limitation are due to wrong or redundant annotation from microRNAs

databases (Fromm et al., 2015). Moreover, confused, and false positive functional analysis can result from an extensively use of simulation over experimental procedure.

The wisest approach in this case is to refer not only to microRNAs databases but also to better annotated databases, such as ensemble! and UCSC. miR genomic location, and epigenetic regulation are all important information to obtain a successful prediction.

2.7 Statistical Analysis

Statistical tests were used to discern between different experimental groups, using Student *t-test* for comparison between two groups, and 1 and 2-way- Analysis of variance (1-way ANOVA and 2-way ANOVA) for more than 2 groups. Student *t-test* was then used for direct comparison regarding gene regulation change induced by fibrotic *stimuli* (TGF-ß, substrate and stretch) and also for single comparison in gain and loss of function experiments. 1-way-ANOVA was used for multiple comparison for analysis between experimental samples greater than 2, the analysis was also accompanied by Tukey Post-Hoc test for comparison between pairs of columns. 2-way-ANOVA was used to investigate differences induced by fibrotic *stimuli* in two different age populations.

All statistical analyses were performed using Prisms. Information regarding power calculation of sample sizes are referred to 2.2.1

3 microRNAs expression in the Bleomycin model of lung fibrosis

3.1 Introduction

Reproducing the entire disease complexity in in an animal model is still impossible. No models so far have been able to fully recapitulate lung fibrosis characteristics univocally. However, strategies such as administration of asbestosis, silica and Bleomycin, or cytokine overexpression (overexpressing TGF-ß, TNF-α or IL-1) represent robust methods to use for research propose (Mouratis & Aidinis, 2011). Among animal fibrotic models, the Bleomycin model of lung fibrosis is one of the better characterised and established in fibrosis research (Moore et al., 2013). Using a single intratracheal administration of Bleomycin, it is possible to reproduce both inflammatory and fibrotic patterns. Bleomycin induces either single or double strand DNA breaks (ssDNA or dsDNA) which lead to tissue injury due to cell apoptosis or necrosis. The intratracheal route limits the tissue damage to the lung. Furthermore, the low expression of Bleomycin metabolising enzymes increases the drug half-life and effectiveness with increase in cell damage. Bleomycin treatment leads to 1) Cell death 2) Inflammation 3) Fibrosis, which together recapitulate the main events of IPF. The main limitation of this model is that it resembles more an acute injury than a chronic disease such as fibrosis (Hatley et al., 2010). Moreover, murine lungs can recover from disease after 28 days (Degryse & Lawson, 2011).

Despite the limitations, the method has proved to be indispensable for drug discovery for antifibrotic therapies and to improve our understanding of the diseases.

As mentioned in the aim section, comprehensive analysis at different time point in the Bleomycin model of lung fibrosis identified in clusters of microRNAs interesting possible target for the developing of therapy against fibrotic diseases. Therefore, microRNAs of interest were selected based on their potential future therapeutic role (Xie et al., 2011). However, this study was based on arrays, therefore there was the necessity to validate the analysis with qPCRs in a lung fibrosis phenotype.

After the phenotype was confirmed at molecular and histopathological level the microRNAs target discovery began. As mentioned in the introduction, the main focus of this work was on three major microRNAs, miR21-a, miR-34a and miR-29. Obviously, all cited microRNAs represent already interesting lead at the moment in clinical trial.

miR-21a has been strongly associated with kidney fibrosis and a synthetic analogue of miR-21a has proved to be a possible cure for Alport disease, which can evolve to kidney fibrosis. Therefore, miR-21a might be involved in the first phase of fibrotic development, which represent most interesting therapeutic window for patient affected by the disease (Ivan G. Gomez et al., 2015). miR-34a has a lung tropism, with significant increase in ageing and in cancer, as it induce lung epithelial survival by *p53* repression (Disayabutr et al., 2016; Hermeking, 2010). miR-29a is considered fundamental in scar formation, this miR can potentially repress most of collagens and represent one of the most interesting target for microRNAs discovery (Slusarz & Pulakat, 2015). Another microRNA included in this experience was miR-378, because of its role in the response to tissue damage and involvement in EMT (Jieun Kim, Hyun, Wang, Lee, & Jung, 2018).

The main aim of this chapter was to identify microRNAs with unique expression profiles in the Bleomycin model of lung fibrosis.

3.2 Materials and methods

C57BL/6J male were treated with Bleomycin to induce a fibrotic phenotype as described in 2.25.

C57BL/6 mice (N=5 per group) were treated with either Bleomycin (mg/g) or vehicle (PBS control group). Mice were grouped in four groups based on the time of culling, such as control group, which received PBS and 3, 10 and 21 days after the intra-tracheal injection of a Bleomycin. C57BL/6 were sacrificed by intraperitoneal injection of pentobarbital sodium. Euthanasia was then confirmed by the end of the circulation and by no sign of reflex. Lungs were dissected and inflated for *ex vivo* lung µCT scans. After inflation, lungs were immersed in a solution at 3% of potassium iodide, used as contrast reagent, and imaged at 20 µm through Skyscan1272 µCT. Next, post-caval lobes were removed for histological analysis, and the remaining lung tissue used to isolate RNA.

3.3 Results

Bleomycin administration holds an obvious limitation due to interindividual biodiversity, as any treatment to any biological organism. The purpose of this chapter was to obtain results on microRNA from lung showing fibrotic phenotypes. For this reason, lungs were analysed at both mRNA (qPCR), protein (histology) and organ level (µCT) to assess the presence of a fibrotic phenotype. The reason why fibrosis was evaluated at different levels was to develop a robust system to correlate fibrosis development with microRNAs expression. To assess this correlation, samples were collected at 3, 10 and 21 days after treatment with Bleomycin, which represent inflammatory phase, apex of and end-point of fibrotic response, respectively. The main reason of this methodology lay in mice capability to rescue the healthy phenotype after 28 days from Bleomycin administration.

3.3.1 µCT Analysis of lungs

Total inflated *ex-vivo* lungs were imaged with a µCT following the setting cited in 2.2.3.

To quantify the fibrosis, X-ray attenuation of lung parenchyma was measured. Increased X-ray attenuation corresponded to a higher amount of soft tissue in the specimen and therefore

indicator of lung density. Major blood vessels were excluded from the analysis (Wheeler, Jones, & Ikonomidis, 2014) Lung parenchyma disruption induced by the treatment, should start a scar formation with having a higher quantity of collagen fibres augments the density of the organ. Density was calculated through dedicated software, which can calculate an object density from the different levels of grey in the reconstructed CT image (fig. 3.1 and 3.2). Therefore, the amount of fibrosis was evaluated as the average X-ray attenuation of the lung tissue (fig. 3.2). However, 2 scatter points in the control group and 1 in the 10 days one were missing due to mistake in lung inflation procedure.

Scans from control group shows a general bright appearance which reflected a healthy lung architecture (fig. 3.1 top left), while in the 3 days Bleomycin group there were fibrotic events (highlighted by the red arrow in fig. 3.1 top right). In progression from the 3 days group, 10 and 21 days Bleomycin groups showed a general increase in voxels with high X-ray attenuation, indicating fibrosis. Moreover, it is possible to appreciate an increase in density around main airways for the 10 and 21 group samples (3.1 bottom).

From qualitative point of view 10 days samples appeared the most fibrotic as it showed darker area compared to 21 days group, which was expected to have the highest degree in fibrosis. However, 3D scans reconstructed images allow a complete vision of the *ex vivo* lung allowing the possibility to quantify the levels of grey for each lung section (fig. 3.2).

Lung density showed a significant 2.3-fold increase from control in 10 days Bleomycin group and a 1.5-fold increase in 21 days Bleomycin group (fig. 3.2). Analysis of the density histogram showed X-ray attenuation for control and 3 days group were mostly represented at lower density range (between 0- 49) while the 10 days and 21 days Bleomycin groups showed a shift to higher X-ray attenuation values (between 87-166, fig.3.3).

The results suggested the presence of fibrosis after 10 and 21 days after treatment with Bleomycin, with a pronounced increase in tissue density around major airways as highlighted by red arrows in figure 3.1.

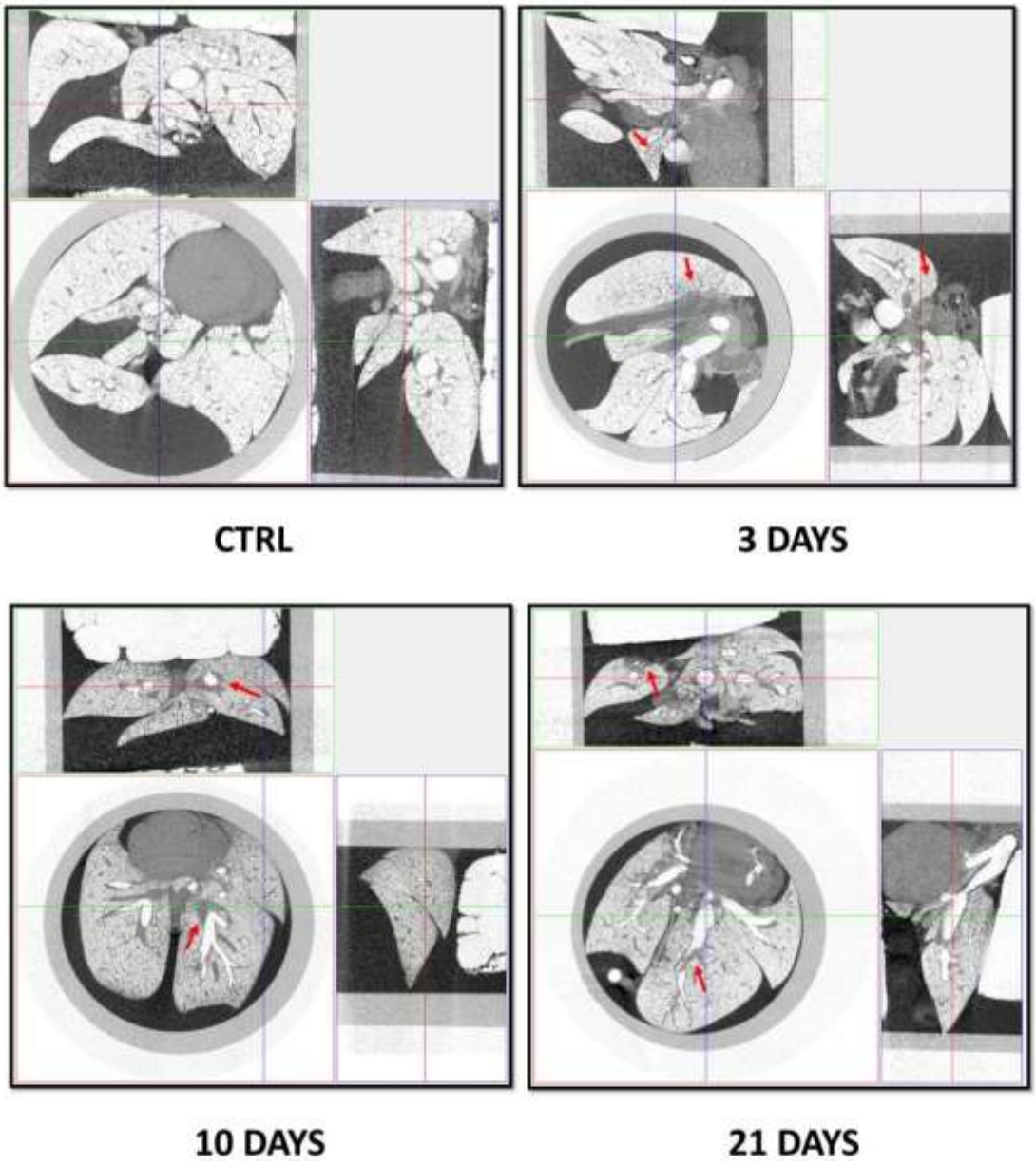

Figure 3.1 Section of mouse lung imaged in X (upper), Y (central) and Z (right) axe. Images were generated and reconstructed from µCT software (Burkel) and saved as snapshot. Diverse colour results from different X-ray adsorption across the tissue. In the figure can be appreciated different level of grey, where the darker indicates area with higher tissue density and whiter area less tissue density. The images are reconstruction of this density map in the three dimensions from Control, 3 days (top) 10 days and 21 days (bottom) after bleomycin treatment. Red arrow highlights tissue with suspect increase in tissue density.

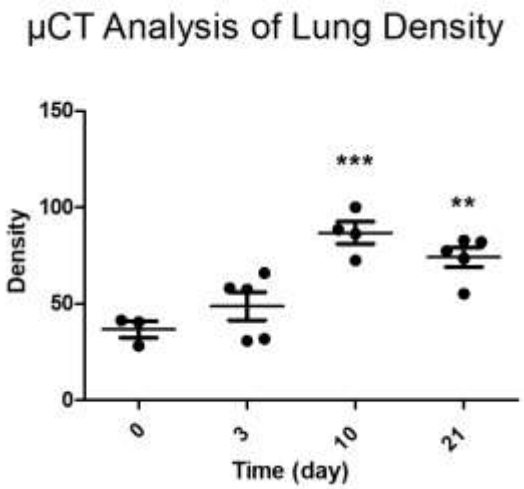

*Figure 3.2 µCT analysis of average lung density after intratracheal administration of Bleomycin. Lungs were obtained after 3, 10 and 21 days after the treatment. The density measurement are on a scale where 0 indicates pure air, and 255 solid soft tissue. Results shown in the figure were significant for 1-way-ANOVA with an overall p-value < 0.001. Turkey post- hoc test was used for single column comparison **: p-value < 0.01 ***: p-value < 0.001.*

3.3.2 Collagen fibre analysis

Picric Acid (Sirius Red) was used as stain for collagen fibres. Lungs were imaged with both brightfield microscopy and polarized light microscopy (shown respectively as A and B) for a qualitative analysis. PLM images were further analysed quantitively. From each sample 3 alveolar areas were arbitrary selected, the area transformed from coloured into scale of grey as 8-bit, collagen fibres in alveoli were then measured as levels of grey (fig 3.8). To produce an unbiased analysis capillary contains higher quantity of collagen fibres were excluded from the areas of interest (as indicated by the yellow arrow in 3.4B). The brightfield image allowed to evaluate the area to use for the quantitative analysis.

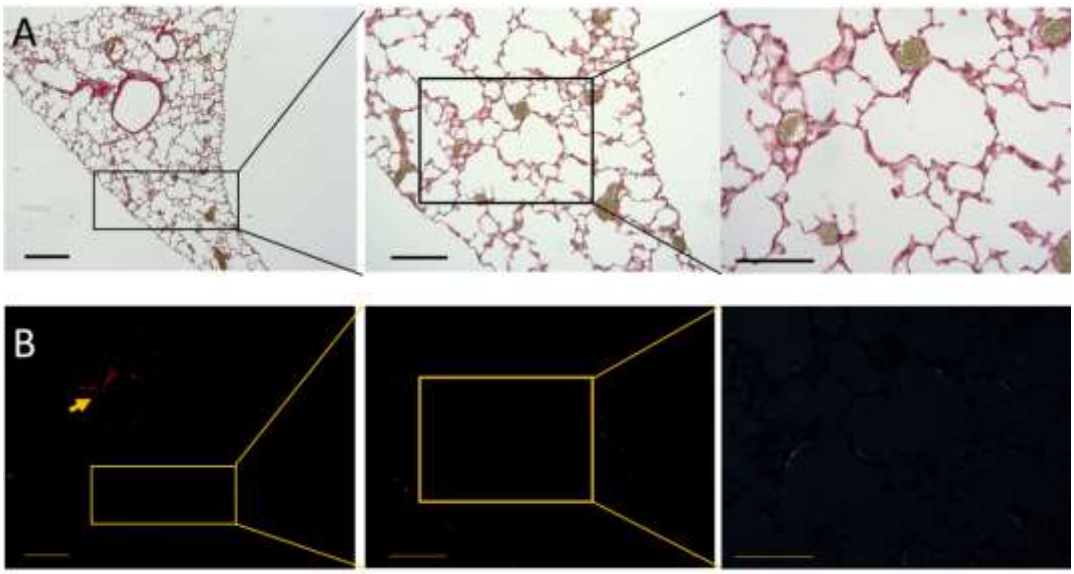

Figure 3.3 Control lungs stained with Sirius Red. Same image obtained using bright- field microscopy (A) and Polarized light microscopy (B). Black and yellow box indicates areas of interest imaged at 4X (left), 10X (centre) and 20X (right) magnification. Lungs show a normal appearance with circular dichroism around capillary (highlighted by RBC stained in green-dark yellow) [scale bar 1.000, 750, 500 µm respectively].

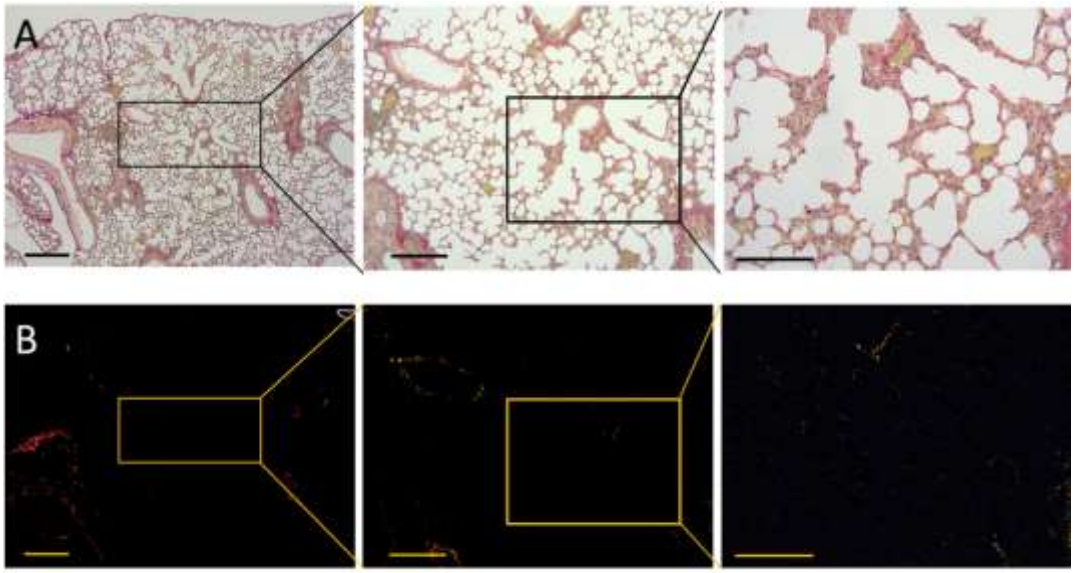

Figure 3.4 Section from 3 days after Bleomycin group, stained with Sirius Red. Same image obtained using bright-field microscopy (A) and Polarized light microscopy (B). Blackand yellow box indicates areas of interest imaged at 4X (left), 10X (centre) and 20X (right) magnification. Images show increase in cell population in the selected area, which might depend on immune infiltration due to treatment with Bleomycin [scale bar 1.000, 750, 500 µm respectively].

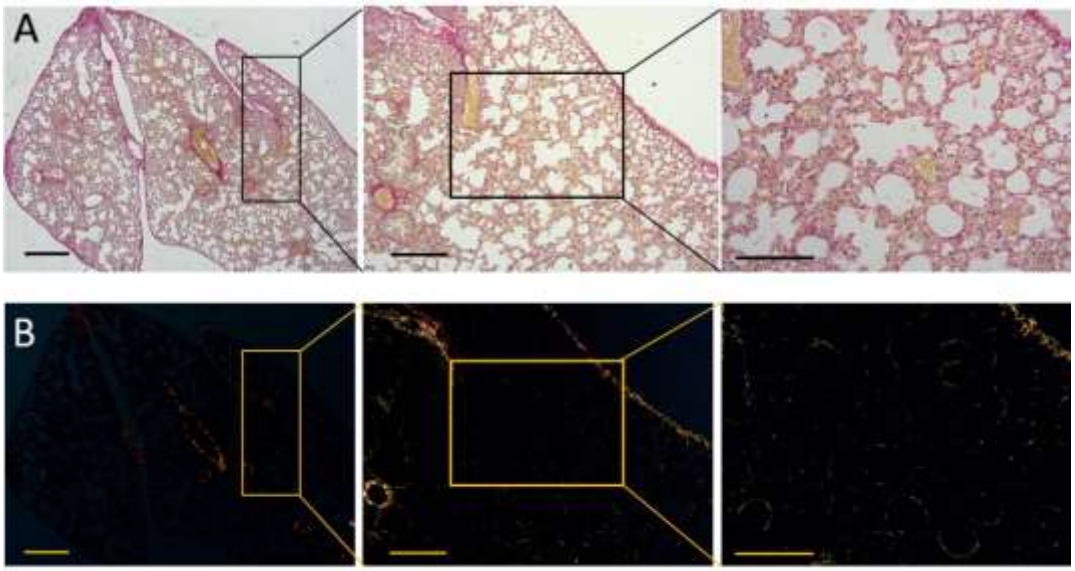

Figure 3.5 Section from 10 days after Bleomycin group, stained with Sirius Red. Same image obtained using bright-field microscopy (A) and Polarized light microscopy (B). Black and yellow box indicates areas of interest imaged at 4X (left), 10X (centre) and 20X (right) magnification. Collagen fibres stains showed a pronounced circular dichroism in alveolar tissue parenchyma. [scale bar 1.000, 750, 500 µm. respectively].

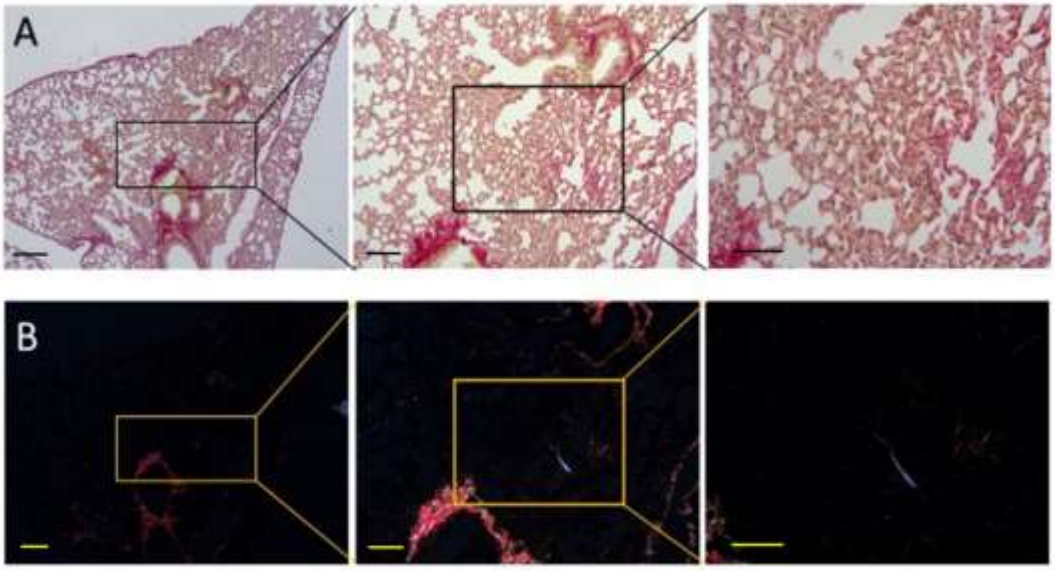

Figure 3.6 Section from 10 days after Bleomycin group, stained with Sirius Red. Same image obtained using bright-field microscopy (A) and Polarized light microscopy (B). Black and yellow box indicates areas of interest imaged at 4X (left), 10X (centre) and 20X (right) magnification. Collagen fibres stains showed a pronounced circular dichroism in alveolar tissue parenchyma. [scale bar 1.000, 750, 500 µm. respectively].

Control lungs showed a normal lung architecture, with a normal distribution of collagen fibres (fig.3.3A). Polarized light microscopy image (fig. 3.3B) did not show any event of dichroism

of note. Sections from lungs 3 days after Bleomycin treatment showed a typical hexagonal shape of lung parenchyma, with an increase in cell density around the alveolar walls, which could reflect the possibility of immune infiltration (fig. 3.4A). Polarized light microscopy showed a little increase in collagen fibres deposition (fig. 3.4B). Ten days after Bleomycin, lungs showed a disrupted lung parenchyma with a significant increase in cell density around alveoli (fig. 3.5A). Polarized light microscopy identified an increase from the control group in terms of dichroism around alveoli (fig. 3.5B).

Twenty one days after Bleomycin treatment, lung sections showed an abnormal lung parenchyma (fig 3.6A). Polarized light microscopy showed increase in collagen fibres deposition highlighted by the dichroism (fig. 3.6B).

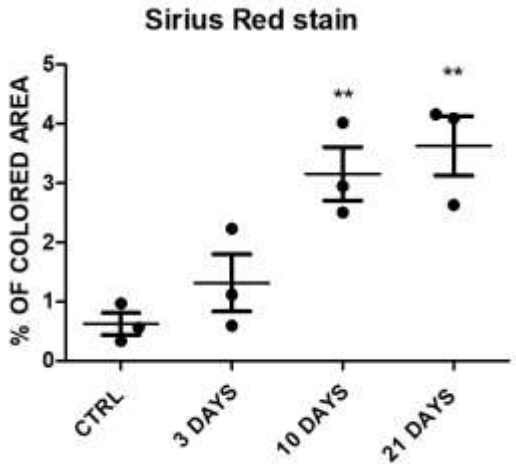

*Figure 3.7 Quantification of collagen fibres content from 3, 10 and 21 days after Bleomycin treatment (n=3). Results in the figure were significant for 1-way ANOVA with an overall p-value < 0.01. Turkey post-hoc test was used for single column comparison with control **: p-value < 0.01.*

The percentage of area with events of dichroism confirmed the increase in collagen fibre deposition for the 10 and 21 days Bleomycin group, with a significant 3-4-fold increase in the stained area from control sections (fig. 3.7).

Histology confirmed the pronounced fibrosis for lung of 10 and 21 days, confirming tomography results. The level of collagen suggested the peak of fibrosis after 10 days from Bleomycin treatment and a possible rescue of the phenotype after 21 day.

3.3.3 ECM gene expression profile

The effect of Bleomycin was studied by analysing the expression of Granzyme ß (GzmB), Col3a1, Col1a1 and Ccn2/Ctgf by quantitative polymerase chain reaction (qPCR) as described in 2.5.4. Col1a1, Col3a1 and Ccn2/Ctgf represents key component of ECM, involved in the response to chronic damage and fibrosis. The rational was to monitor expression of ECM to further confirm fibrosis development at mRNA level. GzmB was included as suggestion from Prof. Bou-Gharios, to provide further information regarding a possible immune infiltration found in the histological sections for the 3 days group (fig. 3.4).

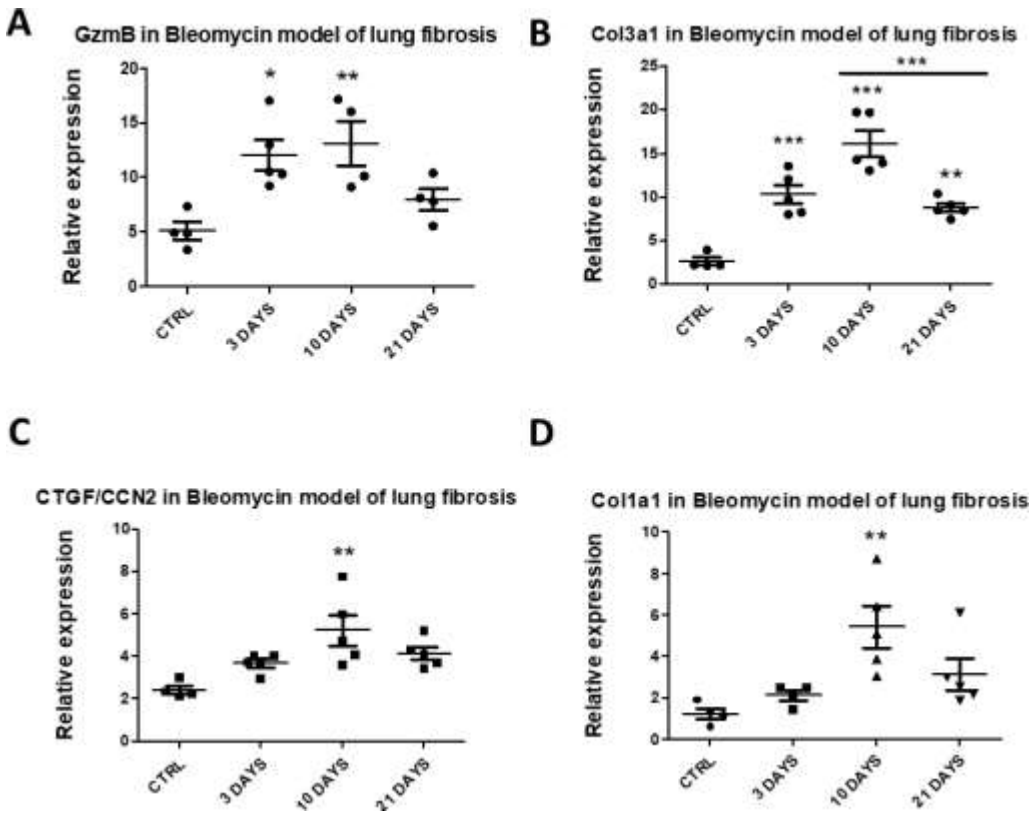

Figure 3.8 Gene expression analysis of Granzyme Beta (A) Collagen 3a1 (B) Connective tissue growth factor (C) and Collagen 1a1 (D) in the Bleomycin model of lung fibrosis. Results shown in the figure were all significant to 1-way ANOVA with an overall p-value < 0.01, p- value < 0.001, p-value < 0.001 and p-value < 0.01 respectively for GzmB, Col3a1, CTGF/CCN2 and Col1a1. Turkey post-hoc test was used for single group comparison with control (n=4).

Granzyme ß (GzmB) showed significant 2 and 4-fold increase from control 3 and 10 days after Bleomycin treatment respectively. After 21 days GzmB level returned to levels close to the

control group (fig. 3.8A).

Collagen 3a1 (Col3a1), one of the most abundant proteins in the lung, showed a 3-fold increase 3 days after the treatment with Bleomycin. This further increased after 10 days, with a 6-fold time increase in Col3a1 expression from control. Col3a1 expression levels decreased 21 days after Bleomycin treatment with a 3-fold increase relative to control and a 45 % decrease in Col3a1 expression compared to the 10 days group (fig 3.8B).

Connective tissue growth factor (Ctgf/Ccn2) showed a significant 2-fold increase from control 10 days after treatment with Bleomycin. Ctgf/Ccn2 levels slightly decreased (20% not significant) from levels at 10 days to 21 days after Bleomycin (fig. 3.8C).

Collagen 1a1 (Col1a1) expression showed a significant 4-fold increase in 10 days group compared to control (fig 3.8D).

Despite pair comparison did not show consistently significance at different time points, all ECM genes showed a progressive increase with a peak at 10 days, indicating that ECM production does not stop despite the pathological appearance. GzmB increase at 3 days after damage induction through Bleomycin further suggests a possible activation of inflammatory machinery.

3.3.4 microRNA expression profiles

The effect of Bleomycin treatment on the expression of miR-34a-5p, miR-21a-5p, miR-29a-3p and miR-378-3p was studied by quantitative polymerase chain reaction (qPCR). Snord68, a small non-coding RNA was used as housekeeping gene. Relative expression was calculated as exponential difference between housekeeping gene and gene of interest (figure 3.9). 1-way ANOVA was used together with Turkey as Post Hoc test for pair comparison.

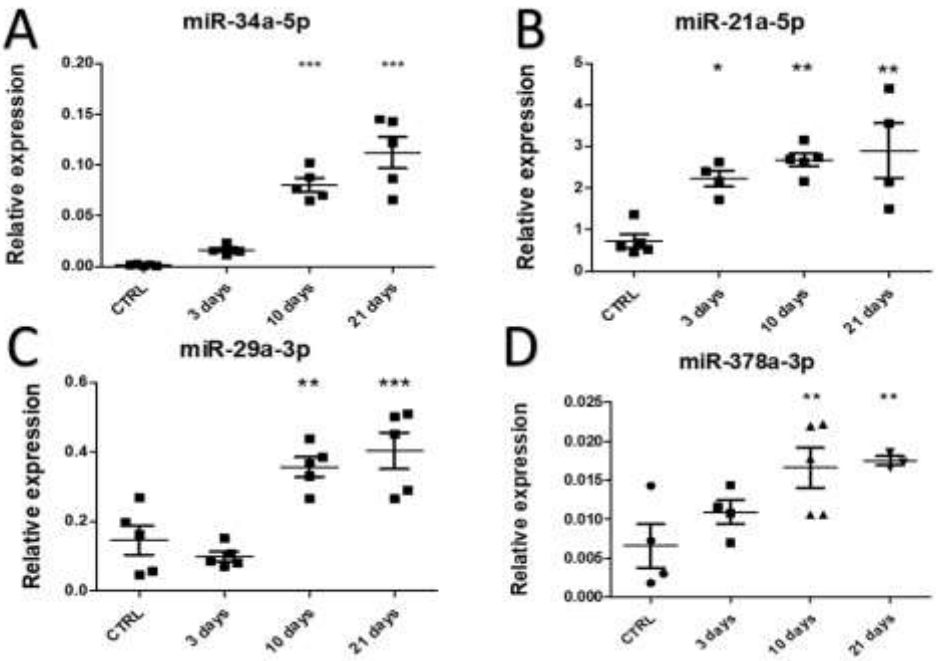

Figure 3.9 miRs expression analysis of miR-34a-5p (A), miR-21a-5p (B), miR-29a-3p (C) and miR-378a-3p (D) in the bleomycin model of lung fibrosis. Results shown in the figure were all significant for 1-way ANOVA with an overall p-value < 0.0001, p-value < 0.001, p-value < 0.0001, p-value < 0.001, respectively for miR-34a-5p, miR-21a-5p, miR-29a-3p and miR- 378a-3p.

Expression of all four miRs increased after Bleomycin treatment, with miR- 21a-5p expression already significantly increased three days after Bleomycin treatment, and all miRs studied significantly increased at days 10 and 21 after Bleomycin treatment.

miR-34a-5p showed a progressive increase in its expression with a 55 and 77-fold increase respectively at 10 and 21 days after Bleomycin treatment from control (fig 3.9A).

Bleomycin progressively increased miR-21a-5p expression with significant 3, 3.7 and 4-fold time increase respectively for 3, 10 and 21 days after Bleomycin treatment from control (fig. 3.9B).

miR-29a-3p expression displayed significant 2.4 and 2.7-fold increase respectively at 10 and 21 days after Bleomycin treatment from control (fig. 3.9C). miR-378a showed a gradual increase in its expression after Bleomycin administration, with significant 4 and 6.6-fold increase respectively for 10 and 21 days groups (fig 3.9D).

3.4 Discussion

Bleomycin sulphate is an antibiotic from *Strptomyces verticullus* and is used to reproduce IPF features in experimental model of fibrosis (Mouratis & Aidinis, 2011).

The main aim of this chapter was to identify microRNAs with unique expression profiles in the Bleomycin model of lung fibrosis. Four microRNAs (miR- 21a, miR-29a, miR-34a, and miR-378a) showed progressive increase in their expression following major fibrotic features such as an increase in lung density and ECM. To obtain information regarding the progressive IPF characteristic, three time points representing start, progression and end stages of fibrosis were selected (3, 10, 21 days after Bleomycin treatment).

In PF, healthy lung parenchyma is replaced by denser scar tissue made of ECMs and an increase in tissue stiffness. Tomography represents the golden standard in clinical practise and represent an incredible tool in experimental biology. CT reconstructs an organ structures as 3D density map, offering the possibility to identify fibrosis progressions and discern between structure at diverse density (capillary, alveoli, bronchioles, etc.). In 2013 Chris Scotton and collaborators developed a preclinical *ex-vivo* methodology for evaluation of drug efficacy using a Bleomycin model of lung fibrosis. The study was supported by *gsk* who had interest in this method to test compound against IPF (Scotton et al., 2013). Therefore, the idea was to replicate the method developed by Scotton and collaborator to use for microRNAs discovery. However, biological biodiversity together with dissection difficulty were source of variability in my experience and represented limitations that I found in the application of this method. In addition, in the *ex-vivo* procedure lungs are filled with diverse volumes of air, which can result in variation in lung total volume. Depending on the amount of air lung might appear more open or close and less or more fibrotic. This limitation was the reason why two lungs were excluded from this analysis as the inflation was not successful. To sum, results from the *ex-vivo* µCT showed an increase in the soft tissue after Bleomycin administration. The increase in soft tissue increased X-ray attenuation from a specimen placed between radioactive source and a detector. However, morphological changes found in fibrotic samples, as the increase in lung stiffness are features common to all Interstitial lung diseases (Nogee et al., 2001). Densitometric analysis of µCT images showed a progressive increase following fibrosis progression. Moreover, higher level of grey, indicating in the analysis X-rays more attenuated by the specimen, were higher represented in the 10 and 21 days groups. Thus, µCT revealed Bleomycin efficiency in reproducing a progressive

fibrotic-like phenotype.

The three-day group did not show any form of fibrosis, as this time point represents a pro-inflammatory phase of IPF (Mouratis & Aidinis, 2011). Fibrotic lung undergoes an acute Th2-immune response characterised by increase in TGF-ß, IL-1ß and TNF-α (Wynn, 2011). Effects of this increase are fibroblast/myofribroblast activation and ECM secretion in the later stage increase (Kendall & Feghali- Bostwick, 2014). In the model developed, GzmB upregulation and the increase in the amount of nucleated cells population in the 3 days group are indicator a pro-inflammatory phase. Moreover, GzmB expression level remained high also in the 10 days group, which is in line with results obtained in the perforin knock out mice subjected to Bleomycin treatment Miyazaki (Miyazaki et al., 2004). However, more detailed evidence (measurement of inflammatory cytokines at transcript and protein level and further IHC for identification of the single nucleate population) are necessary to further confirm this result.

In later stages of fibrosis (10 and 21 days after treatment), stains showed a progressive disruption of hexagonal shape lung parenchymal, clear sign of an unsolved scar. PLM microscopy confirmed a fibrotic appearance of the lungs, highlighted by dense collagenous structure, in line with the increase in fibrillar collagen in IPF (Wynn, 2011).

The fibrotic appearance found in histology was also confirmed at expression level through qPCRs for Col1a1, Col3a1 and Ccn2/Ctgf. Results for both Col1a1 (α1 chain of type-I) and Col3a1 showed significant increase in 10 and 21 days groups, with peaks for both genes at 10 days (fig. 3.9B and D). Col1a1 and Col3a1 decrease at 21 days from 10 days group may represented a possible lung atrophy. In support of this possibility Sirius red staining from 21 days samples showed a marked disruption of lung parenchymal, worse than in 10 days group. Ccn2/Ctgf showed a trend similar to Col1a1 and Col3a1 with significant increase 10 days after bleomycin, with a similar progressive trend. This molecular behaviour in response to Bleomycin is in line with previous study from Leask and collaborators, who suggested a profibrotic role of Ccn2/Ctgf (S. Liu et al., 2011; Sonnylal et al., 2010).

Results obtained from CT scans, histology and gene expression designated in 10 and 21 days, as more fibrotic.

Therapeutic use of miRs is a relatively new strategy in the field of fibrosis, as mentioned in 1.5. The idea beyond the pharmacological administration of those small non-nuclear RNAs, is the

manipulation of their expression to reverse disease outcomes. miRs expression have been found altered in a broad range of disease. One example is represented by repression of miR-34a, now at phase II of clinical trial, against solid lung tumour (Beg et al., 2017). microRNAs can have a single or multiple target, which can regulate a signalling pathways entirely (Avraham & Yarden, 2012). In the Bleomycin model of lung fibrosis all four microRNAs showed a progressive increase in their expression following the gradual fibrotic increase.

miR-34a-5p high relative expression represents the characteristic lung tropism of this microRNA, which showed to be influenced by TGF-ß (Takano et al., 2017). miR-34a has been shown to regulate mechanisms such as apoptosis, senescence, and ageing, which are in line with the increase found in the Bleomycin model of lung fibrosis. Interestingly, Huachun Cui and collaborators showed an amelioration in lung physiology in a conditional epithelial knock out for miR-34a after Bleomycin administration (Cui et al., 2017). Our results are then in line with previous publications, which identify miR-34a-5p as a possible profibrotic microRNA.

miR-21a-5p shows an interesting expression profile in our experimental model of lung fibrosis with a progressive upregulation with highest levels of expression at 10 days (fig. 3.10 B). miR-21a-5p showed a lung tropism, showing a high expression already in the untreated group. After Bleomycin treatment miR- 21a-5p expression gradually increased reaching the highest expression level among all miRs tested. This increases in expression from a healthy lung shows that miR- 21a-5p is a possible pro-fibrotic microRNA. Results are in line with a study from Yamada and collaborators, who showed a similar increase in miR-21a-5p expression in the Bleomycin model of lung fibrosis (Yamada et al., 2013).

miR-29a-3p is increased in the expression at later stages of fibrosis, with significant increase at 10 and 21 days after Bleomycin administration (fig. 3.10 C). Our experimental data are not in line with the work of Montgomery who found a suppression in miR-29a-3p expression in the same animal model of fibrosis (Montgomery et al., 2014; Xiao et al., 2012). To further investigate miR-29a-3p role in lung fibrosis, I tested miR-29a-3p expression using mirmimic and antagomir approach in primary mouse lung fibroblasts (Chapter 6).

miR-378-3p has been involved in muscle differentiation and induction of subsequent apoptosis (Wei et al., 2016). The increase in miR-378a-3p expression indicates possible role for this miR in pulmonary fibrosis.

All microRNAs showed possible profibrotic role in the Bleomycin model of lung fibrosis,

however only miR-21a-5p and miR-34a-5p showed a clear progressive increase in their expression. Another fundamental reason why I focus this experimental study on those two microRNAs regards their relative expression level. miR-34 and miR-21 showed in control lungs CT values arounds 20-22, indicating that at 20^{th} or 22^{nd} cycle there was the exponential increase of the expression. By contrast, miR-378 had a relative expression of smaller order, which might be not identifiable after inhibitory treatments. This, I think is a key parameter to consider as pharmacologic use of microRNAs uses suppression or mimicking their ability as gain and loss of function.

In conclusion, my results show that expression of all four microRNAs studied increased in bleomycin induced lung fibrosis. miR-21a-5p may be of special interest as it already increased at an early stage of the disease before major fibrosis has occurred. It is therefore a potential target for treatment in the early stages of the disease.

4 Effect of fibrotic ECM substrate in a dynamic culture of A549 and MRC5

4.1 Introduction

In pulmonary fibrosis environmental aspects such as unhealthy lifestyle or cigarette smoking, are believed to be important inducers of pulmonary fibrosis (Borie et al., 2013; Ramlee et al., 2016). These *stimuli* trigger prolonged and continuous parenchymal damage or chronic damage, which is considered at the basis of organ fibrosis (Wynn, 2011). *In vitro* systems are at the moment able to reproduce organ structure and cells, thanks to the latest advantages in organoids and stem cells. Wilkinson in 2014 have been able to obtain human lung epithelial leaflet through a complex procedure, with the aim to develop a strategy for personalised medicine (Dan C. Wilkinson et al., 2014). Despite the latest advantages in 3D culture and their reliability, none of the systems that have been developed so far can fully mimic lung complexity. However, *in vitro* studies can provide information regarding cell behaviour and ECM-cell crosstalk in a number of pathologies, such as organ fibrosis.

In organ fibrosis several cell types can contribute to the development of the disease, including immune cells (Th2 response), fibroblasts and myofibroblasts, and epithelial cells that undergo a transition into mesenchymal cells (EMT) (Meltzer & Noble, 2008; Wynn, 2011). Cytokine treatment with TGF-ß at a concentration lower than 10 ng/mL is currently the most used *in vitro* strategy to reproduce disease hallmarks (Fragiadaki et al., 2011). TGF-ß treatment determines TGF-ß receptor activation and a further increase in ECM expression. ECM is a reservoir of growth factors that are trapped in that; in fibrosis, ECM remodelling can be followed by a pathological release of active forms of TGF-ß (Burgstaller et al., 2017). Then, TGF-ß activating its canonical pathway will increase secretion of ECM.

TGF-ß is considered a major regulator of EMT (Kalluri & Weinberg, 2009). EMT accounts for acquisition of polarity and movement, achieved through the loss of epithelial surface markers and acquisition of mesenchymal ones. This results in an increase in the mesenchymal cell pool (fibroblast/myofibroblast) at the site of damage. EMT is not a pathological mechanism and its correlation with fibrosis has only been shown in the kidney, lung, and intestine (Kalluri & Weinberg, 2009). These three organs share similarity in high cell turnover, cell heterogeneity and embryonic origin, and all three form physical barriers against pathogens. It was calculated that

in kidney fibrosis between 15-30% of myofibroblast secreting collagens were originating from epithelial cells (Kalluri & Neilson, 2003). Apart from TGF-ß, several other cytokines, such as WNT, EGF, FGF and others can activate EMT, as described in 1.2 (Kalluri & Weinberg, 2009). However, one transcriptional repressor family sensitive to TGF-ß, Snail, seems to be a master regulator of EMT in all types. Then, transformation of an alveolar cell into a mesenchymal one would dramatically affect the amount fibroblast/myofibroblast and ECM secretion, which can ultimately worse or induce a fibrotic phenotype. Emerging evidence has demonstrated that EMT is strongly influenced by mechanical forces (Gomez, Chen, Gjorevski, & Nelson, 2010). These findings latter may have important implications in the context of lung fibrosis.

Through an involuntary innervation, movement of the diaphragm and chest muscles leads to a below-like movement of the lung. This leads to deformation of the lung tissue which is propagated to lung cells through their attachment to the ECM. During fibrosis lung increase in thickness, due to an increase in collagen content. As mentioned in the introduction collagen has incredibility strength power, with a Young modulus of around 11 GPa, which is the force necessary to unbound a collagen brick covalent bound (Shoulders & Raines, 2009). In addition, stiffer matrix seems to attract and activate myofibroblast to increase collagen and other ECM components (D. J. Tschumperlin et al., 2018). Although stiffness seems to be more important than stretch in fibrosis, I preferred to focus more on this latter, as I was more interested in verifying the effect of a diverse ECM in a dynamic system. Therefore, my idea was to compare two substrates, one representing a healthy ECM using RGD-motif and a profibrotic one using collagen matrix, with or without motion or stretch. The aim was to verify if any of those parameters had an effect on key genes involved in the pathogenesis of lung fibrosis. Moreover, I thought that stretch might have a positive effect on miR-21a, as Li and colleagues had suggested that MRTF-A, considered the transcription factor mechano-sensor, can promote miR-21a in mesenchymal cells (D. J. Tschumperlin et al., 2018). The possibility that microRNAs are also involved in the regulation of the mechanical stimulation is an interesting possibility that I wanted to include in my study and therefore I analysed through qPCR miR-21a and miR-34a expression levels.

4.2 Materials and Methods

A549 or MRC5 cells per well were seeded on either RGD-motif or collagen coated 6 well FlexCell plate, as described in 2.4. RDG-motif was used to mimic a healthy ECM, while collagen was used to mimic a fibrotic ECM. Cells were cultured for 1.5 days and FBS free media was then added to the culture once 60-70 % confluency was reached. TGF-ß at 2 ng/mL was added to the culture to mimic a fibrotic cytokine environment while BSA at 0.1% in PBS was used as vehicle in control groups on both substrates. Mechanical stretch was achieved through Flexcell Tension system as described in 2.4.5. After 6 hours cells were lysed and analysed through qPCRs as described 2.5.4.

4.3 Results

4.3.1 Effect of stretch in A549 and MRC5 cells

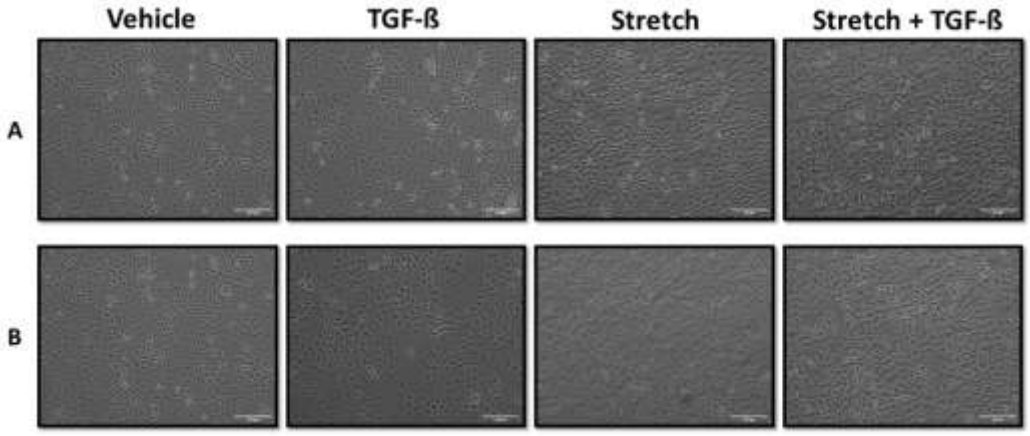

Figure 4.1 A549 seeded on RGD-motif (in A) and Collagen (in B) after treatment. Stretched cells appeared elongated after 6 hours of cyclic stretch using Flexcell system. Treatment with TGF-ß or BSA (Vehicle) did not affect cell morphology. [scale bar 100 µm].

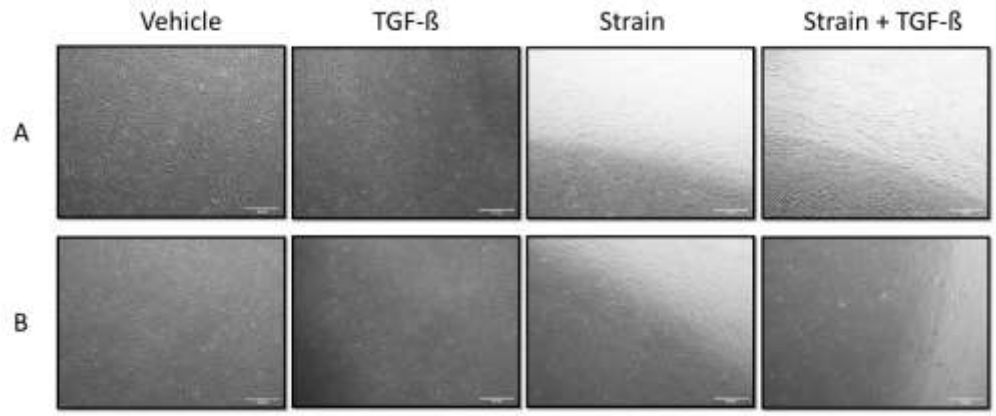

Figure 4.2 MRC5 seeded on RGD-motif (in A) and Collagen (in B). After 6 hours of cyclic stretch using Flexcell system, cells appeared elongated. Treatment with TGF-ß or BSA (Vehicle) did not affect cell morphology [scale bar 100 µm].

For both cell lines, the treatment with TGF-ß or with BSA did not induce visible changes in cell appearance. Cells receiving stretch showed changes in cell shape (more elongated and stretched) as result of stretch at 6% (fig. 4.1 and 4.2 Stretch and Stretch + TGF-ß).

4.3.2 A549 Gene expression profile

The effects of substrate, stretch and fibrotic cytokine environment (TGF-ß) on the adherent adenocarcinoma alveolar cell A549 were studied analysing genes of interest expression (Tab. 2.13 in 2.5) (Col1a1, CCN2/CTGF, SNAI1 and PDGFRα) by Quantitative polymerase chain reaction (qPCR).

*Table 4.1 2-way ANOVA statistic was applied to calculate significative differences induced by the treatments (TGF-ß and stretch; used as row) and the substrate (used as column) for Col1a1 (A), CCN2/CTGF (B) SNAI1 (C) and PDGFRα (D). Top of the figure gives numerical percentage indication on the weight of the single variable including interaction, while bottom figure shows statistical significance where * p-value < 0.05, ** p-value < 0.01 and *** p-value < 0.001.*

A — 2-WAY ANOVA COL1A1

Source of Variation	% of total variation	P value
Interaction	4.14	0.0092
TREATMENT	66.80	< 0.0001
SUBSTRATE	7.56	< 0.0001
Source of Variation	P value summary	Significant?
Interaction	**	Yes
TREATMENT	***	Yes
SUBSTRATE	***	Yes

B — 2-WAY ANOVA CCN2/CTGF

Source of Variation	% of total variation	P value
Interaction	1.90	0.0100
TREATMENT	83.68	< 0.0001
SUBSTRATE	3.69	< 0.0001
Source of Variation	P value summary	Significant?
Interaction	**	Yes
TREATMENT	***	Yes
SUBSTRATE	***	Yes

C — 2-WAY ANOVA SNAI1

Source of Variation	% of total variation	P value
Interaction	0.75	0.7617
TREATMENT	53.08	< 0.0001
SUBSTRATE	5.75	0.0040
Source of Variation	P value summary	Significant?
Interaction	Ns	No
TREATMENT	***	Yes
SUBSTRATE	**	Yes

D — 2-WAY ANOVA PDGFRα

	% of total variation	P value
Interaction	9.60	< 0.0001
TREATMENT	41.89	< 0.0001
SUBSTRATE	30.47	< 0.0001
Source of Variation	P value summary	Significant?
Interaction	***	Yes
TREATMENT	***	Yes
SUBSTRATE	***	Yes

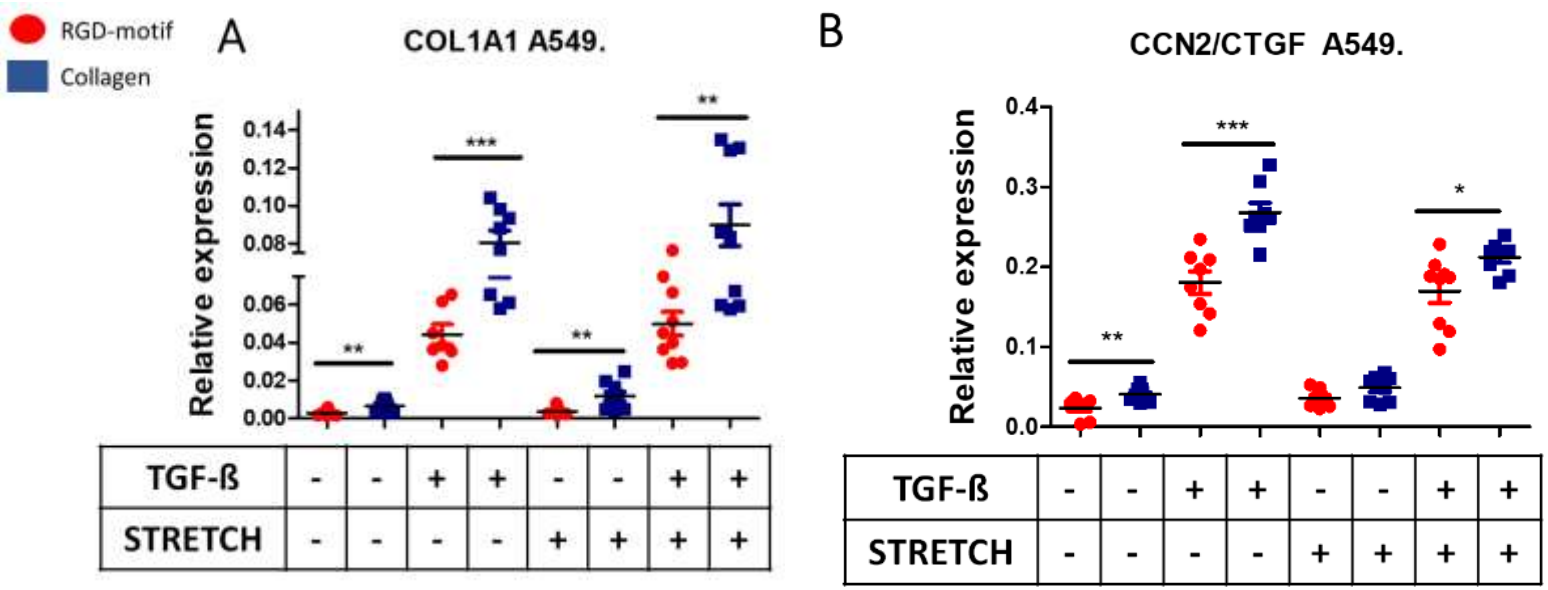

*Figure 4.3 Gene Expression analysis from A549 (n=7) (second part). (Alveolar human cell line) for COL1A1 (A), CCN2/CTGF (B), SNAI1 (C) and PDGFRα (D). Red Scattered circles represented A459 seeded on RGD-motif, while blue scattered squared A549 seeded on collagen (see top-right part of the figure). Treatments are shown by + or – indicating the presence of such variable. Student t-test was used to investigate significant differences. * symbol indicate significance related to substrate. * p-value < 0.05 ** p-value < 0.01, ***p-value < 0.001. (Please note that all results shown in the figure were significant for an overall 1-way ANOVA).*

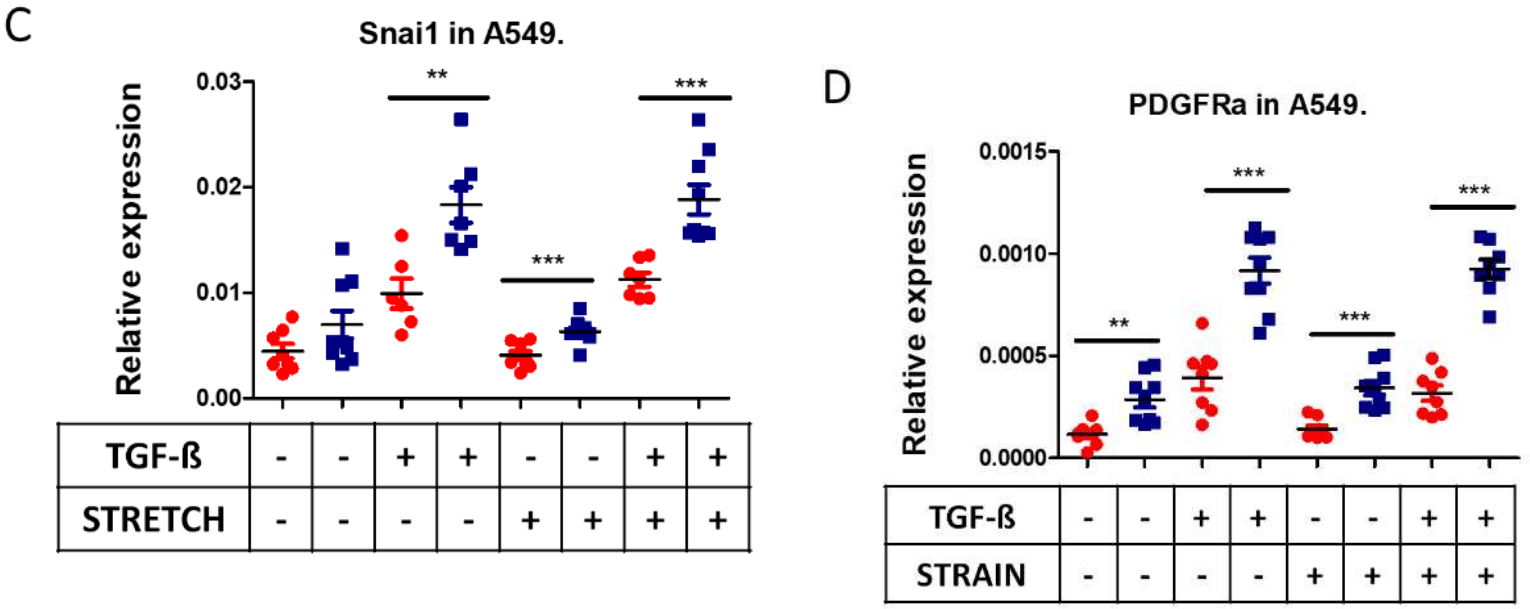

*Figure 4.3 Gene Expression analysis from A549 (n=7) (second part). (Alveolar human cell line) for COL1A1 (A), CCN2/CTGF (B), SNAI1 (C) and PDGFRα (D). Red Scattered circles represented A459 seeded on RGD-motif, while blue scattered squared A549 seeded on collagen (see top-right part of the figure). Treatments are shown by + or – indicating the presence of such variable. Student t-test was used to investigate significant differences. * symbol indicate significance related to substrate. * p-value < 0.05 ** p-value < 0.01, ***p-value < 0.001. (Please note that all results shown in the figure were significant for an overall 1-way ANOVA).*

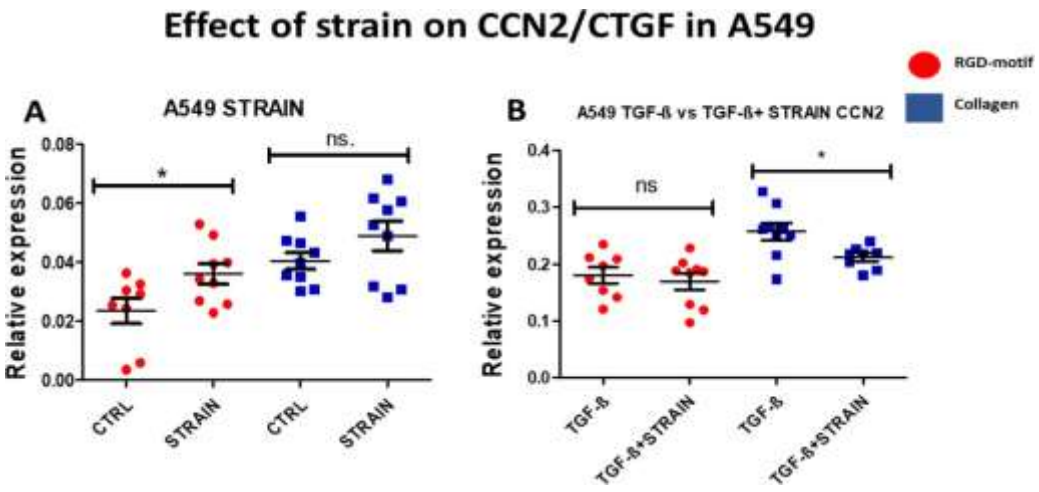

Figure 4.3 (bis) CCN2/CTGF expression level in A549 (n=7). Red circles indicate A549 seeded on RGD- motif, whereas blue squares on collagen. Effect of stretch on cells without TGF-ß (A) and after treatment with TGF-ß (B) for CCN2/CTGF.

Without any stimulation cells cultured on collagen showed higher mRNA expression for all genes studied compared to RGD-motif (fig. 4.2).

Treatment with TGF-ß at 2 ng/mL for 6 hours resulted in significant increase in expression level for all genes analysed, as visible in figure 4.3. Moreover, TGF-ß increased the expression of COL1A1 and CCN2/CTGF of 15 and 6 fold approximately. This response to TGF-ß treatment demonstrated that not only mesenchymal cells, but also epithelial alveolar cells participate in ECM turnover, however, this experiment did not show evidence on protein level.

COL1A1 expression was significantly affected by TGF-ß, treatment resulted in upregulation of COL1A1 expression from control condition on both substrates, with a higher 17-fold time relative increase in the RGD-motif group compared to the 12-fold time increase in collagen group. However, the absolute level of COL1A1 expression was again higher in the collagen group, including TGF-ß together with stretch group (Fig 4.3A and Table 4.1A). Under all conditions, COL1A1 expression was higher in cells cultured on collagen than in cells cultured on the RGD motif. TGF-ß treatment resulted in upregulation of CCN2 expression with higher 6-fold increase from control for collagen group versus a 5-fold increase in RGD-motif group (4.3 B). TGF-ß

treatment induced a proportional similar increase in SNAI1 expression in both substrates from control. After TGF-ß treatment SNAI1 expression was 38% higher in the collagen group compared to RGD-motif (fig 4.3 C). PDGFR expression resulted in a 3.5-fold time relative increase from control in both substrates induce by TGF-ß (fig 4.3 D).

Stretch did not change COL1A1 expression level from controls, and stretch did not affect TGF-ß induced expression of COL1A1 in either the collagen group or cells cultured on the RGD-motif (fig. 4.3 A). Mechanical stretch leads to increases in CCN2/CTGF expression on both substrates, however, this was only significant for cells cultured on the RGD-motif (fig. 4.4A). Stretch condition showed a 54% increase in collagen group compared to the RGD-motif. Stretch did not affect TGF-ß-induced SNAI1 expression (fig. 4.3 C). Stretch at 6% did not significantly affect PDGFRα expression from controls (fig 4.3 D)

Stretch with TGF-ß showed significant increase from control for all genes. However, for COL1A1, SNAI1 and PDGFRα this effect was triggered by the TGF-ß only (fig. 4.3). By contrast, in CCN2/CTGF the combination of the two stimulations resulted in a significant decrease from the TGF-ß group, as effect of stretch over TGF-ß (fig. 4.4 B).

Interesting, 2-way ANOVA analysis showed significant interaction for COL1A1, CCN2/CTGF and PDGFRα, demonstrating that the two stimulation trigger a different response based on which substrate A549 were cultured (Tab. 4.1).

4.3.3 A549 microRNAs expression profile

The effects of substrate, stretch and fibrotic cytokine environment (TGF-ß) on the adherent adenocarcinoma alveolar cell A549 (Tab. 2.11 in 2.5) was studied by analysing expression of microRNAs of interest (miR-21a-5p and miR-34a-5p) by Quantitative polymerase chain reaction (qPCR).

*Table 4.2 2-way ANOVA statistic was applied to calculate significative differences induced by the treatments (TGF-ß and stretch; used as row) and the substrate (used as column) for miR-21a-5p (A) and miR-34a-5p (B). Top of the figure gives numerical percentage indication on the weight of the single variable including interaction, while bottom figure shows statistical significance where * p-value < 0.05, ** p-value < 0.01 and *** p-value < 0.001.*

A

2-way ANOVA miR-21a-5p		
Source of Variation	% of total variation	P value
Interaction	2.56	0.6652
TREATMENT	6.06	0.3034
SUBSTRATE	30.40	< 0.0001
Source of Variation	P value summary	Significant?
Interaction	ns	No
TREATMENT	ns	No
SUBSTRATE	***	Yes

B

2-way ANOVA miR-34a-5p		
Source of Variation	% of total variation	P value
Interaction	1.03	0.9324
TREATMENT	0.31	0.9878
SUBSTRATE	3.68	0.2201
Source of Variation	P value summary	Significant?
Interaction	ns	No
TREATMENT	ns	No
SUBSTRATE	ns	No

*Figure 4.4 microRNA expression level in A549 (n=5) (Alveolar human cell line) for miR-21a-5p (A) and miR-34a-5p (B). Red Scattered circles represented A459 seeded on RGD-motif, while blue scattered squared A549 seeded on collagen (see top-right part of the figure). Treatments are shown by + or – indicating the presence of such variable. (C) miR-21a-5p overall expression comparison between RGD-motif (red circle) and collagen (blue squares). Student t-test was used to investigate significant differences. * symbol indicate significance related to * p-value < 0.05, *** p-value < 0.001*

Figure 4.5A and C shows miR-21a-5p expression level in A549 cells. Table 4.2A shows 2-way ANOVA results for miR-21a-5p, highlighting that only substrate influenced miR-21a-5p expression. Neither TGF-ß nor mechanical stretch affected miR-21a-5p expression in A549 cells. miR-21a-5p expression level showed a highly statistically significant 18% increase in the collagen group compared to the RGD- motif.

Table 4.2 shows 2-way ANOVA result related to figure 4.5B showing miR- 34a-5p expression

level in A549. No significant effects of either treatment or substrate were indicated by 2-way ANOVA (Tab. 4.2B and fig. 4.5B).

Results on microRNAs demonstrated that epithelial cells are strongly influenced by the substrate, while other treatments did not result in any effect detected.

In A549, COL1A1, CCN2/CTF, SNAI1, PDGFRα showed a responsiveness to TGF-ß, while collagen as substrate trigger upregulation from RGD-motif in all genes analysed plus miR-21a. Interestingly, only CCn2/CTGF showed a responsiveness to stretch, highlighting a possible role of CCN2/CTGF as mechano-sensor.

4.3.4 MRC5 Gene expression profile

At this point, I wanted to evaluate the response from the same stimulation in mesenchymal cells, as in general they are considered more important in a context of organ fibrosis. Mesenchymal cells regulate connective tissue homeostasis, sensing and responding to wide a range of *stimuli*, such as cytokines, chemokines, neurotransmitters, oxygen reactive species, hormones, and microRNAs (Kendall & Feghali-Bostwick, 2014). Therefore, using the same setting used for A549 I studied the expression of COL1A1, CCN2/CTGF, SNAI1 and SMAD7 by Quantitative polymerase chain reaction (qPCR). SMAD7 was included in this analysis as its fundamental role in repression ECM secretion in mesenchymal cells. Unfortunately, for time reason I was not able to either test PDGFRα in MRC5 and SMAD7 in A549.

*Table 4.3 2-way ANOVA statistic was applied to calculate significative differences induced by the treatments (TGF-ß and stretch, used as row) and the substrate (used as column) for Col1a1 (A), CCN2/CTGF (B) SNAI1 (C) and SMAD7 (D). Top of the figure gives numerical percentage indication on the weight of the single variable including interaction between variables, while bottom figure shows statistical significance where * p-value < 0.05, ** p-value < 0.01 and *** p-value < 0.001.*

A — 2-WAY ANOVA COL1A1

Source of Variation	% of total variation	P value
Interaction	2.41	0.6345
TREATMENT	4.31	0.3870
SUBSTRATE	10.66	0.0076
Source of Variation	P value summary	Significant?
Interaction	ns	No
TREATMENT	ns	No
SUBSTRATE	**	Yes

B — 2-WAY ANOVA CCN2/CTGF

Source of Variation	% of total variation	P value
Interaction	3.68	0.2224
TREATMENT	46.00	< 0.0001
SUBSTRATE	3.21	0.0516
Source of Variation	P value summary	Significant?
Interaction	ns	No
TREATMENT	***	Yes
SUBSTRATE	ns	No

C — 2-WAY ANOVA SNAI1

Source of Variation	% of total variation	P value
Interaction	7.28	0.0003
TREATMENT	75.49	< 0.0001
SUBSTRATE	0.51	0.2130
Source of Variation	P value summary	Significant?
Interaction	***	Yes
TREATMENT	***	Yes
SUBSTRATE	ns	No

D — 2-WAY ANOVA SMAD7

Source of Variation	% of total variation	P value
Interaction	2.92	0.1565
TREATMENT	61.32	< 0.0001
SUBSTRATE	3.32	0.0160
Source of Variation	P value summary	Significant?
Interaction	ns	No
TREATMENT	***	Yes
SUBSTRATE	*	Yes

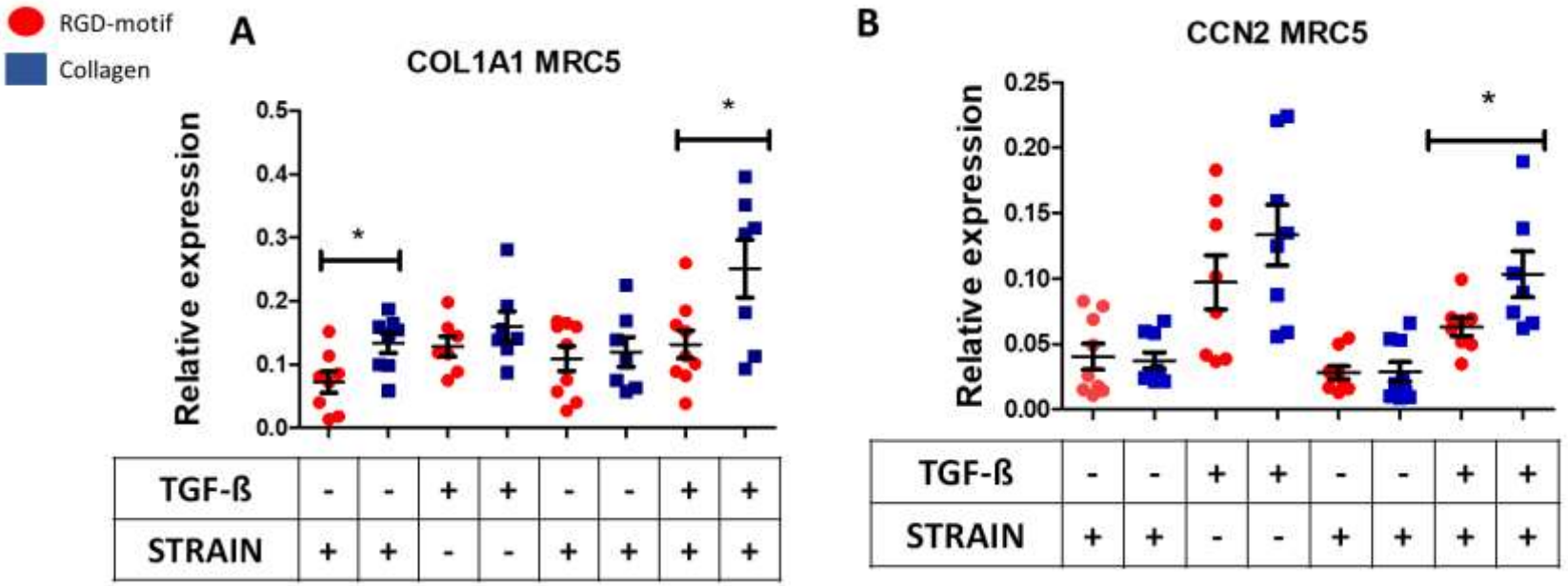

*Figure 4.5 Gene Expression analysis from MRC5 (lung fibroblast human cell line) (first part) for COL1A1 (A), CCN2/CTGF (B), SNAI1 (C) and SMAD7 (D). Red Scattered circles represented MRC5 seeded on RGD-motif, while blue scattered squared MRC5 seeded on collagen (see top-right part of the figure). Treatments are shown by + or – indicating the presence of such variable. Student t-test was used to investigate significant differences. * symbol indicate significance related to substrates * p-value < 0.05. (Please note that all results shown in the figure were significant for an overall 1-way ANOVA except for CCN2/CTGF).*

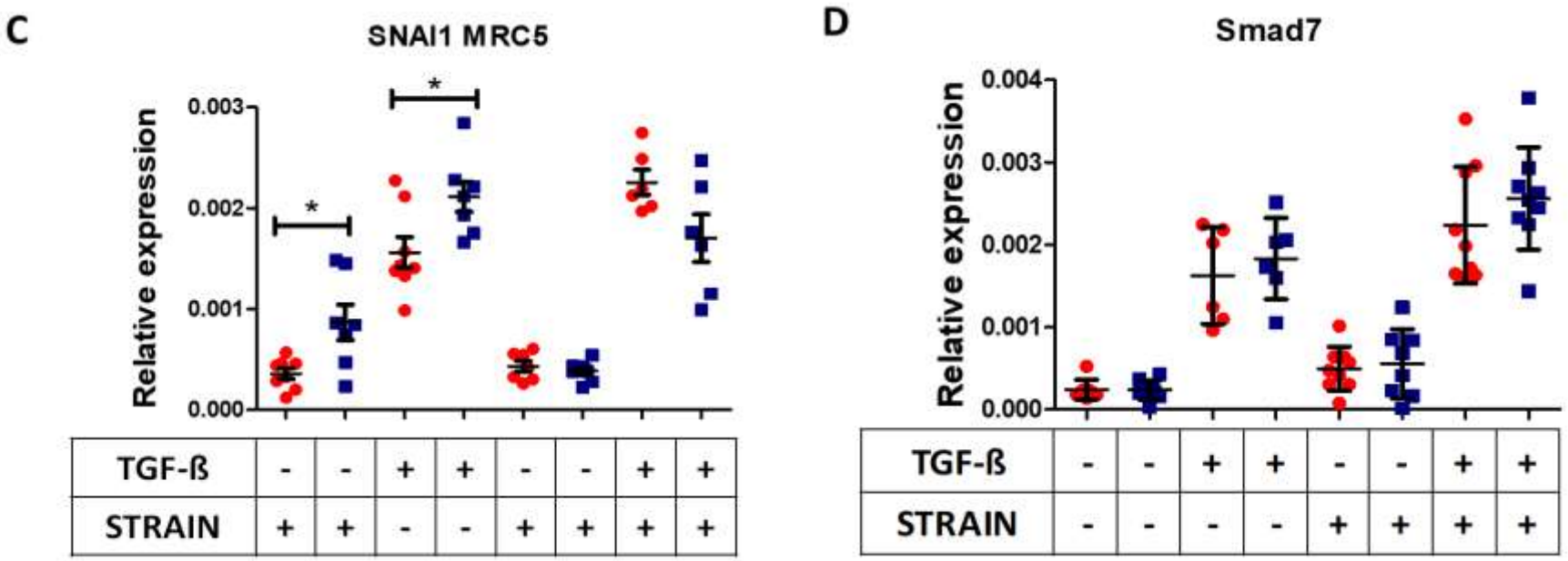

*Figure 4.5 Gene Expression analysis from MRC5 (lung fibroblast human cell line) (second part) for COL1A1 (A), CCN2/CTGF (B), SNAI1 (C) and SMAD7 (D). Red Scattered circles represented MRC5 seeded on RGD-motif, while blue scattered squared MRC5 seeded on collagen (see top-right part of the figure). Treatments are shown by + or – indicating the presence of such variable. Student t-test was used to investigate significant differences. * symbol indicate significance related to substrates * p-value < 0.05. (Please note that all results shown in the figure were significant for an overall 1-way ANOVA except for CCN2/CTGF).*

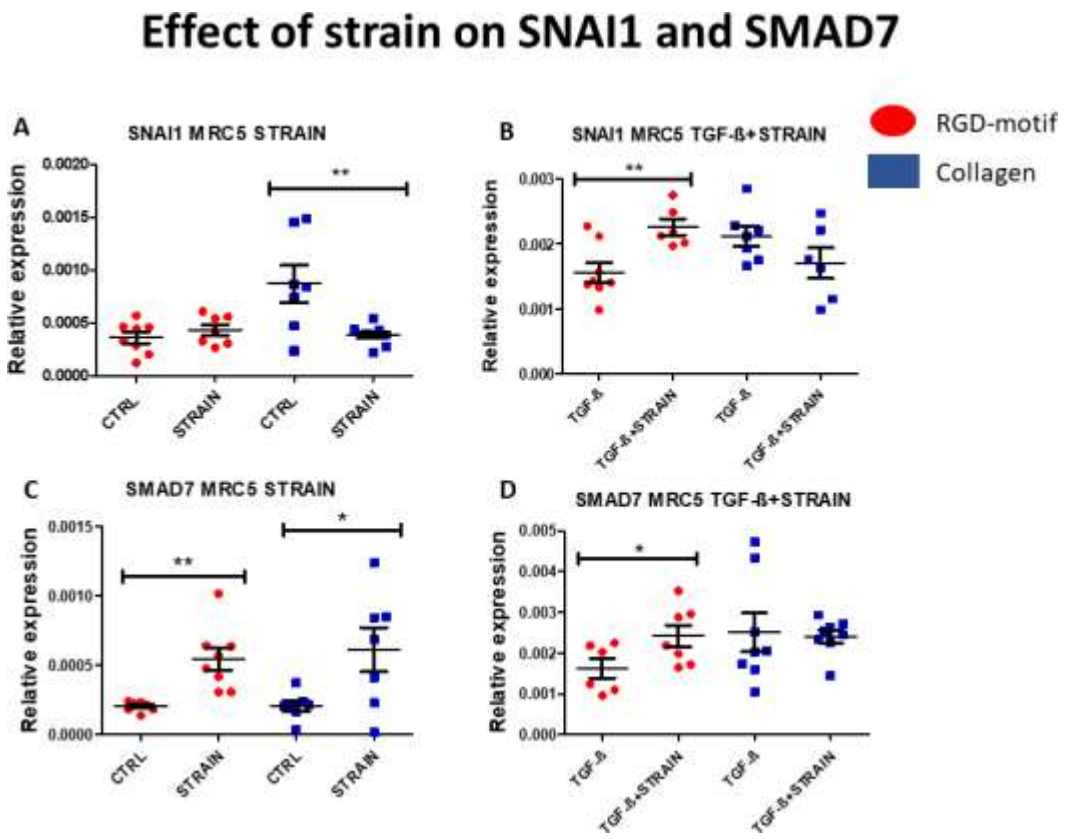

Figure 4.6 SNAI1 (A and B) and SMAD7 (C and D) expression level in MRC5. Red circles indicate MRC5 seeded on RGD-motif, whereas blue squares on collagen. Effect of stretch from control state (A and C) and from a treatment with TGF-ß (B and D) for SNAI1 and SMAD7

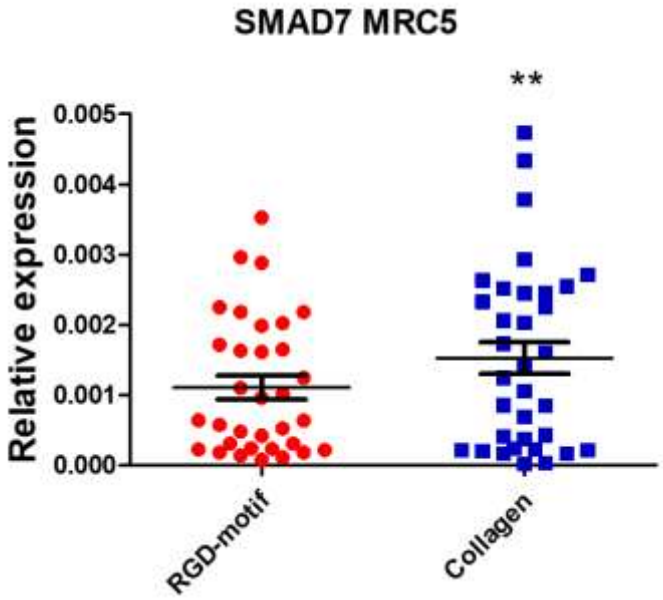

Figure 4.7 Effect of different substrates on SMAD7 expression in MRC5 (n=34). SMAD7 delta CT values were divided in two groups and student t-test for pair comparison showed a significant increase in the collagen group compared to the RGD-motif.

MRC5 showed an expression 10 times higher for COL1A1 compared to A549, while SNAI1 had 10 times lower level in MRC5 compared to A549.

Collagen as substrate induced the expression of COL1A1, SMAD7, while in SNAI1 showed a similar response for samples cultured on collagen, however this trend was lost once stretch was applied on the culture (fig. 4.6, 4.7, 4.8). COL1A1 had a significant 2-fold increase for cells cultured on collagen group compared to cells cultured on the RGD-motif (4.6 A). Cumulative analysis from all sample using paired t-test for SMAD7 highlighted a 27% increase for cells cultured on collagen substrate compared to RGD-motif, as also confirmed by 2-way ANOVA (fig. 4.8 and Tab 4.3).

TGF-ß treatment accounted for a significant 78% increase level in COL1A1 mRNA in RGD-motif from control, while collagen group did not respond to the stimulation. In CC2/CTGF TGF-ß treatment resulted in a 1.5-fold upregulation compared to control on both substrate from control. TGF-ß induced a significant 4 times increase in MRC5 cultured on RGD-motif compared to collagen group for SNAI1 (fig. 4.6 C). TGF-ß treatment induced a 4 time increase in SMAD7 expression for cells cultured on the RGD-motif group, and a 9-fold increase in cells cultured on collagen group compared to untreated groups (Fig 4.6D).

Mechanical stimulation through stretch assay only influenced SNAI1 and SMAD7, interesting CCN2/CTGF was not affect by this stimulation (fig. 4.7). SNAI1 collagen group showed a significant 55% reduction in SNAI1 expression compared to control (fig. 4.7A). Stretch induced a significant increase in SMAD7 expression from controls in both substrates, with a 2-fold increase in cells cultured on RGD-motif and a 3-fold increase in cells cultured on collagen (fig. 4.7C).

Combination of TGF-ß with stretch showed a significant increase for MRC5 cultured on collagen for COL1A1 and CCN2/CTGF with an increase of 91% for COL1A1 and a 63% for CCn2/CTGF from the RGD-motif.

Statistical analysis using 2-way ANOVA resulted in a no significant interaction for COL1A1, CCN2 and SMAD7, which indicates that treatment (TGF-ß and stretch) affected SMAD7 expression in the same direction (increase/decrease in the expression) on both substrates. By contrast, significative interaction for SNAI1 highlights that variables affect gene expression differentially (Tab. 4.3D).

4.4 Discussion

The main focus of the experiments described in this chapter was to investigate the effects of diverse substrates and mechanical stretch on genes and microRNAs believed to be involved in fibrosis, in the two main lung cell lineages: epithelial and mesenchymal.

As mentioned in the introduction, lung compliance refers to V/P relationship, which are altered in many pathological conditions, reflecting alteration to lung structure. Fibrotic lungs need higher pressure to breathe in a same amount of volume of air in inspiration compared to normal lungs (Bela Suki et al., 2011). This characteristic compliance is the result of increase in ECM after chronic damage, which also alter lung mechanical properties (Martinez et al., 2017). Fibrotic alteration dramatically changes lung function and physiology. Understand the cellular response to structural variation appears crucial to develop new antifibrotic therapy. Interesting, fibroblasts produce higher amount of ECM when seed on stiffer ECM (D. J. Tschumperlin et al., 2018). Therefore, the increase in stiffness occurring in fibrosis might have consequences on ECM production. Moreover, a stiffer material is always harder to stretch, therefore a stiffer ECM needs more work, as the product of force per distance to extend the surface during breathing. In addition, in later stages of lung fibrosis lungs there is a lack in stretch due to ECM excess. Therefore, the first hypothesis was to verify if stretch reduces expression of ECM gene upregulated in fibrosis. To assess this, epithelial and mesenchymal lung cells were seeded on an elastic material, coated with two major ECM components representing a healthy and profibrotic set. The system used was similar to the one invented by Wirtz and Dobbs in 2000, who developed a stretch assay for lung cells, using a RGD-motif coated elastic membrane and a sinusoidal stretch (Wirtz & Dobbs, 2000).

Results obtained on stretch suggested a possible protective role of stretch, able to downregulate the expression of COL1A1 and CCN2/CTGF in A549 and upregulate SMAD7 in lung fibroblasts. As suggested by Wirtz and Dobbs work, stretch might regulate ECM turnover and epithelial/mesenchymal communication occurring in foetal alveolar development (Wirtz & Dobbs, 2000). Although results showed in the chapter are not focused on lung development, both results highlight a key role of stretch in regulation of proliferation and ECM turnover. Moreover, mathematical model of lung injury suggested that stretch holds a protective role in tissue repair, which is conceptually in line with results found in this chapter (Savla et al., 2004).

Nevertheless, substrate showed a higher regulative power on ECM and miR gene regulation compared to stretch. Fibrotic substrate (collagen) upregulated COL1A1, CCN2/CTGF, SNAI1, PDGFRα as well as miR-21a-5p expression in A549 cells and COL1A1, SMAD7 in MRC5.

As expected, TGF-ß stimulated the expression of most of the fibrotic genes in both cell types. A549 showed significant upregulation induced by TGF-ß in COL1A1, CCN2/CTGF, SNAI1 and PDGFRα, while in MRC5, TGF-ß stimulated CCN2/CTGF, SNAI1 and SMAD7 expression. By contrast, both microRNAs did not show increased expression induced by TGF-ß treatment. This latest result was not in line with other publication reporting miR-21a and miR-34a responsiveness to TGF-ß (Cui et al., 2017). However, this might be a consequence of the coated membrane, strain, or diverse time points, as Cui and collaborators used a similar setting employing A549.

Collagen type 1 is the major component of fibrillar collagen, which in lung confers organ structural rigidity during the “bellow-like movement” (Laurent, 1986). Moreover, it composes 15% of the organ weight (30% of lung dry weight) and COL1A1 upregulation is a characteristic hallmark in all organ fibrosis (Laurent, 1986; Ricard-Blum, 2011). Thus, during fibrosis, normal tissue parenchyma made of collagen, laminin, elastin, fibronectin, and others protein, is replaced by type-I collagen. In general, COL1A1 showed a good responsiveness to TGF-ß and fibrotic substrate in both A549 and MRC5. Interestingly, MRC5 showed higher control levels of COL1A1 compared to A549, which reflect the difference between epithelial and mesenchymal cells. TGF-ß-induced COL1A1 with higher magnitude in A549 than in MRC5, although COL1A1 expression was relatively higher in MRC5 than A549. In both cell lines, TGF-ß treatment results in relatively higher increase in COL1A1 expression in the RGD-motif group compared to the collagen group. In Epithelial A549 cells, collagen as substrate resulted in a twofold increase in COL1A1 expression under all experimental conditions, while in MRC5 cells cultured on collagen triggered the same effect only in the control group and for the combined TGF-ß and stretch group. These results indicate a possible positive feedback loop during fibrosis where the presence of a matrix rich in collagen type 1 further increases COL1A1 expression. One possible mechanism is that collagen fibres act as ligand for signalling transduction. This possibility is supported by stereospecific bond between collagen GFOGER

motif and integrin α2ß1, which emerged to undergo conformational changes (Mejía et al., 2015). Collagen-induced changes in α2ß1 structure which may activate pathways, resulting in increased COL1A1 expression (Jia, Li, Peng, Ding, & Alexov, 2018). In both wound healing and in fibrosis mechanical stretch and TGF-ß can increase COL1A1 expression (Savla, Olson, & Waters, 2004). My results on COL1A1 expression demonstrate that a fibrotic environment (TGF-ß and collagen as substrate) increases COL1A1 expression in both lung epithelial and mesenchymal cells.

CCN2/CTGF is a protein belonging to CCN family and it is an ECM component. CCN2/CTGF has two main roles, it is an ECM protein, and it is a paracrine modulator for other ECM protein (Hall-Glenn & Lyons, 2011). This protein has been extensively studied in fibrosis and transgenic mouse models have identified it as a pro-fibrotic protein (S. Liu et al., 2011; Sonnylal et al., 2010). CCN2/CTGF showed similar control level between epithelial and fibroblast cells, however A549 were more responsive to TGF-ß, displaying also less variance between technical replicates. A549 showed results similar to COL1A1 with CCN2/CTGF expression increased by both TGF-ß and the collagen substrate. Although TGF-ß treatment stimulated CCN2/CTGF expression in both A549 and MRC5 cells, there were differences in the magnitude of the response between cell lines, with a two-fold increase in MRC5 cells and a 5-fold increase in the A549 cells. In A549 cells the substrate significantly affected the expression of CCN2/CTGF, the RGD-motif group showed a higher relative increase from control state compared to collagen coated plate. CCN2/CTGF expression in the A549 epithelial cells was strongly dependent on the culture substrate, whereas in MRC5 cells this effect was not statistically significant. Stretch strongly affected CCN2/CTGF gene regulation in A549, and although a similar trend was observed in the MRC5 cells, this was not statistically significant. The unexpected high variability in MRC5 may have masked any stretch related effect. Interestingly, in A549 cells, stretch appears to have a protective antifibrotic effect as stretch downregulated CCN2 expression in cells cultured in fibrotic substrate condition (collagen and TGF-ß).

SNAI1 is a DNA binding repressor involved in mesoderm formation during embryogenesis, where it represses E-cadherin expression, and stimulates N- cadherin expression. This is why SNAI1 was characterised as one of most important EMT regulators (Nieto, 2002; Thiery et al., 2009). TGF-ß induces EMT, and EMT is an important process in

organ fibrosis, as it augments the number of resident fibroblasts (Takano et al., 2017). However, the role of SNAI1 in fibroblasts is poorly understood. The results in this chapter are in line with a stimulatory effect of TGF-ß on SNAI1 expression in both cell lines (Hwangbo et al., 2016). Moreover, TGF-ß induced SNAI1 expression ten times more in epithelial A549 than in MRC5 fibroblasts, although a low base line expression in the epithelial A549 cells. Cells on a fibrosis-mimicking substrate, collagen, resulted in higher SNAI1 expression in both cell lines, with levels 10 times higher in A549. The effect of the fibrotic substrate was more pronounced in the A549 cells than in the MRC5 cells. Only in A549, SNAI1 expression was consistently higher when cells were cultured on collagen, which may induce EMT, contributing to fibrosis. Stretch only affects SNAI1 regulation in MRC5, where stretched cultures on collagen showed a downregulation in gene expression. This reduction in SNAI1 expression suggested that stretch may have a protective effect against fibrosis.

PDGFRα is a tyrosine kinase receptor with a high mitogenic activity fundamental for a correct wound healing repair and lung morphogenesis (Whitsett et al., 2018). Although PDGFR α is mesenchymal marker, we wanted to understand its role in epithelial lung cell as bridge between EMT and fibrosis (Wu et al., 2012). Moreover, PDGFR α is the binding receptor for PDGFα, a pro-inflammatory cytokine able to activate myofibroblasts and PDGFRα is known to be activated in fibrosis (Wynn, 2011). As expected, TGF-ß stimulated PDGFRα expression in the A549 cells. Culture of A549 cells on collagen resulted in increased PDGFRα expression under all experimental conditions. Stretch did not affect PDGFRα expression in A549 cells. These results are in line with previous studies suggesting a role of PDGFR α in fibrosis and EMT progression (Wu et al., 2012). A fibrotic environment (TGF-ß and collagen substrate) results in an increase in PDGFR α expression, which may stimulate EMT in A549 epithelial cells. However, results obtained alone cannot be referred to increase in EMT as they lack in pathways analysis on PGDFRα signalling and information on cytoskeleton remodelling in EMT. Possibly, stimulation with PDGFRα agonist (PDGFα) might confirm a role for PDGFRα in EMT.

SMAD7 is an inhibitory intracellular protein involved in the TGF-ß pathway, where it limits TGF-ß signalling cascade, which can also limit fibrosis progression (Lan, 2008; Mouratis & Aidinis, 2011). SMAD7 is induced by TGF-ß, and this results in a negative feedback on TGF-ß activity. As expected, TGF-ß upregulated SMAD7 expression in the MRC5 cells. In addition, mechanical stretch increased SMAD7 expression, suggesting again that stretch may have an

antifibrotic role as it induced SMAD7 expression. This upregulation depending on stretch may be then lost in the course of fibrosis, as tissue become stiffer. Moreover, stretch only upregulated TGF-ß-induced SMAD7 expression when cells were cultured on the RGD-motif, while on collagen stretch no longer increased TGF-ß-induced SMAD7 expression. Therefore, the antifibrotic effect of stretch-induced SMAD7 expression may be lost in a fibrotic environment.

miR-21a-5p is a small non-coding RNA up-regulated in lung tissue from patients affected by lung fibrosis. Predicted alignment algorithms indicate a 8-mer binding site at SMAD7 3'-UTR (Li et al., 2013; G. Liu et al., 2010). In Chapter 3, miR- 21a-5p showed a pro-fibrotic behaviour, displaying a progressive up-regulation parallel to fibrotic progression. TGF-ß does not affect miR-21a-5p expression in epithelial A549 lung adenocarcinoma cells. However, culturing the cells on fibrotic substrate, rich in collagen, miR-21a-5p expression was resulted significantly increased, showing a response to fibrotic stimulation. miR-21a-5p expression was influenced by substrate in epithelial A549 cells, which might affect SMAD7 expression in fibroblasts. Although this study is limited by the use of an adenocarcinoma cell line, our results show an overall agreement with previous publications. Moreover, they clarify the protective role of stretch in lung fibrosis, and a profibrotic role of an ECM rich in collagen.

miR-34a-5p expression has been reported to be related to EMT progression after TGF-ß treatment, key in IPF (Cui et al., 2017). As for miR-21a-5p, miR-34a-5p expression was upregulated in the experimental Bleomycin model of lung fibrosis (Chapter 3). However, in the experiments described in this chapter miR-34a-5p expression cells was not affected by TGF-ß, stretch or the culture substrate in A549. This might depend on the experimental set-up used for this experiment, as the system used can be considered more informative than no-coated plates. TGF-ß concentration, timing, cell variability are variables that could have affected miR-34a-5p levels.

An important limitation which could in principle affect this set-up is undoubtedly substrate thickness, as it can dramatically influence ECM gene expression. In addition, fibronectin, laminins, elastin, and other ECM components are all upregulated during fibrosis. However, results obtained highlighted a stronger induction of collagen substrate compared to RGD-motif, demonstrating a novel role of parenchyma in the stimulation of profibrotic

genes. Understand this crosstalk might highlight novel roles for collagen in fibrosis.

Another limitation of note for the study lay in the use of cell lines, as primary cells can better represent physiological conditions.

In details, as A549 cells are an adenocarcinoma alveolar cell line and therefore cannot be considered the best model to use for a study on fibrosis. However, currently, there are no validated experimental procedures able to generate primary alveolar epithelial culture, except using stem cells or cell sorting. Generation of an alveolar epithelium from stem cells has several important drawbacks, as maintaining of stemness characteristics (Dye, Miller, & Spence, 2016). The cell sorting procedure from small rodents has a low yield. Furthermore, both techniques are labour intensive, take a long time and are quite expensive. On the other hand, the A549 cell line is widely used in lung research, as cells possess several features of alveolar type-I and type-II cells (Junghyun Kim et al., 2018).

MRC5 is an immortalised cell line isolated from the lung of a 14 week-old aborted foetus. Although this cell line cannot represent a mature lung fibroblast, MRC5 are not a cancer cell type and for that can be considered a better cellular model for a study on fibrosis. However, they had a higher level of variability in the response compared to A549.

Unfortunately, due to time constriction qPCRs for SMAD7 in A549 and PDGFRα in MRC5 were not performed.

Table 4.4 and 4.5 summarise all results obtained in this chapter.

Table 4.4 Sum of qPCRs from A549. In the column there are listed the genes and miRs of interest, whereas in the row the different stimulation performed. Up facing arrows (↑) indicates upregulation, while down facing arrows (↓) downregulation in expression

A549	TGF-ß	COLLAGEN SUBSTRATE	STRETCH
COL1A1	↑	↑	-
CCN2/CTGF	↑	↑	↓
SNAI1	↑	↑	-
PDGFRα	↑	↑	-
miR-21a-5p	-	↑	-
miR-34a-5p	-	-	-

Table 4.5 Sum of qPCRs from MRC5. In the column there are listed the genes and miRs of interest, whereas in the row the different stimulation performed. Up facing arrows (↑) indicates upregulation, down facing arrows (↓) downregulation in expression and ↓/↑ indicates a diverse result depending on experimental conditions (TGF-ß and substrate; see fig. 4.7)

MRC5	TGF-ß	COLLAGEN SUBSTRATE	STRETCH
COL1A1	-	↑	-
CCN2/CTGF	↑	-	-
SNAI1	↑	↑	↓/↑
SMAD7	↑	↑	↑

5 Effect of ECM substrates and ageing on mRNA and miR expression in primary mouse lung fibroblasts in a 2D model of Lung Fibrosis

5.1 Introduction

In chapter 4, differences in ECM highlighted a profibrotic role of collagen rich substrate on COL1A1, CCN2/CTGF, SNAI1 PDGFRα and miR-21a-5p expression in epithelial adenocarcinoma alveolar cells (A549), while it slightly increased expression of SMAD7 in immortalised lung fibroblasts (MRC5). As mentioned in 4.4, cells lines are immortalised and clonal, and do not represent a true physiological state, while primary cells are more similar to physiological condition. Therefore, they can represent more reliable system in term of cell cycle and response for *in vitro* studies on fibrosis. Using, then, the same *in vitro* culture system employed for cell lines experiments (chapter 4), I further studied this *in vitro* system in primary lung fibroblasts, due to their strong influence on ECM remodelling and primary role in fibrotic development. The fibrosis related genes analysed were fibrillar collagens (Collagen types 1 and 3), EMT master regulators (Snai1 and Slug), Ccn2/Ctgf and inhibitory Smads (Smad6 and Smad7), as well as fibrosis related microRNAs (miR-21a and miR-34a). Please note that the rational beyond the measurement of Snai1 and Slug mRNAs in fibroblasts refer to their importance as regulators of genes involved in cell motility.

Expression of Col1a1 and Col3a1 is upregulated in lung fibrosis, leading to a change in ECM composition (Ricard-Blum, 2011). Although fibroblasts are known to bind fibrillar collagen *via* integrin $\alpha_1ß_2$ and discoidin receptors, it is unclear if fibrillar collagen holds a feedback activity in fibroblasts (Mejía et al., 2015; Ricard-Blum, 2011). In chapter 4, the results highlighted a possible positive feedback operated by collagenous membrane on expression of key genes in fibrosis in both epithelial and mesenchymal cell lines. Therefore, I studied the cellular responses to a fibrotic-like ECM composed of Collagen in comparison to a non-fibrotic matrix modelled using RGD-motif peptides.

Lung fibrosis mostly affects the elderly, and the reasons for this are currently unclear, although one factor may be an increase ECM crosslinking (King et al., 2000). Moreover, during ageing tissue damage can increase over time which, in combination with lifestyle, genetic and environmental factors, might evolve into a pathological condition.

Obviously, immortalised cell lines do not allow the study of the effects of ageing on cell responses. Furthermore, as mentioned above, cell lines, although useful as model systems, may not completely reflect physiological condition. In contrast primary cells can be used for studies on age, as they can be isolated from model organisms at different ages. However, as mentioned in the introduction, animal ages used in an experiment must refer to the animal age that shows similarities with a human phenotype (also at genetic level). Therefore, in this chapter I performed studies similar to those in Chapter 4 but in primary lung fibroblasts isolated from young adult (3- months-old) and aged (14-15-month-old) mice. The rational beyond the use of this age was that after 12 months of age mice starts to change key physiological parameters, as result of ageing process (Schulte et al., 2019). Therefore, as age has a key role in fibrosis, I wanted to investigate in this *in vitro* model the differences in the response to profibrotic stimulation (TGF-ß and Substrate). In addition, I wanted to further verify stretch protective response found in A549 and MRC5 also in primary mouse lung fibroblasts.

In this setup I also analysed the role of miR-21a and miR-34a, in primary lung fibroblasts (TGF-ß, substrate, stretch and age). The sub-aim of this procedure was to provide key insight for further use in the development of antifibrotic therapy for IPF. Moreover, I wanted to verify if miR-34a was influenced by age. This is because miR-34a has been already extensively documented to be fundamental in different processes correlated with ageing. As mentioned in the introduction, miR-34a targets to p53 and SIRT1 two key proteins involved in cancer and ageing, and that appeared upregulated in the Bleomycin model of lung fibrosis (chapter 3) (Smith-Vikos & Slack, 2012).

The aged mice used in this chapter were also used by Miss Jacquelin Lin, a member of my group, who was studying the role of p38 (MAPK) in aged bones cells and macrophages. Therefore, in order to respect the principle of reduction (3Rs https://www.nc3rs.org.uk/the-3rs), we used mice at an age representative of ageing in both the lung and the skeleton.

5.2 Material and Methods

5.2.1 Cell culture

Primary mouse lung fibroblasts were isolated from young and aged C57BL6/J mice (n=6) according to the method described in 2.5.2. Next, 10^5 cells per well at passage 2 were seeded on either RGD-motif- or collagen-coated 6 well plates from Flexcell as described in 2.5.4. Cells were stimulated with TGF-ß at 2 ng/mL for 6h while 0.1% BSA in PBS was used as vehicle. To mimic lung deformation during breathing, the Flexcell Tension system was set at 6% of stretch and 1 Hz to mimic lung parenchymal dynamics (2.4.5).

5.2.2 mRNA and miR qPCR method and statistical analysis

RNA isolation, reverse-transcription and qPCRs were performed as described in paragraph 2.5. 2-way analysis of variance was used to understand the effects of ageing and substrate and if there was any statically interaction between the two variables in the experiments. Student's t-test was used to analyse the effects of single variables (substrate, ageing and stretch), as described in 2.7.

5.3 Results

5.3.1 Mechanical stretch and ageing modify primary mouse lung fibroblasts shape.

During the 6h of mechanical loading, cells were treated with 2 ng/mL of TGF- ß or vehicle. At the end of the loading, the cells were imaged using a Nikon Inverted TiE microscope (fig. 5.1)

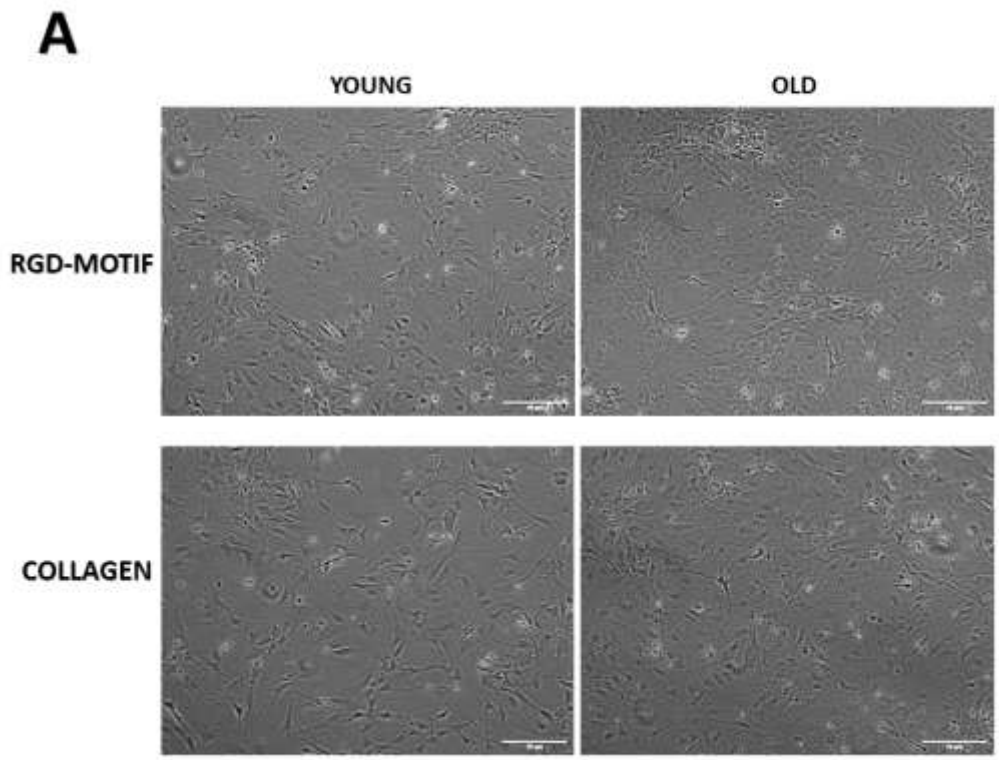

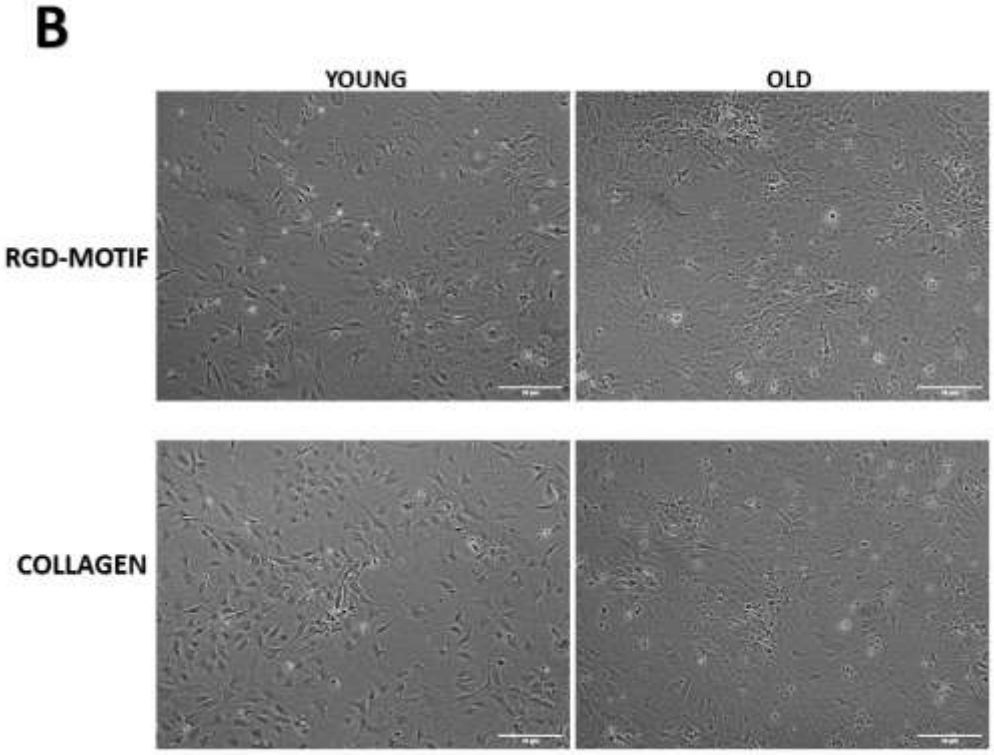
B
YOUNG
OLD
RGD-MOTIF
COLLAGEN

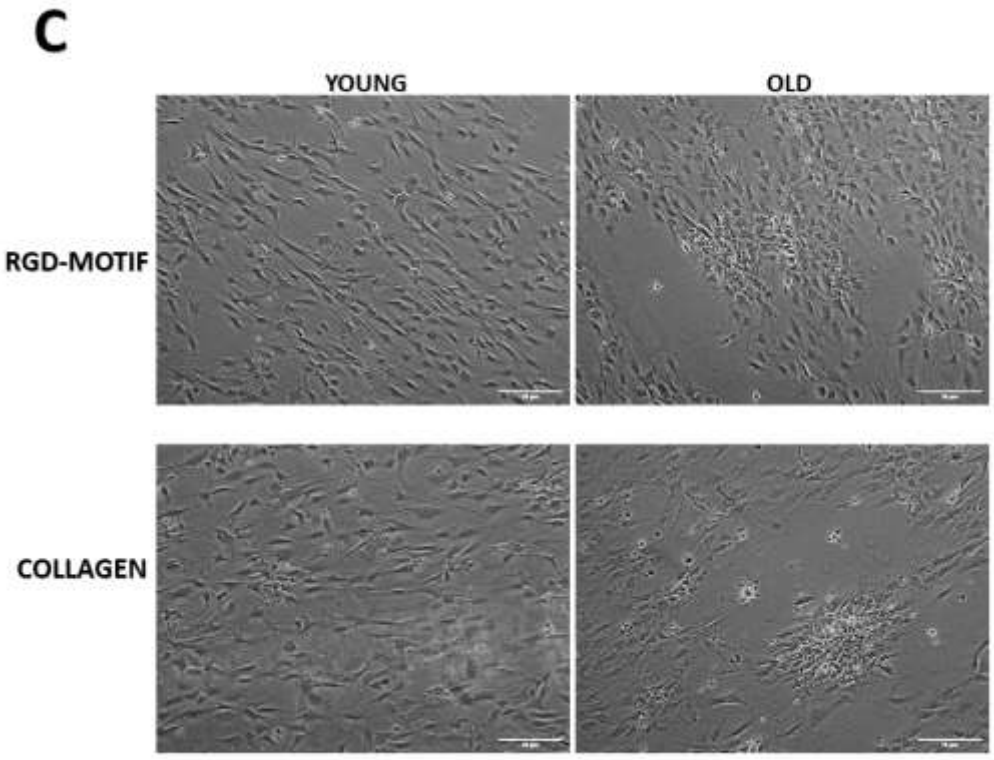
C
YOUNG
OLD
RGD-MOTIF
COLLAGEN

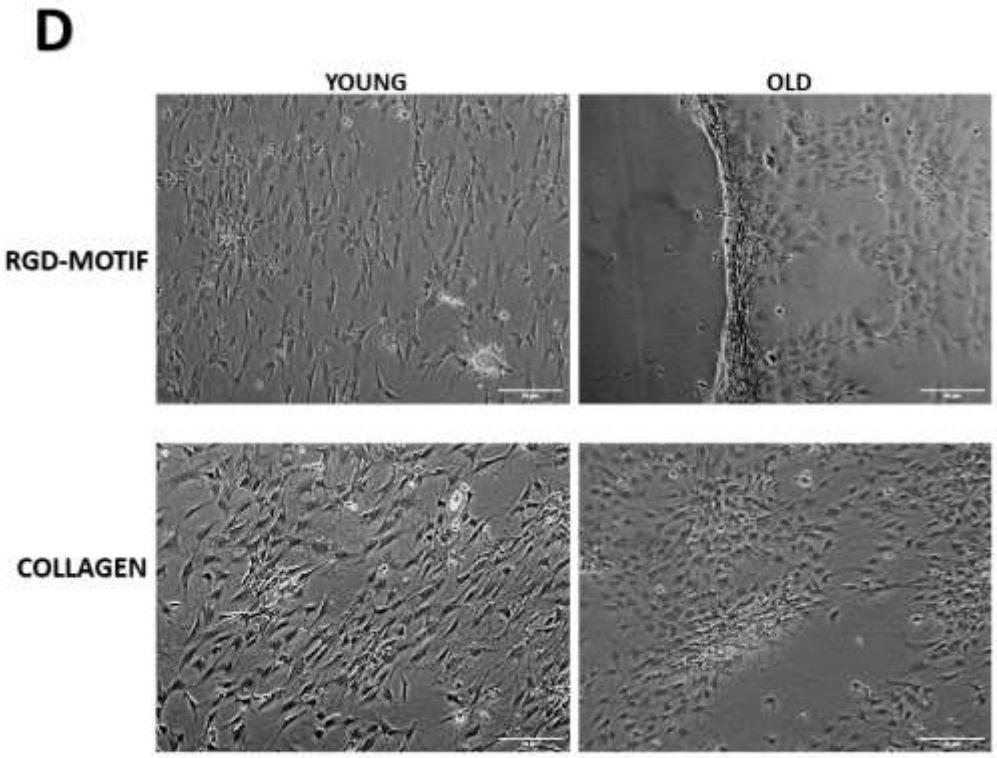

Figure 5.1 Phase contrast images obtained from culture of primary mouse lung fibroblast at 10X magnification. Cells were seeded onto either RGD-motif or collagen (type 1) 6 well plate and treatment with BSA (used as control for TGF-ß effect) and not stretched using the Flex system (used as control for the latter condition A), TGF-ß at 2ng/mL and not stretched (B), Stretched at 6% of Stretch and at 1 Hz and treated with BSA (C) and stretched at 6% of stretch and 1 Hz and treated with TGF-ß at 2 ng/mL. [scale bar 50 µm].

Figure 5.1 shows phase contrast images obtained from the application of the stretch at 6% 1 Hz for 6 hours. At 6% of mechanical stretch cells appear to increase their confluency to the no-stretched cells. Moreover, mechanical stretch appears to lead to a change in cell shape. Application of stretch leads to differences between cultures of young and aged fibroblasts, where stretch seems to stimulate cell aggregation and clumping of cells in cultures from aged mice.

TGF-ß and substrates did not seem to affect cell confluency or shape of the primary fibroblasts.

5.3.2 Gene expression profile

Quantitative polymerase chain reaction (qPCR) for genes of interest was used to investigate the effect of substrate, ageing and stretch on primary mouse lung fibroblasts (n=6).

*Table 5.1 2-way ANOVA results for Col1a1 calculated to identify differences induced by treatments (TGF-ß, Substrate and stretch) and ageing. Top of the figure gives numerical percentage indication on the weight of the single variable including interaction, while bottom figure shows statistical significance where * p-value < 0.05, ** p-value < 0.01 and *** p-value < 0.001.*

2way ANNOVA Col1a1		
Source of Variation	% of total variation	P value
Interaction	10.28	0.0433
TREATMENT	23.28	< 0.0001
AGE	8.01	0.0009
Source of Variation	P value summary	Significant?
Interaction	*	Yes
TREATMENT	***	Yes
AGE	***	Yes

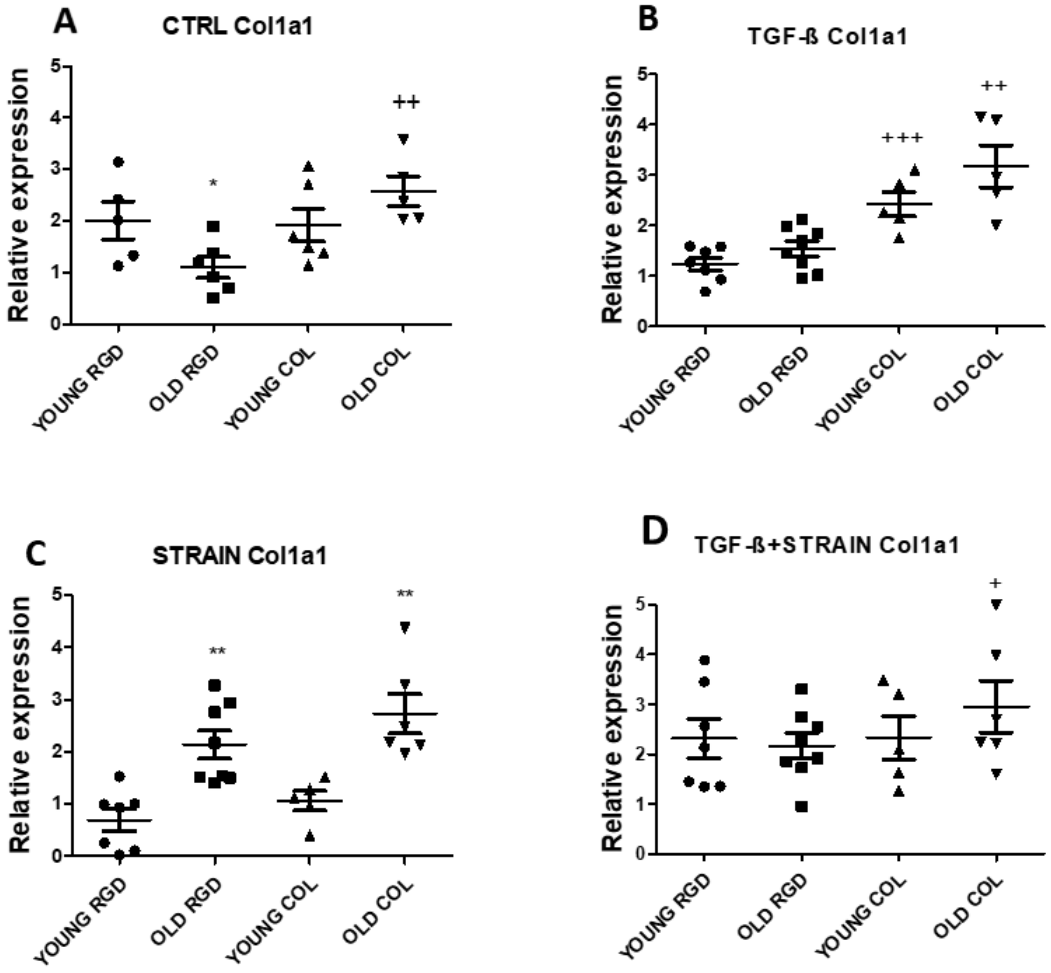
A
CTRL Col1a1
Relative expression
YOUNG RGD
OLD RGD
YOUNG COL
OLD COL
B
TGF-ß Col1a1
C
STRAIN Col1a1
D
TGF-ß+STRAIN Col1a1

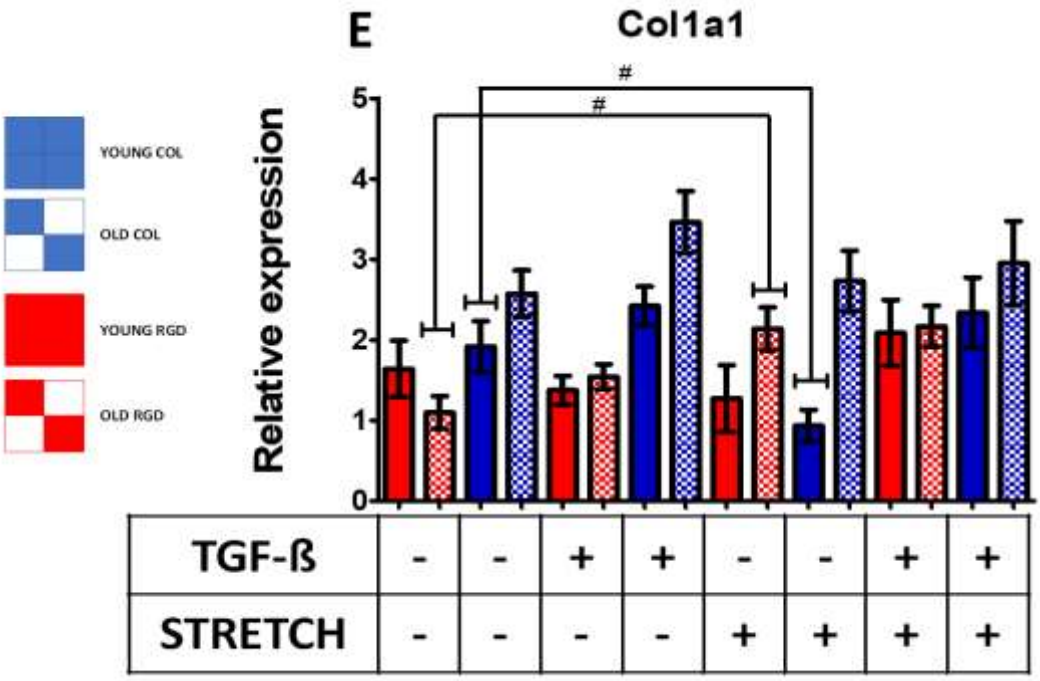

Figure 5.2 Gene Expression analysis from primary mouse lung fibroblast for Col1a1. Scatter dot-plot where each dot represents an individual mouse donor (A-D). A) Control. B) Fibroblasts treated with 2ng/mL of TGF-ß. C) Fibroblasts stretched at 6% of stretch. D)Fibroblasts receiving both 2 ng/mL of TGF-ß and stretch at 6% 1 Hz. E) Sum of all experimental group, where blue bar-charts indicate cell seeded on collagen plate and red bar-charts cells on RGD-motif plate. Patterned bar-charts indicate the old subgroup while the solid ones indicate the young group (panel on graph's left). Student t-test was used to investigate significant differences between two groups. Differences in substrate are indicated by "+", differences in age-related are indicated by "". * and + p-value < 0.05, ** and ++ p-value < 0.01, +++ p-value < 0.001. Differences due to the effect of stretch are indicated by the "#", # p-value < 0.05.*

Analysis by qPCR of Col1A1 expression by 2-way ANOVA indicates a significant effect for the treatment applied to the culture (TGF-ß, substrate and stretch) as well as age. Moreover, significant interaction between age and treatment indicated that the age of the cells affected the response to the treatments (Table 5.1).

In the vehicle control group, the substrate does not affect Col1a1 expression in the fibroblasts from young mice. However, aged fibroblasts show a 2-fold increase in Col1a1 mRNA expression in the cells cultured on collagen compared to those cultured on the RGD-motif. This increase indicates that in non-fibrotic environment old fibroblasts produce more collagen if in contact on collagenous substrate. Moreover, young fibroblasts on RGD-motif showed a significant 1.5-fold increase from the old group on the same substrate (fig. 5.2A).

Therefore, without stimulation old fibroblasts cultured on non-fibrotic ECM produce

less Col1a1.

Treatment with TGF-ß did not significantly increase Col1a1 mRNA expression in fibroblasts cultured on the RGD- motif regardless of the age. Treatment with TGF-ß resulted in higher expression levels of Col1a1 on collagen compared to the RGD-motif for both young and old fibroblasts, respectively 1.7-fold in young and 2.5-fold in old (fig. 5.2B). Therefore, TGF-ß stimulation seems to be stronger for old fibroblast on collagen coated plates.

Stretch alone resulted in a 2-fold increase in Col1a1 expression in the old fibroblast on RGD-motif but not on old cells cultured on collagen. In the young fibroblasts, mechanical stretch leads to a decrease in Col1a1 expression of approximately 2-fold in RGD-motif and 3 fold in collagen (fig. 5.2C and E).

TGF-ß alone and the combination of TGF-ß and stretch resulted in a significant upregulation of Col1a1 in the aged group on the collagen compared to the cells cultured on RGD-motif (fig. 5.2D).

All treatments (substrates, TGF-ß and stretch) and age strongly affected Col1a1 expression. Moreover, substrates and TGF-ß seems to be stronger independent profibrotic stimulation, while stretch seems to have an inhibitory role against Col1a1 increase.

*Table 5.2 2-way ANOVA results for Col3a1 calculated to identify differences induced by treatments (as row: TGF-ß, Substrate and stretch) and ageing (as column). * p-value < 0.05, ** p-value < 0.01 and *** p-value < 0.001 *** p-value < 0.001.*

2way ANNOVA Col3a1		
Source of Variation	% of total variation	P value
Interaction	4.45	0.6342
TREATMENT	18.03	0.0068
AGE	1.08	0.2634
Source of Variation	P value summary	Significant?
Interaction	ns	No
TREATMENT	**	Yes
AGE	ns	No

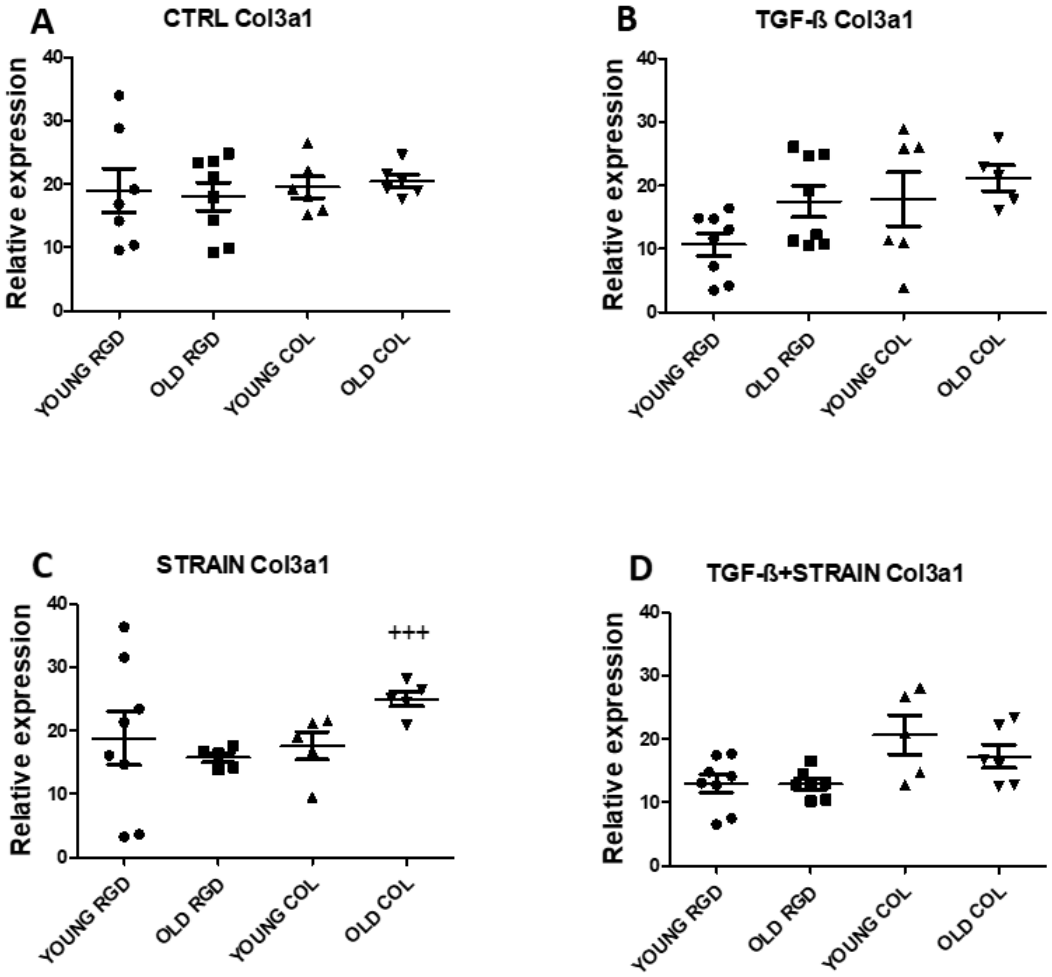
A
CTRL Col3a1
Relative expression
40
30
20
10
0
YOUNG RGD
OLD RGD
YOUNG COL
OLD COL
B
TGF-ß Col3a1
Relative expression
40
30
20
10
0
YOUNG RGD
OLD RGD
YOUNG COL
OLD COL
C
STRAIN Col3a1
Relative expression
+++
40
30
20
10
0
YOUNG RGD
OLD RGD
YOUNG COL
OLD COL
D
TGF-ß+STRAIN Col3a1
Relative expression
40
30
20
10
0
YOUNG RGD
OLD RGD
YOUNG COL
OLD COL

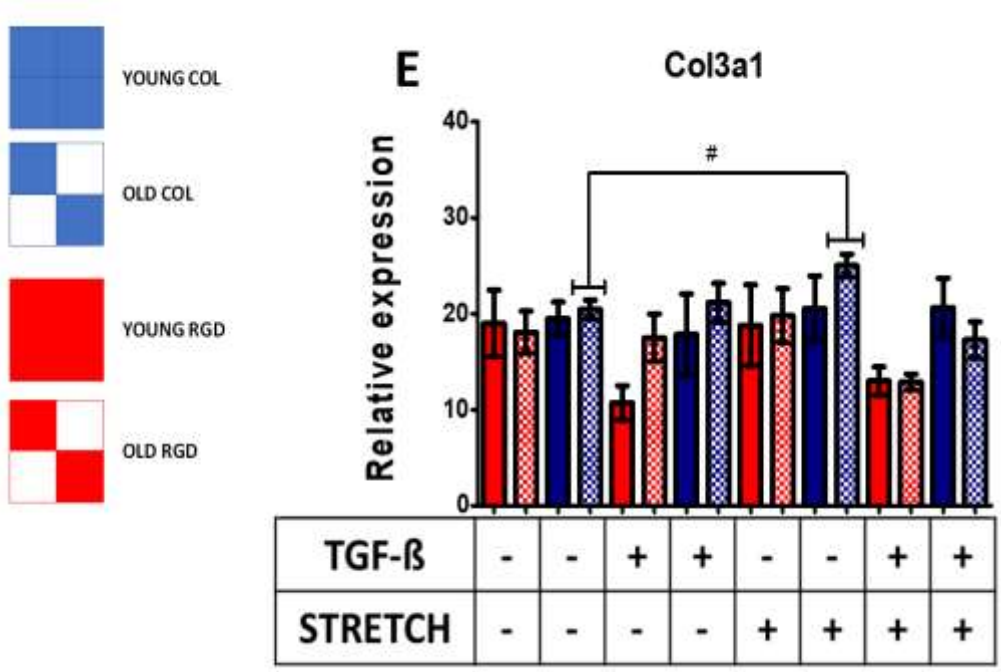

Figure 5.3 Gene Expression analysis from primary mouse lung fibroblast for Col3a1. Scatter dot-plot where each dot represents an individual mouse donor (A-D). A) Controls. B) Fibroblasts treated with 2ng/mL of TGF-ß. C) Fibroblasts stretched at 6% of stretch. D) Fibroblasts receiving both 2 ng/mL of TGF-ß and stretch at 6% 1 Hz. E) Sum of all experimental group, where red circle scatter-dots indicate cell seeded on RGD-motif plate and blue square scatter-dots cells on collagen plate regardless age of the cells (as 2-way ANOVA not significant for age). Student t-test was used to investigate significant differences. Differences in substrate are indicated by p-value < 0.05, +++ p-value <0.001.

2-way ANOVA results showed a significance only for treatments (TGF-ß, substrate and stretch) in total expression variance, which accounted for 18.03% of total percentage variation (Tab. 5.2).

Without stimulation, there are no differences in Col3a1 expression regardless of the age of the donor mice or the substrate on which the cells were cultured (Fig 5.3A).

TGF-ß did not affect Col3a1 expression (fig. 5.3B) in any of the groups. Mechanical stretch resulted in a 14% significant increase in Col3a1 expression for the aged cells cultured on collagen compared to control conditions as well to the same cells cultured on RGD-motif (fig. 5.3C and E).

Stretch alone induced a significant upregulation in Col3a1 expression from a background state in the old group on cultured on collagen.

Combination of stretch and TGF-ß did not result in any significant changes in the level

of expression of Col3a1 compared to the control group (fig.5.3A and fig. 3D).

Results obtained showed that without stimulation levels of Col3a1 are the highest obtained in this experimental setting (see below). Relative expression gives an absolute value, which is influenced only by the house keeping gene used.

*Table 5.3 2-way ANOVA results for Snai1 calculated to identify differences induced by treatments (as row: TGF-ß, Substrate and stretch) and ageing (as column). * p-value < 0.05, ** p-value < 0.01 and *** p-value < 0.001.*

2 way ANNOVA Snai1		
Source of Variation	% of total variation	P value
Interaction	5.82	0.3011
TREATMENT	30.40	< 0.0001
AGE	0.74	0.3002
Source of Variation	P value summary	Significant?
Interaction	ns	No
TREATMENT	***	Yes
AGE	ns	No

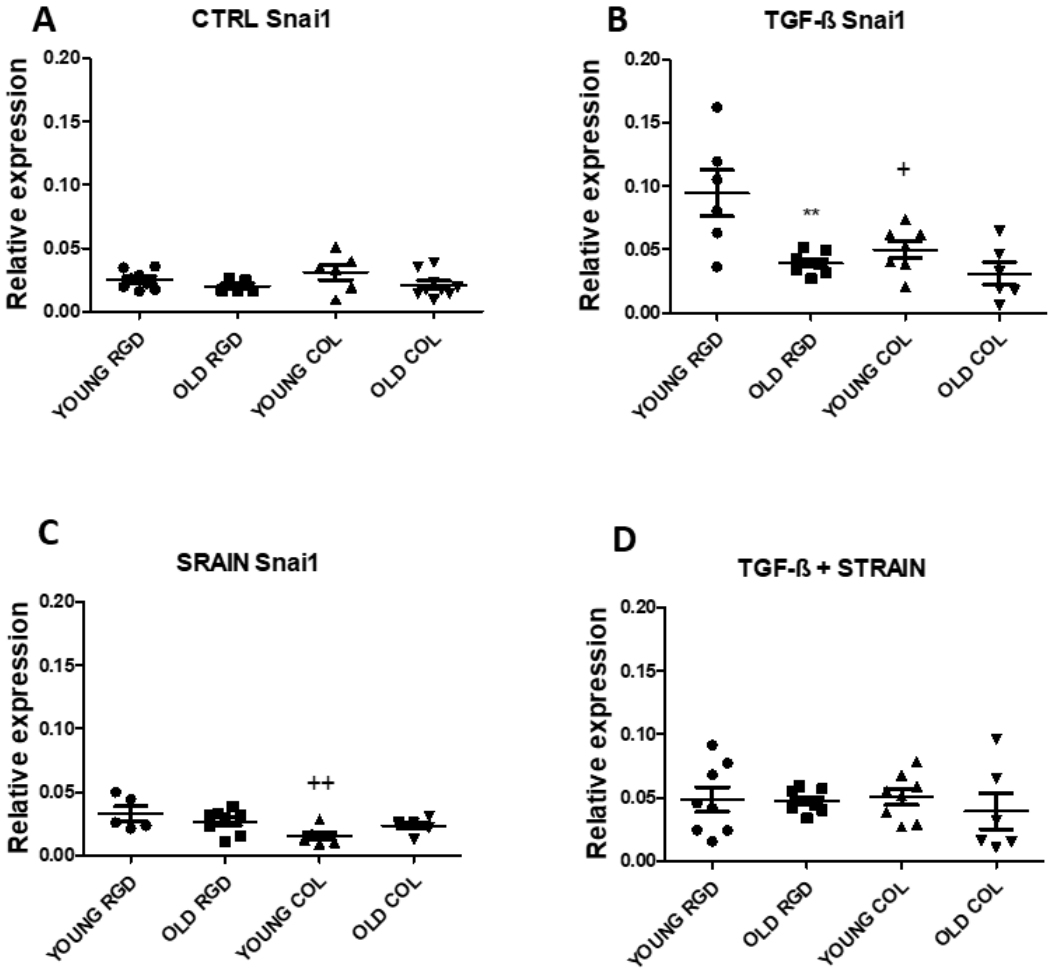
A
CTRL Snai1
Relative expression
0.20
0.15
0.10
0.05
0.00
YOUNG RGD
OLD RGD
YOUNG COL
OLD COL
B
TGF-ß Snai1
Relative expression
**
+
C
SRAIN Snai1
Relative expression
++
D
TGF-ß + STRAIN
Relative expression

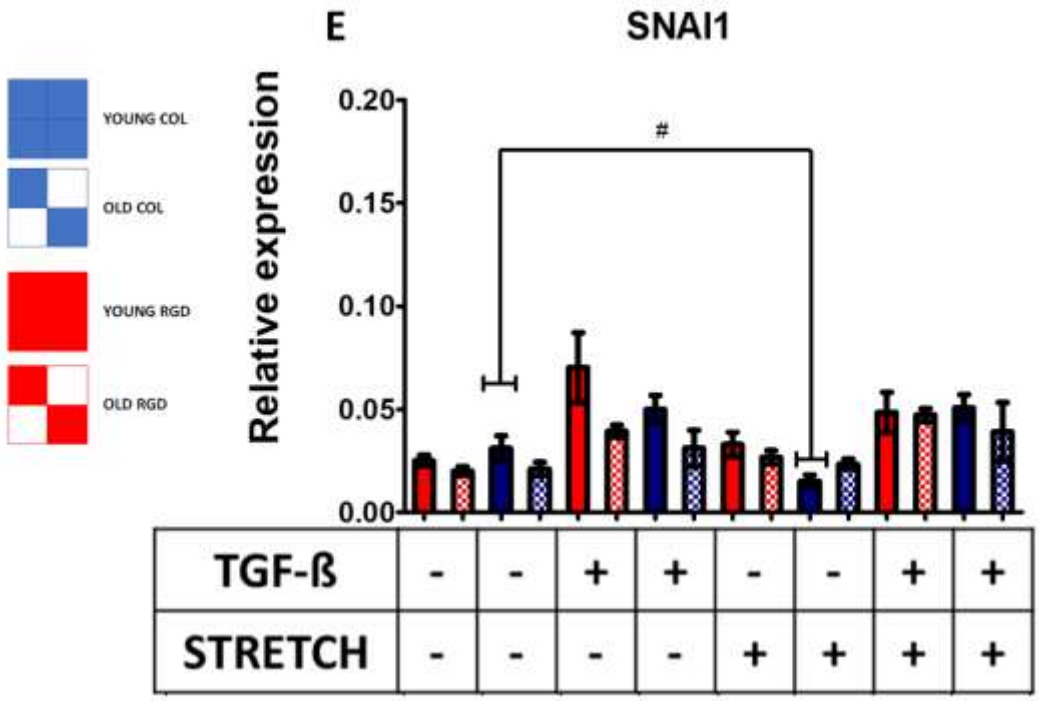

Figure 5.4 Gene Expression analysis from primary mouse lung fibroblast for Snai1. Scatter dot-plot where each dot represents an individual mouse donor (A-D). A) Controls. B) Fibroblasts treated with 2ng/mL of TGF-ß. C) Fibroblasts stretched at 6% of stretch. D) Fibroblasts receiving both 2 ng/mL of TGF-ß and stretch at 6% 1 Hz. E) Sum of all experimental group, where red circle scatter-dots indicate cell seeded on RGD-motif plate and blue square scatter-dots cells on collagen plate regardless age of the cells (as 2-way ANOVA not significant for age). Student t-test was used to investigate significant differences. Differences in substrate are indicated by p-value < 0.05, +++ p-value < 0.001.

Figure 5.4 shows Snai1 expression for all experimental groups used to investigate the effect of ageing, ECM substrates and stretch in primary mouse lung fibroblasts. 2- way ANOVA results indicated a significant effect only for treatment (TGF-ß, substrate and stretch), but not for age (Tab 5.3).

Controls values showed very low relative expression levels (fig. 5.4 A).

TGF-ß treatment induced a significant 2-fold increase from control in cells cultured on RGD-motif (fig. 5.4 B).

Stretch alone in young fibroblasts on collagen resulted in a 2-fold reduction of Snai1 expression from control (fig. 5.4E). Substrate differences accounted for a 45% reduction in Snai1 expression for collagen plates compared to RGD-motif in young fibroblasts (fig 5.4C).

The combination of stretch and TGF-ß did not affect Snai1 expression (fig. 5.4D).

Table 5.4 2-way ANOVA results for Slug calculated to identify differences induced by treatments (as row: TGF-ß, Substrate and stretch) and ageing (as column). p-value < 0.05, ** p-value < 0.01 and *** p-value < 0.001.*

2 way ANNOVA SLUG		
Source of Variation	% of total variation	P value
Interaction	13.00	0.0011
TREATMENT	36.67	< 0.0001
AGE	4.18	0.0043
Source of Variation	P value summary	Significant?
Interaction	**	Yes
TREATMENT	***	Yes
AGE	**	Yes

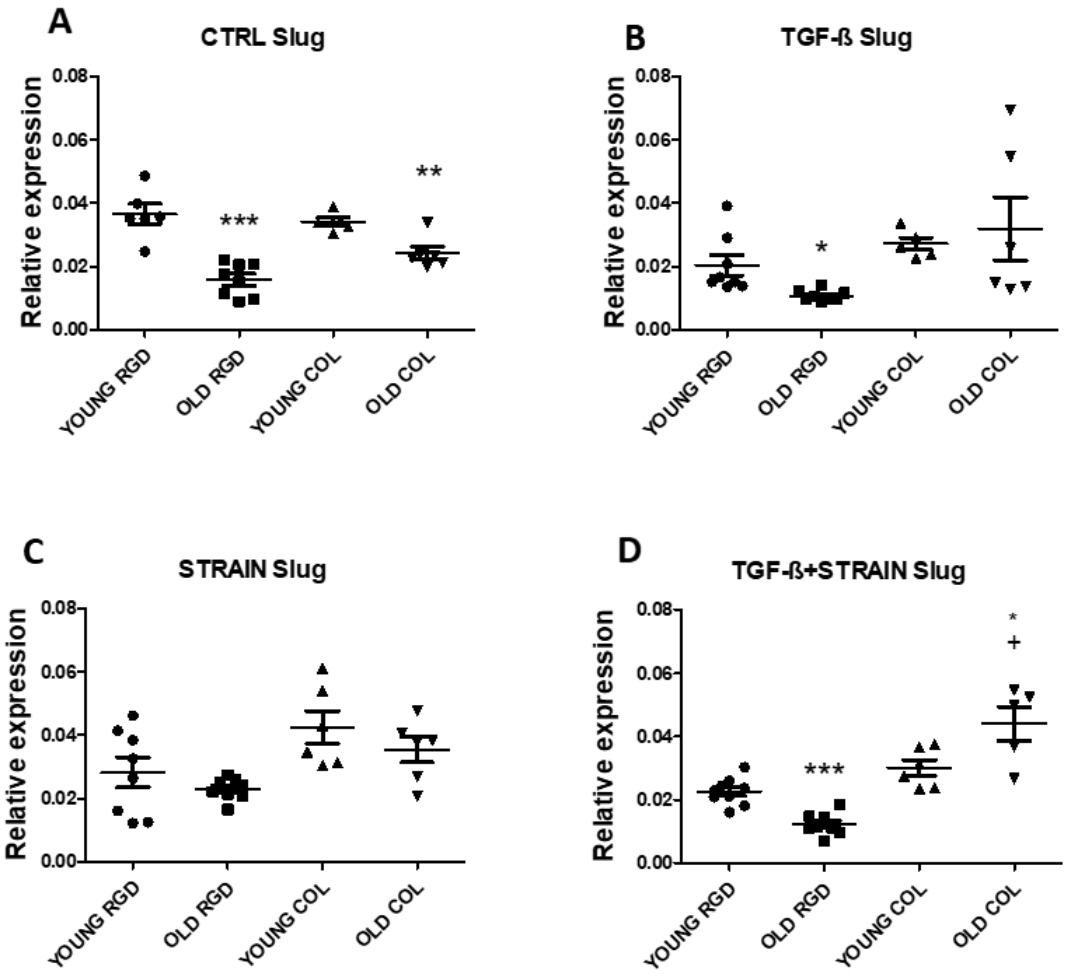
A
CTRL Slug
Relative expression
0.08
0.06
0.04
0.02
0.00
***
**
YOUNG RGD
OLD RGD
YOUNG COL
OLD COL
B
TGF-ß Slug
Relative expression
0.08
0.06
0.04
0.02
0.00
*
YOUNG RGD
OLD RGD
YOUNG COL
OLD COL
C
STRAIN Slug
Relative expression
0.08
0.06
0.04
0.02
0.00
YOUNG RGD
OLD RGD
YOUNG COL
OLD COL
D
TGF-ß+STRAIN Slug
Relative expression
0.08
0.06
0.04
0.02
0.00
***
*
+
YOUNG RGD
OLD RGD
YOUNG COL
OLD COL

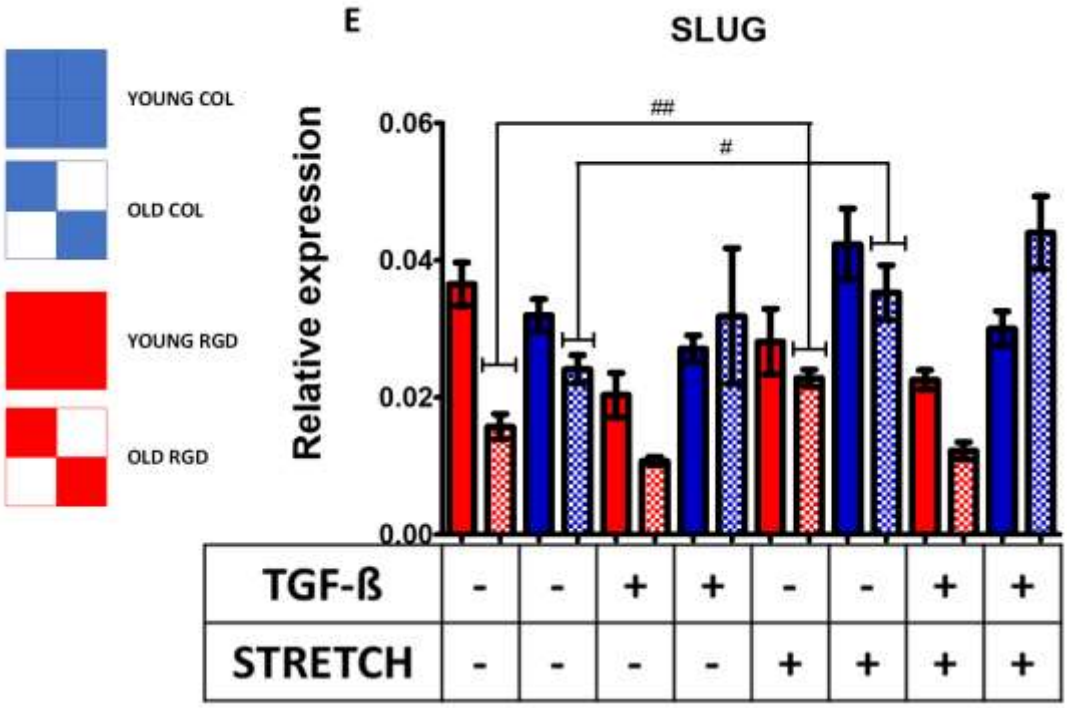

Figure 5.5 Gene Expression analysis from primary mouse lung fibroblast for Slug. A) Control. B) Fibroblasts treated with 2ng/mL of TGF-ß. C) Fibroblasts stretched at 6% of stretch. D) Fibroblasts receiving both 2 ng/mL of TGF-ß and stretch at 6% 1 Hz. E) Sum of all experimental group, where blue bar-charts indicate cell seeded on collagen plate and red bar-charts cells on RGD-motif plate. Patterned bar-charts indicate the old subgroup while the solid ones indicate the young group (panel on graph's left. Student t-test was used to investigate significant differences. Differences in substrate are indicated by "+", differences in age-related are indicated by "". * and + p-value < 0.05, ** p-value < 0.01, *** p-value < 0.001. Differences due to the effect of stretch are indicated by the "#", # p-value < 0.05 and ## p-value < 0.01.*

In the vehicle control groups there are no differences due to substrate. However, aged fibroblasts show consistently a lower expression with a significant decrease of 50% in Slug expression compared to young fibroblasts (fig. 5.5A).

TGF-ß treatment led to a significant 65% decrease in Slug expression from control for the RGD-motif group for both ages (fig. 5.5E).

Mechanical stretch resulted in a significant 1.5-fold increase in Slug expression compared to controls on both substrates (fig. 5.5C). Indicating that stretch induce a diverse response based on the substrate (fig. 5.5 E).

The combination of TGF-ß and stretch resulted in a 45% reduction of Slug expression only in aged fibroblasts cultured on RGD-motif. Aged cells cultured on collagen showed a 30% increase in Slug expression compared to young cells on collagen, and a 3-fold increase compared to aged fibroblast on the RGD-motif (fig. 5.5D).

*Table 5.5 2-way ANOVA results for CCN2 calculated to identify differences induced by treatments (as row: TGF-ß, Substrate and stretch) and ageing * p-value < 0.05, ** p-value < and *** p-value < 0.001.*

2 way ANNOVA CCN2		
Source of Variation	% of total variation	P value
Interaction	1.25	0.9502
TREATMENT	48.80	< 0.0001
AGE	0.04	0.7856
Source of Variation	P value summary	Significant?
Interaction	ns	No
TREATMENT	***	Yes
AGE	ns	No

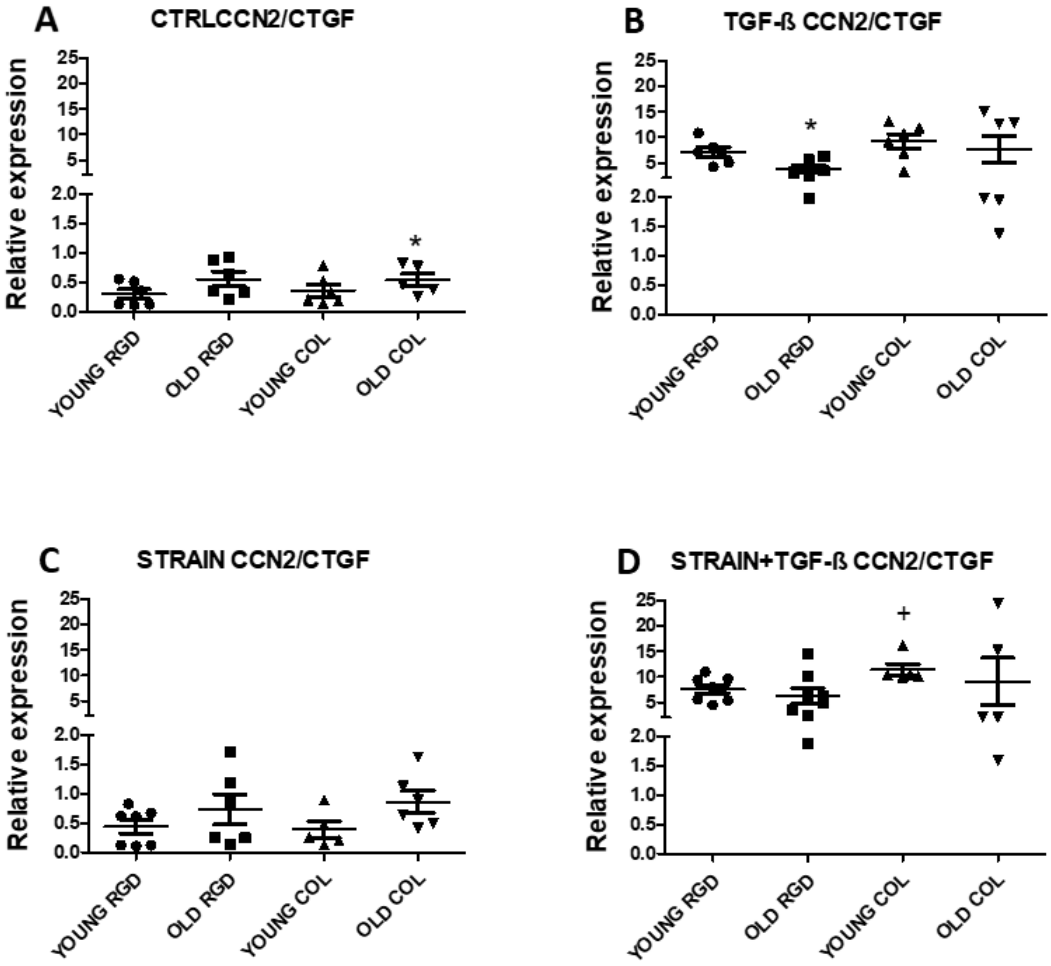

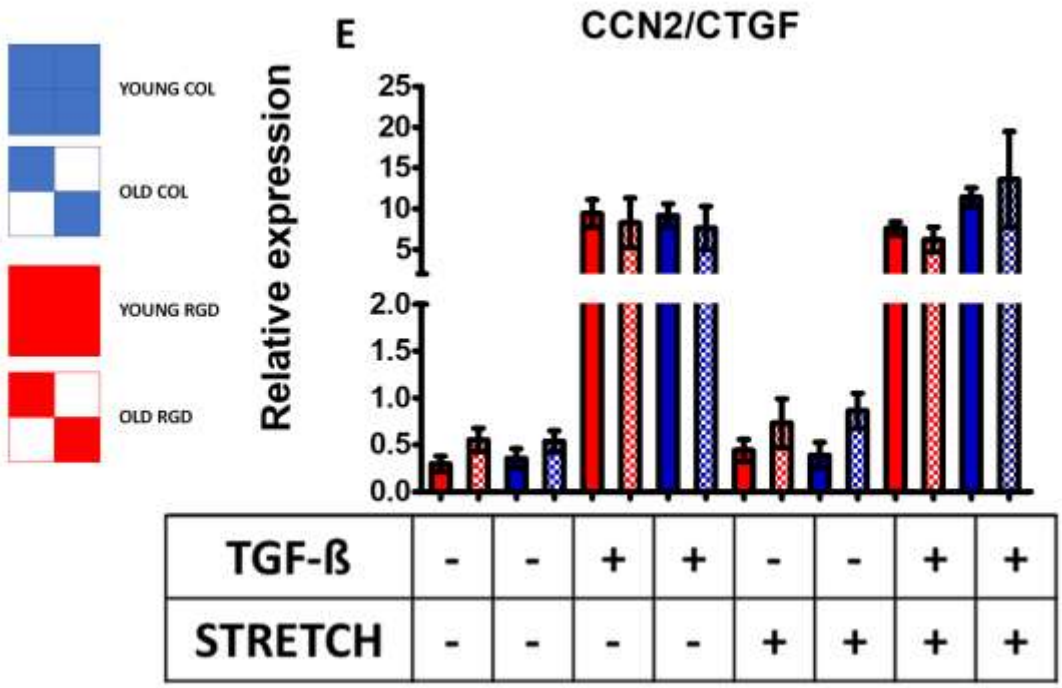

Figure 5.6 Gene Expression analysis from primary mouse lung fibroblast for Ccn2/Ctgf. Scatter dot-plot where each dot represents an individual mouse donor (A-D). A) Controls. B) Fibroblasts treated with 2ng/mL of TGF-ß. C) Fibroblasts stretched at 6% of stretch. D) Fibroblasts receiving both 2 ng/mL of TGF-ß and stretch at 6% 1 Hz. E) Sum of all experimental group, where red circle scatter-dots indicate cell seeded on RGD-motif plate and blue square scatter-dots cells on collagen plate regardless age of the cells (as 2-way ANOVA not significant for age). Student t-test was used to investigate significant differences. Differences in substrate are indicated by p-value < 0.05, +++ p-value <0.001.

Figure 5.6 shows Ccn2/Ctgf expression for all experimental groups used to investigate the effect of ageing, ECM substrates and stretch in primary mouse lung fibroblasts. 2-way ANOVA results showed a significant effect due to treatment (TGF- ß, substrate and stretch), but not for age (Tab. 5.5).

Control groups did not show significant difference due to substrate (fig. 5.6A). TGF-ß treatment induced a significant overall 20-fold increase in Ccn2/Ctgf expression level compared to controls regardless of age or substrate (fig. 5.6E). Stretch did not induce any significant changes in Ccn2/Ctgf expression (fig. 5.6C). Similar to TGF-ß alone, combination of TGF-ß and stretch induced increased expression of Ccn2, which was not different from the increase induced by TGF-ß alone (fig. 5.6E). However, in fibroblasts from young mice, the combined TGF-ß and stretch condition resulted in a significant 41% increase in the collagen group compared to the RGD-motif (fig. 5.6D).

*Table 5.6 2-way ANOVA results for Smad6 calculated to identify differences induced by treatments (as row: TGF-ß, Substrate and stretch) and ageing (as column). Top of the figure gives numerical percentage indication on the weight of the single variable including interaction, while bottom figure shows statistical significance where * p-value < 0.05, ** p- value < 0.01 and *** p-value < 0.001.*

2 way ANNOVA SMAD6		
Source of Variation	% of total variation	P value
Interaction	5.13	0.2256
TREATMENT	21.29	0.0015
AGE	32.02	< 0.0001
Source of Variation	P value summary	Significant?
Interaction	ns	No
TREATMENT	**	Yes
AGE	***	Yes

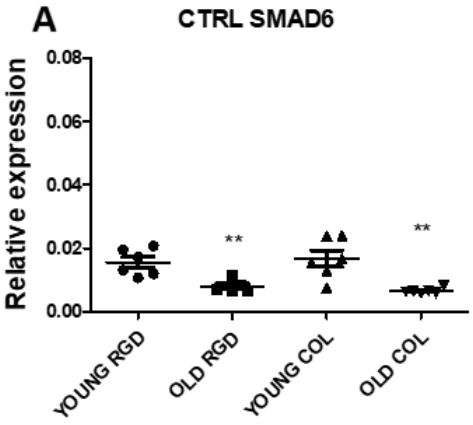
A
CTRL SMAD6
Relative expression
0.08
0.06
0.04
0.02
0.00
**
**
YOUNG RGD
OLD RGD
YOUNG COL
OLD COL

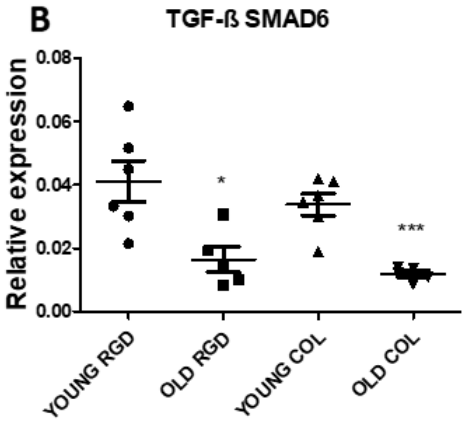
B
TGF-ß SMAD6
Relative expression
0.08
0.06
0.04
0.02
0.00
*
***
YOUNG RGD
OLD RGD
YOUNG COL
OLD COL

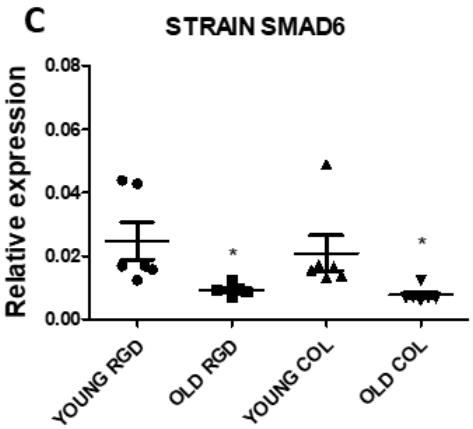
C
STRAIN SMAD6
Relative expression
0.08
0.06
0.04
0.02
0.00
*
*
YOUNG RGD
OLD RGD
YOUNG COL
OLD COL

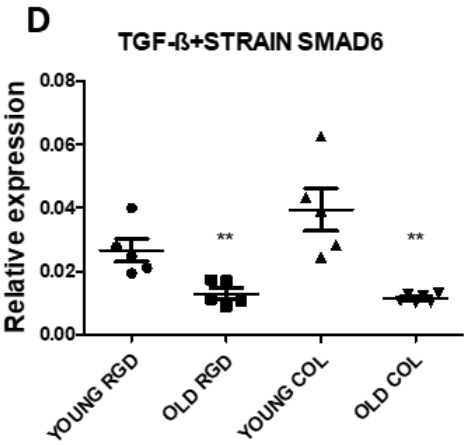
D
TGF-ß+STRAIN SMAD6
Relative expression
0.08
0.06
0.04
0.02
0.00
**
**
YOUNG RGD
OLD RGD
YOUNG COL
OLD COL

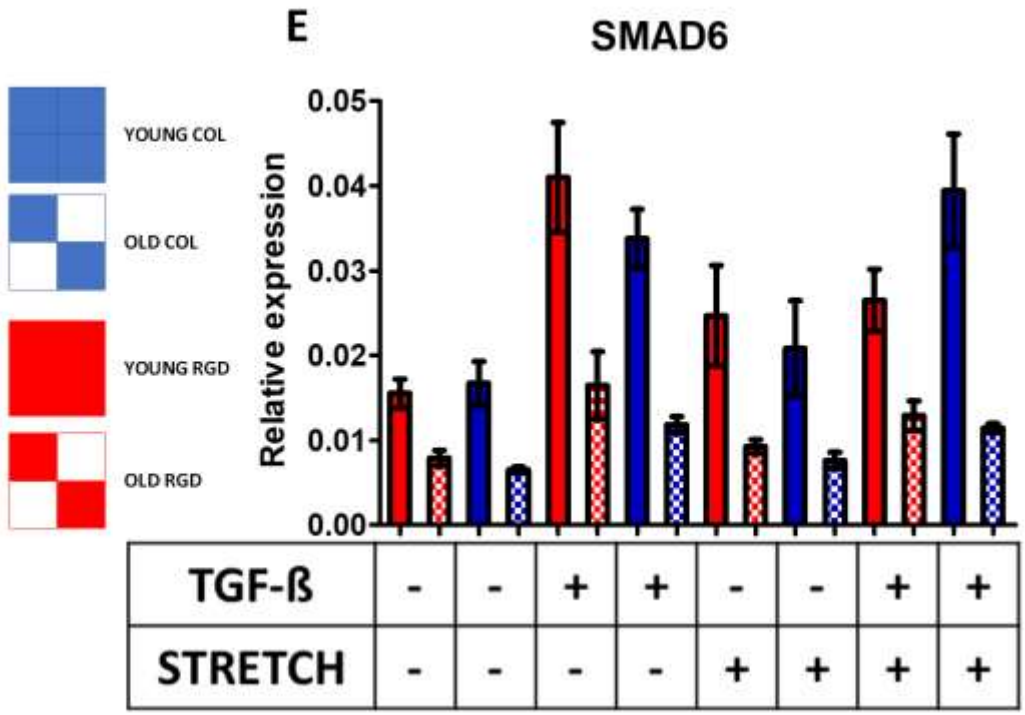

Figure 5.7 Gene Expression analysis from primary mouse lung fibroblast for Smad6. A) Background level (CTRL). B) Fibroblasts treated with 2ng/mL of TGF-ß. C) Fibroblasts stretched at 6% of stretch. D) Fibroblasts receiving both 2 ng/mL of TGF-ß and stretch at 6% 1 Hz. E) Sum of all experimental group, where blue bar-charts indicate cell seeded on collagen plate and red bar-charts cells on RGD-motif plate. Patterned bar-charts indicate the old subgroup while the solid ones indicate the young group (panel on graph's left. Student t-test was used to investigate significant differences. Differences in substrate are indicated by "+", differences in age-related are indicated by "". * p-value < 0.05, ** p-value < 0.01, *** p- value < 0.001.*

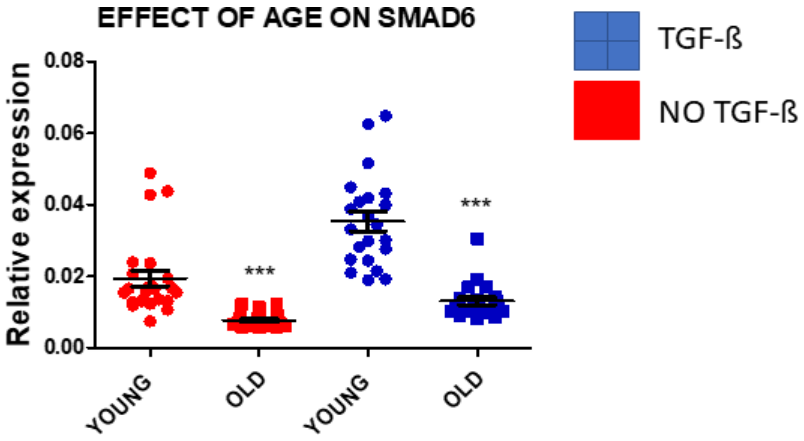

*Figure 5.8 Effect of age on Smad6 expression. Scatter-dot plot where circles indicate young groups and squares old groups regardless on the substrates, red dots represent no TGF-ß treated groups (control and stretch) while blue dots represent TGF-ß treated group (TGF-ß and TGF-ß with stretch). Student t-test was employed to calculate significative difference based on age. *** p-value < 0.001.*

Next, I analysed Smad6 expression to investigate the effect of ageing, ECM substrates and stretch in the primary mouse lung fibroblast culture model. 2-way ANOVA result showed that both treatment (TGF-ß, substrate and stretch) and age highly significantly affect SMAD6 expression. (Tab.5.6). SMAD6 expression is decreased in aged cells compared to young cells under all the experimental conditions studied.

In control cultures, aged fibroblasts showed a significant decrease of Smad6 expression of 49% and 61% compared to young fibroblasts on RGD-motif and collagen respectively (fig.5.7A).

TGF-ß treatment induced an overall significant 2- fold increase in Smad6 expression from control groups (fig. 5.7E). However, Smad6 expression in aged fibroblasts was still decreased but around 60% compared to young fibroblasts irrespective of the substrate (fig. 5.7B).

Stretch did not affect Smad6 expression, and the difference between young and aged fibroblasts was similar to control conditions (fig. 5.7C).

The combination of stretch and TGF-ß resulted in expression level similar to TGF-ß alone, with a 2-fold increase from controls (fig. 5.7E), and a similar difference between young and aged fibroblasts as TGF-ß alone (fig. 5.7D).

To summarise, the factors affecting Smad6 expression in this system are TGF-ß and age, and TGF-ß affects SMAD6 expression with a similar magnitude in both ages analysed (fig. 5.8).

*Table 5.7 2-way ANOVA results for Smad7 calculated to identify differences induced by treatments (as row: TGF-ß, Substrate and stretch) and ageing (as column). Top of the figure gives numerical percentage indication on the weight of the single variable including interaction, while bottom figure shows statistical significance where * p-value < 0.05, ** p- value < 0.01 and *** p-value < 0.001.*

2 way ANNOVA SMAD7		
Source of Variation	% of total variation	P value
Interaction	5.89	0.4071
TREATMENT	31.93	< 0.0001
AGE	3.35	0.0448
Source of Variation	P value summary	Significant?
Interaction	ns	No
TREATMENT	***	Yes
AGE	*	Yes

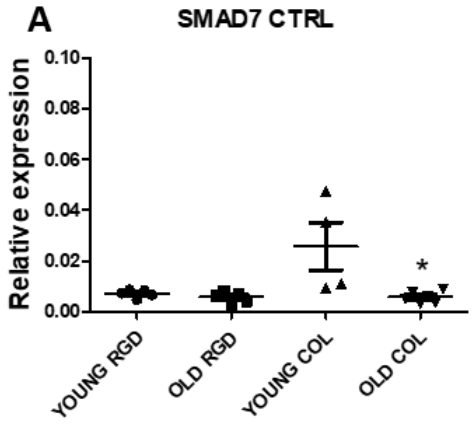
A
SMAD7 CTRL
Relative expression
0.10
0.08
0.06
0.04
0.02
0.00
*
YOUNG RGD
OLD RGD
YOUNG COL
OLD COL

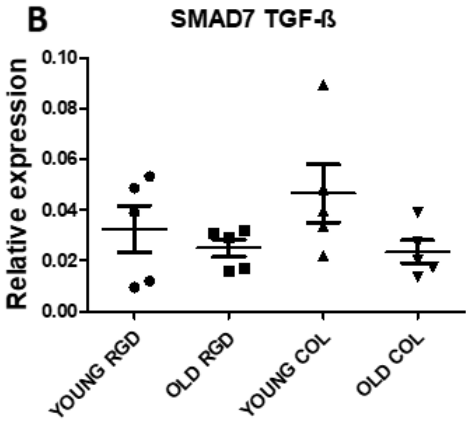
B
SMAD7 TGF-ß
Relative expression
0.10
0.08
0.06
0.04
0.02
0.00
YOUNG RGD
OLD RGD
YOUNG COL
OLD COL

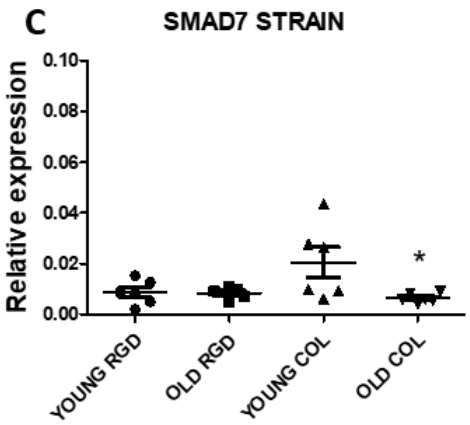
C
SMAD7 STRAIN
Relative expression
0.10
0.08
0.06
0.04
0.02
0.00
*
YOUNG RGD
OLD RGD
YOUNG COL
OLD COL

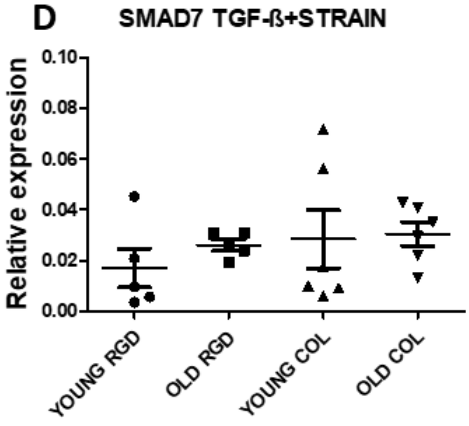
D
SMAD7 TGF-ß+STRAIN
Relative expression
0.10
0.08
0.06
0.04
0.02
0.00
YOUNG RGD
OLD RGD
YOUNG COL
OLD COL

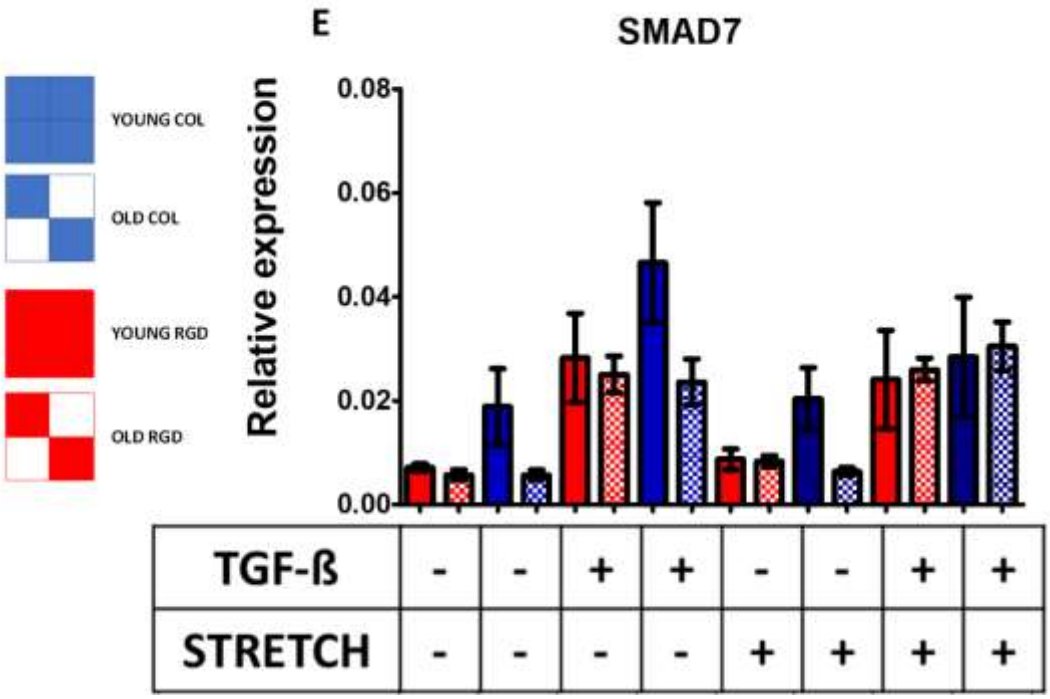

Figure 5.9 Gene Expression analysis from primary mouse lung fibroblast for Smad7. A) Background level (CTRL). B) Fibroblasts treated with 2ng/mL of TGF-ß. C) Fibroblasts stretched at 6% of stretch. D) Fibroblasts receiving both 2 ng/mL of TGF-ß and stretch at 6% 1 Hz. E) Sum of all experimental group, where blue bar-charts indicate cell seeded on collagen plate and red bar-charts cells on RGD-motif plate. Patterned bar-charts indicate the old subgroup while the solid ones indicate the young group (panel on graph's left. Student t-test was used to investigate significant differences.

Figure 5.9 shows Smad7 expression for all experimental groups used to investigate the effect of ageing, ECM substrates and stretch in primary mouse lung fibroblasts.

2-way ANOVA analysis showed a significant effect of both treatment (TGF-ß, substrate and stretch) and ageing. No significant interaction was found between treatment and age, indicating that treatment affects SMAD7 expression the same way for both ages (Tab. 5.7).

Under control conditions, the only significant difference was a 60% decrease in Smad7 expression for aged fibroblasts on collagen compared to young fibroblasts on the same substrate (fig. 5.9A).

TGF-ß treatment induced a 4-fold increase in Smad7 expression for both young and old fibroblasts on RGD-motif, and a 2.5-fold increase for young fibroblasts and a 4-fold increase in old one on collagen plates compared to control conditions (fig. 5.9E).

Although Smad7 levels after TGF-ß treatment appeared to be lower in aged fibroblasts than in young fibroblasts, this was not statistically significant (fig. 5.9B). Mechanical stretch alone showed Smad7 expression levels similar to control conditions, with a similar significant 70% decrease in Smad7 expression in aged fibroblasts on collagen compared to the young

fibroblasts (fig. 5.9C).

The combination of TGF-ß and stretch induced increases in Smad7 levels similar to those of TGF-ß alone (fig. 5.9E). No differences induced by substrate or ageing were found in the analysis (fig. 5.9D).

To summarise, TGF-ß and collagen induce expression of key genes involved in fibrosis, while age seems to upregulate profibrotic genes as Col1a1 and downregulate antifibrotic genes, such as Smad6 and Smad7. Moreover, results obtained in primary lung cells highlighted a possible feedback effect of collagen as substrate for profibrotic genes, as for A549 in chapter 4.

5.3.3 microRNAs expression analysis

Quantitative polymerase chain reaction (qPCR) for microRNAs was used to investigate the effect of substrate, ageing and stretch on primary mouse lung fibroblasts. As mentioned in the introduction of this chapter, the rational was to obtain more information regarding the magnitude of miR-21a and miR-34a response to profibrotic stimulation. Moreover, as in chapter 4 I was not able to complete qPCRs on miR-21a and miR-34a in MRC5, it was critical to obtain information on those miRs for the progression into animal model.

Table 5.7 2-way ANOVA results for miR-34a-5p calculated to identify differences induced by treatments (as row: TGF-ß, Substrate and stretch) and ageing (as column). Top of the figure gives numerical percentage indication on the weight of the single variable including interaction, while bottom figure shows statistical significance where * p-value < 0.05, ** p- value < 0.01 and *** p-value < 0.001.

2way ANNOVA miR-21a-5p		
Source of Variation	% of total variation	P value
Interaction	21.63	< 0.0001
TREATMENT	24.19	< 0.0001
AGE	21.34	< 0.0001
Source of Variation	P value summary	Significant?
Interaction	***	Yes
TREATMENT	***	Yes
AGE	***	Yes

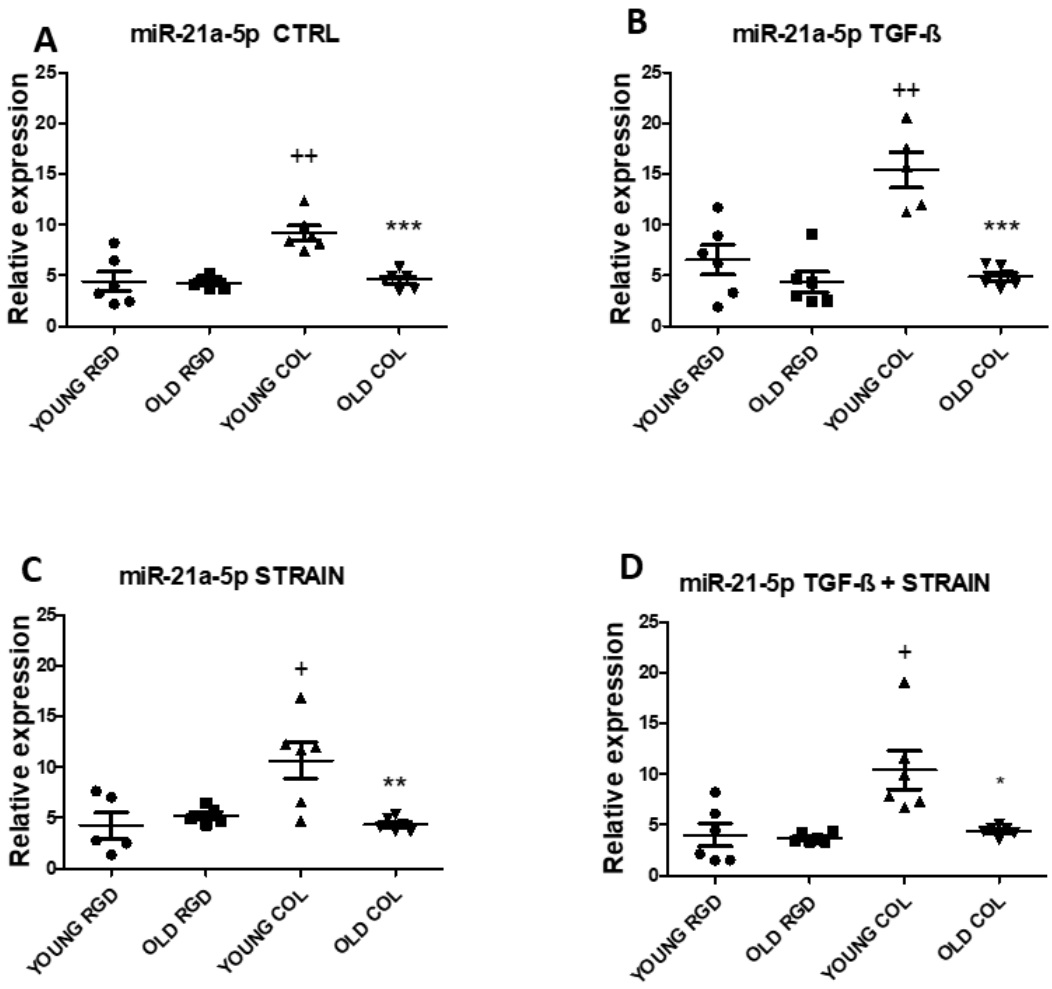
A
miR-21a-5p CTRL
Relative expression
25
20
15
10
5
0
++
***
YOUNG RGD
OLD RGD
YOUNG COL
OLD COL
B
miR-21a-5p TGF-ß
Relative expression
25
20
15
10
5
0
++
***
YOUNG RGD
OLD RGD
YOUNG COL
OLD COL
C
miR-21a-5p STRAIN
Relative expression
25
20
15
10
5
0
+
**
YOUNG RGD
OLD RGD
YOUNG COL
OLD COL
D
miR-21-5p TGF-ß + STRAIN
Relative expression
25
20
15
10
5
0
+
*
YOUNG RGD
OLD RGD
YOUNG COL
OLD COL

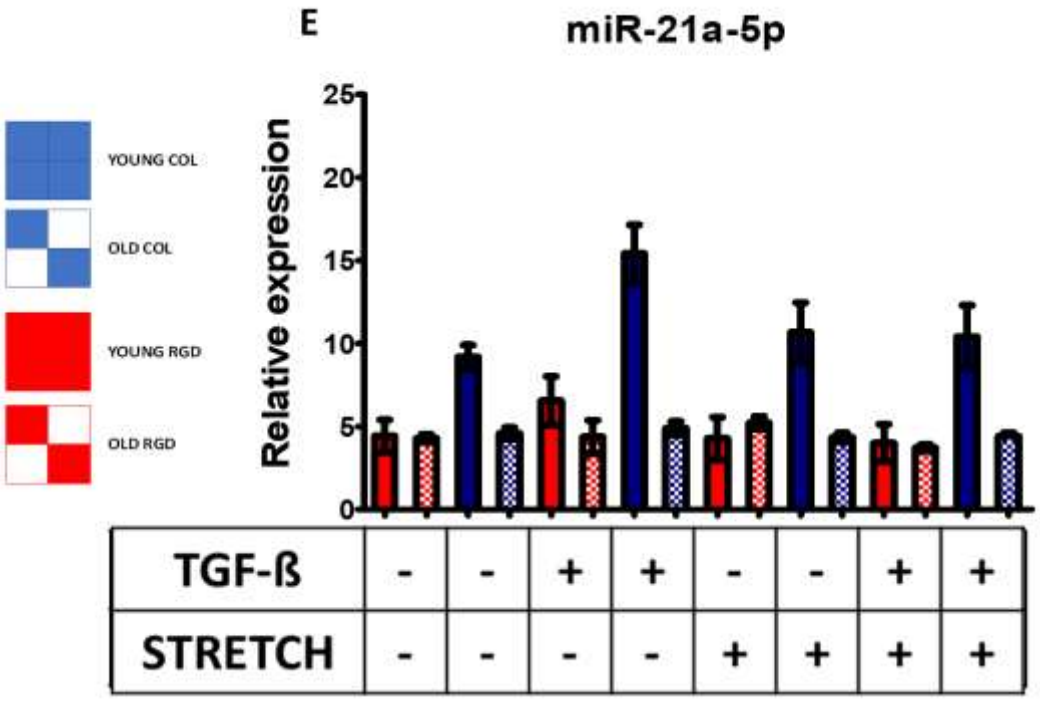

Figure 5.10 microRNA expression analysis from primary mouse lung fibroblast for miR-21a-5p. A) Background level (CTRL). B) Fibroblasts treated with 2ng/mL of TGF-ß. C) Fibroblasts stretched at 6% of stretch. D) Fibroblasts receiving both 2 ng/mL of TGF-ß and stretch at 6% 1 Hz. E) Sum of all experimental group, where blue bar-charts indicate cell seeded on collagen plate and red bar-charts cells on RGD-motif plate. Patterned bar-charts indicate the old subgroup while the solid ones indicate the young group (panel on graph's left. Student t-test was used to investigate significant differences. Differences in substrate are indicated by "+", differences in age-related are indicated by "". * and + p-value < 0.05, ** and ++ p-value < 0.01, *** p-value < 0.001.*

Figure 5.10 shows miR-21a-5p expression for all experimental groups. 2-way ANOVA results showed a significant effect of both treatment (TGF-ß, substrate and stretch) and ageing (Tab. 5.8). Result indicated a significant interaction.

Under control conditions, the substrate induced differences in young fibroblasts, with a 2-fold increase in fibroblasts cultured on collagen compared to cells cultured on the RGD-motif.

TGF-ß induced a 67% increase of miR-21a-5p expression in young fibroblasts cultured on collagen only (fig. 5.10 B and E).

Stretch did not affect miR-21a-5p expression level from control. However, as seen under the other experimental conditions, young fibroblasts on collagen displayed a 2.5- fold increase compared to both young fibroblasts on RGD-motif and old on collagen (fig. 5.10C).

TGF-ß and stretch resulted in a significant 48% decrease in miR-21a-5p expression in

young cells cultured on collagen compared to the same cells stimulated with TGF-ß only (fig. 5.10E). Moreover, young fibroblast on collagen showed a 2.5-fold increase in miR-21 expression compared to young fibroblasts on RGD-motif. For cells cultured on collagen, expression in young cells was 2-fold increase compared to fibroblasts (fig. 5.10D).

Overall, there was very little response to treatment for miR-21a-5p expression, with the exception of young fibroblasts cultured on collagen. The expression of miR-21a-5p was consistently higher in this group compared to all the other groups, and this was the only group that showed a response to TGF-ß.

*Table 5.8 2-way ANOVA results for miR-34a-5p calculated to identify differences induced by treatments (as row: TGF-ß, Substrate and stretch) and ageing (as column). Top of the figure gives numerical percentage indication on the weight of the single variable including interaction, while bottom figure shows statistical significance where * p-value < 0.05, ** p- value < 0.01 and *** p-value < 0.001.*

2way ANNOVA miR-34a-5p		
Source of Variation	% of total variation	P value
Interaction	3.66	0.7618
Treatment	13.44	0.0461
Age	13.22	0.0002
Source of Variation	P value summary	Significant?
Interaction	ns	No
Treatment	*	Yes
Age	***	Yes

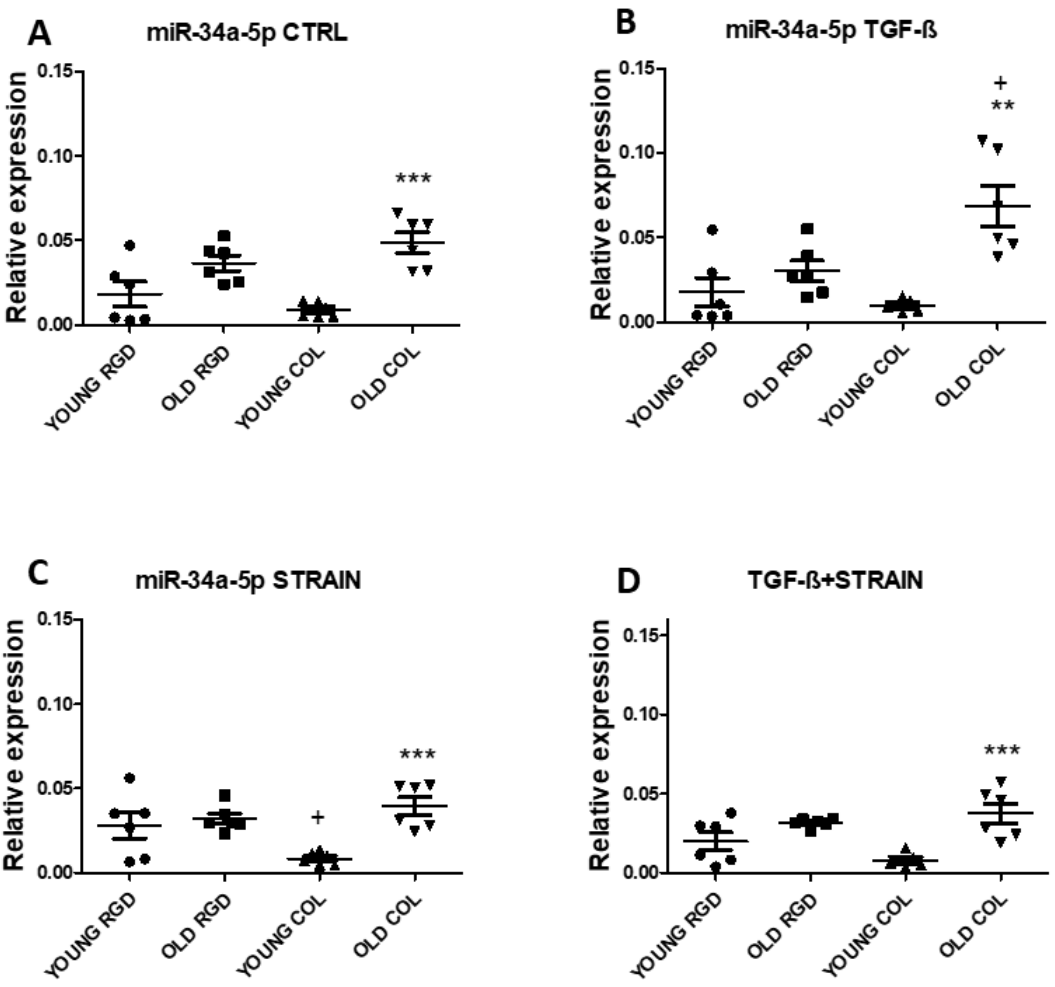
A
miR-34a-5p CTRL
Relative expression
0.15
0.10
0.05
0.00
***
YOUNG RGD
OLD RGD
YOUNG COL
OLD COL
B
miR-34a-5p TGF-ß
Relative expression
0.15
0.10
0.05
0.00
+
**
YOUNG RGD
OLD RGD
YOUNG COL
OLD COL
C
miR-34a-5p STRAIN
Relative expression
0.15
0.10
0.05
0.00
***
+
YOUNG RGD
OLD RGD
YOUNG COL
OLD COL
D
TGF-ß+STRAIN
Relative expression
0.15
0.10
0.05
0.00
***
YOUNG RGD
OLD RGD
YOUNG COL
OLD COL

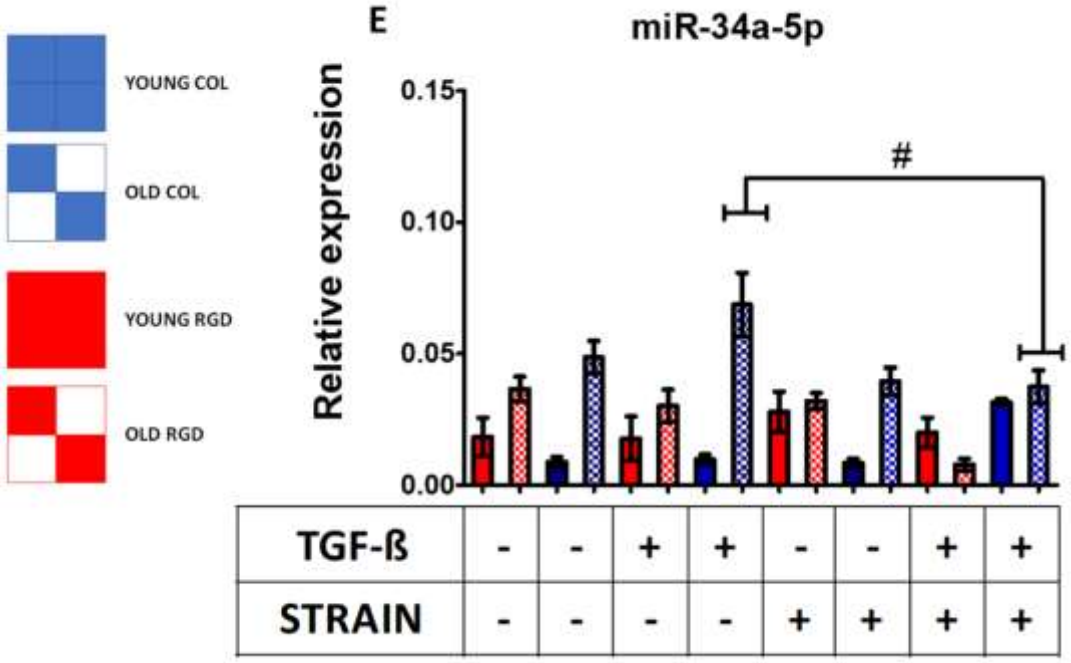

Figure 5.11 microRNA expression analysis from primary mouse lung fibroblast for miR-34a- 5p. A) Background level (CTRL). B) Fibroblasts treated with 2ng/mL of TGF-ß. C) Fibroblasts stretched at 6% of stretch. D) Fibroblasts receiving both 2 ng/mL of TGF-ß and stretch at 6% 1 Hz. E) Sum of all experimental group, where blue bar-charts indicate cell seeded on collagen plate and red bar-charts cells on RGD-motif plate. Patterned bar-charts indicate the old subgroup while the solid ones indicate the young group (panel on graph's left. Student t-test was used to investigate significant differences. Differences in substrate are indicated by "+", differences in age-related are indicated by "". + p-value < 0.05, ** p-value < 0.01, *** and +++ p-value < 0.001. Differences due to the effect of stretch are indicated by the "#", # p- value < 0.05. Note that each datapoint for each experimental group indicates an individual mouse donor.*

Figure 5.11 shows miR-34a-5p expression for all experimental groups used to investigate the effect of ageing, ECM substrates and stretch in primary mouse lung fibroblasts. 2-way ANOVA indicated significant effects of both treatment (TGF-ß, substrate and stretch) and age (Tab. 5.9). However, the effect of ageing had a higher level of significance than treatment. There was no significant interaction between treatment and age, indicating that the response to treatment was not different between the two age groups (Tab. 5.9).

Under control conditions there was a significant 5.5-fold increase in miR-34a-5p expression in the aged cells on collagen compared to the young fibroblasts. A similar increase was observed for cells cultured on RGD-motif, but this was not statistically significant.

Neither TGF-ß, mechanical stretch, or the combination of both affected miR-34a-5p expression compared to control (fig. 5.11E).

However, the substrate the cells were cultured on the age of the cells did affect miR-34a-5p expression. miR-34a-5p expression was generally higher in old fibroblasts. Young fibroblasts displayed 73 % decrease in miR-34a-5p expression on collagen compared to those cultures on RGD-motif. However, aged fibroblasts showed higher miR-34a-5p expression on collagen coated plates. In old fibroblasts on collagen, mechanical stretch induced a 2-fold decrease in TGF-ß induced miR-34a-5p expression but did not affect TGF-ß-induced miR-34a-5p expression in young cells or aged cells cultured on RGD-motif (fig. 5.11E).

Age represent the strongest inducer of miR-34a expression in primary lung fibroblasts.

5.4 Discussion

Transforming grow factor ß (TGF-ß) is considered a key cytokine in fibrosis (Wynn, 2011). Transcriptional activation by Smads is limited by a negative feedback loop operated by inhibitory Smads (Smad6 and Smad7).

In fibrosis, dysregulation in the TGF-ß pathway leads to a constant receptor type 1 activation, resulting in a pathological increase in ECM. TGF-ß pathway activation also leads to epithelial-to-mesenchymal transition (EMT) (Z. Yan, kui, & Ping, 2014). EMT contributes to fibrosis by increasing the number of resident fibroblasts. Mechanical tension (stretch) has also been identified as EMT inductor in cardiomyocytes (Finch-Edmondson & Sudol, 2016). Stretch activation might result in cytoskeletal remodelling, through Slug and Snai1, inducing fibroblasts-dependent ECM remodelling.

Classic *in vitro* molecular and cellular experiments on fibrosis employ TGF-ß treatment at concentrations lower than 10 ng/mL to establish a fibrotic-like phenotype. Those classic model present limitation due to the lack of reproducibility with organism physiology. It is now well accepted that the tissue environment is as important as the cells that compose it. Therefore, understand and then reproduce a tissue environment in terms of cytokine, ECM and stretch can virtually reproduce a tissue environment with maybe less cost than organoids.

Age dramatically affects the response to the chronic damage. During ageing mammalian lose cell replicative power and impaired response have more probability to evolve to a pathological state, as in fibrosis. Clinical evidence highlights a scenario with significant increase in lung fibrosis in aged people, where treatments with Nintenadib and Piredenifidone

only slower disease progression.

Hence, we developed a system able to take in account tissue environment, as cytokines and ECM environment, mechanical stretch, and ageing. This system was used to investigate the response of those stimulations to primary lung fibroblasts. The readout was again mRNA profiling from key genes involved in lung fibrosis pathogenesis and miR-21a and miR-34a.

To investigate the effect of ageing, primary lung fibroblasts were isolated from young (3 months old) and old (15 months old) wild type female C57BL/6 mice. To assess the effect of ECM as substrate on gene regulation, primary mouse lung fibroblasts were cultured on either the RGD-motif or Collagen type 1 coated tissue culture plates. RGD-motif is an Arginine-Glycine-Aspartate repeated motif present in almost all ECM proteins such as fibronectin, vitronectin, fibulin, laminin, collagen, and others, and it is fundamental for cell attachment to matrix (Burgstaller et al., 2017). Collagen is the most abundant ECM protein, which is contributes more than 30% of body dry weight (Ricard-Blum, 2011). However, in pulmonary fibrosis, excess collagen production leads to lung failure. In order to investigate whether matrix composition affects gene regulation during fibrosis, I used RGD-motif as a healthy control and collagen as disease group. Another important feature that I wanted to include in the study is mechanical stretch. The increase in collagen content during fibrosis leads to an increase in lung stiffness, modifying lung elastic properties. Lung deformation is fundamental for correct air intake. Therefore, if the lung becomes stiffer, diaphragm and chest muscles need to operate a higher work, as force per direction, in order to compensate the increase in stiffness (Miller, 2010; Béla Suki et al., 2011). For this reason, stretch was included in the system to have information regarding the effect of stretch on gene regulation.

Using this system, I studied the expression of 7 genes (Col1a1, Col3a1, Slug, Snai1, CCN2/CTGF, Smad6, Smad7) and 2 microRNAs (miR-21a-5p and miR-34a-5p) and found that age, substrate and stretch all affected gene expression in the cultures.

The first observation through phase contrast microscopy regarded cell behaviour. Stretched cultures appear sparser in comparison with the static culture (fig 5.1). Old fibroblasts, regardless of substrates showed signs of cellular distress to the force applied to the culture, as shown in figure 5.1. Old fibroblasts were forming clumps, possibly to overcome the distress induced by mechanical stimulation (fig. 5.1). Percentages of stretch from 10 to

15% have already been reported to induce cell death, in epithelial lung systems and in Hela cells, therefore the percentage used was around 6% of surface elongation (Peñuelas et al., 2013). Moreover, aged lung cells are more susceptible to mechanical force (Valentine et al., 2017). Old primary mouse fibroblasts seem to form clumps to overcome cellular stress induced by the 6% stretch (fig 5.1 C and D).

TGF-ß treatment did not induce any significant change in cell shape and cell-to-cell attachment. Figures were equivalent between groups; however, the use of a phase contrast microscopy limited the quality and quantity of information to discuss.

Regarding gene regulation, I found that expression of Col1a1, Slug, Smad6 and 7 and miR-21a-5p and miR-34a-5p were all influenced by age, whereas the expression of Col3a1, Ccn2/Ctgf and Snai1 were not (Tab. 5.10). Col1a1 and miR- 34a-5p showed an overall increase in expression while Slug, Smad6 and 7 and miR- 21a-5p an overall decrease due to age. The increase in Col1a1 and miR-34a-5p expression is in line with the higher incidence of pulmonary fibrosis in the elder population (King et al., 2000; Stuart et al., 2014). Moreover, Col1a1 showed a higher magnitude increase in the aged group when treated with TGF-ß. Col1a1 increased level in the aged group were also found in the stretch experimental condition (fig. 5.2). Apart from age, Col1a1 expression was also affected by a collagen as substrate and stretch (Tab. 5.1).

The age-related decrease in expression of the inhibitory Smads, Smad6 and Smad7 may partially explain the higher incidence of fibrosis in the elderly population. The mechanism that I propose is that the decrease in inhibitory Smad expression (as negative feedback loop related to age) give rises to increased Smad2/3/4 activation in response to TGF-ß, leading to increased matrix production. Both epigenetic and transcriptomic mechanisms can decrease inhibitory Smad expression (X. Yan et al., 2009). Moreover, Smad7 increased expression have been found in age-related skin cancer, which results in a ubiquitin-ligase dependent TGF-ß degradation (through Smurfs) (Han et al., 2006). Then, considering that fibrosis has an opposite response to cancer in chronic damage, the decrease found with age for Smad6 and 7 is in line with differences in TGF-ß between cancer and fibrosis. In physiological condition a decrease in Smad6 and 7 increases activatory Smads, powering then the fibrosis in ageing. Smad7 overexpression with transgene was demonstrated to revert fibrotic phenotype in the Bleomycin model of lung fibrosis (Nakao et al., 1999). This means that Smad7 holds antifibrotic

properties, however most of those studies does not employ old mice for the Bleomycin model of fibrosis. Therefore, results obtained arise a question on the role of Smad7 in aged fibrotic lung, which might highlight a connection between ageing and fibrosis.

From prediction analysis miR-21a-5p/Smad7 interacts in mammals and while Smad7 holds antifibrotic role, miR-21a-5p showed profibrotic characteristic (see chapter 3 and 4). The possibility of miR-21a-dependant Smad7 inhibition represents one of rational of this PhD project, as if this hypothesis is true miR-21a inhibition should result in a Smad7 increase and *vice versa* (see chapter 6).

Age clearly influenced Slug expression in untreated conditions, where I found an overall downregulation in expression in relation with age. This decrease is in line with Slug intervention in development. TGF-ß condition (fig. 5.5B) showed a decreased expression in old fibroblasts on RGD-motif, whereas a dynamic fibrotic environment triggers an opposite behaviour (fig. 5.5D). Slug is widely study in embryology, and it is a transcriptional repressor involved in neural crest formation, it is a source of smooth muscle vascular cells in lung (Whitsett et al., 2018). Results suggested a role in response to fibrotic stimulation for Slug in fibroblasts for the first time.

Overall miR-34a-5p expression was higher in the aged compared to the young fibroblasts. The increase in miR-34a-5p expression was most pronounced in cells cultured on collagen. Increased expression of this microRNA has previously been shown in aged lung epithelial cells, and to promote organ disfunction related to fibrosis. (Cui et al., 2017a; Smith-Vikos & Slack, 2012).

Main limitation of the study was that expression levels were only assessed at a single time point. The decrease in expression of Smad6 and -7 expression with age strongly suggest increased TGF-ß induced signalling. However, additional experiments, such as Smad phosphorylation studies, need to be performed to confirm this mechanism. In summary, results obtained, identified ageing as profibrotic *stimuli* through inhibition of Smad6 and Smad7 and increase in Col1a1. Collagen as substrate confirmed also in primary cells to be a strong inductor of fibrosis, while stretch confirmed a protective role also in primary mouse lung fibroblasts.

Table 5.9 Sum of qPCRs from primary mouse lung fibroblasts results. In the column there are listed the genes and miRs of interest, whereas in the row the different stimulation performed. Up facing arrows (↑) indicates upregulation, while down facing arrows (↓) downregulation in expression.

	TGF-ß	**COL AS SUBSTRATE**	**STRETCH**	**AGE**
Col1a1	↑	↑↑	↓	↑
Col3a1	↓	-	↑	-
Ccn2/Ctgf	↑↑	-	-	-
Snai1	↑	↑	↓	-
Slug	↓	-	↑	↑
Smad6	↑	↑	-	↓↓
Smad7	↑↑	-	-	↓
miR-21a-5p	↑	↑	↓	-
miR-34a-5p	-	↑	↓	↑↑

6 miR-29a mirmimic and miR-21a antagomiR as therapeutic avenues for pulmonary fibrosis.

6.1 Introduction

Pulmonary fibrosis belongs to Interstitial lung disease family. The disease is characterised by a low survival rate and resistance to drug treatment. Current treatments only treat disease symptoms but so not slow of reverse disease progression (Fischer & Brown, 2015). IPF is the form of fibrosis with the highest mortality, and rational drug design for treatment is difficult as its aetiology is currently unknown (Meltzer & Noble, 2008). Current disease models for IPF do not fully recapitulate the full disease phenotype, and show phenotype overlap with other forms of lung fibrosis. In addition, most models for lung fibrosis although representing major disease features, such as increased lung volume, increased ECM production and collagen crosslinking, are more similar to an acute response than a chronic disease (see introduction). Despite disease phenotypes showing high variability, features such as mesenchymal activation and increased ECM production are considered hallmarks of fibrosis (Kendall & Feghali-Bostwick, 2014). Those hallmarks are mostly the result of the activity of mesenchymal cells, which have been a focus of this experimental thesis. The main strategy for the work presented in this thesis was to first identify microRNAs that are differentially expressed in fibrotic lungs, followed by *in vitro* experiments to study the effect of these microRNAs on fibrotic lung fibroblasts, and finally to test the effect of the most promising microRNAs in a mouse model of IPF.

Currently only Pirfenidone and Nintedanib are accepted for the treatment of PF, which although a low efficacy they reduce PF symptomatology and slow disease progression (Fujimoto et al., 2015). Currently, several strategies are being used to develop better treatments for IPF, such as monoclonal antibodies and microRNAs, targeting ECM protein (as for CCN2/CTGF, SMAD cascade, etc.).

Evidence from *in vitro* and *in vivo,* and clinical data suggest that microRNAs change their expression in response to fibrotic development. As an example miR-21a

and miR-155 were found to be upregulated in patients affected by IPF compared to healthy control subjects (Li et al., 2013). Fine tuning the expression of microRNA, then, might be a potential strategy against lung disease as IPF (Rajasekaran, Rajaguru, & Sudhakar Gandhi, 2015). The basic principle of microRNA therapies is to either mimic the repression activity of the microRNA itself (mirmimic); or repressing the repressor activity of a microRNA (antagomir) (see introduction). For some of those therapies, lead development has now reached phase three clinical trials (miR-34a, miR-92, miR-16 and miR-122). However, it should be noted that only few leads reach this stage, as they have limited applicability (Hanna et al., 2019). microRNAs have a unique mechanism of action, where the 3'-UTR repression can bind to multiple target mRNAs, as it is based on energy favourable events. This unspecific target affinity creates off-target effects that might be lethal or result in an unexpected response. However, experimental evidence based non-ambiguous annotation of microRNA targets could possible predict these off-target effects, and lead to more specifically targeted modified microRNA and prevent or minimise adverse effects. Another limitation of microRNA therapies lies in the vehicle used (PEG, Lipofectamine, etc.), as it affects lead molecular structure, or increases the toxicity or being not adequate for that type of delivery. An example of clever drug administration is represented by the work of Patel and collaborators, who successfully "transfected" a mRNA-PEG-conjugate into mouse lung, which resulted in the expression of the mRNA (Patel et al., 2019). This elegant strategy resulted in a lower toxicity in the experimental model and in low systemic effect, as delivery was localized to animal lung.

microRNA arrays showed that several microRNAs are differentially expressed in the Bleomycin model of fibrosis, several of which target intracellular proteins involved in the TGF-ß signalling pathway, an important target pathway in IPF (Xie et al., 2011). microRNAs can regulate transcripts involved IPF pathogenesis, where increase in a specific ECM protein were correlated with decrease in microRNA expression and *vice versa.* This miRs:mRNA relationship needs to be further validated, as the change in expression might be random. The strategy used in this chapter involved application of both mirmimics and antagomirs, as miR reduction should lead

to an increase of mRNA target, and microRNA overexpression should lead to a decrease in the target gene. Validations of this interactions are needed to understand if variation in a chosen microRNA correlates to amelioration in the fibrotic phenotype. In chapter 3, I showed a progressive increase in 4 microRNAs (miR-21a, miR-34, miR-29a and miR-378) followed by Bleomycin treatment in C57BL/6J. Studies regarding the Bleomycin model of lung fibrosis and clinical target discovery found quite often a miR-29a-3p expression suppression (Montgomery et al., 2014; Slusarz & Pulakat, 2015; Ting Xie et al., 2011). miR-29a-3p has been associated with the regulation of more than 4000 transcripts and shows conservation among vertebrates and connection with diabetes, cancer, and organ fibrosis (Slusarz & Pulakat, 2015b). miR-29a-3p is an evolutionary conserved microRNA and therefore, represents a good candidate for antifibrotic therapy. Thus, using a gain and loss of function approach, I studied the effect of miR-29a-3p in primary mouse lung fibroblasts to clarify its role as ECM regulator. In chapter 5, miR-34a and miR-21a were investigated in primary mouse lung fibroblast in response to different fibrotic *stimuli,* such as TGF-ß, collagen as substrate and aging. miR-21a-5p was significantly influenced by TGF-ß and collagen in mouse lung primary fibroblasts. miR-21a-5p showed an upregulation in epithelial A549 cells induced by collagen type-I substrate (Chapter 4). Results obtained on miR-21a-5p suggested an involvement of this microRNA in fibrosis. Therefore, I focussed on inhibition of miR-21a-5p as a potential antifibrotic therapy *in vivo*.

6.2 *Material and Methods*

Predicted alignment were conducted using TargetScan7.2 (http://www.targetscan.org/vert_72/). (Agarwal et al., 2015). Primary mouse lung fibroblasts were isolated as described in 2.4 and were cultured in DMEM standard media and treated with a scramble sequence, used as control; a mirmimic and antagomir sequence, to boost and inhibit miR-21a-5p and miR-29a-3p expression (ref. 2.4.6). miR-29a-3p and miR-21a-5p were first evaluated in terms of gain and loss of expression through qPCR. Then, Col1a1 and Col3a1 (miR-29a-3p predicted targets, see below) and Col1a1, Col3a1, Ccn2/Ctgf and Smad7 were evaluated in their expression (miR-21a predicted target, see below). Expression level were evaluated using qPCRs as described in 2.5.

Four five month old male C57BL/6J mice for each experimental group received tail vein intravenous injection (*iv.)* once a week of 2 µg/g of cholesterol modified mirmimic and antagomir for miR-21a-5p and scrambled sequence as control, as described in 2.2.5. Fibrosis was induced through intratracheal administration of Bleomycin, as described in chapter 2.2.5. Progression of fibrosis was monitored through in vivo µCT Scans (Quantum GX-2) at the start of the experiment and at 7, 11 and 17 days after Bleomycin administration as described in

On day 18 day, mice were sacrificed, lungs were dissected out inflated filled with O.C.T. (ref.2.2.2). Lungs were analysed first for miR-21a-5p, then for Col1a1 and Smad7 with qPCRs (ref. 2.5). Slides of 5-7 µm were cut using cryotome and then evaluated for collagen presence with Picrosirius red stains (ref. 2.3).

6.3 Results

6.3.1 miR-29a-3p in primary mouse lung fibroblasts

6.3.1.1 miR-29a-3p predicted target on Col1a1 and Col3a1

TargetScan 7.2 is one of the most used bioinformatic tool for microRNAs target identification (ref. 2.9). A list of predicted mRNA targets generated by TargeetScan7.2 algorithm through sequence complementary between mRNA transcript and the miR sequence are shown in Table 6.1. TargetScan7.2 lists all microRNA predicted target based on the number base pair complementarity between microRNA core sequence and target mRNAs 3'-UTR. This rank is generated then based on more energetically favourable events.

Table 6.1 TargetScan7.2 results for miR-29, in the table are shown only the first 12 entries generated by the system. The table shows the name of miR-29a targets, the number and type of binding site as conserved or not among species shows as "conserved site" and "poorly conserved site" and the miRs isoform. In red are highlighted predicted interaction between miR-29a and collagen related genes.

Ortholog of target gene	Gene name	Conserved sites				Poorly conserved sites				
		total	8mer	7mer-m8	7mer-A1	total	8mer	7mer-m8	7mer-A1	6mer sites
TET3	tet methylcytosine dioxygenase 3	**7**	2	4	1	**3**	0	2	1	5
TET1	tet methylcytosine dioxygenase 1	**4**	0	3	1	**0**	0	0	0	1
COL1A1	collagen, type I, alpha 1	**3**	1	0	2	**0**	0	0	0	0
ELN	elastin	**3**	2	1	0	**0**	0	0	0	0
COL4A5	collagen, type IV, alpha 5	**2**	2	0	0	**1**	1	0	0	0
ATAD2B	ATPase family, AAA domain containing 2B	**3**	3	0	0	**0**	0	0	0	0
TET2	tet methylcytosine dioxygenase 2	**4**	2	2	0	**1**	0	1	0	0
ADAMTS17	ADAM metallopeptidase with thrombospondin type 1 motif, 17	**2**	1	1	0	**1**	0	0	1	4
PI15	peptidase inhibitor 15	**3**	1	1	1	**0**	0	0	0	1
IFI30	interferon, gamma-inducible protein 30	**1**	1	0	0	**0**	0	0	0	0
NASP	nuclear autoantigenic sperm protein (histone-binding)	**3**	1	2	0	**0**	0	0	0	0
COL3A1	collagen, type III, alpha 1	**2**	1	0	1	**0**	0	0	0	1

Table 6.1 shows mRNAs targets for miR-29a-3p alignment. Among top 12 predicted target, I focused my attention on mRNAs relevant in terms of ECM, such as collagen type-I, III (highlighted by red boxes). Top entries targets are more favourable events as presented higher number of sequence complementarity and species conservation. However, as in lung Col4a5 is little expressed it was excluded by any further analysis, while Col1a1 and Col3a1 were took in consideration as main constituent of collagen fibres. Please note that collagen 4a5 was not taken in consideration as non-fibrillar.

From the list in Table 6.1, each entry is linked to hyperlinked files, containing

information regarding the conservation miR:mRNA interaction between main species used in experimental biology (fig. 6.1, 6.2 and 6.8), and the base pair interaction between a microRNA of interest and the predicted target (6.2, 6.3 and 6.8).

Predictions on Col1a1 showed one 8-mer and two 7-mer A1 binding sites, while Col3a1 showed one 8-mer and one 7-mer A1 site. 8-mer indicated an exact match to position 2-8 of the mature microRNA followed by an A, and a 7-mer-A1 an exact match to position 2-7 of the mature microRNA followed by an A (Agarwal et al., 2015).

Figure 6.1 miR-29a-3p binding site on Col3a1 3'- UTR and conservation of the binding among the species

Position 877-883 of COL1A1 3' UTR mmu-miR-29a-3p	5' ...CAGUUUGGUAUCAAAGGUGCUAC... |||||| 3' AUUGGCUAAAGUCUACCACGAU	7mer-A1
Position 919-926 of COL1A1 3' UTR mmu-miR-29a-3p	5' ...GUGGGAAGGAAUUUC---UGGUGCUA... ||||| ||||||| 3' AUUGGCUAAAGUCUACCACGAU	8mer
Position 1095-1101 of COL1A1 3' UTR mmu-miR-29a-3p	5' ...GUUUUUUUUCCUGAAGGUGCUAU... |||| |||||| 3' AUUGGCUAAAGUCUA-CCACGAU	7mer-A1

Figure 6.2 Col1a1 3'-UTRs and miR-29a-3p interactions.

Position 235-242 of COL3A1 3' UTR mmu-miR-29a-3p	5' ...CAGUUUGGUAUCAAAGGUGCUAC... |||||| 3' AUUGGCUAAAGUCUACCACGAU	8mer
Position 672-678 of COL3A1 3' UTR mmu-miR-29a-3p	5' ...AAAGACACAUGUUAAGGUGCUAA... |||||| 3' AUUGGCUAAAGUCUACCACGAU	7mer-A1

Figure 6.3 Col3a1 3'-UTR and miR-29a-3p interactions

Figure 6.1 to 6.3 shows sequence complementarity between miR-29a-3p and Col1a1 (fig. 1 and 3) and miR-29a-3p and Col3a1 (fig. 6.2 and 6.3) 3'-UTR and their conservation among species. Interestingly, Col1a1 interactions with miR-29a were not conserved in macaw, chicken, lizard and in Xenopus tropicalis (fig. 6.1), while Col3a1 interaction showed to be conserved among all analysed species (fig. 6.2). Figure 6.2 and 6.3 shows details of miR-29a-3p and target genes interaction, which accounts for energetical favourable interactions.

6.3.1.2 qPCRs results

Primary mouse lung fibroblasts were transfected with 50 nM of scramble sequence (control), 50 nM of mirmimic sequence (stimulator of miR expression) or 50 nM of antagomir sequence (inhibitor of miR expression) for miR-29a-5p.

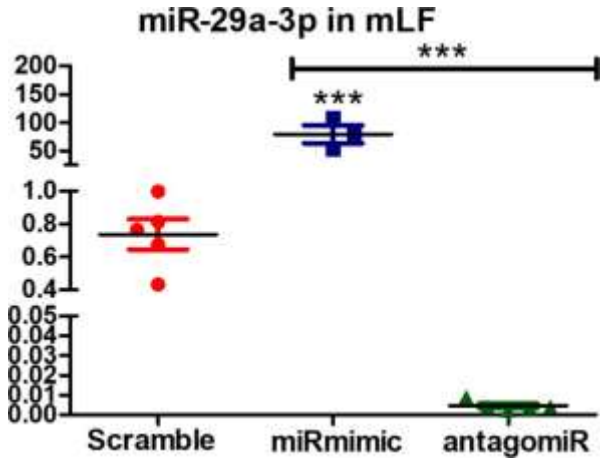

*Figure 6.4 qPCRs from primary mouse lung fibroblasts transfected with 50 M of Scramble (red circles), miRmimic (blue squares) and antagomiR (green triangles) for the miR-29a-3p. Results shown in the figure were significant for 1-way-ANOVA with an overall p-value < 0.001. Turkey post-hoc test was used for single column comparison ***: p-value < 0.001.*

Figure 5 shows expression level for miR-29a-3p. miRmimic group showed a 100-fold time increased from scramble (control) for miR-29a-3p, while antagomir group showed a 99.4% decrease from scramble (control). Expression trend demonstrated that the transfection conditions were partially achieved.

This meant that the transfection of miR-29a-3p was effective in modifying microRNA expression, resulting in the induction of miR expression for mimic group and inhibition for antagomir group (fig. 6.4).

Next, Col1a1 and Col3a1 expression level were evaluated through qPCRs, the rational was to evaluate if the treatment with mirmic and antagogomir were able to modify target expression.

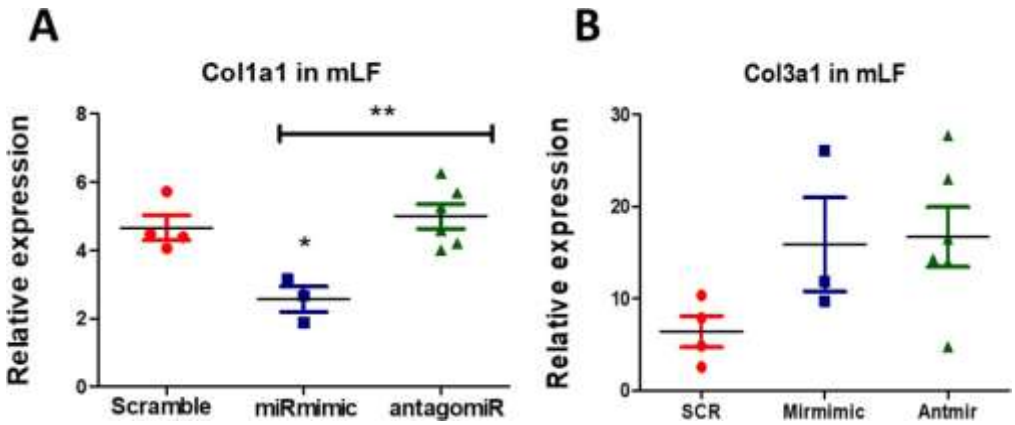

*Figure 6.5 qPCRs results from mLFs transfected with 50 M of Scramble (red circles), miRmimic (blue squares) and antagomiR (green triangles) for col1a1 (A) and col3a1 (B). Col1a1 expression level were significant for 1-way-ANOVA with an overall p-value < 0.01. Turkey post-hoc test was used for single column comparison *: p-value < 0.05, **: p- value < 0.01.*

Figure 6.5 shows the effect of treatments with miR-29a-3p on Col1a1 and Col3a1 mRNAs. Treatment with the mirmimic resulted in a significant 2-fold decrease in Col1a1 expression, while there was no significant upregulation in the antagomir group from scrambled (control). However, antagomir group showed a 50% significant upregulation from miRmimic group (fig.6.5A). Therefore, treatment aiming at modifying miR-29a-3p expression are efficient in fine tuning Col1a1 expression.

Treatments modifying miR-29a-3p expression did not resulted in changes in Col3a1 expression (fig. 6.5B). Therefore, treatments miR-29a-3p analogue did not affect Col3a1 expression.

6.3.2 miR-21a-5p role in models of lung fibrosis

6.3.2.1 miR-21a-5p target Smad7 3'-UTR

TargetScan7.2 results from predicted alignment between miR-21a-5p sequence and genome wise 3'-UTRs, generated a table containing 274 conserved sites and 67 poorly conserved. As mentioned above, TargetScan7.2 output (tab 6.2) contains a hyperlink information regarding miR:mRNA binding and conservation of this predicted interaction between species (fig. 6.6 and 6.7).

Although microRNAs do not need a complete match between sequences, 7 and 8- mer interaction are generally assumed to be more energetic favourable events. Among top list genes, Smad7 (tab. 6.2 highlighted by red box) belonging to TGF-ß canonical pathway, was in the top 15 entries in the list produced by TargetScan7.2. Smad7 showed the presence of an 8-mer conserved site for miR-21a-5p. Figure 6.7 shows the high conservation among species for the predicted alignment, in white in the figure. Smad7 3'-UTR displays conserved sites for miR-21a-5p binding, which is not present only in Macaw, animal that has a different Smad7 3'-UTR. Figure 6.8 shows sequence complementarity and sequence location of predicted alignment, which identified in miR-21a-5p and miR-21c possible target of mRNA-microRNA interaction with Smad7.

This means that miR-21a-5p has affinity to bind Smad7 3'-UTR, which was further evaluated experimentally to identify the role of miR-21a-5p in fibrosis.

Table 6.2 TargetScan7.2 results for miR-21a, in the table are shown only the first 20 entries generated by the system. The table shows the name of miR-21a targets the number of sites of binding and the type of binding, diving them in "conserved site" and "poorly conserved site" and in the last type of miRs isoform. In red is highlighted predicted interaction between miR-21a and Smad7. Please note that the column named "representative miRNA" shows the most probable miR's binding isoform.

Ortholog of target gene	Gene name	Conserved sites				Poorly conserved sites				
		total	8mer	7mer-m8	7mer-A1	total	8mer	7mer-m8	7mer-A1	other sites
GPR64	G protein-coupled receptor 64	**2**	2	0	0	**0**	0	0	0	0
FGF18	fibroblast growth factor 18	**1**	1	0	0	**0**	0	0	0	0
ARMCX1	armadillo repeat containing, X-linked 1	**1**	1	0	0	**0**	0	0	0	0
FASLG	Fas ligand (TNF superfamily, member 6)	**2**	1	1	0	**0**	0	0	0	0
CCL1	chemokine (C-C motif) ligand 1	**1**	1	0	0	**0**	0	0	0	0
SCML2	sex comb on midleg-like 2 (Drosophila)	**2**	1	1	0	**0**	0	0	0	1
AIM1L	absent in melanoma 1-like	**1**	1	0	0	**0**	0	0	0	0
IL12A	interleukin 12A	**1**	1	0	0	**0**	0	0	0	0
ZNF367	zinc finger protein 367	**2**	2	0	0	**0**	0	0	0	0
SPRY1	sprouty homolog 1	**1**	1	0	0	**0**	0	0	0	2
RNFT1	ring finger protein, transmembrane 1	**1**	1	0	0	**0**	0	0	0	0
PELI1	pellino E3 ubiquitin protein ligase 1	**1**	1	0	0	**0**	0	0	0	0
YOD1	YOD1 deubiquitinase	**2**	2	0	0	**0**	0	0	0	1
SMAD7	SMAD family member 7	**1**	1	0	0	**0**	0	0	0	0
SRL	sarcalumenin	**1**	1	0	0	**1**	0	1	0	1
NTF3	neurotrophin 3	**1**	0	1	0	**0**	0	0	0	0
DUSP8	dual specificity phosphatase 8	**1**	1	0	0	**1**	0	0	1	0
ARHGAP24	Rho GTPase activating protein 24	**1**	1	0	0	**0**	0	0	0	1
ELF2	E74-like factor 2	**1**	1	0	0	**0**	0	0	0	1
ZNF704	zinc finger protein 704	**2**	1	1	0	**1**	1	0	0	2
TGFBI	transforming growth factor, beta-induced	**1**	1	0	0	**0**	0	0	0	0

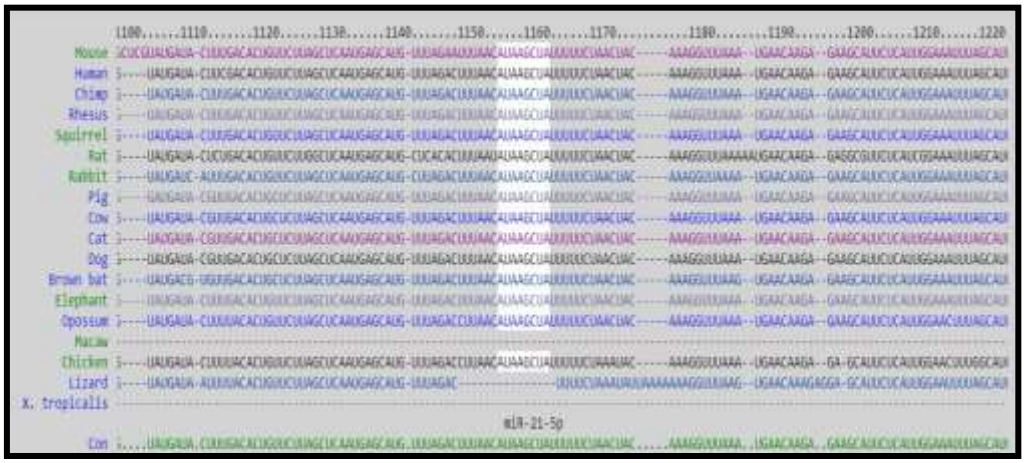

Figure 6.6 Screenshot obtained from TargetScan7.2 showing predicted binding location of miR-21a-5p over 3'-UTR for Smad7 and binding. conservation among species

.

Position 1156-1163 of SMAD7 3' UTR mmu-miR-21a-5p	5' ...UGUUUAGAAUUUAACAUAAGCUA... ||||||| 3' AGUUGUAGUCAGACUAUUCGAU	8mer
Position 1156-1163 of SMAD7 3' UTR mmu-miR-21c	5' ...UGUUUAGAAUUUAACAUAAGCUA... ||||||| 3' AACAUGGUCAGACUAUUCGAU	8mer

Figure 6.7 Smad7 3'_UTRs and miR-21a-5p interaction

6.3.2.2 miR-21a-5p mirmimic and antagomir in primary mouse lung fibroblast

Primary mouse lung fibroblasts were isolated from C57BL/6 and cultured as described in 2.2.2. Cells were transfected with 50 nM of scramble sequence (control), 100 nM of mirmimic sequence (stimulator of miR expression) or 150 nM of antagomir sequence (inhibitor of miR expression) for miR-21a-5p. To assess the effect of TGF-ß, cells were stimulated for 1 hour before lysis with TGF-ß at 2 ng/mL. Cells were incubated for a total of 48 hours in the above mentioned condition, according to 2.2.5. microRNA gain and loss of function was evaluated through qPCR for miR-21a-5p normalised SNORD68 (ref. 2.6) to further assess the effect of a miR- 21a-5p gain and loss of function on Smad7 mRNA (fig. 6.8).

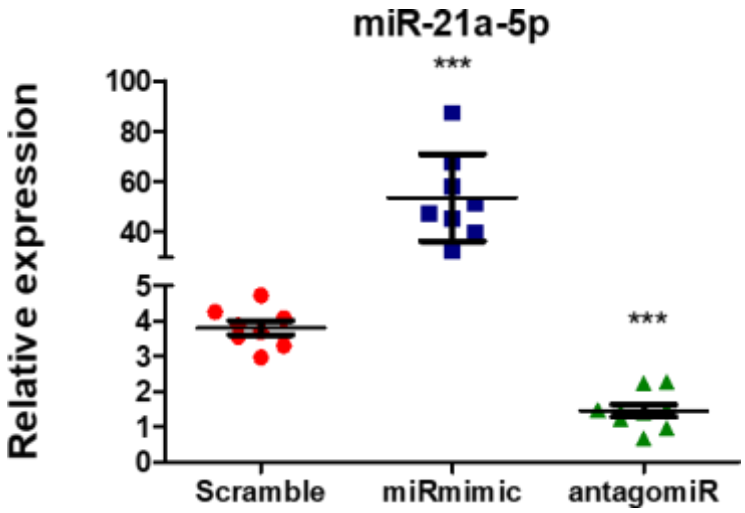

Figure 6.8 miR-21a-5p gain and loss of function in primary mouse lung fibroblasts. qPCRs result from primary mouse lung fibroblasts treated with a scramble (control), mirmimic (upregulation) and antagomiR (downregulation) for miR-21a-5p. Results are significant for 1-way ANOVA with an overall p-value < 0.001. Student T-test was conducted to evaluate single significance of treated group compared to control and it is indicated by the symbol "". *** p-value < 0.001.*

Transfection with mirmimic resulted in a significant 8-fold increase in miR-21a-5p expression, while transfection with antagomir resulted in a 44% decrease in miR-21a-5p expression from control (fig. 6.8). Therefore, treatments with miR-21a-5p analogue were able to fine tuning microRNA expression, with induction of miR-21a-5p for mirmimic group and inhibition in antagomir group (fig. 6.8).

Next, I assessed whether treatment miR-21a-5p mirmimics and antagomirs resulted in significant changes in Smad7 mRNA expression (fig. 6.9). Primary lung fibroblasts were also treated with TGF-ß to reproduce a more fibrotic cytokine environment.

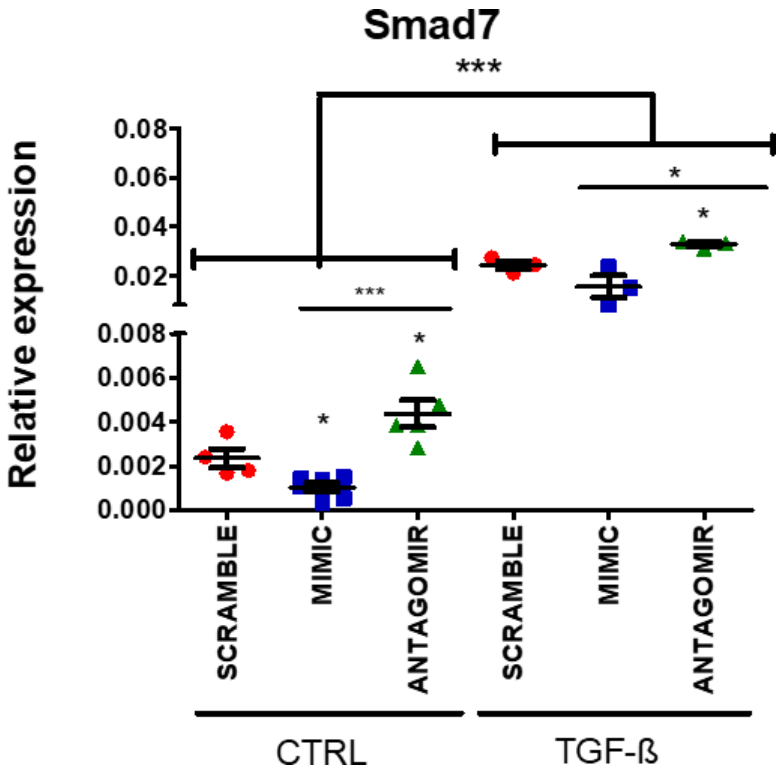

Figure 6.9 Smad7 expression level from gain and loss of function experiments for miR-21a-5p in primary mouse lung fibroblasts. qPCR for Smad7 were conducted to asses if changes in miR-21a-5p expression would affect Smad7 expression. Cells were treated with or without TGF-ß at concentration of 2 ng/mL to reproduce a fibrotic phenotype. Results are significant for 1-way ANOVA with an overall p-value < 0.001. Student T-test was conducted to evaluate significance differences between pairs of columns and are indicated by "". *< p-value 0.05, ** p-value < 0.01 and *** p-value < 0.001.*

In the absence of TGF-ß, there was a significant 56% decrease in Smad7 expression in cells transfected with the mirmimic, and 84% increase in cells treated with the antagomir group. In cells stimulated with TGF-ß, SMAD7 expression increased approximately 10-fold. Although transfection with mirmimic resulted in a 36% reduction in Smad7 expression, this was not statistically significant. Transfection with antagomir resulted in a significant 35% increase in Smad7 expression. SMAD7 expression after TGF-ß stimulation was twice as high in the antagomir treated cells as in the mirmimic treated cells.

Treatments miR-21a-5p analogues were able to fine tuning Smad7 expression, with induction of Smad7 for antagomir group and repression for mirmimic group, regardless of TGF-ß treatment. This meant that increase in miR-21a-5p resulted in

repression in Smad7 and miR-21a-5p repression in Smad7 increase. This suggested that miR-21a-5p can regulate Smad7 expression. Interesting, TGF-ß treatment did not modify the trend induced by treatments with miR-21a-5p analogues.

Next, I wanted to evaluate if modifications in miR-21a-5p would affect the expression of key ECM genes. Therefore, Col1a1, Col3a1 and Ccn2/Ctgf expression were assessed through qPCR, both with and without TGF-ß (Fig. 6.9).

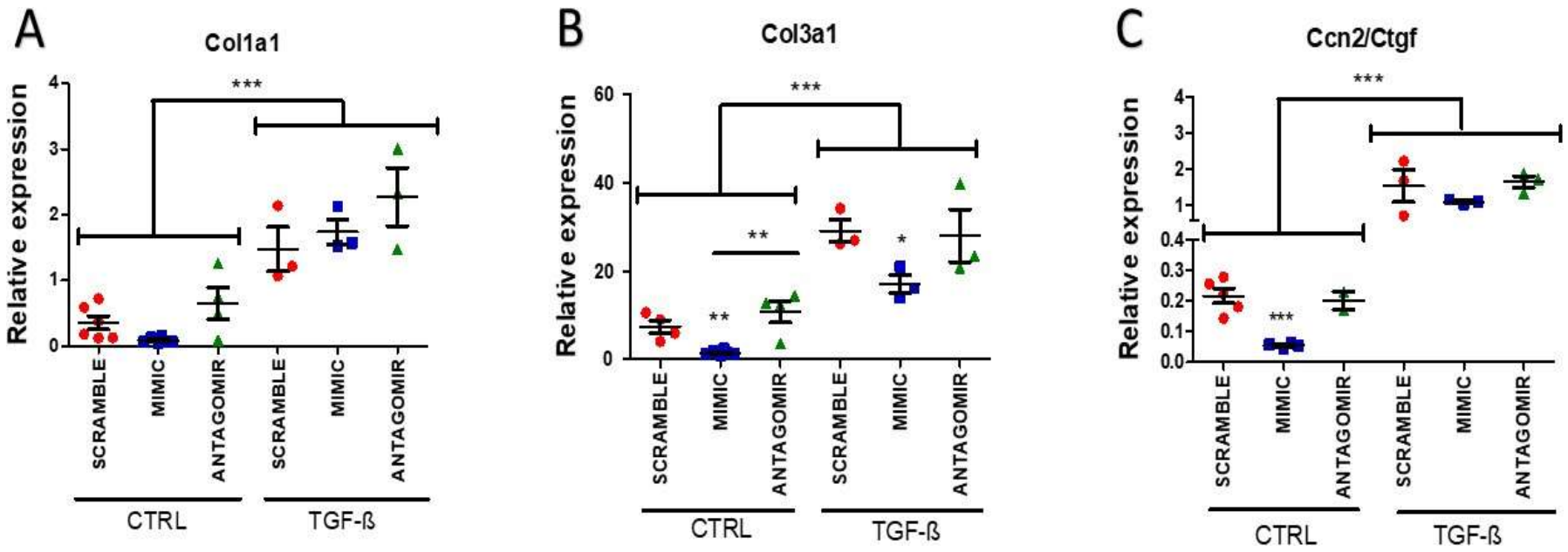

Figure 6.10 qPCRs from miR-21a-5p gain and loss of function experiments for Col1a1 (A), Col3a1 (B) and Ccn2/Ctgf (C) in primary mouse lung fibroblasts. Cells were treated with or without TGF-ß at concentration of 2 ng/mL to reproduce a fibrotic phenotype. Results are significant for 1-way ANOVA with an overall p-value < 0.001. Student T-test was conducted to evaluate significance differences between pairs of columns and are indicated by "". *< p-value 0.05, ** p-value < 0.01 and *** p-value < 0.001.*

Treatment with miR-21a-5p mirmimics and antagoMirs did not significantly affect Col1a1 expression (fig. 6.10A). Col3a1 showed reduction in expression in the mirmimic group of 1.5 for the TGF-ß and 5-fold time in the untreated group compared to each control. Without TGF-ß, Col3a1 antagomir group showed a significant increase of 7.5-fold time from the mirmimic group. In untreated condition, transfection with mirmimic resulted in a significant 74% decrease of Ccn2/Ctgf expression, while the antagomir had no effect on Ccn2/Ctgf expression. TGF-ß stimulation resulted in an overall 11.5-fold time increase in Ccn2/Ctgf expression, however, neither the mirmimic nor the antagomir had any effect on this expression.

Interesting, regardless of TGF-ß stimulation mirmimic group showed a general decrease in the expression of the three main genes involved in fibrosis, despite Smad7 repression.

6.3.2.3 *miR-21a-5p mirmimic and antagomir in the Bleomycin model of lung fibrosis (1)*

miR-21a-5p expression was assessed through qPCRs in liver and lung to measurement the efficacy of the experimental treatment following the method illustrated in 2.2 (fig. 6.11). qPCR for miR-21a-5p from liver samples was performed to assess systemic adsorption for treatments with mirmic and antagomir.

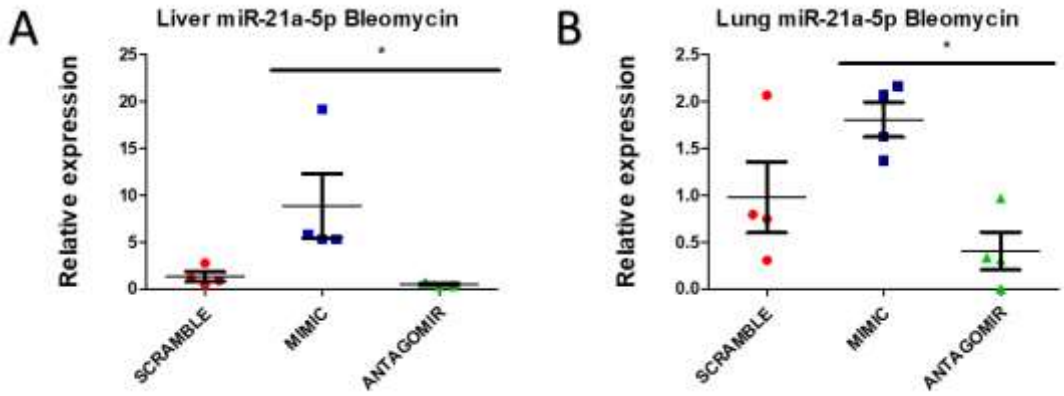

Figure 6.11 miR-21a-5p gain and loss of function in the Bleomycin model of lung fibrosis (n=4). qPCRs result from mice liver (A) and lung (B) treated with a scramble (control red), mirmimic (upregulation blue) and antagomir (downregulation green) sequences for miR-21a-5p. Results are significant for 1-way ANOVA with an overall p-value < 0.05. Student T-test was conducted to evaluate significant differences between pairs of columns, indicated by "" symbol. * p-value < 0.05.*

miR-21a-5p expression in the Liver showed a non-significant 4-fold increase for the mirmimic group and a 68% decrease for antagomir group, resulting in a significant 12-fold increase in the mirmimic group compared to the antagomir group (fig. 6.11A). Lungs showed a significant 3-fold time increase in the mirmimic and a non-significant 25% reduction in the antagomir group from scramble. miR-21a-5p expression increased 4-fold in the mirmimic group compared to the antagomir group (fig. 6.11B). The results demonstrated that treatments with mirmic and antagomir were efficient in fine tune miR-21a-5p expression in circulation, as expected.

Next, Smad7 (predicted target), Col1a1 and Ccn2/Ctgf were evaluated in the lung tissue of the experimental animals.

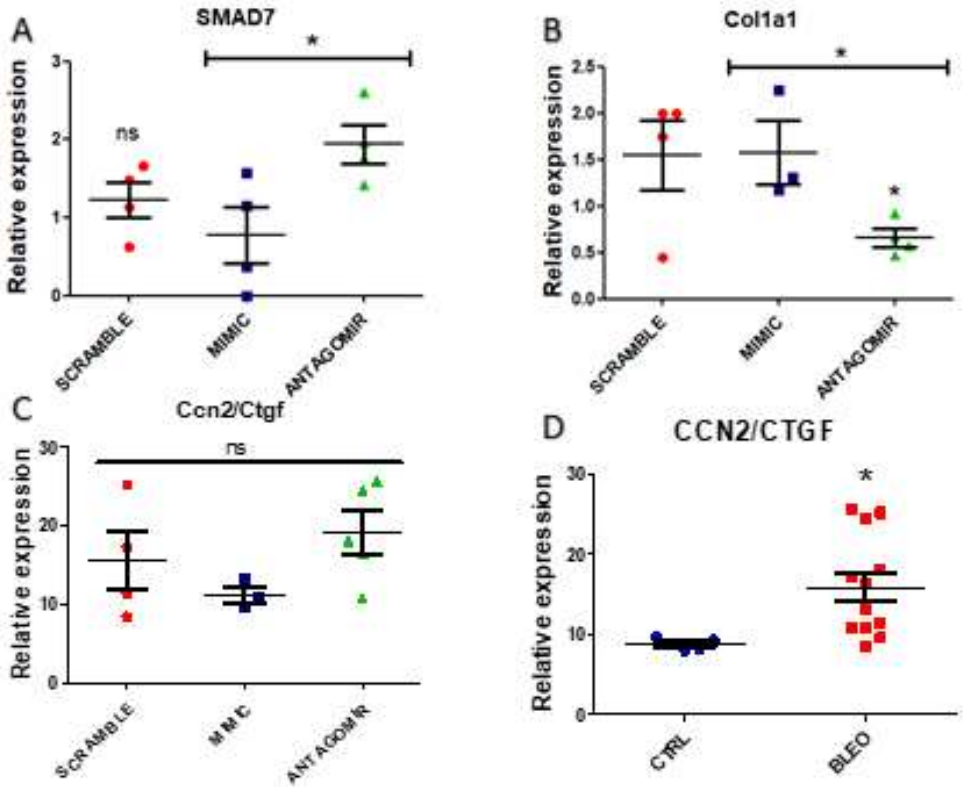

Figure 6.12 qPCRs from miR-21a-5p gain and loss of function experiments for Smad7 (A), Col1a1 (B) and Ccn2/Ctgf (C)in lungs from mice treated with Bleomycin (n=4). Bleomycin was used to recapitulate fibrotic phenotype. Ccn2/Ctgf comparison for samples treated with Bleomycin (in red) and untreated (CTRL in blue) (D). Results in Smad7 and Col1a1 are significant for 1-way ANOVA with an overall p-value < 0.05 for Smad7 and an overall p-value < 0.01 for Col1a1. Student T-test was conducted to evaluate significance differences between pairs of columns and are indicated by "". *< p-value 0.05.*

Smad7 expression levels were decreased by 37% in the miR-21a-5p mirmimic group, however, this was not statistically significant. In the antagomir group SMAD7 expression was increase by 58%. SMAD7 expression was 2.5- time higher in the antagomir group compared to the mirmimic group (fig. 6.12A). This meant that antagomir treatment for miR-21a-5p results in increase in Smad7 expression.

Collagen α1-chain mRNA showed a significant 65% decrease in the antagomir, while there was no significant effect on Col1A1 expression in the mirmimic group (fig. 12B). Interesting, the antagomir group showed for the four mice treated a consistent decrease in Col1a1 expression, which suggest an amelioration in the fibrotic phenotype induce by the treatment.

Ccn2/Ctgf did not showed significant changes induced by the experimental condition (fig. 6.12C), however Bleomycin increase Ccn2/Ctgf expression level from

not Bleomycin treated mice (fig. 6.12D). This meant that treatment with Bleomycin were efficient in reproduce the fibrotic phenotype experimentally.

6.3.2.4 *miR-21a-5p mirmimic and antagomir in the Bleomycin model of lung fibrosis (2)*

In vivo µCT scans imaged lung at different stages during the follow-up study on the role of miR-21a-5p in the Bleomycin model of lung fibrosis. Resulting images at endpoint were further used for qualitative analysis regarding fibrotic development in mice lungs.

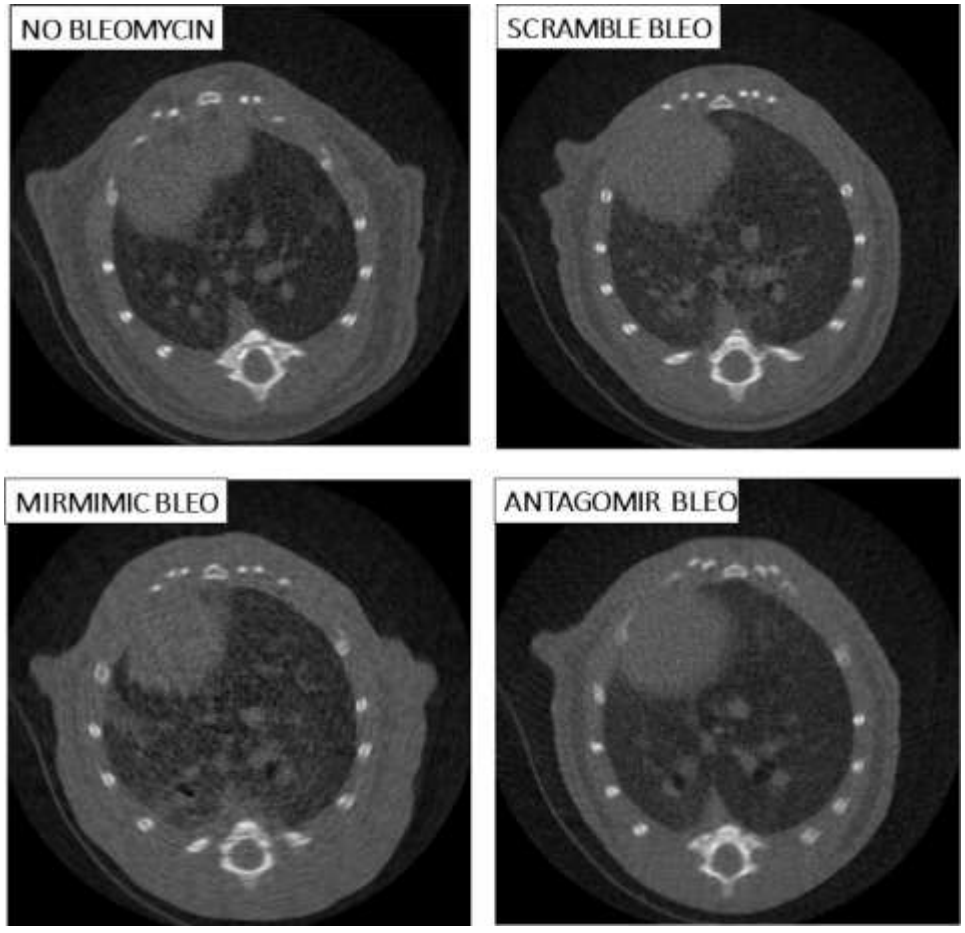

Figure 6.13 Orthogonal mice cross section from lung scanned with µCT from Control (without Bleomycin treatment, top left), scramble (Bleomycin treated, top right), mirmimic (Bleomycin treated, bottom left) and antagomir (Bleomycin treated, bottom left) groups. Grey levels (0-251) were set with 0 (black) indicating air while 251 (white) set as bones. Therefore, soft tissue referred to middle value using this scale setting. White arrow indicated an area that shows a localised attenuation of X-ray that suggest a worsening of fibrotic phenotype.

Lungs treated with Bleomycin showed qualitative increase in ECM contents, represented in lung cross-section as patch of light grey (fig. 6.13) Control group lungs showed areas with light grey, indicating major blood vessel. Both scramble and antagomir groups showed similar light grey patterns, while the mirmimic group shows a quite significant dark area reduction in lung cross-section (fig. 6.13). The increase in grey colour over black, indicated an increase in lung volume with reduction of air capability. This suggested that alveoli are replaced by a thin net of ECM, indicating an increase in fibrosis, which had in the mirmic group the worst phenotype.

6.3.2.5 miR-21a-5p mirmimic and antagomir in the Bleomycin model of lung fibrosis (3)

Sections were visualised and imaged through both Brightfield and Polarized light microscopy, as described in 2.3.

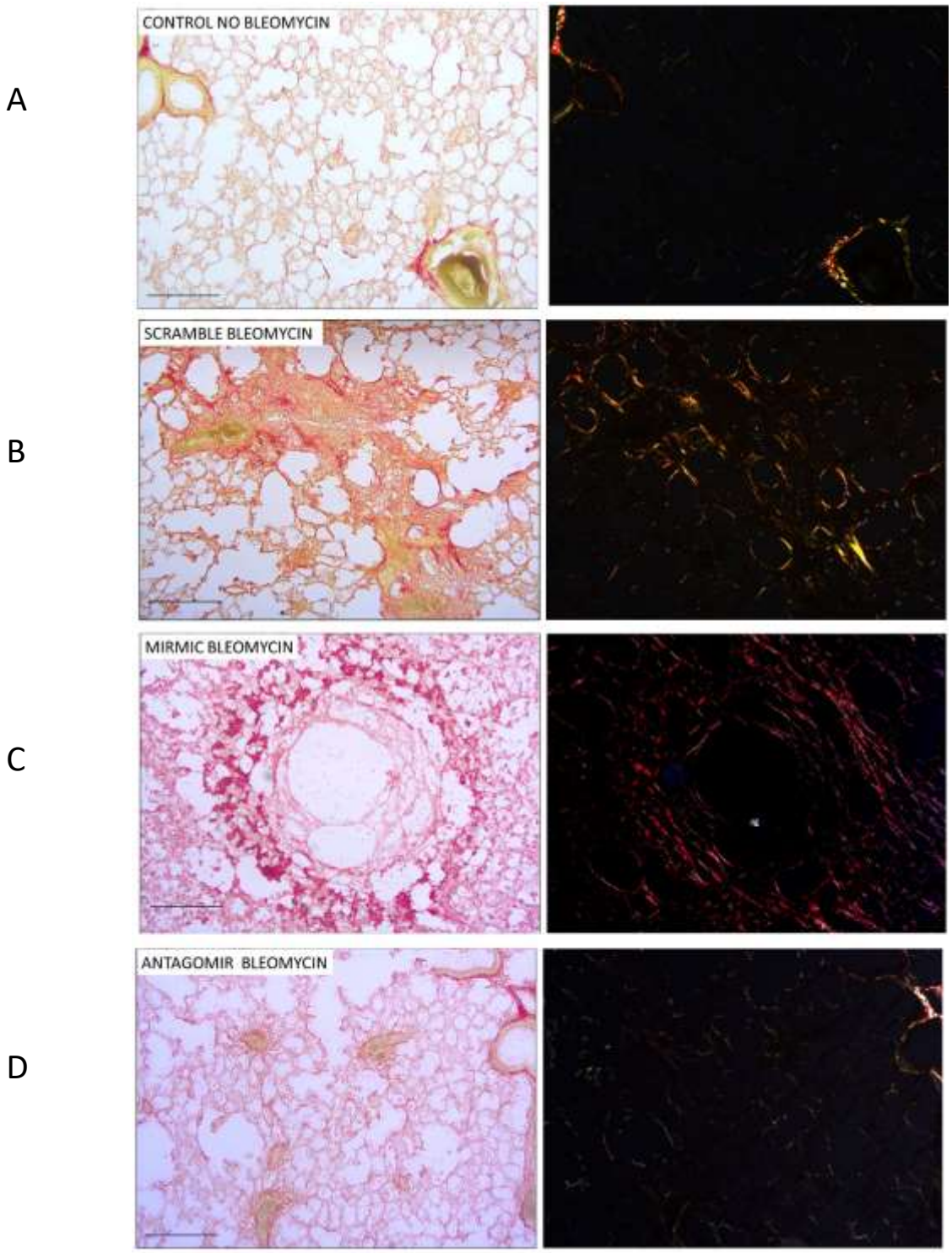

Figure 6.14 Representative images from lung sections from untreated lung (A) and lungs treated with Bleomycin (B-D), stained with Sirius Red and imaged through Brightfield (left) and Polarised light microscopy (right). Lung treated with Bleomycin also received a scramble sequence (B) mirmic (C) and antagomir. From images obtained through polarised light microscopy it is possible to notice an increase in dichroism for Bleomycin treated lungs(B-D). Treatments with miR-21a-5p analogue resulted in worsening of fibrotic phenotype for mirmic group (C) compared to Scramble (B) and antagomir (D). [scale bar 500 µm].

Control lung section shows a normal lung architecture with Picrosirius stain limited to the blood vessels, without positive stain in the alveoli. Polarized light microscopy shows few events of dichroism, most of that with low intensity. (fig. 6.14A).

Lungs from the Bleomycin/scrambled group show tissue aggregates with parenchymal disruption. Polarised light microscopy highlighted event of dichroism around alveoli with bright colour intensification. (fig. 6.14B).

Lung section from Bleomycin/mirmimic group shows tissue degeneration and intensification of red stain around alveoli. Polarized light microscopy showed increased in red colour formation (fig. 6.14C).

Lung section from Bleomycin/antagomir group shows normal appearance of the alveoli. However, polarized light microscopy displayed events of dichroism in the alveolar space (fig. 6.14D).

Section comparison of above showed sections allows to obtain qualitative information regarded treatment combination. Scramble and mirmimic group treated with Bleomycin displayed a higher tissue disruption with clearer level of dichroism highlighted by polarised light microscopy. Antagomir group treated with Bleomycin showed a higher level of tissue integrity and less level of dichroism compared with the other Bleomycin treated groups. Antagomir group showed similarity with control group with a higher dichroism development.

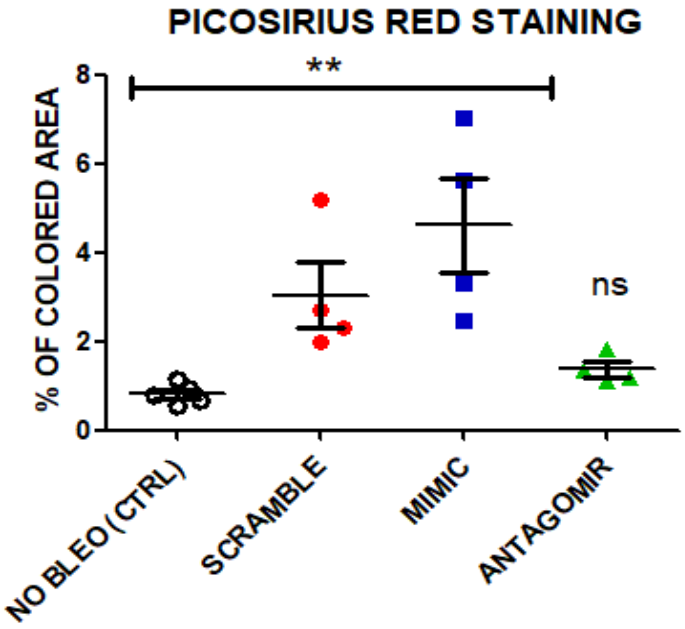

Figure 6.15 Quantification of collagen fibres content from control not treated with Bleomycin (clear circle), scramble treated with Bleomycin (red circle), mirmimic group treated with Bleomycin (blue squares) and antagomir group treated with Bleomycin (green triangles). Results showed are significant for 1-way ANOVA with an overall p-value < 0.01. Student T-test was conducted to evaluate significant differences between pairs of columns, indicated by "" symbol. ** p-value < 0.01.*

Quantification of the polarised light images using image analysis (see Chapter2) showed that Bleomycin treatment resulted in a significant 3.2-fold compared to the no-Bleomycin control group. This was even further increased to a 5-fold increase in polarised light signal in the mirmimic group, however, this was not significantly different from the scramble group. In contrast, treatment with the antagomir did not result in a significant increase in polarised light signal. Moreover, scramble and mirmimic group showed a non-significant 2-fold and 3-fold increased level of collagen fibres formation compared to the antagomir group (fig. 6.15).

Bleomycin treatments were able to induce a fibrotic phenotype, which seem to be rescued by a treatment with antagomir for miR-21a-5p. On the other hand, a treatment that increases miR-21a-5p seem to lead to a worser phenotype when Bleomycin is present.

6.4 Discussion

PF is a debilitating progressive disease where lung parenchyma is replaced by a collagenous scar tissue, which led to a breathing imbalance and death, and currently there are no treatments able to reverse the disease (Wynn, 2011). Reducing collagen fibres deposition by blocking the TGF-ß pathway is a promising strategy for the treatment of IPF (Fujimoto et al., 2015). microRNAs are a promising class of compounds able to block TGF-ß and collagen formation (Rajasekaran et al., 2015). In the present chapter, I focused on the role of miR29a-3p and miR-21a-5p.

miR-29a-3p appears from a comprehensive microRNAs analysis as one of the most encourageing target for antifibrotic therapy (Xie et al., 2011). Thus, to evaluate the benefits in a treatment with miR-29a-3p, a gain and loss of function experiments was performed. The main focus of the procedure was to discover from silico to *in vitro* the role of miR-29a-3p in primary fibroblast, cells considered at basis of fibrosis pathogenesis. To reduce genetic intra-organ variability primary lung fibroblast were employed for the purpose. Although lung is composed by a wide range of mesenchymal cells with different role and characteristic, fibroblasts used for the experiments expressed characteristic proteins common to matrix and myo- fibroblasts, such as, α-smooth actin, vimentin and HSP47 (Whitsett, Kalin, Xu, & Kalinichenko, 2018). Likewise, miR-29a, did not showed pronounced sequences differences between human and mice. TargetScan 7.2 analysis showed for miR-29a-3p microRNA-mRNA interactions, a high level of conservation between mammalian species. Targetscan prediction suggested inhibitory interaction miR-29a-Col1a1 and miR-29a-Col3a1, lung major ECM component, which were conserved in mammalian species. Moreover, 8 and 7-A1 mer complementarity are more probable events as enough stable to maintain a miR- mRNA interaction (Agarwal et al., 2015). 1-way ANOVA showed that treatments were significantly efficient in reproducing a gain and loss of function for miR-29a in primary mouse lung fibroblasts. Although, antagomir group did not showed significant decrease from control (scramble), its expression was 99.4% decreased from miRmimic. qPCRs on Collagen type-I resulted in mirmimic significant downregulation in Col1a1 from both experimental groups, correlated to the increase in the same group in miR-29a-3p expression. By contrast, no changes were detected in Col3a1. Thus, miR-29a-3p mirmic can downregulated Col1a1 expression, but not Col3a1 in primary mouse lung fibroblasts. Interestingly, miR-29a-Col1a1

inhibitory interaction is conserved only in mammalian species, which highlights difference in fibrillar collagen between diverse species (Agarwal et al., 2015). Therefore, this repression might represent a mechanism to reduce fibres formation probably acquired in mammalian evolution. Moreover, miR-29a-3p protective role in fibrosis in response to collagen overexpression is a topic supported by evidence in human fibroblasts, where IPF patients showed miR-29a suppression (Parker et al., 2014). Consistently, miR-29a mirmic leads to decrease in collagen biosynthesis induced by Bleomycin in a mouse model of pulmonary fibrosis. Mice treated with Bleomycin, receiving a therapeutic dose of mirmimic showed a return to a normal lung parenchyma architecture (Montgomery et al., 2014). Results obtained are in line with previous publications and support an antifibrotic role for miR-29a-3p mirmic. In addition, they provide information regarding a selective regulative role for miR-29a on Col1a1, but not on Col3a1 for mouse lung fibroblasts. This fact is important considering that it was postulated that Col1a1 and Col3a1 have a diverse role in fibrillar formation and therefore in fibrosis. Recently, a clinical trial from miRagen is developing a miR-29 mirmic therapy against different forms of organ fibrosis (Gallant-Behm et al., 2019). Therefore, my evidence together with previous work confirmed that miR-29a-3p can be a potential target for disease affecting Collagen turnover. This because it is important to understand that microRNA analogue can be used to fine tune mRNA expression. Evidence showed in chapter are limited by the lack of result on collagen at protein level, however it should be noticed that if Col1a1 is not translated, protein will decrease.

miR-21a has been identified as a profibrotic microRNA in other tissues (Li et al., 2013; G. Liu et al., 2010). As mentioned in the introduction, miR-21a-5p is a potential drug for the treatment of nephropathy (Ivan G. Gomez et al., 2015).

Bioinformatic analysis using TargetScan7.2 identified Smad7 as miR-21a target, presenting an 8-mer binding site from the predicted alignment.

Smad7 is a negative regulator of the TGF-ß pathway, by inhibiting TGF-ß signal transduction and positive feedback on TGF-ß1 receptor. As a result, Smad7 limits TGF-ß-stimulated matrix production. In chapter 4 and 5, I showed that Smad7 expression is induced by TGF-ß and a collagen-based cell culture substrate in both primary mouse lung fibroblasts and in the human MRC5 lung fibroblast cell line (Chapter 4 fig. 6 and 7, chapter 5 fig.10). My findings are in line with previous work identifying Smad7 as a potential inhibitor of organ

fibrosis (Lan, 2008; Troncone et al., 2018; Zhang et al., 2007).

To evaluate if Smad7 is indeed regulated by miR-21a I performed experiments using miR-21a antagomirs (a specific hairpin inhibitor for miR-21a) and mirmimics, both in vitro and in vivo.

Treatment of lung fibroblasts with miR-21a mirmimics resulted in a reduction of Smad7 expression levels, while inhibition of miR-21a using antagomirs resulted in an increase of Smad7 expression. These results indicate that Smad7 is indeed a target for miR-21a.

Quantitative PCRs for Col1a1, Col3a1 and Ctgf/Ccn2 were conducted in the three experimental systems with or without TGF-ß (fig 6.10). ECM expression level showed in all analysed genes a dependency to TGF-ß. Regarding the effect of transfected sequences, Col1a1 and Ccn2/Ctgf did not show significant changes in the TGF-ß treated groups (fig 6.10A and C), while Col3a1 resulted in a significant decrease in mirmimic group compared to control (fig. 6.10B). Col3a1 downregulation triggered by TGF-ß and miR-21a elevated levels, drawing again a possible Col3a1 protective role against fibrosis (chapter 3 and 5).

Next, I investigated the role of miR-21a in the development of pulmonary fibrosis using the *in vivo* mouse model of Bleomycin induced lung fibrosis. Mice were assigned to three experimental groups, receiving either a scramble (control), mirmimic (to increase miR-21a expression) or an antagomir (to inhibit miR-21a expression). Treatment with miR-21a mirmimic resulted in a significant increase in miR-21a in both lung and liver tissue. However, in both livers and lungs the downregulation by the miR-21a antagomir was not significant compared to the scramble control (fig. 6.11). This may be due to intra-individual variation or accelerated clearance of the molecular treatments. Moreover, mice were sacrificed 7 days after the last injection, and therefore the treatment's limited one week half- life, levels in the tissue may have decreased below detection levels.

Smad7 expression was significantly higher in the antagomir treated group compared to the mirmimic group. Although Smad7 levels were higher than scramble control, this difference was not statistically significant, and similarly, the increased levels of Smad7 in the antagomir group was not statistically significant from the scramble control group (fig. 6.12). Statistical limitations between treatment groups may be due to the relatively small group size.

Next, I evaluated the effect of the antagoMir and mirmimicic on expression of fibrosis related genes Ccn2/Ctgf and Col1a1 (fig. 6.12).

Ccn2/Ctgf is a member of CCN family strongly related with fibrosis development.

Through transgenic strategies Leask et al. demonstrated the profibrotic role of CCN2/CTGF gene (S. Liu et al., 2011; Sonnylal et al., 2010). Moreover, a monoclonal antibody for CCN2/CTGF is currently in a phase II clinical trial for the treatment of IPF (Fujimoto et al., 2015; Raghu et al., 2016). Neither the antagomir nor the mirmimic microRNA treatment had any effect on Ccn2/Ctgf expression in the Bleomycin mouse model (fig. 6.12C). Moreover, µCT endpoint scans showed an overall worsening for the mirmimic group indicating that an increase in miR-21a-5p might correlate with increase in ECM (fig. 6.12).

Col1a1 encodes for the α1-chain of type I collagen, which is a major component of mammalian ECM (Vuorio, 1990). Col1a1 changes are strongly related with tissue repair imbalance and organ fibrosis, which is one of the main hallmarks of IPF. Different strategies have been developed during time, targeting collagen biosynthesis and transportation for the cure of fibrosis, however none of them is currently in use for disease treatment (Staab-Weijnitz et al., 2015). The miR-21a-5p mirmimic did not affect Col1a1 expression, although increased level of ECM was found in µCT scans (fig. 6.13). However, treatment with the antagomir lead to a 65% reduction in Col1a1 RNA expression compared to scramble. Hence, inhibition of miR-21a expression might reduce fibrosis through Col1a1 inhibition (fig. 6.15B).

Histology of the lungs confirmed the antagoMir not only inhibition of Col1A1 expression, but also Collagen fibre formation in the Bleomycin model (fig. 6.14). Collagen fibre area was reduced to levels comparable to those in animals that did not receive Bleomycin. In contrast, the mirmimic group displayed an impaired tissue parenchyma with a significant increase in collagen fibre formation (fig. 6.14C).

Interesting miR-21a-5p has affinity for TGF-ß 3'-UTR with an 8-mer site of binding (Tab. 6.1), which theoretically should reduce the autocrine effect of TGF-ß. Results from primary fibroblasts treated with miR-21a-5p mirmic and antagomir, and TGF-ß suggested a possible inhibitory role for miR-21a-5p on TGF-ß. Mirmimic group treated with TGF-ß showed significant decrease from scramble and antagomir group for Ctgf/Ccn2 and Col3a1 expression. However, without TGF-ß stimulation, the mirmic group showed a lower expression for the analysed genes. In addition, *in vivo* results highlighted a phenotypical worsening for mice treated with Bleomycin and mirmic compared to antagomir or scramble.

These results show that miR-21a-5p is a promising candidate for the treatment of PF. *In*

vitro and *in vivo* models of fibrosis resulted in a miR-21a-5p upregulation, leading to a decrease in Smad7 expression. In particular, miR-21a inhibition showed to be a possible strategy for the cure of IPF, as decreased level in miR-21a reflected in Smad7 upregulation. Smad7 upregulation, achieved through miR-21a inhibition, resulted in reduced Col1a1 expression and collagen fibres deposition in the Bleomycin model of lung fibrosis. This latter is in line with previous reports which identified Smad7 upregulation as a promising strategy for the cure of IPF and other types of organ fibrosis (Lan, 2008; Nakao et al., 1999). Moreover, the strategy used to induce Smad7 with antagomir treatment can be considered less toxic and does not modify DNA, which represent benefits for a future therapy. miR-21a gain of function resulted in a worsening of the fibrosis in the animal model, in particular in tissue parenchyma architecture and ECM deposition (fig. 6.11 and 6.13).

To conclude, figure 6.16 proposes the mechanism to explain experimental results obtained on the role of miR-21a inhibition in the *in vitro* and *in vivo model* of fibrosis. In pathological conditions, TGF-ß activates the expression of several ECM gene through a Smad-dependent mechanism. In lung fibroblasts TGF-ß increases also miR-21a expression, leading to Smad7 repression, which augments activatory Smad power and ECM expression. Then if miR-21a is inhibited by a specific miR-21a target, it might be possible to restore Smad7 negative feedback on TGF-ß pathway, limiting ECM production and restoring a healthy phenotype.

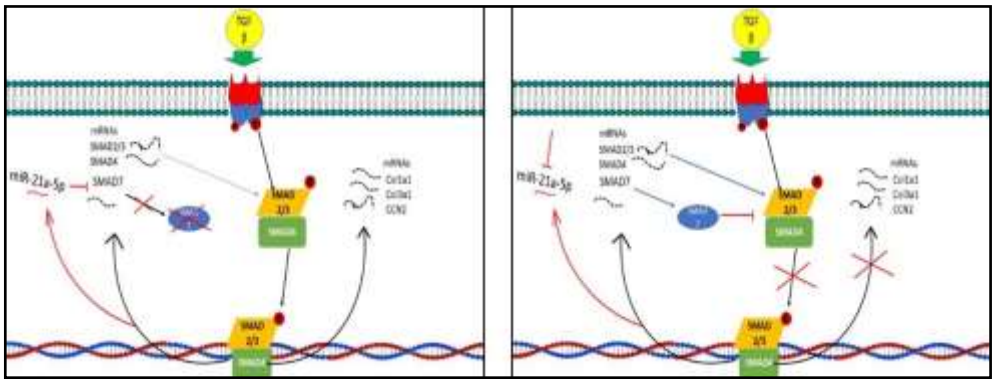

Figure 6.16 Schematic view of the molecular mechanism at the basis of pulmonary fibrosis amelioration through miR-21a-5p inhibition.

7 Discussion

Pulmonary fibrosis is a debilitating progressive disease mostly affecting the elderly. The name “Idiopathic” implies that the underlying cause of IPF is currently unknown. However, IPF is due to dysregulated wound healing repair, characterised by increased matrix production as well as changes in ECM composition, leading to increased tissue rigidity (Vancheri, 2015; Wynn, 2011). The main ECM component overexpressed in fibrosis is collagen (Meltzer & Noble, 2008). So far there has been very limited success in the development of antifibrotic therapies, and the disease usually leads to death within 2-5 years (Wynn, 2011).

The first aim of this PhD project was to identify microRNAs that are differentially expressed in lung fibrosis, and to test whether these miRs or corresponding antagomiRs can suppress lung fibrosis in a mouse model. Using the Bleomycin model, I identified 4 microRNAs (miR-21a-5p, miR-34a-5p, miR-29a-3p and miR-378-5p) as potential pro-fibrotic microRNAs due to progressively increased expression correlated with progression of fibrotic features. However, Montgomery and collaborators found reduced miR-29a-3p expression in the same Bleomycin model of fibrosis (Montgomery et al., 2014).

In vitro experiments using primary mouse fibroblasts demonstrated then that miR-29a-3p overexpression results in a reduction of Col1a1 expression, whereas it has no effect on Col3a1, the other predicted target. Primary mouse lung fibroblasts were used as more relevant cell type in a context of wound healing alteration triggering fibrosis. In conclusion the *in vitro* results obtained confirmed a possible antifibrotic effect previously proposed by Montgomery et al.

miR-21a-5p and miR-34a-5p have previously been identified upregulated in experimental and clinical data on IPF (Cui et al., 2017; Li et al., 2013). Cui and collaborators in 2017 already demonstrated the potential benefit in miR-34a suppression in the mouse model of fibrosis, which was the reason why I focused more on miR-21a, which was not yet studied in this model (Cui et al., 2017).

Of the miRs I identified in the bleomycin model, miR-21a showed the highest expression level, miR-21 expression was significantly increased in the early stages of fibrosis (3 days after Bleomycin treatment), whereas mir-34a and miR-29a were increased only at the late stages, when fibrosis is already apparent (10-21 days after Bleomycin). Therefore, miR-21a suppression might be able to reverse lung fibrosis in early stages of the disease. miR-21a-5p expression also showed an *in vitro* increase dependant on TGF-ß and an ECM rich in collagen type 1, conditions which mimic a pro-fibrotic environment.

Predicted target analyses identified Smad7 as potential target for miR-21a- 5p. Smad7 is a negative regulator of TGF-ß induced signalling and is a potential therapeutic target for treatment of fibrosis (Zhang et al., 2007). Next, I validated the interaction between miR-21a-5p and Smad7 in primary mouse lung fibroblast using mirmimic and antagomir treatments. My results showed mirmimic decreased Smad7 expression, while the antagomir increased Smad7 expression. As increased Smad7 is expected to decrease TGF-ß signalling, I next studied whether miR-21a mirmimics and antagomirs affect development of fibrosis *in vivo* using the Bleomycin model of lung fibrosis. I found that the miR-21a-5p mirmimic increased fibrosis in this model, while the antagomir ameliorated lung fibrosis. miR-21a-5p antagomir increased Smad7 expression in the lungs of the mice, while the mirmimic had no significant effect. The trend in the mirmimic group showed decreased expression of Smad7, however this was not significance due to limitations in statistical power, as only 3-4 animal replicates were used for each experimental group.

This part of the present study provides rational insight regarding a possible pharmacological strategy to prevent the development of lung fibrosis through miR- 21a inhibition. The uses of mirmimic or antagomir treatments as more similar to treatments against IPF and were preferred to a tamoxifen-induced knockout strategy. Moreover, knockout systems would impair epigenetic regulation in response to profibrotic stimulation induced by Bleomycin. This because microRNAs repression has been seen to tune the expression of entire signalling networks (Avraham & Yarden, 2012). However, to demonstrate a reduction in TGF-ß network

activation, the balance between activatory and inhibitory Smads should have been investigated in the antagomir group, for instance by performing western blots for phosphor-SMADS after TGF-ß stimulation.

Tail vein injection (*iv.)* of miR-21a represented a major pharmacokinetic limitation of this experiment, as the intravenous administration can lead to systemic side effects. However, an aerosol administration may be a safer route to take in consideration for the future experiments. Recently, Patel and collaborators have been able to deliver and express PEG-coated polyplexes mRNA only in mouse lungs, which is a suitable strategy also for miRNAs (Patel et al., 2019).

Future possible combinatory strategy employing a pool of microRNAs, like for example combined inhibition of miR-21a and miR-34a, and overexpression of miR-29 might result in a stronger amelioration of lung fibrosis. However, possible off-target effects need to be considered in experimental planning.

Another interesting feature to explore is miR-21a inhibition at early stages of fibrosis, which may ameliorate lung fibrosis through a IL-12 overexpression dependant mechanism in T helper cells (Murugaiyan, Garo, & Weiner, n.d.). IL-12 is a predicted target for miR-21a and its overexpression results in an amelioration in the Bleomycin model of lung fibrosis (Keane et al., 2001). Therefore, miR-21a- repression may increase IL-12 expression triggering amelioration in the Bleomycin model. A possible strategy to investigate this mechanism is evaluating the reduction in immune T-cell infiltration for antagomir group after a Bleomycin treatment.

My next aim was to study the effect of changes in ECM composition analysing the expression of ECM genes and miRs associated with organ fibrosis *in vitro,* using lung epithelial and fibroblast cells. In general, it is reductive to assume that a treatment with TGF-ß is the only driving force in lung fibrosis. Changes occurring in fibrosis regarding matrix composition demonstrated to equally influence the expression of key genes involved in lung fibrosis for both epithelial and fibroblasts cells. The increase in fibrillogenesis during lung fibrosis triggers changes in ECM composition, which holds profibrotic characteristic. However, the

model used was not able to mimic 3D lung septa structure and cannot account that RGD-motif is present also in collagen fibres (Burgstaller et al., 2017). Results showed that a number of genes and both miR-21a-5p and miR-34a-5p were influenced by collagen as substrate.

miR-21a showed a profibrotic-like synergistic effect from TGF-ß treatment and collagen as coated substrate, which was found only in the young fibroblast population. However, as TGF-ß treatment used for the study (2 ng/mL) does not represent a physiological condition, there is the needs to test miR-21a-age-dependency *in vivo*, may be using the Bleomycin model of fibrosis in old mice.

Results identified that Col1a1 expression was influenced by collagen as substrate in a positive feedback manner. Collagen substrate gave rise to increase in Col1a1 expression which powered-up the profibrotic induction by TGF-ß. Moreover, matrix composition, consistently affected the expression of CCN2/CTGF and PDGFRα in epithelial cells and Slug, Smad6, miR-21a and miR-34a in fibroblast cells. This positive feedback effect is in line with the idea that not only RGD-motif, but also collagen, in ECM can transduce signals impacting gene regulation. The interaction between Collagen type-I GFOGER motif and integrin α2ß1 have been experimentally demonstrated and it suggest that α2ß1-GFOGER activate intracellular signalling pathways (Mejía et al., 2015). However, there are no current cellular evidence suggesting this mechanism, which can be key in this field of study. Positive feedback loop effect of collagen substrate on Col1a1 needs also to be further investigated at protein level.

In mammalian lungs, mechanical stretch is generated by diaphragm and chest muscle and transferred first to lung septa and then at cellular level (Bela Suki et al., 2011). Evidence in biomechanics shown that mechanical stretch can exert effects on gene regulation (Junghyun Kim et al., 2018). In lung fibrosis the increase in ECM causes mechanical stretch impairment due to the increase in tissue stiffness (Scotton et al., 2013). Applying mechanical stretch in the culture, I found in both primary and immortalised cells a stretch-dependant protective effect. Stretch decreased expression of CCN2/CTGF, SNAI1 and upregulated SMAD7 in immortalised cell line, and Col1a1, Snai1, miR-21a-5p and miR-34a-5p in primary cells. Interestingly, Col1a1 showed age dependant differential response to mechanical stretch, which raises a

number of questions related to wound healing repair response in ageing.

IPF affects most of the elder population with highest incidence in the 40-70 years old population (Raghu et al., 2011). In my *in vitro* system aged fibroblasts showed increase in Col1a1, Slug and in miR-34a-5p and decrease in Smad6 and Smad7, confirming a stronger profibrotic response in age cells. Hence, ageing decreased TGF-ß repressor and increased expression of profibrotic effectors. Results obtained suggests that increase incidence of lung fibrosis in aged population depends on stronger susceptibility to chronic damage for aged fibroblasts. Future experimental insights are necessary to confirm this effect also on human primary fibroblasts, as interspecies difference may correlate to different mechanism.

In conclusion, the *in vitro* system was able to produce significant results on the effect of cytokines, substrates, and ageing, also taking in consideration cell stretch. However, this model could be improved through the use of 3D lung mimic bioprinting or lung decellurization. This is because those methods can be more representative of lung parenchyma than a coated surface. Moreover, those methods can be taken in account also the direction of stretch, key feature not analysable with Flexcells. Moreover, a 3D system represents more physiological condition and therefore represent a more reliable system to use. Lung decellurization or 3D bioprinting might provide better system to use regarding the effect of fibrotic feature on gene regulation (Parker et al., 2014). However, 3D lung bioprinting is a very recent reality, which have been only able to reproduce lung endothelia but not the epithelia (Albritton & Miller, 2017).

My experiments have shown that miR-21 could be a good target for the development of a novel treatment for IPF.

Bibliography

1 Abercrombie, M. (1979). The cells. *Journal of Clinical Pathology*, *31*, 1–6.

2 Agarwal, V., Bell, G. W., Nam, J. W., & Bartel, D. P. (2015). Predicting effective microRNA target sites in mammalian mRNAs. *ELife*, *4*(AUGUST2015), 1–38. https://doi.org/10.7554/eLife.05005

3 Arakawa, H., Honma, K., Fernandez, I. E., Eickelberg, O., Fischer, A., Brown, (2011). Honeycomb lung: History and current concepts. *American Journal of Roentgenology*, *196*(4), 773–782. https://doi.org/10.2214/AJR.10.4873

4 Armanios, M. (2012). Telomerase and idiopathic pulmonary fibrosis. *Mutation Research - Fundamental and Molecular Mechanisms of Mutagenesis*, *730*(1–2), 52–58. https://doi.org/10.1016/j.mrfmmm.2011.10.013

5 Armanios, M. Y., Chen, J. J.-L., Cogan, J. D., Alder, J. K., Ingersoll, R. G., Markin, C., … Loyd, J. E. (2007). Telomerase Mutations in Families with Idiopathic Pulmonary Fibrosis. *New England Journal of Medicine*, *356*(13), 1317–1326. https://doi.org/10.1056/NEJMoa066157

6 Atkinson, J. M., Pullen, N., Da Silva-Lodge, M., Williams, L., & Johnson, T. S. (2015). Inhibition of thrombin-activated fibrinolysis inhibitor increases survival in experimental kidney fibrosis. *Journal of the American Society of Nephrology*, *26*(8), 1925–1937. https://doi.org/10.1681/ASN.2014030303

7 Bai, S., Shi, X., Yang, X., & Xu, C. (2000). Smad6 as a transcriptional corepressor. *Journal of Biological Chemistry*, *275*(12), 8267–8270. https://doi.org/10.1074/jbc.275.12.8267

8 Bartel, D. P. (2009). MicroRNAs: Target Recognition and Regulatory Functions. *Cell*, *136*(2), 215–233. https://doi.org/10.1016/j.cell.2009.01.002

9 Bonniaud, P., Kolb, M., Galt, T., Robertson, J., Robbins, C., Stampfli, M., … Gauldie, J. (2014). Smad3 Null Mice Develop Airspace Enlargement and Are Resistant to TGF- -Mediated Pulmonary Fibrosis. *The Journal of Immunology*, *173*(3), 2099–2108.

https://doi.org/10.4049/jimmunol.173.3.2099

10 Borie, R., Crestani, B., Dieude, P., Nunes, H., Allanore, Y., Kannengiesser, C., Grandchamp, B. (2013). The MUC5B Variant Is Associated with Idiopathic Pulmonary Fibrosis but Not with Systemic Sclerosis Interstitial Lung Disease in the European Caucasian Population. *PLoS ONE*, *8*(8), 1–6. https://doi.org/10.1371/journal.pone.0070621

11 Burgstaller, G., Oehrle, B., Gerckens, M., White, E. S., Schiller, H. B., & Eickelberg, O. (2017). The instructive extracellular matrix of the lung: basic composition and alterations in chronic lung disease. *European Respiratory Journal*, *50*(1), 1601805. https://doi.org/10.1183/13993003.01805-2016

12 Cai, Y., Yu, X., Hu, S., & Yu, J. (2009). A Brief Review on the Mechanisms of miRNA Regulation. *Genomics, Proteomics and Bioinformatics*, *7*(4), 147–154. https://doi.org/10.1016/S1672-0229(08)60044-3

13 Charan, J., & Kantharia, N. (2013). How to calculate sample size in animal studies? *Journal of Pharmacology and Pharmacotherapeutics*, *4*(4), 303–306. https://doi.org/10.4103/0976-500X.119726

14 Chaudhary, N. I., Schnapp, A., & Park, J. E. (2006). Pharmacologic differentiation of inflammation and fibrosis in the rat bleomycin model. *American Journal of Respiratory and Critical Care Medicine*, *173*(7), 769–776. https://doi.org/10.1164/rccm.200505-717OC

15 Chaudhury, A., & Howe, P. H. (2009). The tale of transforming growth factor-beta (TGFβ) signaling: A soigné enigma. *IUBMB Life*. https://doi.org/10.1002/iub.239

16 Chen, P. H., Chen, X., & He, X. (2013). Platelet-derived growth factors and their receptors: Structural and functional perspectives. *Biochimica et Biophysica Acta - Proteins and Proteomics*. https://doi.org/10.1016/j.bbapap.2012.10.015

17 Chen, Y., & Gridley, T. (2013). The SNAI1 and SNAI2 proteins occupy their own and each other's promoter during chondrogenesis. *Biochemical and Biophysical Research Communications*, *435*(3), 356–360. https://doi.org/10.1016/j.bbrc.2013.04.086

18 Cui, H., Ge, J., Xie, N., Banerjee, S., Zhou, Y., Liu, R.-M., Liu, G. (2017). miR-34a promotes fibrosis in aged lungs by inducing alveolarepithelial dysfunctions. *American Journal of Physiology-Lung Cellular and Molecular Physiology*, *312*(3), L415–L424. https://doi.org/10.1152/ajplung.00335.2016

19 Dan C. Wilkinson, A., A.-O. J., Sucre, J. M. S., Vijayaraj, P., Duraa, A., Richardson, W., Gomperts, B. N. (2014). Development of a Three-Dimensional Bioengineering Technology to Generate Lung Tissue for Personalized Disease Modeling. *Stem Cells Translational Medicine*, *4*, 1344–1351. https://doi.org/10.5966/sctm.2013-0145

20 Degryse, A. L., & Lawson, W. E. (2011). Progress Toward Improving Animal Models for Ipf. *Am J Med Sci*, *341*(6), 444–449. https://doi.org/10.1097/MAJ.0b013e31821aa000.PROGRESS

21 Engel, S., Kim, E. K., Cha, S.-I., Green, G., Naikawadi, R. P., Jones, K. D., Wolters, P. J. (2016). miR-34 miRNAs Regulate Cellular Senescence in Type II Alveolar Epithelial Cells of Patients with Idiopathic Pulmonary Fibrosis. *Plos One*, *11*(6), e0158367. https://doi.org/10.1371/journal.pone.0158367

22 Engel, J., & Bächinger, H. P. (2005). Structure, Stability and Folding of the Collagen Triple Helix (pp. 7–33). Springer, Berlin, Heidelberg. https://doi.org/10.1007/b103818

23 Distler, J. H. W., Györfi, A. H., Ramanujam, M., Whitfield, M. L., Königshoff, M., & Lafyatis, R. (2019). Shared and distinct mechanisms of fibrosis. *Nature Reviews Rheumatology*, *15*(12), 705–730. https://doi.org/10.1038/s41584-019-0322-7

24 Fleischmajer, R., Douglas MacDonald, E., Perlish, J. S., Burgeson, R. E., & Fisher, L. W. (1990). Dermal collagen fibrils are hybrids of type I and type III collagen molecules. *Journal of Structural Biology*, *105*(1–3), 162–169. https://doi.org/10.1016/1047-8477(90)90110-X

25 Fragiadaki, M., Ikeda, T., Witherden, A., Mason, R. M., Abraham, D., & Bou-Gharios, G. (2011). High doses of TGF- potently suppress type I collagen via the transcription factor CUX1. *Molecular Biology of the Cell*,

22(11), 1836–1844. https://doi.org/10.1091/mbc.E10-08-0669

26 Fromm, B., Billipp, T., Peck, L. E., Johansen, M., Tarver, J. E., King, B. L., … Peterson, K. J. (2015). A Uniform System for the Annotation of Vertebrate microRNA Genes and the Evolution of the Human microRNAome. *Annual Review OfGenetics*, *49:213–42*. https://doi.org/10.1146/annurev-genet-120213-092023

27 Frost, S. L., Liu, K., Li, I. M. H., Poulet, B., Comerford, E., De Val, S., & Bou-Gharios, G. (2018). Multiple enhancer regions govern the transcription of CCN2 during embryonic development. *Journal of Cell Communication and Signaling*, *12*(1), 231–243. https://doi.org/10.1007/s12079-017-0440-4

28 Fujimoto, H., Kobayashi, T., & Azuma, A. (2015, January 8). Idiopathic Pulmonary Fibrosis: Treatment and Prognosis. *Clinical Medicine Insights: Circulatory, Respiratory and Pulmonary Medicine*. https://doi.org/10.4137/CCRPM.S23321

29 Gonzalez, D., & Brandan, E. (2019). CTGF/CCN2 from Skeletal Muscle to Nervous System: Impact on Neurodegenerative Diseases. *Molecular Neurobiology*, 1–6. https://doi.org/10.1007/s12035-019-1490-9

30 Gribbin, J., Hubbard, R. B., Le Jeune, I., Smith, C. J. P., West, J., & Tata, L. J. (2006). Incidence and mortality of idiopathic pulmonary fibrosis and sarcoidosis in the UK. *Thorax*, *61*(11), 980–985. https://doi.org/10.1136/thx.2006.062836

31 Guilbert, M., Roig, B., Terryn, C., Garnotel, R., Jeannesson, P., Sockalingum, G. D., … Piot, O. (2016). Highlighting the impact of ageing on type I collagen: Label-free investigation using confocal reflectance microscopy and diffuse reflectance spectroscopy in 3D matrix model. *Oncotarget*, *7*(8), 8546–8555. https://doi.org/10.18632/oncotarget.7385

32 Haley, K. J., Fewell, J. G., Wertheim, B. M., Samokhin, A. O., Yung, L.-M., Khanna, D., … Gladyshev, V. N. (2018). NEDD9 targets COL3A1 to promote endothelial fibrosis and pulmonary arterial hypertension . *Science Translational Medicine*, *10*(445), eaap7294. https://doi.org/10.1126/scitranslmed.aap7294

33 Han, G., Li, A. G., Liang, Y. Y., Owens, P., He, W., Lu, S., … Wang, X. J.

(2006). Smad7-Induced β-Catenin Degradation Alters Epidermal Appendage Development. *Developmental Cell*, *11*(3), 301–312. https://doi.org/10.1016/j.devcel.2006.06.014

34 Handorf, A. M., Zhou, Y., Halanski, M. A., & Li, W. J. (2015). Tissue stiffness dictates development, homeostasis, and disease progression. *Organogenesis*, *11*(1), 1–15. https://doi.org/10.1080/15476278.2015.1019687

35 Hanna, J., Hossain, G. S., & Kocerha, J. (2019). The potential for microRNA therapeutics and clinical research. *Frontiers in Genetics*. https://doi.org/10.3389/fgene.2019.00478

36 Hartmann, C., & Yang, Y. (2020). Chapter 1 - Molecular and cellular regulation of intramembranous and endochondral bone formation during embryogenesis. In J. P. Bilezikian, T. J. Martin, T. L. Clemens, & C. J. B. T.-P. of B. B. (Fourth E. Rosen (Eds.) (pp. 5–44). Academic Press. https://doi.org/https://doi.org/10.1016/B978-0-12-814841-9.00001-4

37 Hashimoto, N., Phan, S. H., Imaizumi, K., Matsuo, M., Nakashima, H., Kawabe, T., … Hasegawa, Y. (2010). Endothelial-mesenchymal transition in bleomycin-induced pulmonary fibrosis. *American Journal of Respiratory Cell and Molecular Biology*, *43*(2), 161–172. https://doi.org/10.1165/rcmb.2009-0031OC

38 Hatley, M. E., Patrick, D. M., Garcia, M. R., Richardson, J. A., Bassel-Duby, R., van Rooij, E., & Olson, E. N. (2010). Modulation of K-Ras-dependent lung tumorigenesis by MicroRNA-21. *Cancer Cell*, *18*(3), 282–293. https://doi.org/10.1016/j.ccr.2010.08.013

39 Hauschka, S. D., & Konigsberg, I. R. (1966). *The influence of collagen on the development of muscle clones. Proceedings of the National Academy of Sciences* (Vol. 55). Biophysical Society Meeting. https://doi.org/10.1073/pnas.55.1.119

40 Heibein, J. A., Goping, I. S., Barry, M., Pinkoski, M. J., Shore, G. C., Green, D. R., & Bleackley, R. C. (2000). Granzyme B–Mediated Cytochrome C Release Is Regulated by the Bcl-2 Family Members Bid and Bax. *The Journal of Experimental Medicine*, *192*(10), 1391–1402.

https://doi.org/10.1084/jem.192.10.1391

41 Henriksen, K., & Karsdal, M. A. (2016). Type I Collagen. In *Biochemistry of Collagens, Laminins and Elastin* (pp. 1–11). Elsevier. https://doi.org/10.1016/B978-0-12-809847-9.00001-5

42 Hermeking, H. (2010). The miR-34 family in cancer and apoptosis. *Cell Death and Differentiation*. Nature Publishing Group. https://doi.org/10.1038/cdd.2009.56

43 Hsia, C. C. W., Hyde, D. M., & Weibel, E. R. (2016). Lung structure and the intrinsic challenges of gas exchange. *Comprehensive Physiology*, *6*(2), 827–895. https://doi.org/10.1002/cphy.c150028

44 Hwangbo, C., Tae, N., Lee, S., Kim, O., Park, O. K., Kim, J., … Lee, J. H. (2016). Syntenin regulates TGF-β1-induced Smad activation and the epithelial-to-mesenchymal transition by inhibiting caveolin-mediated TGF-β type i receptor internalization. *Oncogene*, *35*(3), 389–401. https://doi.org/10.1038/onc.2015.100

45 Ingber, D. E. (2003). Tensegrity I. Cell structure and hierarchical systems biology. *Journal of Cell Science*, *116*(7), 1157–1173. https://doi.org/10.1242/jcs.00359

46 Ishida, Y., & Nagata, K. (2011). Hsp47 as a Collagen-Specific Molecular Chaperone. *Methods in Enzymology*, *499*, 167–182. https://doi.org/10.1016/B978-0-12-386471-0.00009-2

47 Ivan G. Gomez, D. A. MacKenna, B. G. Johnson, V Kaimal, A. M. Roach, S. Ren., N. Nakagawa, C. Xin, R. Newitt, S. Pandya, T. Xia, X. Liu, D. Borza, M. Grafals, S. J. Shankland, J. Himmelfarb, D. Portilla, S. Liu, B. Nelson Chau, and J. S. Duffield (2015), Anti–microRNA-21 oligonucleotides prevent Alport nephropathy progression by stimulating metabolic pathways. *The Journal of Clinical Investigation*, *125*(1), 505. https://doi.org/10.1172/Vehicle

48 Jun, J. Il, & Lau, L. F. (2018). Resolution of organ fibrosis. *Journal of Clinical Investigation*. https://doi.org/10.1172/JCI93563

49 Ken, O., Galvin, J., Burke, A., Atamas, S., & Todd, N. (2018). Interstitial Lung Disease and Pulmonary Fibrosis: A Practical Approach for General

Medicine Physicians with Focus on the Medical History. *Journal of Clinical Medicine*, *7*(12), 476. https://doi.org/10.3390/jcm7120476

50 Kalluri, R., & Neilson, E. G. (2003). Epithelial-mesenchymal transition and its implications for fibrosis. *Journal of Clinical Investigation*, *112*(12), 1776–1784. https://doi.org/10.1172/JCI200320530

51 Kalluri, R., & Weinberg, R. A. (2009). The basics of epithelial-mesenchymal transition. *Journal of Clinical Investigation*. https://doi.org/10.1172/JCI39104

52 Kendall, R. T., & Feghali-Bostwick, C. A. (2014). Fibroblasts in fibrosis: Novel roles and mediators. *Frontiers in Pharmacology*, *5 MAY*(May), 1–13. https://doi.org/10.3389/fphar.2014.00123

53 Kim, Jieun, Hyun, J., Wang, S., Lee, C., & Jung, Y. (2018). MicroRNA-378 is involved in hedgehog-driven epithelial-to-mesenchymal transition in hepatocytes of regenerating liver. *Cell Death and Disease (2018)*. https://doi.org/10.1038/s41419-018-0762-z

54 Kim, Junghyun, Han, S., Lei, A., Miyano, M., Bloom, J., Srivastava, V., … Sohn, L. L. (2018). Characterizing cellular mechanical phenotypes with mechano-node-pore sensing. *Microsystems & Nanoengineering*, *4*, 17091. https://doi.org/10.1038/micronano.2017.91

55 King, J., Costabel, U., Cordier, J. F., DoPico, G. A., DuBois, R. M., Lynch, D.,Smith, C. M. (2000). Idiopathic pulmonary fibrosis: Diagnosis and treatment: International Consensus Statement. *American Journal of Respiratory and Critical Care Medicine*. https://doi.org/10.1164/ajrccm.161.2.ats3-00

56 Kõks, S., Dogan, S., Tuna, B. G., González-Navarro, H., Potter, P., & Vandenbroucke, R. E. (2016). Mouse models of ageing and their relevance to disease. *Mechanisms of Ageing and Development*, *160*, 41–53. https://doi.org/10.1016/j.mad.2016.10.001

57 Kühn, K. (1987). The Classical Collagens: Types I, II, and III. *Structure and Function of Collagen Types*, 1–42. https://doi.org/10.1016/B978-0-12-481280-2.50005-2

58 Kuivaniemi, H., & Tromp, G. (2019). Type III collagen (COL3A1): Gene and

protein structure, tissue distribution, and associated diseases. *Gene*, *707*, 151–171. https://doi.org/10.1016/J.GENE.2019.05.003

59 Kurtz, A., & Oh, S. J. (2012, May). Age related changes of the extracellular matrix and stem cell maintenance. *Preventive Medicine*. https://doi.org/10.1016/j.ypmed.2012.01.003

60 Lagares, D., Santos, A., Grasberger, P. E., Liu, F., Probst, C. K., Rahimi, R. A., Tager, A. M. (2017). Targeted apoptosis of myofibroblasts with the BH3 mimetic ABT-263 reverses established fibrosis. *Science Translational Medicine*, *9*(420), eaal3765. https://doi.org/10.1126/scitranslmed.aal3765

61 Lakatos, H. F., Burgess, H. A., Thatcher, T. H., Redonnet, M. R., Hernady, E., Williams, J. P., & Sime, P. J. (2006). Oropharyngeal aspiration of a silica suspension produces a superior model of silicosis in the mouse when compared to intratracheal instillation. *Experimental Lung Research*, *32*(5), 181–199. https://doi.org/10.1080/01902140600817465

62 Lan, H. Y. (2008). Smad7 as a therapeutic agent for chronic kidney diseases. *Frontiers in Bioscience*, 4984–4992.

63 Laurent, G. J. (1986). Lung collagen: More than scaffolding. *Thorax*, *41*(6), 418–428. https://doi.org/10.1136/thx.41.6.418

64 Lemos, D. R., & Duffield, J. S. (2018). Tissue-resident mesenchymal stromal cells: Implications for tissue-specific antifibrotic therapies. *Science Translational Medicine*, *10*(426), 1–10. https://doi.org/10.1126/scitranslmed.aan5174

65 Leslie, K. O., Cool, C. D., Sporn, T. A., Curran-Everett, D., Steele, M. P., Brown, K. K., … Schwartz, D. A. (2012). Familial idiopathic interstitial pneumonia histopathology and survival in 30 patients. *Archives of Pathology and Laboratory Medicine*, *136*(11), 1366–1376. https://doi.org/10.5858/arpa.2011-0627-OAI

66 Li, P., Zhao, G.-Q., Chen, T.-F., Chang, J.-X., Wang, H.-Q., Chen, S.-S., & Zhang, G.-J. (2013). Serum miR-21 and miR-155 expression in idiopathic pulmonary fibrosis. *Journal of Asthma*, *50*(9), 960–964. https://doi.org/10.3109/02770903.2013.822080

67 Lidzbarsky, G., Gutman, D., Shekhidem, H. A., Sharvit, L., & Atzmon, G. (2018). Genomic Instabilities, Cellular Senescence, and Ageing: In Vitro, In Vivo and Ageing-Like Human Syndromes. *Frontiers in Medicine*, *5*(April), 104. https://doi.org/10.3389/fmed.2018.00104

68 Liu, S., Shi-Wen, X., Abraham, D. J., & Leask, A. (2011). CCN2 is required for bleomycin-induced skin fibrosis in mice. *Arthritis and Rheumatism*, *63*(1), 239–246. https://doi.org/10.1002/art.30074

69 Mack, M. (2018). Inflammation and fibrosis. *Matrix Biology*, *68–69*, 106–121. https://doi.org/10.1016/j.matbio.2017.11.010

70 Makareeva, E., & Leikin, S. (2014). Collagen Structure, Folding and Function. In *Osteogenesis Imperfecta* (pp. 71–84). Elsevier. https://doi.org/10.1016/B978-0-12-397165-4.00007-1

71 Marinković, A., Liu, F., & Tschumperlin, D. J. (2013). Matrices of physiologic stiffness potently inactivate idiopathic pulmonary fibrosis fibroblasts. *American Journal of Respiratory Cell and Molecular Biology*, *48*(4), 422–430. https://doi.org/10.1165/rcmb.2012-0335OC

72 Martinez, F. J., Chisholm, A., Collard, H. R., Flaherty, K. R., Myers, J., Raghu, G., Richeldi, L. (2017). The diagnosis of idiopathic pulmonary fibrosis: current and future approaches. *The Lancet Respiratory Medicine*, *5*(1), 61–71. https://doi.org/10.1016/S2213-2600(16)30325-3

73 Massagué, J. (2008). TGFβ in Cancer. *Cell*, *134*(2), 215–230. https://doi.org/10.1016/j.cell.2008.07.001

74 Massagué, J. (2012). TGFβ signalling in context. https://doi.org/10.1038/nrm3434

75 McGowan, S. E., & Torday, J. S. (1997). the Pulmonary Lipofibroblast (Lipid Interstitial Cell) and Its Contributions To Alveolar Development. *Annual Review of Physiology*, *59*(1), 43–62. https://doi.org/10.1146/annurev.physiol.59.1.43

76 Mejía, E. R., Ospina, J. D., Osorno, L., Márquez, M. A., & Morales, A. L. (2015). Mineralogical Characterization of Chalcopyrite Bioleaching. In *Fourier Transform - Signal Processing and Physical Sciences* (Vol. 101, pp. 47–56). Zhang and Plow. https://doi.org/10.5772/59489

77 Meltzer, E. B., & Noble, P. W. (2008). Idiopathic pulmonary fibrosis. *Orphanet Journal of Rare Diseases*, *3*(1), 1–15. https://doi.org/10.1186/1750-1172-3-8

78 Miller, M. R. (2010). Structural and physiological age-associated changes in ageing lungs. *Seminars in Respiratory and Critical Care Medicine*, *31*(5), 521–527. https://doi.org/10.1055/s-0030-1265893

79 Miyazaki, H., Kuwano, K., Yoshida, K., Maeyama, T., Yoshimi, M., Fujita, M., Nakanishi, Y. (2004). The perforin mediated apoptotic pathway in lung injury and fibrosis. *Journal of Clinical Pathology*, *57*(12), 1292–1298. https://doi.org/10.1136/jcp.2003.015495

80 Montgomery, R. L., Yu, G., Latimer, P. A., Stack, C., Robinson, K., Dalby, C. M., van Rooij, E. (2014). MicroRNA mimicry blocks pulmonary fibrosis. *EMBO Molecular Medicine*, *6*(10), 1347–1356. https://doi.org/10.15252/emmm.201303604

81 Moore, B. B., Lawson, W. E., Oury, T. D., Sisson, T. H., Raghavendran, K., & Hogaboam, C. M. (2013). Animal models of fibrotic lung disease. *American Journal of Respiratory Cell and Molecular Biology*, *49*(2), 167–179. https://doi.org/10.1165/rcmb.2013-0094TR

82 Mori, S., Rönnstrand, L., Yokote, K., Engström, A., Courtneidge, S. A., Claesson-Welsh, L., & Heldin, C. H. (1993). Identification of two juxtamembrane autophosphorylation sites in the PDGF beta-receptor; involvement in the interaction with Src family tyrosine kinases. *The EMBO Journal*, *12*(6), 2257–2264. Retrieved from https://www.ncbi.nlm.nih.gov/pmc/articles/PMC413454/pdf/emboj00078-0037.pdf

83 Mouratis, M. A., & Aidinis, V. (2011). Modeling pulmonary fibrosis with bleomycin. *Current Opinion in Pulmonary Medicine*, *17*(5), 355–361. https://doi.org/10.1097/MCP.0b013e328349ac2b

84 Murray, L. A., Rubinowitz, A., & Herzog, E. L. (2012). Interstitial lung disease: Is interstitial lung disease the same as scleroderma lung disease? *Current Opinion in Rheumatology*. https://doi.org/10.1097/BOR.0b013e3283588de4

85 Nakao, A., Fujii, M., Matsumura, R., Kumano, K., Saito, Y., Miyazono, K., & Iwamoto, I. (1999). Transient gene transfer and expression of Smad7 prevents bleomycin- induced lung fibrosis in mice. *Journal of Clinical Investigation*, *104*(1), 5–11. https://doi.org/10.1172/JCI6094

86 Niederreither, K., D'Souza, R., Metsäranta, M., Eberspaecher, H., Toman, P. D., Vuorio, E., & De Crombrugghe, B. (1995). Coordinate patterns of expression of type I and III collagens during mouse development. *Matrix Biology*, *14*(9), 705–713. https://doi.org/10.1016/S0945-053X(05)80013-7

87 Nieto, M. A. (2002). The snail superfamily of zinc-finger transcription factors. *Nature Reviews Molecular Cell Biology*, *3*(3), 155–166. https://doi.org/10.1038/nrm757

88 Nogee, L. M., Dunbar, A. E., Wert, S. E., Askin, F., Hamvas, A., & Whitsett, J. A. (2001). A Mutation in the Surfactant Protein C Gene Associated with Familial Interstitial Lung Disease. *New England Journal of Medicine*, *344*(8), 573–579. https://doi.org/10.1056/NEJM200102223440805

89 O'Brien, J., Hayder, H., Zayed, Y., & Peng, C. (2018). Overview of microRNA biogenesis, mechanisms of actions, and circulation. *Frontiers in Endocrinology*, *9*(AUG), 1–12. https://doi.org/10.3389/fendo.2018.00402

90 Olson, A. L., Gifford, A. H., Inase, N., Fernández Pérez, E. R., & Suda, T. (2018). The epidemiology of idiopathic pulmonary fibrosis and interstitial lung diseases at risk of a progressive-fibrosing phenotype. *European Respiratory Review*. https://doi.org/10.1183/16000617.0077-2018

91 Orgel, J. P. R. O., Irving, T. C., Miller, A., & Wess, T. J. (2006). Microfibrillar structure of type I collagen in situ. *Proceedings of the National Academy of Sciences*, *103*(24), 9001–9005. https://doi.org/10.1073/pnas.0502718103

92 Parola, M. (2016). Age-dependent changes in extracellular matrix turnover: An under evaluated issue in the approach to chronic liver diseases. *Journal of Hepatology*, *64*(1), 13–15. https://doi.org/10.1016/j.jhep.2015.09.017

93 Patel, A. K., Kaczmarek, J. C., Bose, S., Kauffman, K. J., Mir, F., Heartlein,

M. W., Anderson, D. G. (2019). Inhaled Nanoformulated mRNA Polyplexes for Protein Production in Lung Epithelium. *Advanced Materials*, *31*(8), 1–7. https://doi.org/10.1002/adma.201805116

94 Pereira, R., Khillan, J. S., Helminen, H. J., Hume, E. L., & Prockop, D. J. (1993). *Transgenic Mice Expressing a Partially Deleted Gene for Type I Procollagen (COLlAl) A Breeding Line with a Phenotype of Spontaneous Fractures and Decreased Bone Collagen and Mineral*. Retrieved from https://www.ncbi.nlm.nih.gov/pmc/articles/PMC288013/pdf/jcinvest00037-0341.pdf

95 Rajasekaran, S., Rajaguru, P., & Sudhakar Gandhi, P. S. (2015). MicroRNAs as potential targets for progressive pulmonary fibrosis. *Frontiers in Pharmacology*, *6*(NOV), 1–15. https://doi.org/10.3389/fphar.2015.00254

96 Ramazani, Y., Knops, N., Elmonem, M. A., & Nguyen, T. Q. (2018). Connective tissue growth factor (CTGF) from basics to clinics. *Matrix Biology*, *68–69*, 44–66. https://doi.org/10.1016/j.matbio.2018.03.007

97 Ramlee, M. K., Wang, J., Toh, W. X., & Li, S. (2016). Transcription regulation of the human telomerase reverse transcriptase (hTERT) gene. *Genes*, *7*(8). https://doi.org/10.3390/genes7080050

98 Reiser, K. M., Hennessy, S. M., & Last, J. A. (1987). Analysis of age-associated changes in collagen crosslinking in the skin and lung in monkeys and rats. *Biochimica et Biophysica Acta (BBA) - General Subjects*, *926*(3), 339–348. https://doi.org/10.1016/0304-4165(87)90220-0

99 Ribas, J., Ni, X., Castanares, M., Liu, M. M., Esopi, D., Yegnasubramanian, S., Lupold, S. E. (2012). A novel source for miR-21 expression through the alternative polyadenylation of VMP1 gene transcripts. *Nucleic Acids Research*, *40*(14), 6821–6833. https://doi.org/10.1093/nar/gks308

100 Ricard-Blum, S. (2011). The Collagen Family. *Cold Spring Harbor Perspectives in Biology*, *3*(1), 1–19. https://doi.org/10.1101/cshperspect.a004978

101 Rocha, W., Verreault, A., Almouzni, G., Paik, J., Carey, M., Workman, J. L., Imhof, A. (2007). Activation : MicroRNAs Can. *Science (New York, N.Y.)*,

(December), 1931–1934.

102 Rosas, I. O., Richards, T. J., Konishi, K., Zhang, Y., Gibson, K., Lokshin, A. E., Kaminski, N. (2008). MMP1 and MMP7 as potential peripheral blood biomarkers in idiopathic pulmonary fibrosis. *PLoS Medicine*, *5*(4), 0623–0633. https://doi.org/10.1371/journal.pmed.0050093

103 Russo, V., Klein, T., Lim, D. J., Solis, N., Machado, Y., Hiroyasu, S., Granville, D. J. (2018). Granzyme B is elevated in autoimmune blistering diseases and cleaves key anchoring proteins of the dermal-epidermal junction. *Scientific Reports*, *8*(1), 9690. https://doi.org/10.1038/s41598-018-28070-0

104 Rybinski, B., Franco-Barraza, J., & Cukierman, E. (2014). The wound healing, chronic fibrosis, and cancer progression triad. *Physiological Genomics*. https://doi.org/10.1152/physiolgenomics.00158.2013

105 Schittny, J. C. (2017). Development of the lung. *Cell and Tissue Research*. https://doi.org/10.1007/s00441-016-2545-0

106 Schulte, H., Mühlfeld, C., & Brandenberger, C. (2019). Age-Related Structural and Functional Changes in the Mouse Lung. *Frontiers in Physiology*, *10*(December). https://doi.org/10.3389/fphys.2019.01466

107 Scotton, C. J., Hayes, B., Alexander, R., Datta, A., Forty, E. J., Mercer, P. F., Chambers, R. C. (2013). Ex vivo micro-computed tomography analysis of bleomycin-induced lung fibrosis for preclinical drug evaluation. *European Respiratory Journal*, *42*(6), 1633–1645. https://doi.org/10.1183/09031936.00182412

108 Seyer, J. M., Hutcheson, E. T., & Kang, A. H. (1976). Collagen polymorphism in idiopathic chronic pulmonary fibrosis. *The Journal of Clinical Investigation*, *57*(6), 1498–1507. https://doi.org/10.1172/JCI108420

109 Shi, X., Chen, F., Yu, J., Xu, Y., Zhang, S., Chen, Y. G., & Fang, X. (2008). Study of interaction between Smad7 and DNA by single-molecule force spectroscopy. *Biochemical and Biophysical Research Communications*, *377*(4), 1284–1287. https://doi.org/10.1016/j.bbrc.2008.10.145

110 Shoulders, M. D., & Raines, R. T. (2009). COLLAGEN STRUCTURE AND

STABILITY. *Annual Review of Biochemistry*. https://doi.org/10.1146/annurev.biochem.77.032207.120833

111 Slusarz, A., & Pulakat, L. (2015). The two faces of miR-29. https://doi.org/10.2459/JCM.0000000000000246

112 Smith-Vikos, T., & Slack, F. J. (2012). MicroRNAs and their roles in ageing. *Journal of Cell Science*, *125*(1), 7–17. https://doi.org/10.1242/jcs.099200

113 Sonnylal, S., Shi-wen, X., Leoni, P., Naff, K., Van Pelt, C. S., Nakamura, H., De Crombrugghe, B. (2010). Selective expression of connective tissue growth factor in fibroblasts in vivo promotes systemic tissue fibrosis. *Arthritis and Rheumatism*, *62*(5), 1523–1532. https://doi.org/10.1002/art.27382

114 Steele, M. P., Speer, M. C., Loyd, J. E., Brown, K. K., Herron, A., Slifer, S. H., Schwartz, D. A. (2005). Clinical and pathologic features of familial interstitial pneumonia. *American Journal of Respiratory and Critical Care Medicine*, *172*(9), 1146–1152. https://doi.org/10.1164/rccm.200408-1104OC

115 Steffensen, B., Xu, X., Martin, P. A., & Zardeneta, G. (2002). Human fibronectin and MMP-2 collagen binding domains compete for collagen binding sites and modify cellular activation of MMP-2. *Matrix Biology*, *21*(5), 399–414. https://doi.org/10.1016/S0945-053X(02)00032-X

116 Suki, Béla, Stamenović, D., & Hubmayr, R. (2011). Lung parenchymal mechanics. *Comprehensive Physiology*, *1*(3), 1317–1351. https://doi.org/10.1002/cphy.c100033

117 Takigawa, M. (2018). An early history of CCN2/CTGF research: the road to CCN2 via hcs24, ctgf, ecogenin, and regenerin. *Journal of Cell Communication and Signaling*. https://doi.org/10.1007/s12079-017-0414-6

118 Tallquist, M., & Kazlauskas, A. (2004). PDGF signaling in cells and mice. *Cytokine & Growth Factor Reviews*, *15*(4), 205–213. https://doi.org/10.1016/j.cytogfr.2004.03.003

119 Theocharis, A. D., Manou, D., & Karamanos, N. K. (2019, August 11). The extracellular matrix as a multitasking player in disease. *FEBS Journal*.

Blackwell Publishing Ltd. https://doi.org/10.1111/febs.14818

120 Thiery, J. P., Acloque, H., Huang, R. Y. J., & Nieto, M. A. (2009). Epithelial-mesenchymal transitions in development and disease. *Cell*, *139*(5), 871–890. https://doi.org/10.1016/j.cell.2009.11.007

121 Troncone, E., Marafini, I., Stolfi, C., & Monteleone, G. (2018, June 20). Transforming growth factor-β1/Smad7 in intestinal immunity, inflammation, and cancer. *Frontiers in Immunology*. Frontiers. https://doi.org/10.3389/fimmu.2018.01407

122 Tschumperlin, D., Boudreault, F., & Liu, F. (2011). Recent Advances and New Opportunities in Lung Mechanobiology. *J. Biomech.*, *43*(1), 1–19. https://doi.org/10.1016/j.jbiomech.2009.09.015.Recent

123 Tschumperlin, D. J., Ligresti, G., Hilscher, M. B., & Shah, V. H. (2018). Mechanosensing and fibrosis. *Journal of Clinical Investigation*, *128*(1), 74–84. https://doi.org/10.1172/JCI93561

124 Van Moorsel, C. H. M., Van Oosterhout, M. F. M., Barlo, N. P., De Jong, P. A., Van Der Vis, J. J., Ruven, H. J. T., … Grutters, J. C. (2010). Surfactant protein C mutations are the basis of a significant portion of adult familial pulmonary fibrosis in a dutch cohort. *American Journal of Respiratory and Critical Care Medicine*, *182*(11), 1419–1425. https://doi.org/10.1164/rccm.200906-0953OC

125 White, E., & Mantovani, A. (2014). Spectrum of Tissue Injury and Resolution. *J Pathol*, *229*(2), 141–144. https://doi.org/10.1002/path.4126.Inflammation

126 Whitsett, J. A., Kalin, T. V., Xu, Y., & Kalinichenko, V. V. (2018). Building and Regenerating the Lung Cell by Cell. *Physiological Reviews*, *99*(1), 513–554. https://doi.org/10.1152/physrev.00001.2018

127 Winkelmann, A., & Noack, T. (2010). The Clara cell: A “Third Reich eponym”? *European Respiratory Journal*. https://doi.org/10.1183/09031936.00146609

128 Wirtz, H. R., & Dobbs, L. G. (2000). The effects of mechanical forces on lung functions. *Respiration Physiology*, *119*(1), 1–17. https://doi.org/10.1016/S0034-5687(99)00092-4

129 Wynn, T. A. (2004). Fibrotic disease and the TH1/TH2 paradigm. *Nature Reviews Immunology*, *4*(8), 583–594. https://doi.org/10.1038/nri1412

130 Wynn, T. A. (2011). Integrating mechanisms of pulmonary fibrosis. *The Journal of Experimental Medicine*, *208*(7), 1339–1350. https://doi.org/10.1084/jem.20110551

131 Xie, T., Liang, J., Guo, R., Liu, N., Noble, P. W., & Jiang, D. (2011). Comprehensive microRNA analysis in bleomycin-induced pulmonary fibrosis identifies multiple sites of molecular regulation. *Physiological Genomics*, *43*(9), 479–487. https://doi.org/10.1152/physiolgenomics.00222.2010

132 Yamada, M., Kubo, H., Ota, C., Takahashi, T., Tando, Y., Suzuki, T., Ichinose, M. (2013). *The increase of microRNA-21 during lung fibrosis and its contribution to epithelial-mesenchymal transition in pulmonary epithelial cells*. *Respiratory Research* (Vol. 14). https://doi.org/10.1186/1465-9921-14-95

133 Yan, X., Liu, Z., & Chen, Y. (2009). Regulation of TGF-beta signaling by Smad7. *Acta Biochimica et Biophysica Sinica*, *41*(4), 263–272. https://doi.org/10.1093/abbs/gmp018.Review

134 Yan, Z., kui, Z., & Ping, Z. (2014). Reviews and prospectives of signaling pathway analysis in idiopathic pulmonary fibrosis. *Autoimmunity Reviews*, *13*(10), 1020–1025. https://doi.org/10.1016/j.autrev.2014.08.028

135 Yang, G., Yang, L., Wang, W., Wang, J., Wang, J., & Xu, Z. (2015). Discovery and validation of extracellular/circulating microRNAs during idiopathic pulmonary fibrosis disease progression. *Gene*, *562*(1), 138–144. https://doi.org/10.1016/j.gene.2015.02.065

136 Ye, Z. L., Jin, H. J., & Qian, Q. J. (2015). Argonaute 2: A novel rising star in cancer research. *Journal of Cancer*, *6*(9), 877–882. https://doi.org/10.7150/jca.11735

137 Zhang, S., Fei, T., Zhang, L., Zhang, R., Chen, F., Ning, Y., … Chen, Y.-G. (2007). Smad7 Antagonizes Transforming Growth Factor Signaling in the Nucleus by Interfering with Functional Smad-DNA Complex Formation.

Molecular and Cellular Biology, *27*(12), 4488–4499. https://doi.org/10.1128/MCB.01636-06

138 Zheng, Y., Kong, J., Li, Q., Wang, Y., & Li, J. (2018). Role of miRNAs in skeletal muscle ageing. *Clinical Interventions in Ageing*, *13*, 2407–2419. https://doi.org/10.2147/CIA.S169202

Appendix 1 Mice body weight

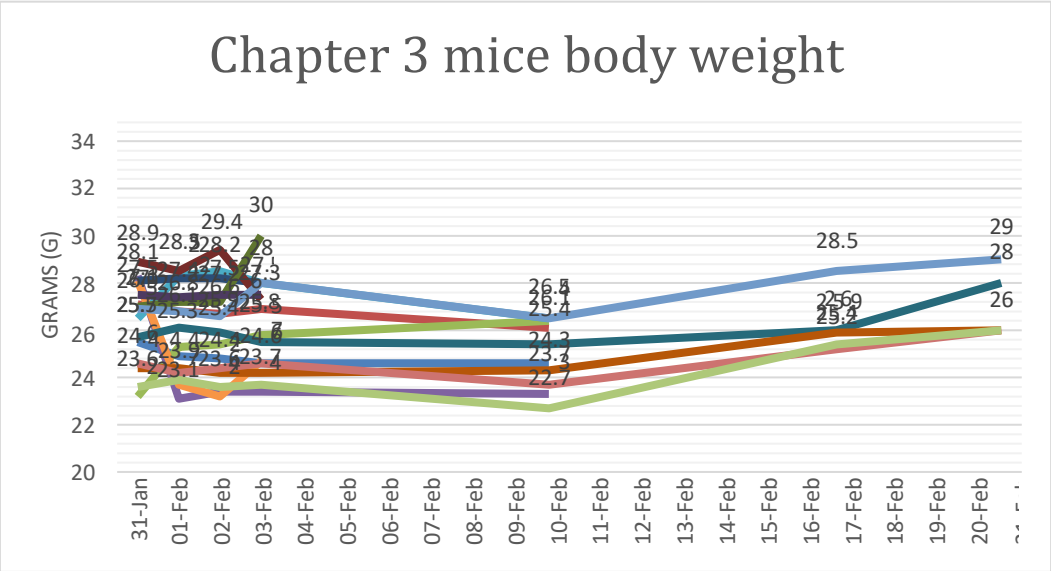

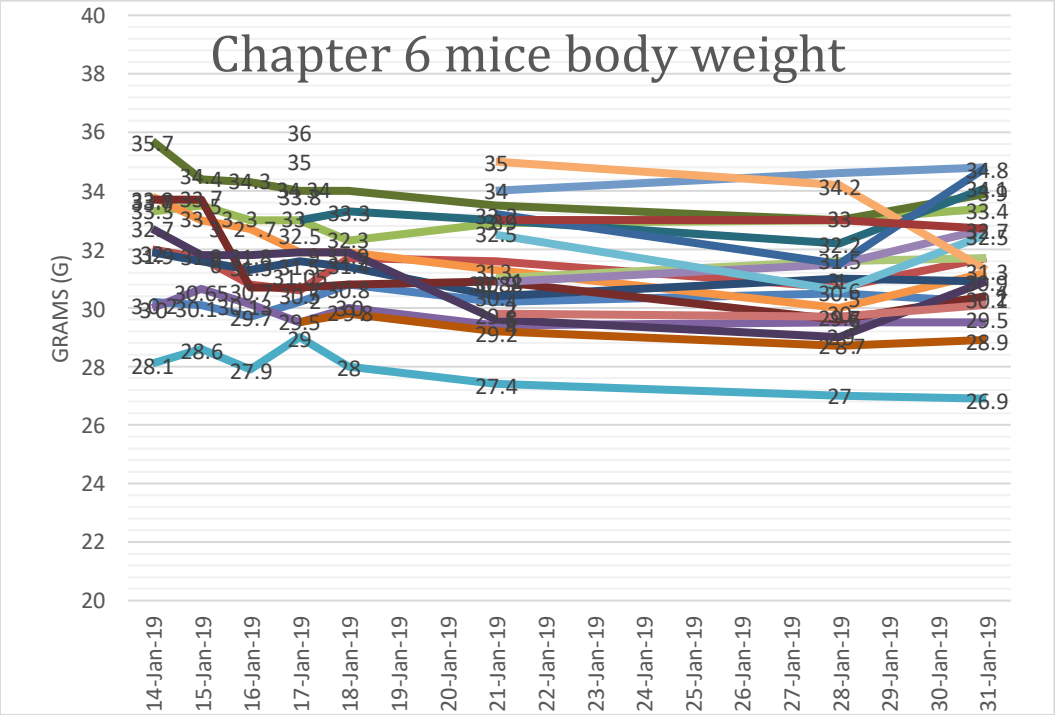

Appendix 2 ImageJ Fiji Macro

Step 1: Conversion 1	
Command	8-bit
Step 2: Thresholding 1	
Mode	Moments dark
Step 3: Conversion	
Command	“Make it Binary”
Step 4: Thresholding 2	
Range of Thresholding	22,255
Step 5: Removing Black Background	
Command	Convert to Mask
Option	BlackBackground FALSE
Step 6: Analysis	
Command	Analyse Particles
	Summarise